

Distribution Dynamics of Biologically Aged RBC Subpopulations: Impact of  
Blood Component Manufacturing Methods, Cryopreservation, and Irradiation

by

Sanaz Hemmmatibardehshahi

A thesis submitted in partial fulfillment of the requirements for the degree of

Master of Science

In

Biopreservation

Department of Laboratory Medicine and Pathology

University of Alberta

© Sanaz Hemmmatibardehshahi, 2024

## **Abstract**

The quality of red blood cell concentrates (**RCCs**) is influenced by storage duration, donor variability, and processing methods. RCCs contain heterogeneous subpopulations of red blood cells (**RBCs**), ranging from young (**Y-RBC**) to old (**O-RBC**), each with distinct structural and biochemical characteristics. A higher proportion of O-RBCs contributes to storage lesions and decreased post-transfusion survival rates. Understanding how manufacturing methods impact the distribution of RBC subpopulations is crucial in estimating the quality of RCCs. Additionally, cryopreservation processes result in approximately 15% loss of vulnerable RBCs due to osmotic and freezing stress. Investigating how different RBC subpopulations respond to these stresses can provide insights into RBC variability in response to cryopreservation techniques and minimize RBC loss. Gamma irradiation, a common practice in transfusion medicine, has been linked to increased hemolysis and supernatant potassium (**K<sup>+</sup>**) levels. Studying RBC subpopulations' responses to irradiation can help develop strategies to minimize irradiation-induced lesions by achieving a favorable ratio of Y- to O-RBCs in units undergoing irradiation. This thesis explored how manufacturing methods, cryopreservation, and irradiation affect various biologically aged RBC subpopulations. It compared the density-based distribution of RBCs, osmotic parameters, irradiation-induced lesions, and recovery rates of Y- and O-RBCs after thawing and irradiation during hypothermic storage.

Density-based Percoll<sup>®</sup> separation was employed to evaluate the impact of manufacturing methods on the distribution of RBCs in RCCs produced by whole blood filtration (**WBF**) and red cell filtration (**RCF**) methods. The membrane water ( $L_p$ ) and solute permeability ( $P_s$ ), osmotic fragility, and osmoscan parameters of Y- and O-RBC subpopulations were measured using stopped-flow and ektacytometry. The biotinylation technique was used to assess the recovery

rate of spiked young and old bio-labeled RBCs (**Y-** and **O-BioRBCs**) in RCC units post-thaw. The impact of gamma irradiation on Y- and O-RBC subpopulations was assessed by measuring oxidative hemolysis, supernatant  $K^+$ , and p50 before and after irradiation during hypothermic storage. The biotinylation approach was implied to evaluate the recovery of Y- and O-RBCs after irradiation.

The comparative analysis of RCCs processed using RCF and WBF methods revealed that RCCs processed with the WBF method exhibited higher RBC counts, hemoglobin (**Hb**), hematocrit (**HCT**), and volume. Despite variations observed in individual units, the overall ratio of Y- to O-RBCs remained consistent across all units regardless of the processing method employed. The stopped-flow experiment revealed that O-RBCs have higher  $L_p$  values followed by Y-RBCs, with unseparated RBCs (**U-RBCs**) showing the lowest  $L_p$  values across all NaCl solutions at 4 and 20 °C ( $p < 0.0001$ ). O-RBCs displayed a higher  $P_s$  value than Y-RBCs during deglycerolization, indicating faster glycerol efflux ( $p < 0.0001$ ). Furthermore, Y-RBCs exhibited higher  $O_{hyper}$ ,  $EI_{max}$ , and lower rigidity compared to O-RBCs, suggesting greater shear stress tolerance ( $p < 0.0001$ ). Despite these findings, no advantages in Y-RBC post-deglycerolization survival were observed. The irradiation results show that hemolysis levels and supernatant  $K^+$  significantly increased after gamma irradiation during hypothermic storage for all RBC subpopulations, with Y- and O-RBCs consistently exhibiting higher hemolysis levels than U-RBCs. Oxidative hemolysis increased across all subpopulations ( $p < 0.0001$ ), with O-RBCs showing a more pronounced trend ( $p = 0.0110$ ). p50 values were decreased across all RBC subpopulations following irradiation. The number of Y- and O-BioRBCs decreased during hypothermic storage, with no significant differences observed between RBC subpopulations.

In conclusion, although WBF-derived RCCs had higher levels of HCT, Hb, RBC counts, and volume, the distribution of Y- and O-RBCs in RCCs was not significantly influenced by manufacturing methods. Variations observed in the distribution of RBCs in RCCs are likely attributed to donor factors rather than the manufacturing method. This highlights the importance of considering donor-related factors when assessing RCC composition. Despite Y-RBCs exhibiting lower membrane permeability and superior osmoscan parameters, no advantage in their post-deglycerolization survival was observed. The hemolysis and supernatant  $K^+$  levels increased in Y- and O-RBCs following irradiation, suggesting comparable membrane damage. The impaired antioxidant capacity of O-RBCs leads to a more pronounced increase in oxidative hemolysis post-gamma irradiation. Despite these differences, no significant variations in RBC survival were observed across RBC subpopulations. Further research is needed to elucidate the complex factors influencing RBC behavior post-irradiation and during hypothermic storage. This research enriches our understanding of how processing methods may impact RBC subpopulations in RCCs, providing valuable insights into optimizing methodologies, considering the diverse subpopulations within RCCs.

## **Preface**

This thesis represents an original work conducted by Sanaz Hemmatibardehshahi, undertaken with the invaluable assistance of several individuals and institutions. I am deeply grateful to Carly Olafson and the Canadian Blood Service (CBS) in Calgary and Edmonton, Canada, for providing whole blood cells essential for Chapter Two of this study. Furthermore, I extend my gratitude to Caroline Picon, an intern student from the Polythech Celmont School of Engineering, France, for her contributions to achieving the goals outlined in Chapter Two. Portions of this Chapter were presented at the CSTM 2024 Annual Meeting on May 23<sup>rd</sup>, 2024.

Chapter Three of this thesis was made possible through the generous support of Dr. Andrew Holt, who provided access to the stopped-flow apparatus crucial for collecting the main data presented in this chapter. Additionally, I am thankful for the resources provided by the Flow Cytometry Facility at the University of Alberta, which significantly contributed to the success of this study. Portions of Chapter Three were presented at the 17<sup>th</sup> Annual Earl W. Davie Symposium on November 16<sup>th</sup>, 2023, the Bench to Bedside Research Symposium on November 30<sup>th</sup>, 2023, and were presented at the Cryo2024 Annual Conference on July 23<sup>rd</sup>, 2024, as well as the CSTM 2024 Annual Meeting on May 23<sup>rd</sup>, 2024.

Chapter Four was completed with the continued assistance of Carly Olafson, Candice Seeger, Jackie Lee, and Blood4Research who were involved in arranging the irradiation of units and tubes and providing the blood component required for this study. The Flow Cytometry Facility at the University of Alberta also played a crucial role in facilitating this research. A portion of the findings from Chapter Four was presented at the CSTM Annual Meeting on May 23<sup>rd</sup>, 2024.

I am profoundly grateful for the collaboration, guidance, and support provided by all individuals and institutions involved in this research endeavor. Their contributions have been instrumental in the successful completion of this thesis.

## **Acknowledgement**

I am deeply grateful to my supervisor, Dr. Jason Acker, for his steadfast guidance, support, and mentorship throughout the entirety of my thesis. His expertise, encouragement, and unwavering dedication have profoundly shaped my academic and professional journey.

I extend my heartfelt appreciation to Dr. Olga Mykhailova, whose inspirational guidance and encouragement propelled me forward and engaged me in diverse projects, providing invaluable experiences across various domains. Special thanks are owed to Dr. Andrew Holt, whose generosity in granting access to the state-of-the-art stopped-flow fluorimeter and assistance in developing the assay were indispensable for the creation of Chapter 2.

I am indebted to the participants, including Wenhui Li, Carly Olafson, Celina Phan, Rafay Osmani, Nishaka William, Mackenzie Brandon-Coatham, and Jayme Kurach, whose contributions were pivotal to the success of this study. I am also grateful to Faranak Yadegari from Dr. Elliott's lab for her invaluable support and assistance with the electric coulter counter. I express sincere gratitude to April Xu, our dedicated lab assistant, for her kindness and invaluable support throughout this project.

My heartfelt thanks go to my committee members, Dr. Gwen Clarke and Chris Ward from the Faculty of Medicine & Dentistry - Laboratory Medicine & Pathology Department, for their invaluable feedback, insights, and encouragement.

I am grateful to Jackie Lee and Candice Seeger at Canadian Blood Services in Edmonton for their invaluable assistance with the irradiation study. Special thanks are also extended to Winnie Eng from the NetCAD Blood4Research Centre for her consistent cooperation in providing blood units for this study.

I am also deeply grateful to the Government of Alberta for their invaluable support through the Alberta Graduate Excellence Scholarship (AGES). This scholarship provided financial assistance and recognized my commitment to academic excellence, greatly impacting this research.

Lastly, I extend my deepest gratitude to my family and friends for their unwavering love, encouragement, and understanding throughout this journey. Their steadfast support has been my source of strength and motivation.

## Table of Contents

Abstract.....	ii
Preface.....	v
Acknowledgement .....	vi
<b>Chapter 1 Introduction.....</b>	<b>1</b>
1.1 Biological Age-Dependent Changes and Quality Assessment in Red Blood Cell Concentrates .....	2
1.2 Exploring Biological Age-Dependent Density Profiles of Red Blood Cells: Implications for Cell Separation and Age Profiling.....	4
1.3 Impact of Donor Sex and Age on Red Blood Cell Quality and Transfusion Outcomes.....	5
1.4 Impact of Manufacturing Methods on Red Blood Cell Quality in Red Blood Cell Concentrates .....	7
1.5 Cryopreservation of Red Blood Cells: Methods, Mechanisms, and Implications for Transfusion Medicine.....	8
1.5.1 Cryoprotective Agents in Red Blood Cell Cryopreservation.....	9
1.5.2 Comparative Methods for Cryopreservation of Red Blood Cells: High Glycerol-Slow Cooling vs. Low Glycerol-Rapid Cooling .....	10
1.5.3 Osmotic Parameters of RBCs and Their Implications for Cryopreservation.....	12
1.6 Variations in RBC Membrane Permeability: Implications for Cryopreservation Efficiency .....	17
1.7 Challenges and Techniques in Measuring Red Blood Cell Volume Changes: Stopped-Flow Spectroscopy Approaches .....	18
1-8 Biotinylation of RBCs .....	20
1.9 Gamma Irradiation of Red Blood Cells: Standard Practice and Global Guidelines .....	21
1.9.1 Impact of Irradiation on Red Blood Cell Storage Lesion and Membrane Integrity: Mechanisms and Consequences .....	22
1.10 Conclusion.....	23

1.11 Rationale.....	24
1.11.1 Clinical Relevance.....	24
1.12 Hypothesis and Objectives .....	25
1.13 References.....	28
<b>Chapter 2 Impact of Blood Component Manufacturing Methods on the Age Distribution of Red Blood Cells in Stored Red Cell Concentrates .....</b>	<b>47</b>
2.1 Introduction.....	48
2.2 Methods and Materials.....	50
2.2.1 Red Cells Concentrate (RCC) Manufacturing .....	50
2.2.2 Red Cell Filtration Processing Method .....	51
2.2.3 Whole Blood Filtration Processing Method.....	52
2.2.4 Density-Fractionation using Percoll® Separation Method .....	53
2.2.5 Estimating Median Density of Each RCCs .....	54
2.2.6 Statistical Analysis and Data Reporting.....	55
2.3 Results.....	56
2.3.1 Comparative Analysis of RBC Indices in RCCs Processed by RCF and WBF Methods	56
2.3.2 Variation in Distribution of RBC Subpopulations across RCCs Processed Using WBF and RCF.....	57
2.4 Discussion.....	58
2.4.1 Assessing RBC Indices Variation across RCCs Produced by Different Methods.....	59
2.4.2 Density-Based Distribution of RBC Subpopulations in RCCs Produced by Different Methods.....	60
2.5 Conclusion .....	61
2.6 References.....	78
<b>Chapter 3 Exploring Osmotic Characteristics and Survival of Red Blood Cell Subpopulation Extremes Following Cryopreservation: A Biotinylation Approach .....</b>	<b>83</b>

3.1 Introduction.....	84
3.1.2 Impact of Biological Aging on RBC Membrane Properties .....	84
3.1.3 Variability in RBC Membrane Characteristics: Donor Traits and Manufacturing Methods .....	85
3.2 Materials and Methods:.....	86
3.2.1 Red Cell Concentrate (RCC) Selection and Pooling.....	86
3.2.2 Density-Fractionation using Percoll® Separation.....	87
3.2.3 Biotinylation of Red Blood Cells .....	88
3.2.4 Spiking the Pooled Unit with Young and Old Biotin-labelled RBCs .....	90
3.2.5 Equilibrium RBC Volume Measurement.....	90
3.2.6 Preparation of Stopped-Flow Experimental Solutions.....	91
3.2.7 Stopped-Flow Spectrophotometer Setup and Measurement of RBC Volume Kinetics...	92
3.2.8 Measurement of Glycerol Permeability .....	93
3.2.9 Conversion from Fluorescence to Volume.....	94
3.2.10 Calculating the Osmotically Inactive Fraction of RBC Subpopulations.....	95
3.2.11 Calculating the Water Permeability ( $L_p$ ) and Glycerol Permeability ( $P_s$ ).....	96
3.2.12 Arrhenius Activation Energies .....	97
3.2.13 RBC Osmotic Deformability Assessment.....	97
3.2.14 Measurement of Hemolysis.....	98
3.2.15 Oxidative Hemolysis .....	100
3.2.16 Osmotic Hemolysis .....	100
3.2.17 Osmotic Fragility.....	101
3.2.18 Glycerolization of RCCs .....	102
3.2.19 Deglycerolization of RCCs .....	103
3.2.20 Tracing Biotin-labeled RBCs in Cryopreserved RCCs.....	103

3.2.21 Statistical Analysis .....	105
3.3 Results.....	105
3.3.1 Correlation Analysis of Relative RBC Volumes and Autofluorescence Across NaCl Concentrations.....	105
3.3.2 Osmotically Inactive Fraction ( $V_b$ ) Analysis Reveals Subpopulation Variances.....	106
3.3.3 Fluorescence Dynamics in Red Blood Cells: Subpopulation Variation and Osmotic Responsiveness.....	106
3.3.4 Water Permeability of RBC Subpopulations .....	107
3.3.5 Solute Permeability ( $P_s$ ) and Water Permeability ( $L_p$ ) of RBC Subpopulations During Glycerolization and Deglycerolization.....	108
3.3.6 Arrhenius Energy .....	108
3.3.7 Rheological and Osmotic Properties of Red Blood Cell Subpopulations.....	108
3.3.8 Hemolytic Variability in Red Blood Cell Subpopulations.....	110
3.3.9 Survival of RBC Subpopulation Post-Deglycerolization.....	111
3.4 Discussion.....	111
3.4.1 Fluorescence Intensity Variations and Hemoglobin Concentration in RBC Subpopulations Under Osmotic Stress.....	111
3.4.2 Variations in Red Blood Cell Membrane Permeability Across Subpopulations with Differing Biological Ages .....	112
3.4.3 Temperature Dependency of Water Permeability in Biologically Aged RBC Subpopulations .....	113
3.4.4 Deformability Analysis of Young and Old RBC Subpopulations .....	114
3.4.5 Osmotic Hemolysis and Antioxidant Capacity of Young and Old RBC Subpopulations .....	115
3.4.6 Biological Age and Recovery Rate of Biotinylated RBCs .....	115
3.5 Conclusion .....	116
3.6 References.....	159

<b>Chapter 4 Exploring the Impact of Gamma Irradiation on Biologically Young and Old Subpopulations of Red Blood Cells</b> .....	168
4.1 Introduction.....	169
4.1.1 Impact of Gamma-Irradiation on Red Blood Cells .....	169
4.1.2 RBC Biological Aging .....	170
4.2 Method and Material.....	171
4.2.1 Red Cell Concentrate (RCC) Selection and Pooling.....	171
4.2.2 Density-Fractionation using Percoll® Separation .....	171
4.2.3 Biotinylation of Red Blood Cell.....	172
4.2.4 Spiking the Pooled Unit with Young and Old Biotin-Labeled RBCs.....	173
4.2.5 Blood Component Irradiation Procedure: .....	173
4.2.6 Measurement of Hemolysis.....	174
4.2.7 Measurement of Supernatant Potassium (K <sup>+</sup> ) .....	175
4.2.8 p50 Measurement .....	175
4.2.9 Tracing Biotin-labeled RBC Subpopulations in Irradiated RCCs .....	176
4.2.10 Statistical Analysis .....	176
4.3 Results.....	176
4.3.1 Hemolytic Variability in Red Blood Cell Subpopulations.....	176
4.3.2 Measurement of Supernatant K <sup>+</sup> in RBC Subpopulations.....	177
4.3.3 Dynamic Changes in p50 Values across RBC Subpopulations .....	178
4.3.4 RBC Survival Post-Irradiation .....	178
4.4 Discussion.....	179
4.4.1 Impact of Irradiation on Hemolysis Levels in RBC Subpopulations.....	179
4.4.2 Impact of Irradiation on Oxidative Hemolysis Levels in RBC Subpopulations .....	180
4.4.3 Effect of Gamma Irradiation on Supernatant K <sup>+</sup> Levels in RBC Subpopulations .....	181

4.4.4 Effects of Irradiation on p50 Values and Post-Irradiation Survival of RBC Subpopulations .....	182
4.5 Conclusion .....	183
4.6 References .....	203
<b>Chapter 5 General Discussion and Concluding Remarks</b> .....	<b>209</b>
5.1 Assessing the Impact of Manufacturing Methods on the Distribution of RBC Subpopulations in Red Cell Concentrates .....	210
5.2 Comparative Analysis of Osmotic Characteristics and Post-Deglycerolization Survival in Red Blood Cell Subpopulations .....	211
5.4 Effects of Biotinylation on Red Blood Cell Properties .....	214
5.5 Conclusion.....	214
5.6 References .....	217
<b>Bibliography</b> .....	<b>220</b>

## List of Tables

Table 3-1 RBC Indices Measured for RCCs .....	118
Table 3-2 RBC Indices for Subpopulation Extremes .....	119
Table 3-3 Calibration Factors for Coulter Counter-Based Measurement of RBC Volumes	120
Table 3-4 Stopped-Flow Experimental Solutions .....	121
Table 3-5 Experimental Solutions Osmolality Measurements .....	122
Table 3-6 Osmometer Control Data .....	123
Table 3-7 Equilibrium RBC Volume in Various NaCl Solutions .....	124
Table 3-8 Fluorescence Intensity of RBCs at Equilibrium's Final 3 Seconds.....	125
Table 3-9 The Correlation Between Relative RBC Volume and Autofluorescence .....	126
Table 3-10 $L_p$ Values Among RBC Subpopulations in Various NaCl Solutions .....	127
Table 3-11 $L_p$ and $P_s$ Values Across RBC Subpopulations during Glycerolization and Deglycerolization.....	128
Table 4-1 RBC Indices Measured for RCCs .....	185
Table 4-2 RBC Indices for Subpopulation Extremes .....	186

## List of Figures

Figure 2-1 Comparison of Red Cell Filtration and Whole Blood Filtration Processing Methods .....	62
Figure 2-2 Preparation of Percoll Density Gradients for RBC Subpopulation Isolation .....	63
Figure 2-3 Comparison of Hemoglobin Levels between RCF and WBF Methods.....	64
Figure 2-4 Comparison of Red Blood Cell Counts between RCF and WBF Methods .....	65
Figure 2-5 Comparison of Mean Corpuscular Volume (MCV) between RCF and WBF Methods .....	66
Figure 2-6 Comparison of Hematocrit (HCT) Levels between RCF and WBF Methods.....	67
Figure 2-7 Comparison of Estimated Median Density between RCF and WBF Methods....	68
Figure 2-8 Comparison of Red Cell Distribution Width (RDW) between RCF and WBF Methods .....	69
Figure 2-9 Comparison of Mean Corpuscular Hemoglobin Concentration (MCHC) between RCF and WBF Methods .....	70
Figure 2-10 Comparison of Final Volume Ratios in RCCs Processed with Different Methods .....	71
Figure 2-11 Unit-to-Unit Comparison of Density-Based Proportion of Red Blood Cells ....	72
Figure 2-12 Analysis of Young Proportion of RBC Subpopulations in RCCs Processed Using Different Methods.....	73
Figure 2-13 Analysis of Old Proportion of RBC Subpopulations in RCCs Processed Using Different Methods.....	74
Figure 2-14 Comparative Analysis of Density Distribution of RCCs Processed Using Different Methods.....	75
Figure 2-15 Comparison of Young to Old RBC Ratio across Units Processed Using Different Manufacturing Methods.....	76
Figure 2-16 Mixed Effect Analysis of Aggregate Data on Young to Old RBC Ratio .....	77

Figure 3-1 Osmoscan Curve and LORCA Indices .....	129
Figure 3-2 Gate Selection for Cell Population Identification.....	130
Figure 3-3 Linear Regression Analysis of Relative Equilibrium Volume (V/V0) and Fluorescence (F/F0).....	131
Figure 3-4 Boyle-van't-Hoff Equation: $V_b$ Calculation in RBC Subpopulations .....	132
Figure 3-5 Effect of NaCl Concentration on Fluorescence Intensity of RBC Subpopulations at Different Temperatures.....	133
Figure 3-6 RBC Responses to NaCl: Volume and Autofluorescence .....	134
Figure 3-7 Correlation between RBC Volume and Fluorescence Intensity in Different RBC Subpopulations .....	135
Figure 3-8 Dynamics of RBC Fluorescence and Volume During Glycerolization and Deglycerolization Processes .....	136
Figure 3-9 Analysis of $L_p$ Values of RBC Subpopulations Across NaCl Solutions at 4 °C	137
Figure 3-10 Analysis of $L_p$ Values of RBC Subpopulations Across NaCl Solutions at 20 °C .....	138
Figure 3-11 Analysis of RBC Subpopulation $P_s$ Values During Glycerolization and Deglycerolization Processes .....	139
Figure 3-12 Comparison of RBC Subpopulation $L_p$ Values During Glycerolization and Deglycerolization Processes .....	140
Figure 3-13 Analysis of RBC Subpopulation $E_a$ Values Across NaCl Solutions .....	141
Figure 3-14 Elongation Analysis of RBC Subpopulations as a Function of Shear Stress ..	142
Figure 3-15 Impact of Biotinylation on RBC Elongation .....	143
Figure 3-16 Comparison of RBC Rigidity ( $K_{EI}$ ) Among Subpopulations .....	144
Figure 3-17 Effect of Biotinylation on RBC Rigidity ( $K_{EI}$ ) .....	145
Figure 3-18 Analysis of $O_{hyper}$ Values among RBC Subpopulations .....	146
Figure 3-19 Effect of Biotinylation on $O_{hyper}$ Values in RBC Subpopulations .....	147

Figure 3-20 Comparison of Maximum Elongation Index ( $EI_{max}$ ) Among RBC Subpopulations .....	148
Figure 3-21 Impact of Biotinylation on Maximum Elongation Index ( $EI_{max}$ ) in RBC Subpopulations .....	149
Figure 3-22 Comparison of Elongation Index at Hypertonic Osmolality ( $EI_{hyper}$ ) Among RBC Subpopulations .....	150
Figure 3-23 Impact of Biotinylation on Elongation Index at Hypertonic Osmolality ( $EI_{hyper}$ ) in RBC Subpopulations .....	151
Figure 3-24 Comparison of Osmolality for Maximum Elongation Index ( $O(EI_{max})$ ) among RBC Subpopulations .....	152
Figure 3-25 Comparison of Initial Hemolysis Levels Post-RBC Separation among Subpopulations .....	153
Figure 3-26 Comparison of Oxidative Hemolysis Levels Across RBC Subpopulations ....	154
Figure 3-27 Effect of Biotinylation on Oxidative Hemolysis in RBC Subpopulations .....	155
Figure 3-28 Comparison of Osmotic Hemolysis Among RBC Subpopulations .....	156
Figure 3-29 Comparison of Osmotic Fragility Among RBC Subpopulations .....	157
Figure 3-30 Tracking Changes in the Numbers of Biolabeled RBC Subpopulations Post-Deglycerolization.....	158
Figure 4-1 Arrangement of Tubes and Placement of Radsure Stickers for Irradiation.....	187
Figure 4-2 Hemolysis Levels Post-irradiation in Different RBC Subpopulations .....	188
Figure 4-3 Comparative Hemolysis Levels in Young and Old RBC Subpopulations .....	189
Figure 4-4 Correlation between Biotinylation and Hemolysis.....	190
Figure 4-5 Comparison of Hemolysis Levels between Irradiated and Non-irradiated RCCs .....	191
Figure 4-6 Correlation Between RBC Senescence and Oxidative Hemolysis .....	192
Figure 4-7 Impact of Irradiation on Oxidative Hemolysis Levels during Hypothermic Storage.....	193

Figure 4-8 Impact of Irradiation on Oxidative Hemolysis in RBC Subpopulations .....	194
Figure 4-9 Correlation Between Biotinylation and Oxidative Hemolysis Levels in RBC Subpopulations .....	195
Figure 4-10 Comparison of Supernatant K <sup>+</sup> Levels during Hypothermic Storage after Irradiation .....	196
Figure 4-11 Comparison of Supernatant K <sup>+</sup> Levels Across RBC Subpopulation After Irradiation .....	197
Figure 4-12 Analysis of K <sup>+</sup> Levels in Irradiated and Non-irradiated RBC Subpopulations	198
Figure 4-13 Comparison of K <sup>+</sup> Levels Between Irradiated and Non-Irradiated RCCs.....	199
Figure 4-14 Dynamic Changes in p50 Values Across RBC Subpopulations Following Irradiation .....	200
Figure 4-15 Comparison of p50 Values Between Irradiated and Non-Irradiated RBC Subpopulations .....	201
Figure 4-16 Post-Irradiation Survival Dynamics of Different RBC Subpopulations.....	202

## **Abbreviations:**

RCCs:	Red blood cell concentrates
RBC:	Red blood cell
Y-RBC:	Young red blood cell
O-RBC:	Old red blood cell
U-RBC:	Unseparated red blood cell
SP-RBC:	Spiked pooled red blood cell
Hb:	Hemoglobin
HCT:	Hematocrit
MCV:	Mean corpuscular volume
MCHC:	Mean corpuscular hemoglobin concentration
PS:	Phosphatidylserine
CD47:	Cluster of differentiation 47
ATP:	Adenosine triphosphate
DPG:	2,3-Diphosphoglycerate
metHb:	Methemoglobin
EMD:	Estimated median density
MCH:	Mean corpuscular hemoglobin
PRP:	Platelet-rich plasma
WBF:	Whole blood filtration
RCF:	Red-cell filtration method
WB:	Whole blood

CPP:	Cell-poor plasma
CPAs:	Cryoprotective agents
LGM:	Low Glycerol Medium
HGM:	High Glycerol Medium
AQP1:	Aquaporin-1
AQP3:	Aquaporin-3
UT-B:	Urea Transporter B
$L_p$ :	Water Permeability
$P_s$ :	Osmotic Permeability to Solutes
$V_b$ :	Osmotically Inactive Cell Volume
$E_a$ :	Arrhenius Activation Energy
$K^+$ :	Potassium (ion)
TBARS:	Thiobarbituric Acid Reactive Substances
MDA:	Malondialdehyde
ROS:	Reactive Oxygen Species
LDH:	Lactate Dehydrogenase
Gy:	Grays (unit of ionizing radiation)
TA-GVHD:	Transfusion-Associated Graft Versus Host Disease
WBCs:	White Blood Cells
NHS:	N-hydroxysuccinimide
Gy:	Grays (unit of ionizing radiation)
AABB:	Association for the Advancement of Blood & Biotherapies
CSA:	Canadian Standards Association

**Chapter 1**  
**Introduction**

## 1.1 Biological Age-Dependent Changes and Quality Assessment in Red Blood Cell Concentrates

Red blood cell concentrates (**RCCs**) are globally used as a lifesaving therapeutic method. (1,2) Despite improvements in stored blood components, transfusion of **RCCs** is still associated with an increased risk of adverse clinical events. (3–10) Recent studies have focused on the effects of storage duration on the quality of blood products and their clinical consequences; however, the quality of **RCCs** may also depend on factors such as donor-to-donor variability and the biological age of **RBCs**. (1,2,9–12) The normal lifespan of red blood cells (**RBCs**) in blood circulation is 120 days, and during this time, **RBCs** undergo the biological aging process. (13) Biological aging process results in the formation of heterogeneous subpopulations of **RBC**, consisting of recently matured (young, **Y-RBC**) to senescent (old, **O-RBC**) **RBCs**. (13,14) Biological aging significantly affects various **RBC** quality parameters, including their ability to withstand oxidative and osmotic stress and their recovery rate following processing methods and storage. Therefore, the proportion of **Y-** to **O-RBCs** in **RCCs** may serve as a reliable marker of **RCC** quality, influenced by donor-related factors and pre-transfusion procedures, including manufacturing methods, irradiation, and hypothermic storage.

Biological aging induces a gradual transformation in the shape of **RBCs**, transitioning from discocytes to spherocytes. (15,16) This process involves microvesiculation, generating small phospholipid vesicles (0.04 - 1.5  $\mu\text{m}$  in diameter) and altering the membrane composition and integrity. (17–22) The shedding of membrane fragments and intracellular cytoplasm via microvesiculation leads to a decrease in the mean cell volume (**MCV**) and an increase in the mean corpuscular hemoglobin concentration (**MCHC**), ultimately resulting in an increased density of **RBCs**. (13,14,23–26) Typically, **Y-RBCs** demonstrate higher **MCV** and morphology index, along with a relatively lower **MCHC** compared to old **O-RBCs**. (27) The translocation of phosphatidylserine (**PS**) molecules to the outer leaflet of the membrane occurs during aging, signaling phagocytic cells for clearance from circulation. (14,17,28–41) Additionally, the expression of **CD47**, an erythrocyte surface antigen that prevents the clearance of **RBCs** from circulation, diminishes during **RBC** biological aging. (42)

The RBC biological aging process is associated with a decline in metabolic activity and progressive failure of cellular homeostasis and antioxidant defenses. Despite the robust antioxidant machinery of RBCs (43–45), the absence of biosynthetic capacity and protein renewal makes RBCs vulnerable to cumulative effects of oxidation and glycation, altering protein structure and function. (46–48) The concentration of adenosine triphosphate (ATP), the primary energy source in RBCs, significantly declines during biological aging due to reduced glycolytic efficiency. (14) The RBC ion concentrations are balanced through ATP-dependent pumps, including sodium/potassium pumps ( $\text{Na}^+/\text{K}^+$ ) and  $\text{Ca}^{2+}$ -ATPase pumps. (49) With decreased ATP during RBC aging, the activity of the  $\text{Na}^+/\text{K}^+$  pump in uptaking  $\text{K}^+$  declines, resulting in the accumulation of  $\text{K}^+$  in the extracellular milieu. (50) A decrease in ATP level affects the function of the  $\text{Ca}^{2+}$ -ATPase pump, leading to the accumulation of  $\text{Ca}^{2+}$  in the RBC cytoplasm. This accumulation triggers the microvesiculation and activation of calcium-sensitive  $\text{K}^+$  channels, ultimately leading to cell shrinkage, cytoskeleton protein degradation, PS exposure, and  $\text{K}^+$  leakage from the RBCs. Additionally, declining ATP levels progressively impair the antioxidant system of RBCs, subsequently leading to an increased concentration of methemoglobin (**metHb**) by biological aging. (14) Hemoglobin (**Hb**) and protein modifications through oxidation, phosphorylation, and aggregation play crucial roles in regulating RBC homeostasis and lifespan. (28–31,51–58) Additionally, decreased ATP levels result in reduced progression through the Ruperport-Leubering shunt, leading to lower levels of 2,3-diphosphoglycerate (**2,3-DPG**). 2,3-DPG facilitates the binding of oxygen to Hb and its subsequent release into the tissues. (59) Reduced 2,3-DPG levels in RBCs during aging enhance the RBC affinity for oxygen and impair oxygen exchange between Hb and the body's tissues. (60) These age-dependent modifications collectively reduce the post-transfusion recovery rate of RBCs by reducing deformability and elongation, increasing cell rigidity, and heightening the susceptibility of RBCs to osmotic, oxidative, and mechanical stress. (14,33,61,62) Understanding these biological age-related alterations in RBCs is crucial for assessing the quality of RCCs by considering the distribution of young and old RBCs in the final blood component, as well as for profiling RBCs according to their biological age.

## 1.2 Exploring Biological Age-Dependent Density Profiles of Red Blood Cells: Implications for Cell Separation and Age Profiling

During the RBC biological aging process, they become denser, marked by decreased surface-to-volume ratio and elevated MCHC. (13,14,27,34) Y-RBCs and O-RBCs can be separated using density fractionation through Percoll<sup>®</sup> centrifugation. (63) The concept of separating RBCs based on their age-dependent density profile was first proposed by Key in 1921, who observed that reticulocytes (immature RBCs) tend to concentrate at the top layer of centrifuged RBC columns. (64) Piomelli et al. introduced the Neocell system, leveraging the lower buoyant density of reticulocytes in autologous plasma during centrifugation to enrich Y-RBCs in the top one-third of the RBC layer. (63) Building upon these findings, Hogan et al. developed a technique utilizing the automated cell processor 215 (ACP<sup>®</sup> 215) to separate Y-RBCs (neocytes) based on their buoyant density in autologous plasma during centrifugation, achieving neocyte enrichment in the top one-third of the RBC layer. (65) In the context of separating Y- and O-RBCs, automated cell processors can be programmed to perform density gradient centrifugation or other separation techniques to isolate RBC subpopulations based on their age-related characteristics. (66) Additionally, volume-fractionation techniques, such as counter-flow centrifugation, sort RBCs by their size as passing through narrow channels or filters. However, inconsistencies arise between density and volume-fractionation results. (66)

Another practical approach to separate Y- and O-RBCs is using fluorescence-activated cell sorting (FACS) based on specific surface markers associated with RBC age. This method relies on the differential expression of markers such as CD47 or band-3 on the surface of RBCs, which change with RBC biological aging. By labeling RBCs with fluorescent antibodies targeting these markers, FACS can effectively sort RBC subpopulations based on biological age. (67) Immunomagnetic separation (IMS) and magnetic-activated cell sorting (MACS) are potential methods for separating RBC subpopulations. IMS involves using magnetic beads conjugated with antibodies targeting surface markers specific to Y- or O-RBCs for isolation, such as the very youngest erythrocytes identified by transferrin positivity (**Trf+Ret**) in peripheral blood. (68) MACS utilizes a column-based separation method, where target cells labeled with magnetic particles conjugated to specific antibodies are retained within the column by a magnetic field while unlabeled cells are washed away. (69) These methods, while effective, may have

limitations in high-throughput applications due to time-consuming antibody binding and washing steps. Additionally, microfluidic devices can sort cells based on parameters, including size, shape, and surface markers, utilizing microscale channels and structures and leveraging fluid mechanics and surface forces for precise sorting. (70,71) However, challenges such as complex device design, limited throughput, high costs, and sensitivity to sample variations may affect the effectiveness of this method in RBC separation.

Despite the advancements in RBC separation techniques, density-fractionation remains the most common method to demonstrate the heterogeneity of the RBC population and can be employed for the age profiling of RCCs and the calculation of the estimated median density (EMD). (34,63,65,72) The estimated median density denotes the density at which Y- and O-RBCs are separated in a 1:1 ratio. In other words, the estimated median density of RCCs is determined based on a 1:1 separation ratio of Young (less dense) RBCs/ Old (dense) RBCs. Density-based separation methods like Percoll<sup>®</sup> centrifugation effectively categorize RBCs into distinct subpopulations based on density. (66) HbA1c, also known as glycated hemoglobin, serves as a reliable marker for confirming the predominant presence of young or old RBC subpopulations in separated fractions. (73) As RBCs age, they are exposed to glucose over time, leading to the glycation of hemoglobin molecules. Consequently, the level of HbA1c increases with the age of RBCs, making it a useful parameter for confirming the biological age of separated RBC subpopulations. Higher HbA1C levels indicate older RBCs, while lower levels suggest younger RBCs. (73) Additionally, assessing the band 4.1a:4.1b ratio is another confirmation method for distinguishing between Y- and O-RBC subpopulations. (35) As RBCs age, the band 4.1a:4.1b ratio increase indicates older RBCs, while a lower ratio suggests younger ones. By analyzing HbA1c levels and the band 4.1a:4.1b ratio, researchers can ensure that the separated RBC subpopulations accurately represent young and old RBCs. (35)

### **1.3 Impact of Donor Sex and Age on Red Blood Cell Quality and Transfusion Outcomes**

In recent years, discussions surrounding the variability of RCCs have extended beyond consideration of RCC chronological age alone. (2,74–76) Donor-related factors, including sex and age, can significantly impact the properties of donated blood and the quality of the final products. (1,2,11,12,27,74–86) RCCs from male and female donors exhibit differences in several

key aspects, including their hematocrit (**HCT**), Hb concentration, oxygen delivery capacity, RBC count, iron homeostasis indexes, deformability, rigidity, and storability (87–90), with RCCs from male donors demonstrating higher levels of Hb, HCT, and RBC count compared to those from female donors. RCCs from female donors have demonstrated superior quality measurements, including less susceptibility to storage-induced hemolysis, mechanical fragility, and better rheological properties compared to RBCs from male donors. (27) Moreover, investigations into the impact of donor age on RCC quality have yielded intriguing results, indicating transfusion of RBCs from older donors (typically defined as >45 years) has been associated with a decreased transfusion-related mortality rate. (88) Chasse et al. findings suggested that RBC transfusion from younger donors or female donors was significantly associated with increased mortality. (91) However, conflicting findings persist in the literature, with the SCANDAT2 database reporting no association between donor age and sex with mortality rate after RBC transfusion. (87) The conflicting findings in previous studies may stem from a narrow focus on mortality outcomes when assessing RCC quality, neglecting other potential transfusion-related reactions or patient clinical conditions. This discrepancy highlights the necessity for deeper investigations into donor-related factors influencing RCC quality and transfusion outcome. One potential explanation for the variability in RBC quality based on donor characteristics is the distribution of RBCs with varying biological ages within the blood products. Mykhailova et al. found a correlation between the distribution of RBC subpopulations within RCCs and donor sex and age. (92,93) Specifically, RCCs from male donors exhibited higher EMDs compared to those from female donors, with a strong positive correlation observed between EMDs and MCHC post-collection. These findings underscore the intricate relationship between donor demographics and the biophysical properties of RCCs, shedding light on potential mechanisms underlying the observed differences in RCC quality. (92–94) Recent research has shed light on the influence of donor sex and age on the distribution of RBC subpopulations, yet further investigation is needed to understand the impact of processing methods on RBC distribution and its mechanisms and clinical implications.

## 1.4 Impact of Manufacturing Methods on Red Blood Cell Quality in Red Blood Cell Concentrates

The quality of RCCs depends on several other factors, including blood manufacturing methods. There are two main RCC processing methods: the top/top, PLT-rich plasma (**PRP**), whole blood filtration (**WBF**), termed B2, and the top/bottom, buffy coat (**BC**), red-cell filtration method (**RCF**), termed B1. While the Canadian Blood Service (**CBS**) has transitioned away from B2, it's worth noting that the B2 method is still used in the US and other countries. These methods are different in processing time, hold duration and temperature of the whole blood before processing, the stage of processing where leukoreduction occurs, and the speed and length of centrifugation, causing a density gradient in the RBC column from the top (Y-RBCs) to the bottom (O-RBCs). (95–97) In the WBF method, units are cooled in insulated shipping containers and filtered in the refrigerator within 72 hours of the stop-bleeding time. The filtered whole blood units are centrifuged at  $4552 \times g$  for 6 minutes. Platelet-poor plasma (**PRP**) and RBCs are both extracted through the top outlet of the main collection bag. (97,98) In the RCF method, whole blood units are rapidly cooled to room temperature 18-24 °C and held overnight before centrifugation. The hard spin centrifugation ( $3907 \times g$  for 10 min) provides enough time and centrifugal force to compact RBCs at the bottom of the bag and results in a cell-poor plasma (**CPP**) on top of the buffy coat layer. The collection set has one outlet at the top and another at the bottom of the collection bag. CPP is squeezed out from the upper outlet while packed RBCs are extracted from the bottom outlet. (97,99) The CPP flow is faster than the RBC flow based on its lower viscosity, resulting in the buffy coat and top layer of packed RBC (mostly containing Y-RBCs) moving upward. As the packed RBCs are squeezed out from the bottom outlet, the buffy coat and top layer of packed RBCs remain in the middle of the bag (45 to 50 mL). (98,100) Leukoreduction of the RBC unit in the RCF method is done at room temperature within 24 hours of the stop-bleeding time. (99,101) While in the RCF method, a significant volume of less dense RBCs remains within the collection bag during buffy coat removal (97–99) in the WBF method, a small volume of denser RBCs remains at the bottom of the collection bag. (97) A study conducted by Canadian Blood Services comparing the quality of RCCs produced using different processing methods analyzed data from 572 RBC units categorized by production method. It was found that all units met mandated guidelines for HCT, hemolysis, and Hb levels. However,

significant differences were observed among units produced using different methods. RCC units produced by the RCF method had lower Hb content, HCT, and volume compared to those produced by the WBF method. (95,97) Despite the overall similarity in quality, the study highlights a lack of equivalency across RBC products manufactured by different methods, suggesting further investigation into these differences and their potential implications for transfusion outcomes. (97) Previous studies have demonstrated that units processed using WBF exhibited higher membrane water permeability and hemolysis compared to those processed using RCF. Additionally, RCF-derived units display significantly higher supernatant  $K^+$  and significantly lower supernatant  $Na^+$  at all testing points compared to WBF-derived units. (102) Almizraq et al. study on the immunomodulatory effects of supernatants from RCCs manufactured using different methods demonstrated that RCCs processed using the WBF method induce higher interleukin-8 (IL-8) production in monocytes compared to RCCs processed using RCF, suggesting a potential pro-inflammatory effect of RCCs processed with WBF. (103) These findings suggest that blood manufacturing methods impact immunomodulation and quality of stored RBCs during hypothermic storage, warranting further investigation into their clinical implications and underlying mechanisms.

### **1.5 Cryopreservation of Red Blood Cells: Methods, Mechanisms, and Implications for Transfusion Medicine**

Cryopreservation is a potential long-term storage strategy for maintaining the quality of RBCs for commercial and medical purposes. (104) Cryopreserved RCCs can be stored for up to 10 years, allowing for a reliable inventory of rare blood types, individuals with adverse antibody problems, and civil emergency and military applications. (105,106) However, the cryopreservation process can impact the integrity and functionality of RBCs, potentially affecting their osmotic properties and survival after transfusion. (107,108) Cell membrane plays a critical role in RBC cryopreservation, as it regulates the transport of water and solutes across the cell membrane during osmotic changes. (107,108) During cryopreservation, RBCs are frozen and stored at subzero temperatures ( $<-65\text{ }^{\circ}\text{C}$ ) where biochemical reactions do not occur. To effectively cryopreserve RBCs, the goal is to prevent the two causes of freezing injury: slow cooling and rapid cooling rate. Slow cooling can cause the formation of ice crystals in the extracellular space and intensify the osmotic efflux of water from the cell. Osmotic efflux of water increases the concentration of

intracellular solutes, causing potential cell damage due to solute toxicity. On the other hand, rapid cooling results in the supercooling of the cell cytoplasm and the formation of ice crystals inside the cells. (109)

### **1.5.1 Cryoprotective Agents in Red Blood Cell Cryopreservation**

Cryoprotective agents (CPAs) protect biological systems from injury during freezing. These CPAs are commonly used in RBC cryopreservation and categorized into two primary groups based on their protective mechanisms: permeating and non-permeating. Permeating CPAs penetrate the cell membrane and act as additional intracellular solvents, thereby reducing the concentration of intracellular solutes and protecting cells from slow-freezing injury. Examples of permeating CPAs are dimethyl sulfoxide (**Me<sub>2</sub>SO or DMSO**), glycerol, ethylene, and propylene glycol. Non-permeating CPAs do not penetrate the cell membrane leading to cell dehydration and increased solute concentration inside the cell. This process depresses the freezing point of the intracellular solution, thereby preventing rapid freezing injury. Among non-permeating CPAs are sugars, polymers, and starches [hydroxyethyl starch (**HES**), polyvinylpyrrolidone (**PVP**)]. (110,111) In 1940, for the first time, Dr. Charles Drew demonstrated that human RBCs can be frozen and later reconstituted. (112) In 1950, after Polge and Smith discovered the protective effect of glycerol during the freezing of spermatozoa (113), glycerol was used for the cryopreservation of RBCs. (114) The first successful transfusion of human RBC frozen in glycerol was reported in 1951. (115) To enable the removal of CPA from RBCs after thawing, Huggins et al. developed the “cytoagglomeration” method in 1963. (116) This method involves the agglomeration or clumping of RBCs, which facilitates RBC separation from the surrounding solution containing the CPA. This method relies on the reversible binding of  $\gamma$ -globulins in plasma to lipoproteins on RBC membranes at an acidic pH. By reducing the ionic strength of the solution,  $\gamma$ -globulins precipitate along with RBCs. After discarding the supernatant, the process is repeated multiple times to eliminate the CPA. RBCs can be resuspended by increasing the ionic strength or pH of the solution. (116) The main issue with cytoagglomeration was the clumping of cells, compromising the quality of RBCs, resulting in poor post-thaw recovery and increased hemolysis rates.

The introduction of the Automated Cell Processor (ACP<sup>®</sup> 215) has streamlined the deglycerolization process and provided a closed system, decreasing the potential for bacterial

contamination and extending the post-deglycerolization expiry date. (117) This automated system uses a closed-loop centrifugal washing bowl to expose the cells to a series of saline wash steps, removing the excess glycerol and concentrating the cells. Additionally, this system is approved for post-process storage of the deglycerolized RBCs for up to 2 weeks. (118) Deglycerolization of cryopreserved RCCs using the Haemonetics ACP<sup>®</sup> 215 cell processor, employing dual centrifugation processing with AS-3 or ESOL additive, ensures that RCCs meet regulatory standards for blood quality, with storage periods of up to 14 days both before processing and after deglycerolization. (118) This approach results in RCCs with optimal hemoglobin content, reduced processing alerts, shorter deglycerolization time, and superior maintenance of ATP levels. (119,120) The advancements in cryopreservation technologies, coupled with the advent of automated cell processors, have extended the storage periods post-deglycerolization. This extension has resulted in enhanced transfusion outcomes, improved patient care, and greater availability of blood inventory.

### **1.5.2 Comparative Methods for Cryopreservation of Red Blood Cells: High Glycerol-Slow Cooling vs. Low Glycerol-Rapid Cooling**

The most common methods used for RBC clinical cryopreservation involve the high glycerol-slow cooling (**HGM**) and the low glycerol-rapid cooling (**LGM**) methods. (111) The high glycerol-slow cooling method is performed by adding the glycerol to RBCs to a final concentration of about 40% (w/v) and cooling at 1 °C/min to storage temperature below -68 °C. (121) While for the low glycerol-rapid cooling method, RBCs are mixed with an equal volume of the solution containing 28% glycerol, 3% mannitol, and 0.65% NaCl, to achieve the final glycerol concentration of 14% (v/v). The RBC-glycerol mixture is then frozen by immersion in liquid nitrogen (-196 °C) and stored there. (122) For deglycerolization with the high glycerol-slow cooling method, RCCs are subjected to rapid thawing in a 37 °C water bath and glycerol removal by a series of washes using sodium chloride solutions with decreasing concentrations. (121) In the low glycerol-rapid cooling method, RBCs are thawed in a warm water bath (42-45 °C) and deglycerolized with a single wash with 16% mannitol in 0.9% NaCl and two washes with isotonic saline. (122) According to Valeri et al. results, the average RBC freeze-thaw-wash recovery (the percentage of RBCs left in the sample after deglycerolization) through the high glycerol-slow cooling method was  $85.2 \pm 5.9\%$  (mean  $\pm$  SD) and the average 24-hour post-

transfusion survival (the percentage of transfused RBCs present in recipient's circulation 24 hours after transfusion) was 83%. (117) The average RBC freeze-thaw-wash recovery, using the low glycerol-rapid cooling method, was 95.9%, and the average 24-hour post-transfusion survival was  $96 \pm 1.5\%$  (mean  $\pm$  SD). (122) An alternative method for RBC cryopreservation is using non-permeating CPAs such as HES. In this method, RBCs are mixed with HES (molecular weight 200,000 Da, degree of substitution 0.5) to a final HES concentration of 11.5% (w/w). RBCs are frozen by immersion into liquid nitrogen and stored below  $-130\text{ }^{\circ}\text{C}$ . RBCs are thawed in a warm water bath, and HES is either left in RBC suspensions or removed by a single wash with isotonic saline. (123) Thomas reported the average recovery of RBCs cryopreserved with HES to be  $98.8 \pm 0.3\%$  (mean  $\pm$  SD). (124,125)

Cryopreserved RBCs demonstrate comparable functional properties to fresh RBCs after thawing and deglycerolization. Research indicates that cryopreserved RBCs maintain normal oxygen transport capacity, 2,3-DPG levels, and ATP concentration, with minimal hemolysis and supernatant potassium ( $\text{K}^+$ ) levels within acceptable limits. (126–128) Cryopreservation appears to maintain the integrity of the RBC membrane, as indicated by consistent levels of PS externalization, CD47 expression, and microvesiculation before freezing, immediately after thawing, and during hypothermic storage control. (40) These findings suggest that the freeze-thaw process prevents the onset of storage-related lesions. While cryopreserved RBCs have been clinically used since the 1960s, there is a lack of randomized clinical studies comparing them with hypothermic-preserved RBCs. Initial studies suggest comparable safety and efficacy between cryopreserved RBCs and hypothermic-preserved RBCs. (129) Post-transfusion hemolysis level, free Hb, bilirubin, platelet counts, and serum creatinine levels were not different between patients transfused with cryopreserved RBCs or hypothermic-preserved RBCs. (129) A component transfusion therapy program at Cook County Hospital in Chicago utilizing cryopreserved RBCs led to a notable reduction in transfusion reaction incidence from 0.57% to 0.11%. (130) O'Brien et al. documented the use of cryopreserved RBCs in vascular surgery and extracorporeal circulation, showing that thawed and deglycerolized RBCs exhibited no significant differences compared to fresh heparinized RBCs after prolonged circulation. (131) Although cryopreserved RBCs were widely used in USA centers during the 1960s and 1970s, concerns regarding cost, delayed availability, and short half-life after thawing have led to diminished usage. (130–133)

### 1.5.3 Osmotic Parameters of RBCs and Their Implications for Cryopreservation

The cell membrane plays a pivotal role in mediating cellular responses to osmotic stress caused by cryopreservation; however, the involvement of different membrane components in this process is poorly understood. (109,134–136) The cell membrane regulates osmotically induced changes in the cell volume during freezing by governing the transport of water and solutes between the cytoplasm and the extracellular milieu. (134,137) Osmosis is a fundamental process involving the movement of solvent from a solution of lower solute concentration to one of higher solute concentration across a semi-permeable membrane that allows solvent passage but blocks solute. (138) When human RBCs are exposed to a hypo- or hypertonic solution, they achieve a new equilibrium cell volume through osmosis much faster than most other cell types. This phenomenon is due to the exceptionally high water permeability of human RBCs facilitated by its membrane. The water permeability of RBCs is generally higher than that of lipid membranes, suggesting the presence of a non-lipid component in the RBC membrane that enhances water transport. Additionally, the low activation energy for water transport in human RBCs (14–20 kJ/mol) suggests an aquaporin pathway for water transportation through the RBC membrane. Inhibition studies suggest that approximately 90% of water transport in RBCs is attributed to Aquaporin-1 (**AQP1**) channels, with a minor contribution from other membrane proteins like Urea Transporter B (**UT-B**) and Aquaporin-3 (**AQP3**). (139,140) AQP1 in the human RBC membrane is the primary membrane protein responsible for transferring water molecules and facilitating the water permeability of the RBC membrane. (139,140) AQP3 is an aquaglyceroporin that transports water, glycerol, and small solutes across the plasma membrane. Glycerol transport kinetics vary among mammalian species, with human RBCs demonstrating relatively fast glycerol transport compared to most others. The reflection coefficient for glycerol transport in human RBCs demonstrating the amount of glycerol that can pass through the membrane, is reported to range from 0.52 to 0.88. (141) This phenomenon is attributed to variations in membrane lipid composition and the presence of glycerol transporter proteins. There are two main glycerol transporter proteins found on the RBC membrane: AQP3 and Aquaporin-9 (**AQP9**). These aquaporin proteins facilitate glycerol transport across the RBC membrane, playing a crucial role in glycerol permeability and the cryopreservation process. (142) The activation energy required for glycerol transport in human RBCs has been reported to range from 15 kJ/mol to 40 kJ/mol. (142–145). In contrast, the activation energy for glycerol

transport through lipid bilayers is notably higher, typically ranging from approximately 50 to 80 kJ/mol (146,147), implying the existence of a hydrophilic pathway within the bilayer that lowers the energy barrier for glycerol transport in human RBCs. AQP3 is identified as the primary glycerol transporter in human RBCs. Studies involving AQP3-null RBCs demonstrate significantly reduced glycerol permeability, supporting AQP3's role in glycerol transport. (143,145) AQP3 displays complex behavior in transporting water and glycerol, which is influenced by pH. This suggests a mechanism wherein successive hydrogen bonding with AQP3 may alter the functionality of these proteins.

Osmotic parameters regulate the movement of water and solute through the cell membrane. Water permeability ( $L_p$ ) represents the ability of the cell membrane to allow water molecules to pass through. Osmotic permeability to solutes ( $P_s$ ) describes the rate at which solutes cross the cell membrane.  $L_p$  and  $P_s$  are typically determined by measuring the rate of cell volume change when placed in an anisotonic environment. (140) The osmotically inactive cell volume ( $V_b$ ) is the volume of the cell that does not participate in the osmotic behavior of the cell. Arrhenius activation energy ( $E_a$ ) describes the temperature dependence of the membrane permeability to water and solutes. (148) Several mathematical models exist for calculating these permeability parameters. These include Jacobs and Stewart equation which incorporates membrane thickness into the permeability constant, a three-parameter model developed by Kedem and Katchalsky, including water and solute permeability and solute-solvent interaction, sigma ( $\sigma$ ) (149,150), a classic two-parameter, water, and solute permeability (2P), (150) and a one-parameter (solute permeability) model introduced by Mazur and colleagues. (142)

Jacob et al. proposed a method to establish a universal measure of cell membrane permeability, adaptable to various experimental settings (**Eq 1-1**). (151,152) The equation introduced a constant representing the amount of a substance passing through a unit cell surface in a unit of time while accounting for concentration gradients across the cell membrane. It integrated membrane thickness into the permeability constant, combining it with the true diffusion constant. The equation also provided conversion factors based on cell volume and surface area for comparisons and conversions. It described a numerical method for solving the differential equations governing water and solute penetration into the cell, enabling the determination of permeability constants from experimental data. (151,152) This method involves

simultaneous penetration equations for water and the solute, solved numerically to find the initial and minimum cell volumes over time. These volumes, along with the time of minimum volume attainment, allow direct reading of permeability constants from a prepared chart, facilitating quantitative assessment of cell permeability under diverse experimental conditions.

$$\frac{dV}{dt} = L_p ART (\sigma(C_s^i - C_s^e) + (C_i^i - C_i^e)) \quad \text{(Equation 1-1)}$$

$$\frac{dS}{dt} = P_s A \frac{(C_s^i - C_s^e)}{10^{15}} + (1 - \sigma) \frac{(C_s^i - C_s^e)}{2} \times \frac{\frac{dV}{dt}}{10^{15}}$$

$V$  is the cell volume ( $\mu\text{m}^3$ ),  $t$  is the time (min),  $L_p$  is the water permeability ( $\mu\text{m}/\text{min}/\text{atm}$ ),  $A$  is the cell surface area, either constant at a specified value or the area of a sphere with a volume of the cell ( $\mu\text{m}^2$ ),  $R$  is the gas constant (L-atm/mole/K),  $T$  is the absolute temperature (K),  $\sigma$  (sigma) is the reflection coefficient (dimensionless),  $C_s^i$ ,  $C_s^e$  are the intracellular, extracellular concentration of permeant solute (Moles),  $C_i^i$ ,  $C_i^e$  are the intracellular, extracellular concentration of impermeant solute (Moles),  $S$  is the number of solute molecules (Moles),  $P_s$  is the solute permeability ( $\mu\text{m}/\text{min}$ ), and  $10^{15}$  is the factor to convert from L to  $\mu\text{m}^3$ .

The Kedem and Katchalsky mathematical model (**KK**) is commonly used to analyze experiments and determine cell membrane permeability parameters (**Eq 1-2**). This approach involves three key parameters:  $L_p$ ,  $P_s$ , and a reflection coefficient ( $\sigma$ ), introduced to characterize flux interactions between water and solute. (150) The KK equation, while widely used, presents certain drawbacks, particularly regarding the complexity introduced by the parameter sigma, leading to frequent misunderstandings and misinterpretations among cryobiologists. Recent discoveries in molecular biologies, such as the identification of aquaporins, suggest that co-transport is often improbable in natural biological membranes, rendering sigma and the KK equation unnecessary. (153) Instead, a classic two-parameter (**2P**) equation (**Eq 1-3**) proves to be simpler and more appropriate in many cases, yielding comparable results to the KK equation when a common channel for solute and solvent is absent. (149) Simulation experiments demonstrate the equivalence of these equations in various scenarios, advocating for a simpler approach in cryobiological research. Additionally, when multiple transport pathways are present,

the 2P formalism provides a more economical and suitable description compared to the KK equation, especially when a phenomenological approach suffices to capture the complexity of transport phenomena. Through simulation techniques, it was demonstrated that both the 2P and KK formalisms yield similar results for  $L_p$  and  $P_s$  in the absence of cotransport channels. (153)

$$J_v = L_p \Delta p + \sigma \Delta \pi \quad \text{(Equation 1-2)}$$

$$J_s = P_s (\pi_2 - \pi_1)$$

$$J_v = L_p \Delta p \quad \text{(Equation 1-3)}$$

$$J_s = P_s (\pi_2 - \pi_1)$$

$J_v$  represents the volume flow of the solution,  $J_s$  represents the solute flux,  $\Delta p$  is the hydrostatic pressure difference,  $\Delta \pi$  is the osmotic pressure differences,  $\sigma$  is the reflection coefficient,  $L_p$  is the water permeability,  $P_s$  is the solute permeability, and  $\pi_1$  and  $\pi_2$  are the osmotic pressures on either side of the membrane.

Mazur et al. proposed two methods to estimate the permeability coefficient of glycerol ( $P$ ): one based on the time taken for cells to hemolysis in hyperosmotic glycerol solutions that were hypotonic compared to sodium chloride and the other based on the time taken for cells suspended in hyperosmotic glycerol solutions in isotonic saline to undergo osmotic shock when abruptly diluted with isotonic saline (Eq 1-4). (142) The equations derived by Mazur to estimate the  $P$  in human RBC are as follows:

$$V(t) = \frac{M_{iso} + 1000 p e(t) S(t)}{M_{de} + P_{se}} \quad \text{(Equation 1-4)}$$

$$S(t) = \frac{M_{de} V(t)}{1000}$$

$$P_{se} = \frac{ds/dt}{A(C_{se} - C_{si})}$$

$$V_d(t) = \frac{M_{iso}V_{iso}}{M_{de} + pe(t)S_e}$$

$$P_{se} = \frac{ds/dt}{A(C_{se} - C_{si})} + \frac{(1 - u)S_e dv/dt}{V_{iso}(C_{se} - C_{si})}$$

$V(t)$  is the volume of water in the cell at time  $t$ ,  $S(t)$  is the mole of solute in the cell at time  $t$ ,  $M_{iso}$  is the molality of non-permeating solutes in isotonic cells,  $pe(t)$  is the activity coefficient of external glycerol,  $S(t)$  is the relative volume of water in the cell at time  $t$ ,  $M_{de}$  is the osmolality of non-permeating salts in the external medium,  $A$  is the cell surface area,  $C_{se}$  and  $C_{si}$  are the external and internal concentration of solute, respectively,  $u$  is the reflection coefficient,  $V_{iso}$  is the relative volume of water in isotonic cells,  $M_d$  is the total osmolality of the external medium after dilution,  $ds/dt$  represents the rate of change of solute concentration inside the cell over time, and  $dV/dt$  is the rate of change of cell volume with time.

The KK equation, despite its comprehensive consideration of pressure gradients, introduces complexity due to the requirement of multiple parameters. Conversely, the Mazur equation offers simplicity but may lack precision in intricate scenarios. In contrast, the Jacob equation, by accurately addressing membrane thickness, emerges as a robust method for determining permeability constants. Its incorporation of membrane characteristics enhances its reliability in quantitatively assessing cell permeability. Moreover, the Jacob equation's ability to provide a universal measure adaptable to diverse experimental settings underscores its potential as a valuable tool in cellular permeability studies. These osmotic parameters can be used in mathematical modeling to predict an optimized cryopreservation protocol. CryoSim6 software was developed by Dr. Locksley McGann at the University of Alberta, Canada (154), uses the phase diagrams of extracellular and intracellular solutions, osmotic properties of the cell membrane, and their temperature dependencies to estimate changes in cell volume during cryopreservation. This information, in turn, is used to predict the probability of cell injury due to increased concentration of intra- and extracellular solutes and intracellular ice formation. (154–156) Karlsson et al. demonstrate it is possible to mathematically predict the proper procedure for CPA addition and removal, prevent excessive cell swelling or shrinking, and reduce CPA toxicity by minimizing exposure time to CPA. (157) Toxicity during CPA addition and removal

can also be mathematically modeled and minimized using the toxicity cost function, the approach recently reported by Benson et al. (158). Mathematical modeling is useful for optimizing complex problems such as cryoprotectant addition and removal, freezing rates, and avoiding toxicity. A key parameter required for these modeling approaches is cell membrane permeability. (159–162)

### **1.6 Variations in RBC Membrane Permeability: Implications for Cryopreservation Efficiency**

In North America, RBCs are preserved using a high glycerol-slow cooling method, with deglycerolization performed using ACP<sup>®</sup> 215, a process that takes about 45 minutes per RCC. (118) Recent efforts aimed at expediting deglycerolization through continuous glycerol removal and reducing deglycerolization time to less than a minute led to unexpected findings. (163–165) Membrane transport modeling designed for rapid glycerol removal from RBCs resulted in significantly higher hemolysis values than anticipated. (164) Lahmann et al. investigated the reasons behind this increased hemolysis by measuring glycerol permeability of the RBC membrane using a coulter counter, covering the full range of glycerol concentrations encountered during RBC cryopreservation. (139,166) They employed a refined mathematical optimization approach to account for concentration dependence and cell-to-cell variability in glycerol permeability, systematically examining the effects of assumed distribution in permeability values on the resulting optimized methods. (166) Lahmann et al. found that the permeability of the RBC membrane to glycerol varies from cell to cell within a single donor, and prolonged deglycerolization times were observed to reduce hemolysis, suggesting a subpopulation with lower glycerol permeability. (166) In a separate study, Jay and Rowlands analyzed erythrocyte permeability to various foreign substrates, particularly glycerol, and observed a wide variation in the permeability coefficient to glycerol among erythrocytes, following a Gaussian distribution. (167) The analysis revealed a correlation between swelling time, stress time, and hemolysis time, providing insights into erythrocyte permeability and its distribution within populations. These studies contribute valuable insights into the mechanisms underlying osmotic hemolysis and erythrocyte membrane permeability, enhancing our understanding of cell biology and transport phenomena. (167)

The permeability of RBC membranes varies widely at the individual and cell-to-cell levels. (166) Donor-specific traits, including age, sex, and ethnicity, influence the osmotic characteristics of RBCs, with older blood donors exhibiting higher water permeability in RBCs. (168) Besides donor factors and subpopulation of RBCs, manufacturing methods can also impact the osmotic characteristics of RBCs. Alshalani et al. found that units processed using a WBF manufacturing method exhibited significantly higher membrane water permeability throughout storage compared to units manufactured using the RCF method. Units prepared by the WBF method exhibited higher hemolysis and supernatant  $K^+$  compared to those processed by the RCF method, emphasizing the impact of the manufacturing process on membrane-related lesions. (95,102) Additionally, hypothermic storage significantly increased RBC membrane permeability, hemolysis, supernatant  $K^+$ , and reduced deformability, indicating membrane degradation. (168) Collectively, these findings, along with freeze-thaw-wash recovery of  $85.2 \pm 5.9\%$ , suggest that osmotically fragile RBCs, particularly older ones, may be more susceptible to loss during the osmotic stress induced by cryopreservation, highlighting the imperative consideration of RBC characteristics in optimizing cryopreservation protocols. The hypothesis posits that variations in osmotic characteristics, including water and solute permeability and deformability parameters in O-RBCs, contribute to their loss during cryopreservation using the high glycerol-slow cooling method.

### **1.7 Challenges and Techniques in Measuring Red Blood Cell Volume Changes: Stopped-Flow Spectroscopy Approaches**

It is critical to know cell osmotic parameters, including membrane permeability to water and solute, to design effective cryopreservation procedures for cells and tissues and avoid osmotic and freezing injury. (153,169,170) In this intricate process, the cell membrane emerges as a pivotal player by regulating the balance of water and solutes between the cell's interior and the extracellular milieu. The membrane function becomes critical during freezing when osmotic changes can jeopardize cell integrity. To determine cell membrane permeability, one needs to measure the rate of cell volume changes when placed in an anisotonic environment. (171)

The quick response of RBCs to anisotonic conditions poses challenges, particularly in accurately measuring their volume changes in response to osmotic stress. (172) Traditional

methods, such as electronic particle counters, employ electrical impedance to count and size suspended particles in a conductive liquid. The device works by aspirating a cell suspension through a glass tube with a small pore, measuring the voltage drop caused by each cell passing through. (173) By adjusting device settings, different cell sizes can be counted, and frequency distribution curves can be plotted to study variations in cell volume. The instrument is calibrated using artificial beads to establish a relationship between threshold units and cell volume. (173) As RBCs swell or shrink in response to osmotic changes, their size can be detected and quantified by the coulter counter. However, this method is less effective due to the speed of volume change in RBCs in response to anisotonic conditions. (174) In recent decades, flow cytometry has advanced significantly, with biological staining commonly used for imaging during the process to trace cell volume and morphology indexes. (175) However, staining can alter cell physiology, and conventional imaging often produces two-dimensional results, posing challenges for accurate volume measurements. (176,177) Interferometric phase microscopy (**IPM**) offers a solution by measuring cell parameters without staining but faces difficulties in decoupling cell refractive index (**RI**) and thickness. (178–180) Turko et al. introduce an improved three-wavelength IPM system for quantitative imaging spectroscopy during flow cytometry. The system accurately measures RBC parameters using a non-linear equation, which offers potential applications in biomedical research. (181) Another common approach in measuring cell volume is microfluidic systems, where RBCs are introduced into channels or chambers with precise dimensions under controlled flow rates and pressure gradients. As RBCs pass through the channels, their dimensions and behavior can be observed and analyzed using various techniques, such as microscopy or impedance sensing. (182–184) Microfluidic systems pose challenges due to their requirement for specialized equipment and expertise in the design, fabrication, operation, and handling of samples, especially when dealing with small volumes or complex biological samples. Consequently, researchers often turn to a technique called stopped-flow spectroscopy to assess RBC osmotic permeability. Stopped-flow spectroscopy can quantify rapid changes in RBC volume over time and is commonly used to measure RBC osmotic permeability. (172,185) By mixing RBCs with solutions of different osmolarities and monitoring changes in light absorbance or fluorescence intensity, the kinetics of volume changes can be analyzed. Two stopped-flow approaches are commonly used: light scattering and self-quenching of a fluorescent dye. (186)

Scattering experiments involve measuring changes in light scattering intensity when cells experience volume changes due to exposure to osmotic gradients. (187) The method relies on the principle that scattered light intensity is proportional to the size and refractive index of the scattering particles. Cells are typically exposed to osmotic gradients in a stopped-flow apparatus, and the resulting change in cell volume is monitored by measuring scattered light intensity at a specific wavelength. Time-dependent changes in scattering intensity are recorded and analyzed to extract information about cell volume changes. (186,187) However, scattering experiments may lack detailed insights into internal cell dynamics, and interpreting data requires careful consideration of factors like cell size distribution and refractive index. Fluorescence self-quenching experiments utilize changes in the fluorescence intensity of a fluorescent dye contained within cells to measure volume changes. (185) Cells are loaded with a fluorescent dye like carboxyfluorescein (CF), which undergoes self-quenching at high concentrations. (186,188) As cells experience volume changes in response to osmotic gradients, the fluorescence intensity of the dye alters accordingly. Fluorescence intensity is monitored over time, and mathematical models are utilized to analyze the data and extract parameters, such as changes in cell volume and water permeability. The direct correlation between fluorescence intensity and cell volume offers sensitive and precise measurements suitable for studying individual cells or small populations. (187,189) However, calibration and considerations of factors like choice of fluorescent dye and dye leakage are crucial for accurate results. Specifically, in the context of RBCs, the autofluorescent properties of Hb and its self-quenching characteristics can be utilized to effectively measure volume changes in RBCs when exposed to anisotonic gradients. (107,168,174) Zhurova et al. developed a method to capture rapid changes in RBC volume in response to anisotonic solutions, using changes in intrinsic hemoglobin fluorescence intensity. This method does not require the addition of any fluorescent dye and overcomes the limitations of the traditionally used methods. (107)

### **1-8 Biotinylation of RBCs**

Several techniques have been developed and utilized over the past century to assess the recovery of RBCs post-transfusion. Among these methods, radioactive labeling with isotopes such as chromium-51 ( $^{51}\text{Cr}$ ) and biotinylation have emerged as prominent approaches. Each method offers unique strengths and weaknesses, influencing its applicability and accuracy in

assessing transfusion recovery. One of the main limitations of using  $^{51}\text{Cr}$  for assessing RBC kinetics is radiation exposure. Additionally, this method doesn't allow the concurrent investigation of multiple populations of RBCs within a single individual. In contrast, biotinylation involves using sulfo-NHS-LC-Biotin, a water-soluble and membrane-impermeable reagent that binds permanently to proteins on the RBC surface. The NHS group of biotin reacts with amine groups on the outer leaflet of the RBC membrane and forms stable amide bonds, which can be detected by combination with fluorochrome. (190,191) This method offers several advantages, including the ability to track multiple RBC populations simultaneously within the same individual. Biotinylation eliminates the risk of radiation exposure and enhances the suitability of this approach for studying RBC kinetics in various populations, including fetuses, infants, children, and pregnant women. (192–194) Back et al. introduced the standardized biotinylation protocol, which provides a safe, reliable, and efficient method for labeling RBCs, making it suitable for clinical research purposes. (190,194) Biotinylated RBCs accurately reflect RBC survival when detected by flow cytometry, showing a close correlation with corrected  $^{51}\text{Cr}$ -based measurements. The biotin-based method is a safe and effective alternative to the traditional radioactive method for measuring RBC survival. (195)

### **1.9 Gamma Irradiation of Red Blood Cells: Standard Practice and Global Guidelines**

Gamma irradiation of RCCs is used to prevent transfusion-associated graft versus host disease (**TA-GVHD**), a rare but usually fatal complication in recipients at risk. TA-GVHD occurs when viable donor T-lymphocytes proliferate and engraft in susceptible recipients after transfusion. TA-GVHD results in significant morbidity and mortality in approximately 80 to 90 % of affected individuals. Gamma irradiation prevents DNA replication in the white blood cells (**WBCs**) that may be present in RCCs. (196) Irradiation of leukoreduced RCCs is the standard care for patients at risk of GVHD, including immune deficient individuals, intrauterine transfusions, and allogeneic stem cell recipients. (197) There are divergent guidelines from global health bodies regarding irradiation practices. The Association for the Advancement of Blood & Biotherapies (**AABB**) and the Canadian Standards Association (**CSA**) have suggested that irradiation can be performed at any time during storage (up to day 42), irradiated RBCs can be stored for up to 28 days not exceeding the original expiry date, and required a minimum dose of 25 grays (**Gy**) to the midpoint of the component and 15 Gy to the entire component. (198,199) The Council of Europe guidelines have

advised that RBCs may be irradiated up to 28 days after collection but must be transfused as soon as possible and no later than 14 days post-irradiation and no later than 28 days after collection.

(200) This is very much distinct from the British Committee for Standards, stating that RBCs may be irradiated at any time up to 14 days after collection and may be stored for an additional 14 days.

(201)

### **1.9.1 Impact of Irradiation on Red Blood Cell Storage Lesion and Membrane Integrity: Mechanisms and Consequences**

Irradiation through different mechanisms accelerates the RBC storage lesion (202), causing biochemical changes and altering RBC metabolism. (203) Radiation induces oxidative stress in RBCs by generating reactive oxygen species (**ROS**) through the ionization of water molecules, producing superoxide radicals ( $O_2^{\bullet-}$ ) and hydroxyl radicals ( $\bullet OH$ ). These highly reactive species can damage various cellular components, including proteins, lipids, and nucleic acids. Byproducts of lipid peroxidation, such as thiobarbituric acid reactive substances (**TBARS**) and malondialdehyde (**MDA**), serve as biomarkers for assessing oxidative stress. They can also compromise membrane integrity, leading to structural and functional alterations in RBCs. (204,205) Radiation-induced oxidative stress affects the metabolomics of RBCs by targeting enzymes involved in glycolysis and the Krebs cycle, disrupting ATP production. Consequently, ATP levels decrease in irradiated RBCs during hypothermic storage, increasing the susceptibility of gamma-irradiated RBCs to hemolysis. The impaired metabolomics system of RBCs directly and indirectly affects its homeostasis by disrupting the function of ion transporters and channels that rely on ATP, such as  $Ca^{2+}$ -ATPase and  $Na^+/K^+$  pump. (206–209) The  $Na^+/K^+$  pump is a pivotal player in maintaining the electrochemical gradient across the RBC membrane by actively pumping  $Na^+$  out of the cell and  $K^+$  into the cell. (210) The  $Ca^{2+}$ -ATPase pump maintains intracellular  $Ca^{2+}$  concentration by actively transporting  $Ca^{2+}$  out of the cell. (211) These pumps and channels help regulate cell volume, membrane integrity, and signal transduction (212), and any disruption in their function can lead to changes in intracellular ion concentrations. (206–209) The impaired function of  $Ca^{2+}$ -ATPase and  $Na^+/K^+$  pump resulting in the accumulation of  $Ca^{2+}$  in RBC cytoplasm and impaired ability of RBC to uptake  $K^+$ . Elevated levels of cytosolic  $Ca^{2+}$  in RBCs prompt the formation of cell membrane microvesicles and activate phospholipid scramblase as well as calcium-sensitive  $K^+$  channels. Activation of these channels and impaired function of the  $Na^+/K^+$  pump in

reuptaking the  $K^+$  leads to  $K^+$  efflux, cell shrinkage, and increased supernatant  $K^+$ . (213,214) Irradiation also disrupts the integrity of RBC membranes and associated proteins, leading to the release of Hb and lactate dehydrogenase (**LDH**), which accelerates aging processes. (215–218) This ultimately reduces the function and viability of RBCs post-transfusion. (217,219–222) This considerable rise in  $K^+$  levels and hemolysis increases the risk of post-transfusion hyperkalemia and subsequent cardiac complications, particularly in neonates or patients undergoing massive transfusions. (218,220,223,224) The increase in supernatant  $K^+$  and hemolysis levels becomes more pronounced with extended post-irradiation storage duration. (224–226)

Additionally, donor sex and age have been demonstrated to impact radiation-induced lesions on RBCs, with female donors exhibiting lower levels of hemolysis and potassium both before and after gamma irradiation. (3,90,227) Previous studies have consistently reported this phenomenon, noting that stored RBC units from female donors, particularly young females, demonstrate greater resistance to mechanical and oxidative stress. (227,228) This resistance may be attributed to the presence of a higher proportion of Y-RBCs with better antioxidant defense mechanisms in RCCs from premenopausal female donors due to their monthly blood loss. (229) Further investigation into the impact of donor characteristics on irradiation is warranted.

## **1.10 Conclusion**

In conclusion, the comprehensive review of osmotic parameters, glycerol transport variability, and the impact of gamma irradiation and manufacturing method on RBCs reveals significant insights into optimizing cryopreservation and irradiation practices, as well as producing RBCs with favorable Y- to O-RBC ratios. Understanding the distribution of RBC subpopulations, their susceptibility to cryopreservation-induced stress, and the consequences of gamma irradiation on their integrity is crucial for enhancing transfusion efficiency and minimizing post-transfusion complications. By considering factors such as donor characteristics, manufacturing methods, cryopreservation protocols, and irradiation, our goal is to develop strategies that sustain and maintain the quality of RBC products, ultimately leading to improved transfusion outcomes.

## 1.11 Rationale

### 1.11.1 Clinical Relevance

The effectiveness of RCCs in transfusion medicine is subject to various factors, including but not limited to storage duration, manufacturing techniques, donor-related variables, and the proportion of different RBC subpopulations within the RCC. Different studies revealed that transfusion of RCCs containing predominantly Y-RBCs prolongs post-transfusion survival, and the higher presence of O-RBCs within the RCCs is associated with a higher level of hemolysis, accumulation of side products of aging, and impaired oxygen delivery post-transfusion due to a rapid clearance of O-RBCs by the spleen. (27,62,230,231) Additionally, Piomelli et al. demonstrated that the post-transfusion survival of Y-RBCs is significantly greater than the O-RBCs using a  $^{51}\text{Cr}$ -labeling method in a rabbit model. (63) These results align with Triadou et al. findings, demonstrating that the post-transfusion survival of  $^{51}\text{Cr}$ -labeled Y-RBCs obtained from 60 human donors was markedly higher than that of unseparated  $^{51}\text{Cr}$ -labeled RBCs after reinfusion into two splenectomized patients. (230) Cohen et al. illustrate a decrease in the average transfusion requirement to sustain hemoglobin levels among splenectomized thalassemia patients who exclusively receive Y-RBCs compared to those who are administered conventional RCC units. (62) Hence, assessing the effectiveness of RCCs necessitates determining the proportions of Y- and O-RBCs within them, as a higher presence of O-RBCs can lead to RCC quality degradation. (231)

This study investigated the impact of pre-storage processing methods used in transfusion medicine, including component manufacturing methods, cryopreservation, and irradiation, on the distribution of RBC subpopulations. The setup and processing steps involved in blood component collection, such as filtration, centrifugation, and extraction, result in the isolation of different subpopulations of RBC. We postulate that during the buffy coat removal step, the top layer of RBCs, which contains Y-RBCs with lower density, may be lost. (97–99) While in the WBF method, a small volume of O-RBCs with a higher density is left at the bottom of the collection bag. (97) We hypothesize that RCCs generated through the WBF method may exhibit a higher ratio of Y- to O-RBCs compared to RCCs produced through the RCF method. This study can provide insights into optimizing processing methods, leading to the production of RCCs with a favorable proportion of Y-RBCs. This optimization may prolong the post-transfusion survival of RBCs, enhance transfusion efficiency, and mitigate the side effects of

RBC aging, including impaired oxygen delivery. (27) Furthermore, the literature suggests that variations in osmotic characteristics, including water and solute permeability parameters of RBCs, contribute to RBC loss during cryopreservation. Understanding the distribution of RBC subpopulations within RCC units can offer valuable insights for enhancing cryopreservation efficiency. By targeting RCCs with a favorable ratio of Y- to O-RBCs, we can potentially improve the recovery rate of RBCs after deglycerolization. This strategic approach not only optimizes cryopreservation protocols to suit the composition of RBC subpopulations but also allows for more rapid deglycerolization steps by reducing variability in the distribution of biologically aged RBC subpopulations. The deglycerolization process can be streamlined by minimizing variability, ensuring consistency and efficiency in RBC recovery. This optimization endeavor aims to enhance overall preservation efficiency, thereby facilitating the availability of high-quality RBC products for transfusion purposes. Finally, this thesis aimed to investigate the susceptibility of Y-RBCs and O-RBCs to destruction following gamma irradiation, focusing on hemolysis, supernatant  $K^+$ , p50, and oxidative hemolysis in irradiated RBC subpopulations. The RBC aging process is characterized by a reduction in the metabolic activity of RBCs and a diminished capacity of O-RBCs to maintain cellular homeostasis and antioxidant defenses. Consequently, the metabolic pathways involved in the synthesis and regeneration of ATP and 2,3-DPG become less efficient in O-RBCs. This decrease in 2,3-DPG levels results in impaired oxygen delivery post-transfusion. (27,230) The observed increase in hemolysis and supernatant  $K^+$  levels in irradiated RCCs poses risks of post-transfusion complications, especially in vulnerable patient populations. (218,220,223,224) It is postulated that the compromised membrane and antioxidant defense mechanisms of O-RBCs significantly contribute to the observed increase in hemolysis, supernatant  $K^+$  levels, and impaired oxygen delivery during storage.

### **1.12 Hypothesis and Objectives**

Blood component manufacturing will affect the distribution of Y- and O-RBCs in stored RCCs, with units containing a higher proportion of O-RBCs being more susceptible to product quality degradation following cryopreservation and gamma irradiation.

The research objectives of the proposed project are the following:

- 1. Determine the Impact of the Blood Component Manufacturing Method on the Proportion of the Y- and O-RBCs in Stored RCCs:** In Chapter 2, we investigated the influence of blood component manufacturing methods, specifically WBF and RCF processes, on the relative proportions of Y- and O-RBCs within stored RCCs. Utilizing whole blood units obtained from the Canadian Blood Services' Blood4Research program and a split study design where units were subjected to different processing procedures. The Percoll<sup>®</sup> separation method was employed to calculate the EMD and assess the distribution of RBCs. The primary objective was to determine whether RCCs produced via the WBF method exhibit a higher ratio of Y- to O-RBCs compared to those produced via the RCF method from the same donor. This research aimed to provide a comprehensive understanding of how various manufacturing methods impact the age distribution of RBCs in stored RCCs.
- 2. Compare Osmotic Parameters and Evaluate Recovery Post-Deglycerolization in Y- and O-RBC Subpopulations:** In Chapter 3, we evaluated the osmotic properties of Y- and O-RBC subpopulations to explore variations in  $L_p$ ,  $V_b$ ,  $E_a$ ,  $P_s$ ,  $O_{\text{hyper}}$ , and  $EI_{\text{max}}$  which could affect the survival of RBCs after deglycerolization. By examining how these RBC subpopulations respond to osmotic and freezing stresses relevant to cryopreservation, this study aimed to gain insights into optimizing cryopreservation strategies, considering the distinct characteristics of Y- and O-RBCs. It was expected that O-RBCs would exhibit elevated  $L_p$  and  $P_s$  values, as well as higher  $E_a$ , owing to their compromised membrane function. Additionally, O-RBCs were expected to have a higher  $V_b$ , potentially due to the increased concentration of Hb and greater loss of water during aging. The recovery of spiked Y- and O-BioRBCs were measured following the RCC deglycerolization process. Y-BioRBCs were expected to exhibit higher post-deglycerolization recovery compared to O-BioRBCs. This insight offers the opportunity to enhance recovery rates of RBCs in the cryopreservation process by ensuring the presence of a desirable ratio of Y- to O-RBCs.
- 3. Compare Oxidative Stress, p50, and Supernatant K<sup>+</sup> in Y- and O-RBC Subpopulations Post-Irradiation and Evaluate Recovery of Y- and O-BioRBCs during Hypothermic Storage Post-Irradiation:** Chapter 4 compared the responses of Y- and O-RBC subpopulations to gamma irradiation, focusing on supernatant K<sup>+</sup>

concentration, oxidative hemolysis, and O<sub>2</sub> affinity. Measurements were taken before irradiation, immediately after irradiation, and on days 7 and 14 post-irradiation during hypertonic storage. The findings contribute to optimizing irradiation strategies, considering the distinct characteristics of Y- and O-RBC subpopulations. It was anticipated that O-RBCs would display elevated supernatant K<sup>+</sup> levels and increased hemolysis due to compromised membrane function. Additionally, O-RBCs were expected to exhibit higher O<sub>2</sub> affinity, linked to decreased 2,3-DPG concentration and increased methemoglobin post-irradiation. The recovery of Y- and O-BioRBCs was assessed following irradiation in RCC units. Y-RBCs were expected to demonstrate higher post-irradiation recovery rates compared to O-RBCs. By evaluating the recovery of these distinct RBC subpopulations, our goal was to investigate the possible relationship between these subpopulations and their recovery post-irradiation. It was anticipated that O-RBCs would experience more rapid loss after irradiation than Y-RBCs.

## 1.13 References

1. Ramirez-Arcos S, Marks DC, Acker JP, Sheffield WP. Quality and Safety of Blood Products. *Journal of Blood Transfusion*. 2016;2016:2482157.
2. Tzounakas VL, Georgatzakou HT, Kriebardis AG, Voulgaridou AI, Stamoulis KE, Foudoulaki-Paparizos LE, et al. Donor variation effect on red blood cell storage lesion: A multivariable, yet consistent, story. *Transfusion (Paris)*. 2016;56(6):1274–86.
3. Jordan A, Chen D, Yi QL, Kanias T, Gladwin MT, Acker JP. Assessing the influence of component processing and donor characteristics on quality of red cell concentrates using quality control data. *Vox Sang*. 2016;111(1):8–15.
4. Dumaswala UJ, Dumaswala RU, Levin DS, Greenwalt TJ. Improved red blood cell preservation correlates with decreased loss of bands 3, 4.1, acetylcholinesterase, and lipids in microvesicles. *Blood*. 1996;87(4):1612–6.
5. Turner TR, Lautner L, Hill A, Howell A, Skeate R, Acker JP. Evaluating the quality of red blood cell concentrates irradiated before or after cryopreservation. *Transfusion (Paris)*. 2020;60(1):26–9.
6. Mollison PL. The introduction of citrate as an anticoagulant for transfusion and of glucose as a red cell preservative. *British Journal of Haematology*. 2000;108(1):13–8.
7. Bratosin D, Leszczynski S, Sartiaux C, Fontaine O, Descamps J, Huart JJ, et al. Improved storage of erythrocytes by prior leukodepletion: Flow cytometric evaluation of stored erythrocytes. *Communications in Clinical Cytometry*. 2001;46(6):351–6.
8. Wang D, Sun J, Solomon SB, Klein HG, Natanson C. Transfusion of older stored blood and risk of death: A meta-analysis. *Transfusion (Paris)*. 2012;52(6):1184–95.
9. Hod EA, Spitalnik SL. Harmful effects of transfusion of older stored red blood cells: Iron and inflammation. *Transfusion (Paris)*. 2011;51(4):881–5.
10. Lannan KL, Sahler J, Spinelli SL, Phipps RP, Blumberg N. Transfusion immunomodulation - the case for leukoreduced and (perhaps) washed transfusions. *Blood Cells, Molecules, and Diseases [Internet]*. 2013;50(1):61–8.
11. Heddle NM, Arnold DM, Acker JP, Liu Y, Barty RL, Eikelboom JW, et al. Red blood cell processing methods and in-hospital mortality: A transfusion registry cohort study. *Lancet haematology*. 2016;3(5):e246–54.
12. Bakkour S, Acker JP, Chafets DM, Inglis HC, Norris PJ, Lee TH, et al. Manufacturing method affects mitochondrial DNA release and extracellular vesicle composition in stored red blood cells. *Vox Sang*. 2016;111(1):22–32.

13. D'Alessandro A, Blasi B, D'Amici GM, Marrocco C, Zolla L. Red blood cell subpopulations in freshly drawn blood: Application of proteomics and metabolomics to a decades-long biological issue. *Blood Transfusion*. 2013;11(1):75–87.
14. Bosman GJCGM, Werre JM, Willekens FLA, Novotný VMJ. Erythrocyte ageing in vivo and in vitro: Structural aspects and implications for transfusion. *Transfusion Medicine*. 2008;18(6):335–47.
15. Almizraq RJ, Seghatchian J, Acker JP. Extracellular vesicles in transfusion-related immunomodulation and the role of blood component manufacturing. *Transfusion and Apheresis Science*. 2016;55(3):281–91.
16. Weisel JW, Litvinov RI. Red blood cells: the forgotten player in hemostasis and thrombosis. *Journal of Thrombosis and Haemostasis*. 2019;17(2):271–82.
17. Bosman GJCGM, Lasonder E, Groenen-Döpp YAM, Willekens FLA, Werre JM, Novotný VMJ. Comparative proteomics of erythrocyte aging in vivo and in vitro. *Journal of Proteomics*. 2010;73(3):396–402.
18. D'Alessandro A, D'Amici GM, Vaglio S, Zolla L. Time-course investigation of sagm-stored leukocyte-filtered red blood cell concentrates: From metabolism to proteomics. *Haematologica*. 2012;97(1):107–15.
19. Malka R, Delgado FF, Manalis SR, Higgins JM. In vivo volume and hemoglobin dynamics of human red blood cells. *PLoS Computational Biology*. 2014 Oct 9;10(10):e1003839.
20. Kameneva M V., Garrett KO, Watach MJ, Borovetz HS. Red blood cell aging and risk of cardiovascular diseases. *Clinical Hemorheology and Microcirculation*. 1998;18(1):67–74.
21. Blasi B, D'Alessandro A, Ramundo N, Zolla L. Red blood cell storage and cell morphology. *Transfusion Medicine*. 2012;22(2):90–6.
22. Simak J, Gelderman MP. Cell membrane microparticles in blood and blood products: potentially pathogenic agents and diagnostic markers. *Transfusion Medicine Reviews*. 2006 Jan;20(1):1-26.
23. Nash GB, Meiselman HJ. Red cell and ghost viscoelasticity. Effects of hemoglobin concentration and in vivo aging. *Biophysical Journal*. 1983;43(1):63–73.
24. Bocci V. Determinants Of Erythr Ocyte Ageing: A Reappraisal. *British Journal of Haematology*. 1981;48(4):515–22.
25. Linderkamp O, Meiselman HJ. Geometric, osmotic, and membrane mechanical properties of density-separated human red cells. *Blood*. 1982 Jun;59(6):1121-7.

26. Sutura SP, Gardner RA, Boylan CW, Carroll GL, Chang KC, Marvel JS, Kilo C, Gonen B, Williamson JR. Age-related changes in deformability of human erythrocytes. *Blood*. 1985 Feb;65(2):275-82.
27. Mykhailova O, Olafson C, Turner TR, D'Alessandro A, Acker JP. Donor-dependent aging of young and old red blood cell subpopulations: Metabolic and functional heterogeneity. *Transfusion (Paris)*. 2020;60(11):2633–46.
28. Kiefer CR, Snyder LM. Oxidation and erythrocyte senescence. *Current Opinion in Hematology*. 2000 Mar;7(2):113-6.
29. Kay MMB, Goodman SR, Sorensen K, Whitfield CF, Wong P, Zaki L, et al. Senescent cell antigen is immunologically related to band 3. *Proceedings of the National Academy of Sciences of the United States of America*. 1983;80(6 D):1631–5.
30. Lutz HU, Stammer P, Fasler S. Preferential formation of C3b-IgG complexes in vitro and in vivo from nascent C3b and naturally occurring anti-band 3 antibodies. *Journal of Biological Chemistry*. 1993;268(23):17418–26.
31. Khandelwal S, Saxena RK. A role of phosphatidylserine externalization in clearance of erythrocytes exposed to stress but not in eliminating aging populations of erythrocyte in mice. *Experimental Gerontology*. 2008;43(8):764–70.
32. Willekens FLA, Roerdinkholder-Stoelwinder B, Groenen-Döpp YAM, Bos HJ, Bosman GJCGM, van den Bos AG, et al. Hemoglobin loss from erythrocytes in vivo results from spleen-facilitated vesiculation. *Blood*. 2003;101(2):747–51.
33. Pionelli S, Seaman C. Mechanism of red blood cell aging: Relationship of cell density and cell age. *American Journal of Hematology*. 1993;42(1):46–52.
34. Bosch FH, Werre JM, Roerdinkholder-Stoelwinder B, Huls TH, Willekens FLA, Halie MR. Characteristics of red blood cell populations fractionated with a combination of counterflow centrifugation and Percoll separation. *Blood*. 1992;79(1):254–60.
35. Mueller TJ, Jackson CW, Dockter ME, Morrison M. Membrane skeletal alterations during in vivo mouse red cell aging. Increase in the band 4.1a:4.1b ratio. *Journal of Clinical Investigation*. 1987;79(2):492–9.
36. Lutz HU, Stammer P, Fasler S, Ingold M, Fehr J. Density separation of human red blood cells on self forming Percoll gradients: correlation with cell age. *Biochimica et Biophysica Acta*. 1992 Mar 5;1116(1):1-10.
37. Rettig MP, Low Philip S. PS, Gimm JA, Mohandas N, Wang J, Christian JA. Evaluation of biochemical changes during in vivo erythrocyte senescence in the dog. *Blood*. 1999;93(1):376–84.
38. Ando K, Beppu M, Kikugawa K, Nagai R, Horiuchi S. Membrane proteins of human erythrocytes are modified by advanced glycation end products during aging in the

- circulation. *Biochemical and Biophysical Research Communications*. 1999 Apr 29;258(1):123-7.
39. I Chin-Yee, N Arya MS d'Almeida. The red cell storage lesion and its implication for transfusion. *Transfusion Science*. 1997 Sep;18(3):447–58.
  40. Holovati JL, Wong KA, Webster JM, Acker JP. The effects of cryopreservation on red blood cell microvesiculation, phosphatidylserine externalization, and CD47 expression. *Transfusion (Paris)*. 2008 Aug;48(8):1658–68.
  41. Stadnick H, Onell R, Acker JP, Holovati JL. Eadie-Hofstee analysis of red blood cell deformability. *Clinical Hemorheology and Microcirculation*. 2011;47(3):229–39.
  42. Anniss AM, Sparrow RL. Expression of CD47 (integrin-associated protein) decreases on red blood cells during storage. *Transfusion and Apheresis Science*. 2002 Dec;27(3):233-8.
  43. Paolo Arese, Franco Turrini, Evelin Schwarzer. Band 3/complement-mediated recognition and removal of normally senescent and pathological human erythrocytes. *Cellular Physiology and Biochemistry*. 2005;16(4–6):133–46.
  44. Lutz HU. Naturally occurring anti-band 3 antibodies in clearance of senescent and oxidatively stressed human red blood cells. *Transfusion Medicine and Hemotherapy*. 2012 Oct;39(5):321-7.
  45. Lutz HU, Bogdanova A. Mechanisms tagging senescent red blood cells for clearance in healthy humans. *Frontiers in Physiology*. 2013 Dec 25;4:387.
  46. González Flecha, F., Castello, P., Gagliardino, J. et al. Molecular Characterization of the Glycated Plasma Membrane Calcium Pump. *The Journal of Membrane Biology*. 171, 25–34 (1999).
  47. Keller MA, Piedrafita G, Ralser M. The widespread role of non-enzymatic reactions in cellular metabolism. *Current Opinion in Biotechnology*. 2015 Aug;34:153-61.
  48. Piedrafita G, Keller MA, Ralser M. The Impact of Non-Enzymatic Reactions and Enzyme Promiscuity on Cellular Metabolism during (Oxidative) Stress Conditions. *Biomolecules*. 2015 Sep 10;5(3):2101-22.
  49. Lew VL, Tiffert T. On the Mechanism of Human Red Blood Cell Longevity: Roles of Calcium, the Sodium Pump, PIEZO1, and Gardos Channels. *Frontiers in Physiology*. 2017 Dec 12;8:977.
  50. Hess JR. Red cell storage. *Journal of Proteomics*. 2010 Jan 3;73(3):368-73.
  51. Snyder LM, Garver F, Liu SC, Leb L, Trainor J, Fortier NL. Demonstration of haemoglobin associated with isolated, purified spectrin from senescent human red cells. *British Journal of Haematology*. 1985;61(3):415–9.

52. Snyder LM, Fortier NL, Trainor J, Jacobs J, Leb L, Lubin B, et al. Effect of hydrogen peroxide exposure on normal human erythrocyte deformability, morphology, surface characteristics, and spectrin-hemoglobin cross-linking. *Journal of Clinical Investigation*. 1985;76(5):1971–7.
53. Snyder LM, Leb L, Piotrowski J, Sauberman N, Liu SC, Fortier NL. Irreversible spectrin-haemoglobin crosslinking in vivo: a marker for red cell senescence. *British Journal of Haematology*. 1983 Mar;53(3):379-84.
54. Samaja M, Rubinacci A, Motterlini R, de Ponti A, Portinaro N. Red cell aging and active calcium transport. *Experimental Gerontology*. 1990;25(3–4):279–86.
55. Giel J.C. G.M. Bosman FLAW and JMW. Erythrocyte aging- a more than superficial.pdf. *Cellular Physiology and Biochemistry*. 2005;16:1–8.
56. Lee TH, Kim SU, Yu SL, Kim SH, Park DS, Moon HB, Dho SH, Kwon KS, Kwon HJ, Han YH, Jeong S, Kang SW, Shin HS, Lee KK, Rhee SG, Yu DY. Peroxiredoxin II is essential for sustaining life span of erythrocytes in mice. *Blood*. 2003 Jun 15;101(12):5033-8.
57. Nagababu E, Chrest FJ, Rifkind JM. Hydrogen-peroxide-induced heme degradation in red blood cells: the protective roles of catalase and glutathione peroxidase. *Biochimica et Biophysica Acta*. 2003 Mar 17;1620(1-3):211-7.
58. Gonzales R, Auclair C, Voisin E, Gautero H, Dhermy D, Boivin P. Superoxide dismutase, catalase, and glutathione peroxidase in red blood cells from patients with malignant diseases. *Cancer Research*. 1984 Sep;44(9):4137-9.
59. Oski FA. The unique fetal red cell and its function. E. Mead Johnson Award address. *Pediatrics*. 1973 Mar;51(3):494-500.
60. Högman CF, Löf H, Meryman HT. Storage of red blood cells with improved maintenance of 2,3-bisphosphoglycerate. *Transfusion (Paris)*. 2006 Sep;46(9):1543–52.
61. Orbach A, Zelig O, Yedgar S, Barshtein G. Biophysical and Biochemical Markers of Red Blood Cell Fragility. *Transfusion Medicine and Hemotherapy*. 2017;44(3):183–7.
62. Cohen AR, Schmidt JM, Martin MB, Barnsley W, Schwartz E. Clinical trial of young red cell transfusions. *The Journal of Pediatrics*. 1984;104(6):865–8.
63. Piomelli S, Seaman C, Reibman J, Tytun A, Graziano J, Tabachnik N, et al. Separation of younger red cells with improved survival in vivo: an approach to chronic transfusion therapy. *Proceedings of the National Academy of Sciences of the United States of America*. 1978;75(7):3474–8.
64. Key Ja. Studies On Erythrocytes, With Special Reference To Reticulum, Polychromatophilia And Mitochondria. *Arch Intern Med (Chic)*. 1921;28(5):511–549.

65. Hogan VA, Blanchette VS, Rock G. A simple method for preparing neocyte-enriched leukocyte-poor blood for transfusion-dependent patients. *Transfusion (Paris)*. 1986;26(3):253–7.
66. Bosch FH, Werre JM, Roerdinkholder-Stoelwinder B, Huls TH, Willekens FL, Halie MR. Characteristics of red blood cell populations fractionated with a combination of counterflow centrifugation and Percoll separation. *Blood*. 1992 Jan 1;79(1):254-60.
67. An, X., Chen, L. (2018). Flow Cytometry (FCM) Analysis and Fluorescence-Activated Cell Sorting (FACS) of Erythroid Cells. In: Lloyd, J. (eds) *Erythropoiesis. Methods in Molecular Biology*, vol 1698. Humana Press, New York, NY.
68. Abramsson-Zetterberg L, Carlsson R, Sand S. The use of immunomagnetic separation of erythrocytes in the in vivo flow cytometer-based micronucleus assay. *Genetic Toxicology and Environmental Mutagenesis*. 2013;752(1–2):8–13.
69. Owen CS, Sykes NL. Magnetic labeling and cell sorting. *J Immunol Methods*. 1984 Oct 12;73(1):41-8.
70. Maria, M.S., Chandra, T.S. & Sen, A.K. Capillary flow-driven blood plasma separation and on-chip analyte detection in microfluidic devices. *Microfluid Nanofluid* 21, 72 (2017).
71. Torres-Castro K, Acuña-Umaña K, Lesser-Rojas L, Reyes DR. Microfluidic Blood Separation: Key Technologies and Critical Figures of Merit. *Micromachines (Basel)*. 2023 Nov 18;14(11):2117.
72. J. Albert Key Md. Studies On Erythrocytes, With Special Reference To Reticulum, Polychromatophilia And Mitochondria. *Arch Intern Med (Chic)*. 1921;28(5):511–49.
73. Beltran Del Rio M, Tiwari M, Amodu LI, Cagliani J, Rodriguez Rilo HL. Glycated Hemoglobin, Plasma Glucose, and Erythrocyte Aging. *Journal of Diabetes Science and Technology*. 2016 Nov 1;10(6):1303–7.
74. Tarasev M, Chakraborty S, Alfano K. RBC mechanical fragility as a direct blood quality metric to supplement storage time. *Military Medicine*. 2015 Mar 1;180(3):150–7.
75. Sparrow RL. Red blood cell components: time to revisit the sources of variability. *Blood Transfusion*. 2017 Mar;15(2):116-125.
76. Bosman GJ. Survival of red blood cells after transfusion: processes and consequences. *Frontiers in Physiology*. 2013 Dec 18;4:376.
77. Sparrow RL. Time to revisit red blood cell additive solutions and storage conditions: a role for "omics" analyses. *Blood Transfusion*. 2012 May;10 Suppl 2(Suppl 2):s7-11.

78. Garraud O, Tissot JD. Blood and Blood Components: From Similarities to Differences. *Frontiers in Medicine (Lausanne)*. 2018 Apr 9;5:84.
79. Tzounakas VL, Anastasiadi AT, Drossos P V., Karadimas DG, Valsami S, Stamoulis KE, et al. Sex-related aspects of the red blood cell storage lesion. *Blood Transfusion*. 2021;19(3):224–36.
80. van Cromvoirt AM, Fenk S, Sadafi A, Melnikova EV, Lagutkin DA, Dey K, Petrushanko IY, Hegemann I, Goede JS, Bogdanova A. Donor Age and Red Cell Age Contribute to the Variance in LORCA Indices in Healthy Donors for Next Generation Ektacytometry: A Pilot Study. *Frontiers in Physiology*. 2021 Mar 2;12:639722.
81. Hazegh K, Fang F, Bravo MD, Tran JQ, Muench MO, Jackman RP, et al. Blood donor obesity is associated with changes in red blood cell metabolism and susceptibility to hemolysis in cold storage and in response to osmotic and oxidative stress. *Transfusion (Paris)*. 2021 Feb 1;61(2):435–48.
82. Daly A, Raval JS, Waters JH, Yazer MH, Kameneva M v. Effect of blood bank storage on the rheological properties of male and female donor red blood cells. *Clinical Hemorheology and Microcirculation*. 2014;56(4):337–45.
83. D'Alessandro A, Zimring JC, Busch M. Chronological storage age and metabolic age of stored red blood cells: are they the same? *Transfusion*. 2019 May;59(5):1620-1623.
84. R J Dern, R P Gwinn, J J Wiorkowski. Studies on the preservation of human blood. I. Variability in erythrocyte storage characteristics among healthy donors. *Journal of Laboratory and Clinical Medicine*. 1966 Jun;67(6):955–65.
85. Melzak KA, Spouge JL, Boecker C, Kirschhöfer F, Brenner-Weiss G, Bieback K. Hemolysis Pathways during Storage of Erythrocytes and Inter-Donor Variability in Erythrocyte Morphology. *Transfusion Medicine and Hemotherapy*. 2021 Feb 1;48(1):39–47.
86. Barshtein G, Gural A, Zelig O, Arbell D, Yedgar S. Preparation of packed red blood cell units in the blood bank: Alteration in red blood cell deformability. *Transfusion and Apheresis Science*. 2020 Jun;59(3):102738.
87. Edgren G, Ullum H, Rostgaard K, Erikstrup C, Sartipy U, Holzmann MJ, et al. Association of donor age and sex with survival of patients receiving transfusions. *JAMA Internal Medicine*. 2017;177(6):854–60.
88. Heddle NM, Cook RJ, Liu Y, Zeller M, Barty R, Acker JP, et al. The association between blood donor sex and age and transfusion recipient mortality: an exploratory analysis. *Transfusion (Paris)*. 2019;59(2):482–91.
89. Fergusson DA, Chassé M, Timmouh A, Acker JP, English S, Forster AJ, Hawken S, Shehata N, Thavorn K, Wilson K, Tuttle A, Perelman I, Cober N, Maddison H, Tokessy M. Pragmatic, double-blind, randomised trial evaluating the impact of red blood

cell donor sex on recipient mortality in an academic hospital population: the innovative Trial Assessing Donor Sex (iTADS) protocol. *BMJ Open*. 2021 Feb 23;11(2):e049598.

90. Kanas T, Lanteri MC, Page GP, Guo Y, Endres SM, Stone M, et al. Ethnicity, sex, and age are determinants of red blood cell storage and stress hemolysis: Results of the REDS-III RBC-Omics study. *Blood Advances*. 2017;1(15):1132–41.

91. Chasse M, Tinmouth A, English SW, Acker JP, Wilson K, Knoll G, et al. Association of blood donor age and sex with recipient survival after red blood cell transfusion. *JAMA Internal Medicine*. 2016;176(9):1307–14.

92. Mykhailova O, Brandon-Coatham M, Phan C, Yazdanbakhsh M, Olafson C, Yi QL, Kanas T, Acker JP. Red cell concentrates from teen male donors contain poor-quality biologically older cells. *Vox Sang*. 2024 Feb 28.

93. Mykhailova O, Brandon-Coatham M, Durand K, Olafson C, Xu A, Yi QL, Kanas T, Acker JP. Estimated median density identifies donor age and sex differences in red blood cell biological age. *Transfusion*. 2024 Feb 29.

94. Cloutier M, Cognasse F, Yokoyama APH, Hazegh K, Mykhailova O, Brandon-Coatham M, et al. Quality assessment of red blood cell concentrates from blood donors at the extremes of the age spectrum: The BEST collaborative study. *Transfusion (Paris)*. 2023 Aug 1;63(8):1506–18.

95. Hansen AL, Kurach JDR, Turner TR, Jenkins C, Busch MP, Norris PJ, et al. The effect of processing method on the in vitro characteristics of red blood cell products. *Vox Sang*. 2015;108(4):350–8.

96. Radwanski K, Garraud O, Cognasse F, Hamzeh-Cognasse H, Payrat JM, Min K. The effects of red blood cell preparation method on in vitro markers of red blood cell aging and inflammatory response. *Transfusion (Paris)*. 2013;53(12):3128–38.

97. Acker JP, Hansen AL, Kurach JDR, Turner TR, Croteau I, Jenkins C. A quality monitoring program for red blood cell components: In vitro quality indicators before and after implementation of semiautomated processing. *Transfusion (Paris)*. 2014;54(10):2534–43.

98. Devine D v., Howe D. Processing of whole blood into cellular components and plasma. *ISBT Science Series*. 2010;5(n1):78–82.

99. Högman CF, Eriksson L, Hedlund K, Wallvik J. The Bottom and Top System: A New Technique for Blood Component Preparation and Storage. *Vox Sang*. 1988;55(4):211–7.

100. Card RT, Mohandas N, Perkins HA, Shohet SB. Deformability of stored red blood cells. *Transfusion (Paris)*. 1982;22(2):96–101.

101. Acker JP, Hansen AL, Kurach JDR, Turner TR, Croteau I, Jenkins C. A quality monitoring program for red blood cell components: In vitro quality indicators before and

after implementation of semiautomated processing. *Transfusion (Paris)*. 2014;54(10):2534–43.

102. Alshalani A, Howell A, Acker JP. Impact of blood manufacturing and donor characteristics on membrane water permeability and in vitro quality parameters during hypothermic storage of red blood cells. *Cryobiology*. 2018 Feb 1;80:30–7.

103. Almizraq RJ, Norris PJ, Inglis H, Menocha S, Wirtz MR, Juffermans N, et al. Blood manufacturing methods affect red blood cell product characteristics and immunomodulatory activity. *Blood Advances*. 2018;2(18):2296–306.

104. Sputtek A, Sputtek R. Cryopreservation in *Transfusion Medicine and Hematology*. In: *Life in the Frozen State*. CRC Press; 2004. p. 483–504.

105. Hess JR. Red cell freezing and its impact on the supply chain. *Transfusion Medicine*. 2004 Feb;14(1):1-8.

106. Sputtek A. Cryopreservation of red blood cells and platelets. *Methods in Molecular Biology*. 2007;368:283-301.

107. Zhurova M, Olivieri A, Holt A, Acker JP. A method to measure permeability of red blood cell membrane to water and solutes using intrinsic fluorescence. *Clinica Chimica Acta*. 2014;431:103–10.

108. Zhurova M, McGann LE, Acker JP. Osmotic parameters of red blood cells from umbilical cord blood. *Cryobiology*. 2014;68(3):379–88.

109. Mazur P, Leibo SP, Chu EH. A two-factor hypothesis of freezing injury. Evidence from Chinese hamster tissue-culture cells. *Experimental Cell Research*. 1972;71(2):345-55.

110. McGann LE. Differing actions of penetrating and nonpenetrating cryoprotective agents. *Cryobiology*. 1978 Aug;15(4):382-90.

111. Scott KL, Lecak J, Acker JP. Biopreservation of red blood cells: Past, present, and future. *Transfusion Medicine Reviews*. 2005;19(2):127–42.

112. BloodBook.com. (2024, March 4). Blood banking. Retrieved March 4, 2024, from <http://www.bloodbook.com/banking.html>

113. Polge C, Smith AU, Parkes AS. Revival of spermatozoa after vitrification and dehydration at low temperatures. *Nature*. 1949 Oct 15;164(4172):666.

114. Smith AU. Prevention of haemolysis during freezing and thawing of red blood-cells. *The Lancet*. 1950 Dec 30;2(6644):910-1.

115. Mollison PL, Sloviter HA. Successful transfusion of previously frozen human red cells. *The Lancet*. 1951 Nov 10;2(6689):862-4.

116. Huggins CE. Reversible agglomeration used to remove dimethylsulfoxide from large volumes of frozen blood. *Science* (1979). 1963;139(3554):504–5.
117. Robert Valeri C, Ragno G, Pivacek LE, Srey R, Hess JR, Lippert LE, et al. A multicenter study of in vitro and in vivo values in human RBCs frozen with 40-percent (wt/vol) glycerol and stored after deglycerolization for 15 days at 4°C in AS-3: Assessment of RBC processing in the ACP<sup>®</sup> 215. *Transfusion (Paris)*. 2001;41(7):933–9.
118. Bandarenko N, Hay SN, Holmberg J, Whitley P, Taylor HL, Moroff G, et al. Extended storage of AS-1 and AS-3 leukoreduced red blood cells for 15 days after deglycerolization and resuspension in AS-3 using an automated closed system. *Transfusion (Paris)*. 2004 Nov;44(11):1656–62.
119. Turner TR, Acker JP. A Canadian perspective on the use and preparation of cryopreserved red cell concentrates. *Transfusion and Apheresis Science*. 2020 Aug;59(4):102853.
120. Hansen AL, Turner TR, Kurach JDR, Acker JP. Quality of red blood cells washed using a second wash sequence on an automated cell processor. *Transfusion (Paris)*. 2015 Oct 1;55(10):2415–21.
121. Meryman HT, Hornblower M. A method for freezing and washing red blood cells using a high glycerol concentration. *Transfusion (Paris)*. 1972;12(3):145–56.
122. Arthur W. Rowe, E. Eyster, A. Kellner. Liquid nitrogen preservation of red blood cells for transfusion: A low glycerol — Rapid freeze procedure. *Cryobiology*. 1968;5(2):119–28.
123. Horn EP, Sputtek A, Standl T, Rudolf B, Kühnl P, Schulte am Esch J. Transfusion of autologous, hydroxyethyl starch-cryopreserved red blood cells. *Anesthesia & Analgesia*. 1997 Oct;85(4):739-45.
124. Thomas MJ, Parry ES, Nash SG, Bell SH. A method for the cryopreservation of red blood cells using hydroxyethyl starch as a cryoprotectant. *Transfusion Science*. 1996 Sep;17(3):385-96.
125. Sputtek A, Bacher C, Langer R, Kron W, Henrich HA, Rau G. Kryokonservierung von Human-erythrozyten mit Hydroxyethylstärke (HES)--Teil 2: Vitalitätsanalytik [Cryopreservation of human erythrocytes with hydroxyethyl starch (HES)--Part 2: Analysis of survival]. *Infusionsther Transfusionsmed*. 1992 Dec;19(6):276-82.
126. Lagerberg JWM, Truijens-De Lange R, De Korte D, Verhoeven AJ. Altered processing of thawed red cells to improve the in vitro quality during postthaw storage at 4°C. *Transfusion (Paris)*. 2007 Dec;47(12):2242–9.
127. Valeri CR, Srey R, Tilahun D, Ragno G. The in vitro quality of red blood cells frozen with 40 percent (wt/vol) glycerol at -80°C for 14 years, deglycerolized with the

Haemonetics ACP<sup>®</sup> 215, and stored at 4°C in additive solution-1 or additive solution-3 for up to 3 weeks. *Transfusion (Paris)*. 2004 Jul;44(7):990–5.

128. Lecak J, Scott K, Young C, Hannon J, Acker JP. Evaluation of red blood cells stored at -80°C in excess of 10 years. *Transfusion (Paris)*. 2004 Sep;44(9):1306–13.

129. Moss GS, Valeri CR, Brodine CE. Clinical experience with the use of frozen blood in combat casualties. *The New England Journal of Medicine*. 1968 Apr 4;278(14):747-52.

130. Telischi M, Hoiberg R, Rao KR, Patel AR. The use of frozen, thawed erythrocytes in blood banking: a report of 28 months' experience in a large transfusion service. *American Journal of Clinical Pathology*. 1977 Aug;68(2):250-7.

131. O'brien TG, Haynes LL, Hering AC, Tullis JL, Watkins E Jr. The use of glycerolized frozen blood in vascular surgery and extracorporeal circulation. *Surgery*. 1961 Jan;49:109-29.

132. Tulis JL, Haynes LL, Pyle HM, Wallach S, Pennell RB, Sproul MT, Khoubesserian A. Clinical use of frozen red cells. *Archives of Surgery*. 1960 Jul;81:151-4.

133. Perrault R, Jackson JR, Martin-Villar J, Smiley RK. Experience with the use of frozen blood. *Canadian Medical Association Journal*. 1967 Jun 10;96(23):1504-9.

134. Mazur P. The Role of Cell Membranes in The Freezing of Yeast and Other Single Cells. *Annals of the New York Academy of Sciences*. 1965;125(2):658–76.

135. Nagashima H, Kashiwazaki N, Ashman RJ, Grupen CG, Seamark RF, Nottle MB. Removal of cytoplasmic lipid enhances the tolerance of porcine embryos to chilling. *Biology of Reproduction*. 1994 Oct;51(4):618-22.

136. J E Lovelock. The denaturation of lipid-protein complexes as a cause of damage by freezing. *Proceedings of the Royal Society B: Biological Sciences* . 1957 Dec 17;17(147(929)):427–33.

137. Hall, John E. *Guyton and Hall Textbook of Medical Physiology*. 13th ed., W B Saunders, 2015

138. Mazur P. kinetics of water loss from cells at subzero temperatures and the likelihood of intracellular freezing. *The Journal of General Physiology*. 1963 Nov;47(2):347-69.

139. Lahmann JM, Benson JD, Higgins AZ. Concentration dependence of the cell membrane permeability to cryoprotectant and water and implications for design of methods for post-thaw washing of human erythrocytes. *Cryobiology*. 2018 Feb;80:1-11.

140. Benga G, Borza T. Diffusional water permeability of mammalian red blood cells. *Comparative Biochemistry and Physiology Part B: Biochemistry & Molecular Biology*. 1995 Dec;112(4):653-9.

141. Owen JD, Eyring EM. Reflection coefficients of permeant molecules in human red cell suspensions. *The Journal of General Physiology*. 1975 Aug;66(2):251-65.
142. Mazur P, Miller RH. Permeability of the human erythrocyte to glycerol in 1 and 2 M solutions at 0 or 20 degrees C. *Cryobiology*. 1976 Oct;13(5):507-22.
143. Campos E, Moura TF, Oliva A, Leandro P, Soveral G. Lack of Aquaporin 3 in bovine erythrocyte membranes correlates with low glycerol permeation. *Biochemical and Biophysical Research Communications*. 2011 May 13;408(3):477-81
144. Carlsen A, Wieth JO. Glycerol transport in human red cells. *Acta Physiologica Scandinavica*. 1976 Aug;97(4):501-13.
145. Roudier N, Ripoché P, Gane P, Le Pennec PY, Daniels G, Cartron JP, et al. AQP3 deficiency in humans and the molecular basis of a novel blood group system, GIL. *Journal of Biological Chemistry*. 2002 Nov 29;277(48):45854-9.
146. De Gier J, Mandersloot JG, Hupkes JV, McElhaney RN, Van Beek WP. On the mechanism of non-electrolyte permeation through lipid bilayers and through biomembranes. *Biochimica et Biophysica Acta*. 1971 Jun 1;233(3):610-8.
147. Tirri LJ, Schmidt PC, Pullarkat RK, Brockerhoff H. Studies on the hydrogen belts of membranes: II. Non-electrolyte permeability of liposomes of diester, diether, and dialkyl phosphatidylcholine and cholesterol. *Lipids*. 1977 Oct;12(10):863-8..
148. Ross-Rodriguez LU, Elliott JAW, McGann LE. Investigating cryoinjury using simulations and experiments. 1: TF-1 cells during two-step freezing (rapid cooling interrupted with a hold time). *Cryobiology*. 2010 Aug;61(1):38-45.
149. Kedem O, Katchalsky A. A physical interpretation of the phenomenological coefficients of membrane permeability. *The Journal of General Physiology*. 1961 Sep;45(1):143-79.
150. Kedem O, Katchalsky A. Thermodynamic analysis of the permeability of biological membranes to non-electrolytes. *Biochimica et Biophysica Acta*. 1958 Feb;27(2):229-46.
151. Jacobs MH. The simultaneous measurement of cell permeability to water and to dissolved substances. *Journal of Cellular Physiology*. 1933 Feb;2(4):427-44.
152. Jacobs MH, Stewart DR. A simple method for the quantitative measurement of cell permeability. *Journal of Cellular Physiology*. 1932 Feb;1(1):71-82.
153. Kleinhans FW. Membrane permeability modeling: Kedem-Katchalsky vs a two-parameter formalism. *Cryobiology*. 1998 Dec;37(4):271-89.
154. McGann LE, Elliott JAW. Optimization of cryopreservation protocols using computer simulations. *Cryobiology*. 2003;47(3):255.

155. Ross-Rodriguez LU, Elliott JAW, McGann LE. Characterization of cryobiological responses in TF-1 cells using interrupted freezing procedures. *Cryobiology*. 2010 Apr;60(2):106–16.
156. McGann LE, Ebertz SL, Elliott JAW. Optimal cooling rates from osmotic simulation of cellular low temperature responses. *Cryobiology*. 2002;45(3):255.
157. Karlsson JO, Younis AI, Chan AW, Gould KG, Eroglu A. Permeability of the rhesus monkey oocyte membrane to water and common cryoprotectants. *Molecular Reproduction and Development*. 2009 Apr;76(4):321-33.
158. Benson JD, Kearsley AJ, Higgins AZ. Mathematical optimization of procedures for cryoprotectant equilibration using a toxicity cost function. *Cryobiology*. 2012 Jun;64(3):144–51.
159. Lovelock JE. The haemolysis of human red blood-cells by freezing and thawing. *Biochimica et Biophysica Acta*. 1953 Mar;10(3):414-26.
160. Mazur P, Cole KW. Roles of unfrozen fraction, salt concentration, and changes in cell volume in the survival of frozen human erythrocytes. *Cryobiology*. 1989 Feb;26(1):1-29.
161. Pegg DE, Diaper MP. On the mechanism of injury to slowly frozen erythrocytes. *Biophysical Journal*. 1988 Sep;54(3):471-88.
162. Meryman HT. Modified model for the mechanism of freezing injury in erythrocytes. *Nature*. 1968 Apr 27;218(5139):333-6.
163. Lusianti RE, Higgins AZ. Continuous removal of glycerol from frozen-thawed red blood cells in a microfluidic membrane device. *Biomicrofluidics*. 2014 Oct 28;8(5):054124.
164. Lusianti RE, Benson JD, Acker JP, Higgins AZ. Rapid removal of glycerol from frozen-thawed red blood cells. *Biotechnology Progress*. 2013 May-Jun;29(3):609-20.
165. Zhou X, Liu Z, Shu Z, Ding W, Du P, Chung JH, et al. A dilution-filtration system for removing cryoprotective agents. *Journal of Biomechanical Engineering*. 2011 Jan 31;133(2).
166. Lahmann JM, Sanchez CC, Benson JD, Acker JP, Higgins AZ. Implications of variability in cell membrane permeability for design of methods to remove glycerol from frozen-thawed erythrocytes. *Cryobiology*. 2020 Feb 1;92:168–79.
167. Jay AW, Rowlands S. The stages of osmotic haemolysis. *The Journal of Physiology*. 1975 Nov;252(3):817-32.
168. Alshalani A, Acker JP. Red blood cell membrane water permeability increases with length of ex vivo storage. *Cryobiology*. 2017 Jun;76:51-58.

169. Liu J, Mullen S, Meng Q, Critser J, Dinnyes A. Determination of oocyte membrane permeability coefficients and their application to cryopreservation in a rabbit model. *Cryobiology*. 2009 Oct;59(2):127–34.
170. Ebertz SL, McGann LE. Cryoprotectant permeability parameters for cells used in a bioengineered human corneal equivalent and applications for cryopreservation. *Cryobiology*. 2004 Oct;49(2):169–80.
171. Verkman AS. Water permeability measurement in living cells and complex tissues. *The Journal of Membrane Biology*. 2000 Jan 15;173(2):73-87.
172. Agre P, Smith B L, Baumgarten R, Preston G M, Pressman E, Wilson P, Illum N, Anstee D J, Lande M B, Zeidel M L. Human Red Cell Aquaporin CHIP 11. Expression during Normal Fetal Development and in a Novel Form of Congenital Dyserythropoietic Anemia. *Journal of Clinical Investigation*. 1994;94(3):1050-1058.
173. Grant JL, Britton MC Jr, Kurtz TE. Measurement of red blood cell volume with the electronic cell counter. *American Journal of Clinical Pathology*. 1960 Feb;33:138-43.
174. Mariia Zhurova. Cryobiological characteristics of red blood cells from human umbilical cord blood. University of Alberta; 2013.
175. Watanabe M, Uehara Y, Yamashita N, Fujimura Y, Nishio K, Sawada T, et al. Multicolor detection of rare tumor cells in blood using a novel flow cytometry-based system. *Cytometry Part A*. 2014 Mar;85(3):206–13.
176. Heitzer E, Auer M, Gasch C, Pichler M, Ulz P, Hoffmann EM, et al. Complex tumor genomes inferred from single circulating tumor cells by array-CGH and next-generation sequencing. *Cancer Research*. 2013 May 15;73(10):2965–75.
177. Cohen-Maslaton S, Barnea I, Taieb A, Shaked NT. Cell and nucleus refractive-index mapping by interferometric phase microscopy and rapid confocal fluorescence microscopy. *Journal of Biophotonics*. 2020 Sep;13(9):e202000117.
178. Rappaz B, Cano E, Colomb T, Kühn J, Depeursinge C, Simanis V, Magistretti PJ, Marquet P. Noninvasive characterization of the fission yeast cell cycle by monitoring dry mass with digital holographic microscopy. *Journal of Biomedical Optics*. 2009 May-Jun;14(3):034049.
179. Jang Y, Jang J, Park Y. Dynamic spectroscopic phase microscopy for quantifying hemoglobin concentration and dynamic membrane fluctuation in red blood cells. *Optics Express*. 2012 Apr 23;20(9):9673-81.
180. Mir, Mustafa, Zhuo Wang, Krishnarao Tangella, and Gabriel Popescu. Diffraction Phase Cytometry: blood on a CD-ROM. *Optical Society of America*. 16 February 2009 / Vol. 17, No. 4.

181. Turko NA, Shaked NT. Erythrocyte volumetric measurements in imaging flow cytometry using simultaneous three-wavelength digital holographic microscopy. *Biomedical Optics Express*. 2020 Nov 1;11(11):6649.
182. Wang M, Liang H, Chen X, Chen D, Wang J, Zhang Y, Chen J. Developments of Conventional and Microfluidic Flow Cytometry Enabling High-Throughput Characterization of Single Cells. *Biosensors (Basel)*. 2022 Jun 23;12(7):443.
183. Béné MC. Microfluidics in flow cytometry and related techniques. *International Journal of Laboratory Hematology*. 2017 May;39 Suppl 1:93-97. DIO:10.1111/ijlh.12669. PMID: 28447416.
184. Honrado C, Bisegna P, Swami NS, Caselli F. Single-cell microfluidic impedance cytometry: from raw signals to cell phenotypes using data analytics. *Lab on a Chip Journal*. 2021 Jan 5;21(1):22-54.
185. Chen PY, Pearce D, Verkman AS. Membrane water and solute permeability determined quantitatively by self-quenching of an entrapped fluorophore. *Biochemistry*. 1988 Jul 26;27(15):5713-8.
186. Wachlmayr J, Hanneschlaeger C, Speletz A, Barta T, Eckerstorfer A, Siligan C, Horner A. Scattering versus fluorescence self-quenching: more than a question of faith for the quantification of water flux in large unilamellar vesicles? *Nanoscale Advances*. 2021 Oct 18;4(1):58-76.
187. Stetefeld J, McKenna SA, Patel TR. Dynamic light scattering: a practical guide and applications in biomedical sciences. *Biophysical Reviews*. 2016 Dec;8(4):409-427.
188. Pal N, Dev Verma S, Singh MK, Sen S. Fluorescence correlation spectroscopy: an efficient tool for measuring size, size-distribution and polydispersity of microemulsion droplets in solution. *Analytical Chemistry*. 2011 Oct 15;83(20):7736-44.
189. Petrášek Z, Schwille P. Precise measurement of diffusion coefficients using scanning fluorescence correlation spectroscopy. *Biophysical Journal*. 2008 Feb 15;94(4):1437-48.
190. de Back DZ, Vlaar R, Beuger B, Daal B, Lagerberg J, Vlaar APJ, et al. A method for red blood cell biotinylation in a closed system. *Transfusion (Paris)*. 2018 Apr 1;58(4):896-904.
191. Mock DM, Nalbant D, Kyosseva S V., Schmidt RL, An G, Matthews NI, et al. Development, validation, and potential applications of biotinylated red blood cells for posttransfusion kinetics and other physiological studies: evidenced-based analysis and recommendations. *Transfusion*. 2018. Vol. 58, Issue 8, p. 2068-81.
192. Mock DM, Matthews NI, Zhu S, Strauss RG, Schmidt RL, Nalbant D, et al. Red blood cell (RBC) survival determined in humans using RBCs labeled at multiple biotin densities. *Transfusion (Paris)*. 2011 May;51(5):1047-57.

193. Mock DM, Lankford GL, Widness JA, Burmeister LF, Kahn D, Strauss RG. RBCs labeled at two biotin densities permit simultaneous and repeated measurements of circulating RBC volume. *Transfusion (Paris)*. 2004 Mar;44(3):431–7.
194. Mock DM, Matthews NI, Zhu S, Burmeister LF, Zimmerman MB, Strauss RG, et al. Red blood cell (RBC) volume can be independently determined in vivo in humans using RBCs labeled at different densities of biotin. *Transfusion (Paris)*. 2011 Jan;51(1):148–57.
195. Mock DM, Lankford GL, Widness JA, Burmeister LF, Kahn D, Strauss RG. Measurement of red cell survival using biotin-labeled red cells: Validation against <sup>51</sup>Cr-labeled red cells. *Transfusion (Paris)*. 1999;39(2):156–62.
196. Moroff G, Luban NLC. The irradiation of blood and blood components to prevent graft-versus-host disease: Technical issues and guidelines. *Transfusion Medicine Reviews*. 1997;11(1):15–26.
197. Treleaven J, Gennery A, Marsh J, Norfolk D, Page L, Parker A, et al. Guidelines on the use of irradiated blood components prepared by the British Committee for Standards in Haematology Blood Transfusion task force. *British Journal of Haematology*. 2011;152(1):35–51.
198. Gammon R. Standards for blood banks and transfusion services. Bethesda M, editor. Association for the Advancement of Blood & Biotherapies (AABB); 2020.
199. Canadian Standards Association. CAN/CSA-Z902:20 Blood and blood components. Toronto, ON; 2020.
200. European Directorate for the Quality of Medicines and Health Care. Guide to the preparation, use and quality assurance of blood components. 20th ed. Strasbourg, France: Council of Europe Publishing; 2020. 188–189 p.
201. Treleaven J, Gennery A, Marsh J, Norfolk D, Page L, Parker A, et al. Guidelines on the use of irradiated blood components prepared by the British Committee for Standards in Haematology Blood Transfusion task force. *British Journal of Haematology*. 2011 Jan;152(1):35–51.
202. de Korte D, Thibault L, Handke W, Harm SK, Morrison A, Fitzpatrick A, et al. Timing of gamma irradiation and blood donor sex influences in vitro characteristics of red blood cells. *Transfusion (Paris)*. 2018;58(4):917–26.
203. Patel RM, Roback JD, Uppal K, Yu T, Jones DP, Josephson CD. Metabolomics profile comparisons of irradiated and nonirradiated stored donor red blood cells. *Transfusion (Paris)*. 2015;55(3):544–52.
204. Katharia R, Chaudhary R, Agarwal P. Prestorage gamma irradiation induces oxidative injury to red cells. *Transfusion and Apheresis Science*. 2013 Feb;48(1):39–43.

205. Relevy H, Koshkaryev A, Manny N, Yedgar S, Barshtein G. Blood banking-induced alteration of red blood cell flow properties. *Transfusion*. 2008 Jan;48(1):136-46.
206. Brugnara C, Churchill WH. Effect of irradiation on red cell cation content and transport. *Transfusion (Paris)*. 1992;32(3):246-52.
207. Pribush A, Agam G, Yermiahu T, Dvilansky A, Meyerstein D, Meyerstein N. Radiation damage to the erythrocyte membrane: the effects of medium and cell concentrations. *Free Radical Research*. 1994 Sep;21(3):135-46.
208. Weinmann M, Hoffmann W, Rodegerdts E, Bamberg M. Biological effects of ionizing radiation on human blood compounds ex vivo. *Journal of Cancer Research and Clinical Oncology*. 2000 Oct;126(10):584-8.
209. Moreira OC, Oliveira VH, Benedicto LBF, Nogueira CM, Mignaco JA, Fontes CFL, et al. Effects of  $\gamma$ -irradiation on the membrane ATPases of human erythrocytes from transfusional blood concentrates. *Annals of Hematology*. 2008 Feb;87(2):113-9.
210. Apell HJ, Nelson MT, Marcus MM, Lauger P. Effects of the ATP, ADP and inorganic phosphate on the transport rate of the Na<sup>+</sup>,K<sup>+</sup>-pump. *Biochimica et Biophysica Acta*. 1986 May 9;857(1):105-15.
211. Axelsen KB, Palmgren MG. Evolution of substrate specificities in the P-type ATPase superfamily. *Journal of Molecular Evolution*. 1998 Jan;46(1):84-101.
212. Strehler EE, Treiman M. Calcium pumps of plasma membrane and cell interior. *Current Molecular Medicine*. 2004 May;4(3):323-35.
213. El Kenz H, Corazza F, Van Der Linden P, Chabab S, Vandenvelde C. Potassium content of irradiated packed red blood cells in different storage media: is there a need for additive solution-dependent recommendations for infant transfusion? *Transfusion and Apheresis Science*. 2013 Oct;49(2):249-53.
214. Xu D, Peng M, Zhang Z, Dong G, Zhang Y, Yu H. Study of damage to red blood cells exposed to different doses of  $\gamma$ -ray irradiation. *Blood Transfusion*. 2012;10(3):321-30.
215. Zimmermann R, Schoetz AM, Frisch A, Hauck B, Weiss D, Strobel J, et al. Influence of late irradiation on the in vitro RBC storage variables of leucoreduced RBCs in SAGM additive solution. *Vox Sang*. 2011 Apr;100(3):279-84.
216. P Agarwal, V L Ray, N Choudhury, R K Chaudhary. Effect of pre-storage gamma irradiation on red blood cells. *Indian Journal of Medical Research*. 2005 Nov;122(5):385-7.
217. Patidar GK, Joshi A, Marwaha N, Prasad R, Malhotra P, Sharma RR, et al. Serial assessment of biochemical changes in irradiated red blood cells. *Transfusion and Apheresis Science*. 2014;50(3):479-87.

218. Harm SK, Raval JS, Cramer J, Waters JH, Yazer MH. Haemolysis and sublethal injury of RBCs after routine blood bank manipulations. *Transfusion Medicine*. 2012;22(3):181–5.
219. Winter KM, Johnson L, Webb RG, Marks DC. Gamma-irradiation of deglycerolized red cells does not significantly affect in vitro quality. *Vox Sang*. 2015 Oct 1;109(3):231–8.
220. Hauck B, Oremek D, Zimmermann R, Ruppel R, Troester B, Eckstein R. Influence of irradiation on in vitro red-blood-cell (RBC) storage variables of leucoreduced RBCs in additive solution PAGGS-M. *Vox Sang*. 2011 Jul;101(1):21–7.
221. Serrano K, Chen D, Hansen AL, Levin E, Turner TR, Kurach JDR, et al. The effect of timing of gamma-irradiation on hemolysis and potassium release in leukoreduced red cell concentrates stored in SAGM. *Vox Sang*. 2014;106(4):379–81.
222. Moroff G, Luban NLC. The influence of gamma irradiation on red cell and platelet properties. *Transfusion Science*. 1994;15(2):141–8.
223. Lee AC, Reduque LL, Luban NLC, Ness PM, Anton B, Heitmiller ES. Transfusion-associated hyperkalemic cardiac arrest in pediatric patients receiving massive transfusion. *Transfusion (Paris)*. 2014 Jan;54(1):244–54.
224. Vraets A, Lin Y, Callum JL. Transfusion-associated hyperkalemia. *Transfusion Medicine Reviews*. 2011 Jul;25(3):184–96.
225. Rühl H, Bein G, Sachs UJ. Transfusion-associated graft-versus-host disease. *Transfusion Medicine Reviews*. 2009 Jan;23(1):62–71.
226. McCoy NC, Yu M, Sullivan JA, Spiegel DM, Leitman SF. The effect of prestorage irradiation red cell survival on posttransfusion. *Transfusion (Paris)*. 1992;32(6):525–8.
227. Kanas T, Sinchar D, Osei-Hwedieh D, Baust JJ, Jordan A, Zimring JC, et al. Testosterone-dependent sex differences in red blood cell hemolysis in storage, stress, and disease. *Transfusion (Paris)*. 2016;56(10):2571–83.
228. Raval JS, Waters JH, Seltsam A, Scharberg EA, Richter E, Kameneva M V., et al. Menopausal status affects the susceptibility of stored RBCs to mechanical stress. *Vox Sang*. 2011 May;100(4):418–21.
229. Rifkind JM, Araki K, Mohanty JG, Suda T. Age dependent changes in erythrocyte membrane function. *Progress in Clinical and Biological Research*. 1985;195:159–72.
230. Triadou, P., R. Girot, D. Rebibo, D. Lemau, B. Mattlinger, P. Bolo, M. Maier, and L. Barritault. Neocytopheresis: a new approach for the transfusion of patients with thalassaemia major. *European Journal of Pediatrics* (1986) 145: 10–13.

231. Tuo WW, Wang D, Liang WJ, Huang YX. How cell number and cellular properties of blood-banked red blood cells of different cell ages decline during storage. *PLoS One*. 2014 Aug 28;9(8):e105692.

## **Chapter 2**

### **Impact of Blood Component Manufacturing Methods on the Age Distribution of Red Blood Cells in Stored Red Cell Concentrates**

## 2.1 Introduction

RCCs are critical in medical transfusion therapy, yet concerns persist regarding their quality and efficacy. (1,2) Despite advancements to improve the quality of stored blood components for better transfusion outcomes, (3–7) transfusion of RCCs is still associated with an increased risk of adverse clinical events. (8–10) While extensive research has focused on the impact of storage duration on RCC quality, (9,10) other factors, such as donor variability and blood manufacturing methods, play significant roles. (1,2,11,12) The quality of RCCs is significantly affected by manufacturing methods, underscoring the clinical importance of understanding processing techniques and product composition variances.

Studies have shown that even minor differences in processing methods within the same organization can lead to notable alterations in blood component quality. (13–16) Evaluation of RBC *in vitro* quality primarily follows regulatory standards, which vary across regions. This variance contributes to regional differences in product composition. While meeting regulatory standards ensures product safety, it may not fully capture the subtle impacts of processing modifications. There are two main RCC processing methods: the WBF and RCF. (14,17,18) In the WBF method, units are cooled and filtered in the refrigerator within 72 hours of the stop-bleeding time. The filtered whole blood is centrifuged at  $4552 \times g$  for 6 minutes. PRP and RBCs are both extracted through the top outlet of the main collection bag. (14,19) In the RCF method, whole blood units are rapidly cooled to room temperature 18-24 °C and held overnight before centrifugation. The hard spin centrifugation ( $3907 \times g$  for 10 min) provides enough time and centrifugal force to compact RBCs at the bottom of the bag and results in a CPP on top of the buffy coat layer. CPP is squeezed out from the upper outlet while packed RBCs are extracted from the bottom outlet. (14,20) As the RBCs are squeezed out from the bottom outlet, the buffy coat and top layer of packed RBCs remain in the middle of the bag (45 to 50 mL). (19,21) Leukoreduction of the packed RBCs is then done at room temperature within 24 hours of the stop-bleeding time. (14,20) Studies have consistently demonstrated that RCCs processed using RCF methods exhibit lower HCT, Hb, RBC count, MCV, and blood volume compared to WBF-derived units. (14,17) Furthermore, RCF-derived RCCs have

shown higher ATP, morphological indices, and p50 values, indicating differences in metabolic and oxygen-binding capacities. (14) According to Canadian Blood Service Quality Control (CBS-QC) data, RCF-derived RCCs exhibit a hemolysis failure rate of 0.5%, while WBF-derived RCCs have a higher rate of 5.2% (unpublished findings). Moreover, results from the Quality Monitoring Program reveal that a greater proportion of WBF-derived RCCs fail to meet hemolysis criteria compared to RCF-derived RCCs. However, this variation in hemolysis levels may be attributed to a combination of donor factors and variations in blood processing techniques. (14) Additionally, manufacturing methods have been found to affect the characteristics of extracellular vesicles within RCCs and their immunomodulatory impact after transfusion. RCCs derived from the RCF method exhibit fewer platelet and white blood cell-derived vesicles and result in a reduced inflammatory response compared to WBF-derived RCCs. (22–24) These collective findings underscore the intricate relationship between manufacturing methods and the quality of RCCs, highlighting the imperative for additional research to comprehensively understand the mechanisms underlying these differences and optimize processing techniques.

RCCs consist of a heterogeneous population of RBCs spanning a range of biological ages. (25,26) The biological aging process in RBCs is associated with membrane remodeling (23,27), reduced metabolic activity, and progressive failure of cellular homeostasis. (28–41) RCCs with a greater proportion of O-RBCs may contribute to increased hemolysis, decreased cellular recovery, reduced oxygen delivery, and metabolic instability. (42–45) Studies have shown that RCCs enriched with Y-RBCs exhibit extended post-transfusion survival (41,46) and decreased transfusion requirements in patients receiving predominantly Y-RBCs. (43,47) Assessing the quality of RCCs involves determining the proportions of Y- and O-RBCs. (48) The distribution of Y-RBCs versus O-RBCs in RCCs is influenced by donor-related factors (49,50) and blood component manufacturing methods. Y-RBCs, characterized by their lower density compared to O-RBCs, can be effectively separated from O-RBCs through centrifugation. (43,46) Previous studies have elucidated that under the influence of centrifugal force, RBCs tend to stratify within a density gradient within the blood bag, with Y-RBCs preferentially settling at the top and O-RBCs gravitating towards the bottom of the bag

due to their higher density. (46,51,52) Considering the centrifugation-induced density gradient in RBCs within the blood bag, we hypothesized that manufacturing steps involving centrifugation and subsequent extraction of RBCs and plasma from either the top or bottom outlet may yield to extraction of different RBC subpopulations and impact the overall quality of RCCs. In the RCF method, CPP and RBCs are squeezed out from the top and bottom outlets, respectively, while a significant volume of blood and buffy coat remain within the collection bag. (14,19,20) We hypothesized that the uppermost layer of RBCs, predominantly including Y-RBCs with lower density, is lost during the buffy coat removal step. On the contrary, in the WBF method, plasma and RBCs are extracted from the upper outlet, leaving behind a residual volume of RBCs at the bottom of the collection bag. (14) We presumed that these cells at the bottom of the bag are denser and primarily composed of O-RBCs. This study investigated how manufacturing methods affect the proportion of Y- and O-RBCs and the EMD of RCCs from the same donor. Whole blood units from the Canadian Blood Services' Blood4Research program were divided into halves, each undergoing either the WBF or RCF process. We hypothesize that RCCs produced through the WBF method may exhibit a higher ratio of Y- to O-RBCs compared to those generated through the RCF method. The distribution of RBC subpopulations and EMD of RCCs was calculated using the Percoll<sup>®</sup> separation method. The study outcomes can help to refine processing techniques, facilitating the production of RCCs with an ideal Y- to O-RBC ratio, thus extending the post-transfusion survival of RBCs and improving transfusion efficacy.

## **2.2 Methods and Materials**

### **2.2.1 Red Cells Concentrate (RCC) Manufacturing**

Whole blood units were collected into citrate-phosphate-dextrose (CPD) in a MacoPharma collection set (LQT 7291 LX Leucoflex LCR-Diamond quadruple bottom-and-top system, CPD/SAGM 500 mL, MacoPharma, Tourcoing, France) and preserved at room temperature (20-22 °C) by the Canadian Blood Services Blood4Research program. The whole blood units used in our experiments were within two days of their collection to ensure optimal integrity. Twelve units were collected from a diverse group of healthy

volunteers of different ages and sexes. Five units were from female donors with an average age of  $58.4 \pm 23$  years old, and seven units were from male donors with an average age of  $54.8 \pm 28$  years old. Approval for the study was obtained from both the University of Alberta Health Research Ethics Board (Biomedical Panel; Protocol #PRO00103459) and the Canadian Blood Services Research Ethics Board (Protocol #2020.005).

Whole blood units and their collection bag were weighed using a scale (GSE 574, Scale System, Michigan, USA) to determine the exact weight of the whole blood. Whole blood units were divided into two equal parts. The whole blood was thoroughly mixed and securely attached to a dried WBF collection bag (DQE710X LX Leucoflex MTL1 top-and-top system, CPD/SAGM 500 mL, MacoPharma, Tourcoing, France) using a sterile connection device (TERUMO sterile tubing welder, TSCD-II<sup>®</sup>, Tokyo, Japan). Before transferring the blood, the CPD solution was drained from the bags, and we utilized dried bags. The whole blood was then transferred from the RCF collection bag into the WBF bag, with the weight of the transferred blood accurately measured using the scale. After transferring half of the whole blood into the WBF collection bag, the tube connections were detached using sterile sealing (Sebra<sup>®</sup> Modle 2600, Omni<sup>™</sup> Sealer, Arizona, USA). Subsequently, each half underwent either RCF or WBF methods to investigate their impact on the distribution of RBC subpopulations.

### **2.2.2 Red Cell Filtration Processing Method**

The RCF method starts with whole blood collection with 70 ml of CPD-anticoagulant (1:7 ratio). Whole blood undergoes a rapid cooling at room temperature (18-24 °C) after collection, followed by an overnight holding period before centrifugation. However, in this study, units sourced from Calgary were promptly shipped and received within a two-day timeframe after collection. Upon arrival, they were promptly subjected to processing procedures without delay. The hard spin centrifugation (Thermo Scientific Sorvall RC3BP Plus Refrigerated Centrifuge, CAN NO: 75007533 Germany); (Rotor setting: HBB-6 rotor,  $3907 \times g$  for 10 minutes at 20 °C, pre-warming the centrifuge to 18-24 °C before the procedure), effectively compacted RBCs at the bottom of the bag and resulted in a CPP

layer at the top of the buffy coat. The collection set features outlets at the top and bottom of the bag. At Canadian Blood Services, an automatic blood processing device (Compomat G4, Fresenius-Kabi, Bothell, WA) is employed for semiautomated component separation. However, due to the absence of access to semiautomated component separation equipment in our case, a manual component separator (4R4414, Fenwal Plasma Extractor, Deerfield, IL USA) was used. Following centrifugation, the CPP was pressed out from the top outlet, and the packed RBCs were drained into a distinct RBC bag via the lower outlet. The standard residual volume following the RCF method typically ranges between 45-50 mL, and given our halved whole blood separation approach, an estimated minimum of 22-25 mL of the buffy coat was anticipated. The endpoint of drainage was determined to ensure a minimum residual volume of 22-25 mL, encompassing both the buffy coat and RBCs. To accurately assessing the end point, an empty bag containing 23 mL of solution was utilized, allowing for visual estimation of the volume of the remaining buffy coat in the bag. The mean residual volume in our study cohort was  $29.42 \pm 5.73$  mL (CV: 19.47%). Subsequently, the SAGM was passed through the leukoreduction filter to prime it before filtering the RBCs. Before this filtration, half of the SAGM volume (55 mL) was withdrawn to ensure the precise ratio of SAGM to RBCs according to our halved whole blood separation approach. Buffy coat volume in the original collection bag was measured to verify its volume fell within the estimated range. In this study, the hold period before leukoreduction spanned 52 to 54 hours after stop-bleeding time ([Figure 2-1 A](#)).

### **2.2.3 Whole Blood Filtration Processing Method**

The WBF method at Canadian Blood Services starts with whole blood collection from healthy donors using CPD in a MacoPharma collection set. Whole blood units are cooled and filtered within 72 hours of the stop-bleeding time in a refrigerated environment (1-6 °C). However, in our unique case, the units were transported from Calgary to Edmonton Canadian Blood Service after collection at room temperature. Upon receiving the units, we promptly split them into RCF and WBF collection bags, and those designated for the WBF method were immediately cooled and filtered in a refrigerated environment (1-6 °C). The duration before filtration encompassed 52 to 54 hours from the bleeding time.

Following filtration, the whole blood units were centrifuged using the following settings: HBB-6 rotor,  $4552 \times g$  for 6 minutes at  $4\text{ }^{\circ}\text{C}$ . Following centrifugation, the PRP and packed RBCs were pressed out from the top outlet. The standard procedure involves using a semiautomated component separator post-centrifugation to extract PRP and packed RBCs. However, due to limited access to such equipment, a manual component separator was utilized. This manual approach involved careful transfer of PRP and RBCs by gently pushing them out from the top outlet into two separate bags. The endpoint of the separation process was determined when minimal plasma remained, and the interface between PRP and RBCs appeared clear. RBCs were directly transferred into the final bag, including 55 mL SAGM and mixed through inversion ([Figure 2-1 B](#)). The residual packed RBCs in the WBF collection bag were retained for subsequent analysis. Furthermore, the filters utilized for both WBF and RCF were backwashed with SAGM and set aside for further analysis.

#### **2.2.4 Density-Fractionation using Percoll<sup>®</sup> Separation Method**

A density-based Percoll<sup>®</sup> separation method was utilized to explore the density distribution and diversity of RBCs within each RCC. This method relies on Percoll<sup>®</sup> density gradient centrifugation, which enables the fractionation of RBCs into distinct subpopulations based on density. For RCC density profiling, an aliquot of 50 mL from each RCC unit was collected into 50 mL conical tubes. The sampling entails mixing the blood unit, inserting a sampling site coupler into the blood bag, and swabbing it with alcohol. A desired volume of packed cells was slowly drawn out, using a syringe and needle, following safety measures. Blood was dispensed drop-wise into a labeled tube to prevent hemolysis, and the unit was subsequently stored in a refrigerator. (51) An aliquot of 1 mL RBCs was analyzed on a cell counter (DXH 520, Beckman Coulter, Mississauga, ON, Canada) to measure the RBC indices, including the MCHC and MCV. Mykhailova et al. introduced an approach to predict the required density of Percoll<sup>®</sup> for fractionating RBCs based on the MCHC and MCV measurements, revealing a positive correlation between MCHC and the density profile of RBCs. (52,53) Using the MCHC and MCV measurements, the Percoll<sup>®</sup> densities required to create a comprehensive density panel for characterizing the RBCs were estimated.

Percoll<sup>®</sup> solutions with varying densities were prepared according to predetermined tables using Percoll<sup>®</sup> (CAS No: 45-001-794, Cytiva 17089109, Uppsala, Sweden), 1.5 M NaCl solution (CAS No: 7647-14-5, Sigma-Aldrich. Co, St. Louis, Missouri, USA), and distilled water. Eight round-bottom tubes, each containing a specific density of Percoll<sup>®</sup> (ranging from 1.088 to 1.100 g/mL), were carefully arranged for each RCC. A 3 mL volume of each Percoll<sup>®</sup> solution was sampled into the respective tubes. A 1 mL aliquot of RBCs was gently layered onto the density gradient of Percoll<sup>®</sup> solutions, ensuring minimal mixing between layers. The tubes were centrifuged at 3041 x g for 15 minutes at 20 °C (acceleration 4, deceleration 1) (Eppendorf 5810R—15 Amp Version, Germany). Following centrifugation, less dense RBCs (Y-RBCs) were carefully isolated into corresponding tubes and the remaining Percoll<sup>®</sup> solution was discarded from tubes with a vacuum flask, leaving the dense RBC (O-RBCs) pellet undisturbed at the bottom. Isolated RBC subpopulations were washed by adding phosphate buffered saline (CAN No: 10-010-049, **PBS** (×1) pH 7.4, Gibco<sup>TM</sup>, Life Technologies Corporation, New York, USA) to each tube, and tubes were centrifuged at 1500 x g for 10 minutes at 20 °C (acceleration 9, deceleration 4). After centrifugation, all supernatants were discarded using a vacuum flask, leaving an equivalent volume of PBS atop packed RBCs to attain a hematocrit range of 40-55%. Adjustments were made visually by adding or removing PBS as needed ([Figure 2-2](#)).

### **2.2.5 Estimating Median Density of Each RCCs**

The RBC indices for each subpopulation were measured using a hematology analyzer. The volume of each RBC subpopulation was measured using a calibrated adjustable-volume pipette to estimate the proportion of each subpopulation. These pipettes allow users to manually adjust the volume by turning a screw or dial on the pipette. To measure sample volumes, the pipette tip was placed at the bottom of the tube, and samples were aspirated by gently adjusting the screw on top. The pipette volume was selected visually, and once chosen, the pipette was adjusted to the smaller volume. The sample was then aspirated, and the screw was slowly turned until all the samples were drawn, ensuring no residual RBCs remained. An appropriate calibrated pipette was chosen based on visual inspection of the volume, for instance, samples ranging between 200 to 500 µL were

measured using a 500  $\mu$ L pipette. This allowed precise control and adjustment of the pipetting volume as needed for accurate volume measurement. The isolated RBC portions were calculated by multiplying the measured volume by the total number of isolated RBCs. The resulting age profiles were represented by skewed Gaussian distributions, and the medians of these distributions were denoted as the EMD of the RCCs.

### **2.2.6 Statistical Analysis and Data Reporting**

In this study, data analysis was conducted utilizing GraphPad Prism software (version 9.5.0, GraphPad Software, San Diego, CA, USA). The statistical analyses comprised the calculation of descriptive statistics such as mean, standard deviation (SD), and standard error of the mean (SEM). To address the repeated measures nature of the study, we implemented statistical techniques specifically designed for such scenarios. Mixed-effects models and repeated measures ANOVA were employed to appropriately account for within-subject variability. These methods allow for the consideration of both between-subject and within-subject variations, ensuring robust analysis and interpretation of the data. In detail, mixed-effects models are advantageous for handling correlated data, such as repeated measures, by incorporating random effects that account for individual variability while accounting for fixed effects, such as treatment conditions or time points. Graphs featuring error bars representing SEM/SD were generated to visually represent the data. Results are presented as mean  $\pm$  SEM/SD, with statistical significance denoted by \*:  $p < 0.05$  (statistically significant), \*\*:  $p < 0.01$  (highly statistically significant), \*\*\*:  $p < 0.001$  (very highly statistically significant), and \*\*\*\*:  $p < 0.0001$  (extremely statistically significant). By utilizing these advanced statistical approaches, we were able to effectively address the repeated measures design of the study, providing reliable and insightful analyses while ensuring the validity of our conclusions.

## 2.3 Results

### 2.3.1 Comparative Analysis of RBC Indices in RCCs Processed by RCF and WBF Methods

A comparative analysis of Hb levels between the RCF and WBF methods using the Student t-test revealed a significant difference. Hb levels were notably lower in units prepared using the RCF method compared to RCCs processed using the WBF method ( $p < 0.0001$ ) ([Figure 2-3](#)). Moreover, a significant disparity in the number of RBCs was observed between RCCs processed by different methods, with RCCs processed with the WBF method demonstrating a higher RBC count compared to the RCF method ( $p < 0.0001$ ) ([Figure 2-4](#)). The MCV exhibited a significant difference between the two groups of units, with units processed with WBF demonstrating a lower MCV compared to that of RCF ( $p < 0.0001$ ) ([Figure 2-5](#)). However, this difference was not significant in some units (Unit#: unit 5 sourced from senior female donors with an average age of 78, and units 9 and 12 sourced by male donors aged 23 and 42, respectively). Significant differences in HCT level were observed between units processed with the WBF method and those processed with the RCF method, with units processed by WBF demonstrating a higher HCT level ( $p < 0.0001$ ) ([Figure 2-6](#)). The estimated median density did not exhibit any significant differences between RCCs produced by RCF and WBF methods ( $p > 0.9999$ ) ([Figure 2-7](#)). Red cell distribution width (**RDW**), a measure of the variation in RBC sizes, showed significant differences between units processed using two different methods ( $p < 0.0001$ ). RCCs produced using the WBF method demonstrated higher RDW compared to those of the RCF method, indicating higher variability in cell size. This discrepancy was more pronounced in specific units, specifically units 1, 7, and 10, where the divergence in RDW values between the two methods was significant. However, in other units, this discrepancy did not attain statistically significant levels ([Figure 2-8](#)). While no significant differences were observed in MCHC values among RCC units processed using different methods, analysis using the Student's t-test revealed that MCHC levels were higher in units processed using the WBF method compared to those processed using the RCF method ( $p = 0.0107$ ) ([Figure 2-9](#)). Analyzing the volume of RCCs revealed that units processed using the WBF method exhibited a higher final volume compared to

those processed using the RCF method ( $p=0.0012$ ) ([Figure 2-10](#)). The ratio of the final volume to the initial volume was calculated to ensure accurate comparisons and mitigate any potential impact of initial volume variations on the final volume of the units. This approach helped standardize the comparison and eliminate any disparities in the initial volume that might have influenced the final volume measurement of the units.

### **2.3.2 Variation in Distribution of RBC Subpopulations across RCCs Processed Using WBF and RCF**

Unit-to-unit analysis of the distribution of RBC subpopulations revealed variation between units processed using different methods. In units 3, 4, 5, 7, 8, 9, 11, and 12, a significantly higher proportion of Y-RBCs was observed at each density in the units processed using the RCF method compared to those processed using the WBF method. Conversely, in units 1, 2, 6, and 10, no significant differences were observed in the proportion of Y-RBCs among RCCs produced using different manufacturing methods. Regarding the old proportion of RBC subpopulations, variation was observed between different units. In units 1, 2, 3, 9, and 11, no significant differences were observed in the proportion of O-RBCs in RCCs processed using different manufacturing methods. However, units 4, 5, 6, 7, 8, 10, and 12 demonstrated a significantly higher proportion of O-RBCs at each density in RCCs processed using the RCF method compared to those processed using the WBF method ([Figure 2-11](#)).

Upon analyzing the density-based proportion of Y-RBCs within identical units processed using different methods, no significant differences were found in the cumulative data from all RCC units ( $p=0.3134$ ). Interestingly, while differences were observed when analyzing unit-to-unit variances, the cumulative data analysis across all units did not reveal any significant differences ([Figure 2-12](#)). Likewise, cumulative data demonstrated no significant difference in the proportion of O-RBCs between units processed using either the RCF or WBF methods ( $p=0.4974$ ) ([Figure 2-13](#)). The cumulative data on the density distribution of RBCs demonstrated no significant differences between the two different methods ([Figure 2-14](#)).

Analysis of the ratio between biologically Y-RBCs and O-RBCs across units processed using different manufacturing methods revealed no significant differences. Despite variations observed in the proportions of Y-RBCs and O-RBCs within individual units, the overall ratio of Y-RBCs to O-RBCs remained consistent across all units regardless of the processing method employed ([Figure 2-15](#)). Mixed effect analysis of aggregate data from all units revealed no significant shifts in the ratio of Y-to-O- RBCs between units processed using different manufacturing methods ( $p=0.8278$ ) ([Figure 2-16](#)). The analysis of residual RBC indices in the buffy coat and the WBF collection bag revealed no statistically significant differences in MCHC and MCV values ( $p=0.0637$  and  $p=0.2916$ , respectively). Additionally, the examination of RBC indices from the RBCs collected during the filter backwash showed no significant differences between the groups.

## 2.4 Discussion

The study conducted a comprehensive analysis, comparing the impact of WBF and RCF methods on the density-based distribution of RBC subpopulations. Notably, significant differences were observed in various parameters. Hb levels were significantly lower in RCCs processed with the RCF method compared to those processed with the WBF method ([Figure 2-3](#)). Additionally, the number of RBCs was higher in RCCs processed using the WBF method compared to the RCF method ([Figure 2-4](#)), suggesting a potential advantage of the WBF method in preserving RBC integrity during processing. The final volume between RCCs processed using the WBF and RCF methods underscores potential efficiency disparities in processing techniques, with RCCs processed using the WBF demonstrating higher final volume ([Figure 2-10](#)). Moreover, differences in MCV and HCT levels were observed, with RCCs processed with WBF showing lower MCV and higher HCT levels compared to RCF ([Figure 2-5](#), [Figure 2-6](#)). Interestingly, while no significant differences were found in the estimated median density of RCCs processed using different methods, significant variations were observed in RDW ([Figure 2-8](#)), indicating differences in RBC size variability between the two methods. Unit-to-unit analysis revealed variations in the proportion of Y- and O-RBC subpopulations, with specific units showing significant differences ([Figure 2-11](#)). However, when analyzing cumulative data across all units, no significant differences were found in the proportion of

Y- and O-RBCs between the two methods ([Figure 2-12](#), [Figure 2-13](#)). Overall, these findings provide valuable insights into the impact of the RCF and WBF methods on the distribution of RBCs within the RCC and the efficiency and quality of RCC transfusion.

#### **2.4.1 Assessing RBC Indices Variation across RCCs Produced by Different Methods**

Previous investigations have illuminated substantial disparities in RCCs produced using distinct manufacturing methods. (14) However, previous studies have generally overlooked the potential impact of donor characteristics, such as age and sex, on RBC distribution within RCCs. (14,17) Mykhailova et al. demonstrated variability in the RBC distribution within the RCC among individual blood donors of different sexes and ages, with a shift observed over hypothermic storage time. (52,53) Remarkably, the sex of donors was found to be significantly associated with the distribution of RBCs, with male RCC units containing a higher proportion of dense RBCs (O-RBCs) compared to their female counterparts. (52,53) In this study, this gap was addressed by eliminating donor-related variables through the splitting approach of whole blood units. In this approach, each half underwent a different processing method. The results of this study align with previous research, emphasizing the significant influence of manufacturing methods on the composition of RCCs. RCF-derived RCCs demonstrated lower HCT, Hb, RBC count, and volume compared to WBF-derived RCCs. While Hb loss occurs during leukoreduction in both methods, the significantly lower level of Hb, HCT, RBC count, and volume in RCF-derived RCCs compared to WBF-derived RCC could potentially be explained by the loss of RBCs associated with the buffy coat separation step. These findings are in line with previous studies, which have consistently shown that RCCs produced by the RCF method have significantly lower HCT, Hb, RBC count, and volume compared to those produced by the WBF method. (14) The disparity in MCV between the two groups of units suggests distinct characteristics in the size and morphology of RBCs resulting from the different processing methods. Contrary to our expectations, the MCV results revealed that RCCs derived through the RCF method exhibited higher MCV compared to those derived through the WBF method in 7 out of 12 units. Considering the inverse relationship between the volume of RBCs and their biological age (40,54,55), the lower MCV values in WBF-derived RCCs suggest a higher proportion of O-RBCs in these units. However,

these findings contradict previous studies, which have indicated that RCCs derived through the WBF method typically have higher MCV values. (14) This discrepancy in MCV may be associated with the increased hold time before processing whole blood. Overnight holding of whole blood at room temperature has been shown to affect RBCs differently compared to those processed within a 4-hour time frame, including decreased supernatant  $K^+$  level and higher hemolysis rates. (56,57) However, there is no available data on the impact of holding time on RBC volume.

#### **2.4.2 Density-Based Distribution of RBC Subpopulations in RCCs Produced by Different Methods**

Analyzing EMD results demonstrated no significant differences in the EMD of RCCs processed using different methods. EMD represents the density at which the ratio of Y- to O-RBCs is 1:1. Considering that the density distribution of RBCs follows a Gaussian curve, with Y-RBCs on one end and O-RBCs on the other, the EMD acts as the threshold defining the distribution of RBCs along this curve, ensuring an equal partitioning of the spectrum. Therefore, even though the EMD remains consistent, the distribution of Y- and O-RBCs at either end of the spectrum may vary, resulting in similar EMD values despite differences in the proportion of Y-RBCs and O-RBCs. Unit-to-unit analysis of the density-based distribution of RBC subpopulations highlighted further variability between units. While specific units exhibited consistent differences in the proportion of RBC subpopulations between the two processing methods, others showed no significant disparities. Examining the proportion of biological Y-RBCs revealed that RCCs processed via the RCF method (units 3, 4, 5, 7, 8, 9, 11, and 12) exhibited a significantly higher proportion of Y-RBCs compared to those processed using the WBF method. This finding contradicts our initial hypothesis, which anticipated lower Y-RBC proportions in RCF-derived RCCs. Conversely, analyzing the proportion of biological O-RBCs indicated that RCCs processed via the WBF method (units 4, 5, 6, 7, 8, 10, and 12) displayed a significantly higher percentage of O-RBCs compared to those processed using the RCF method, which is in alignment with our hypothesis regarding higher O-RBC proportions in WBF-derived RCCs. However, the cumulative analysis of the density-based proportion of Y- and O-RBCs across all units revealed no significant differences, suggesting that

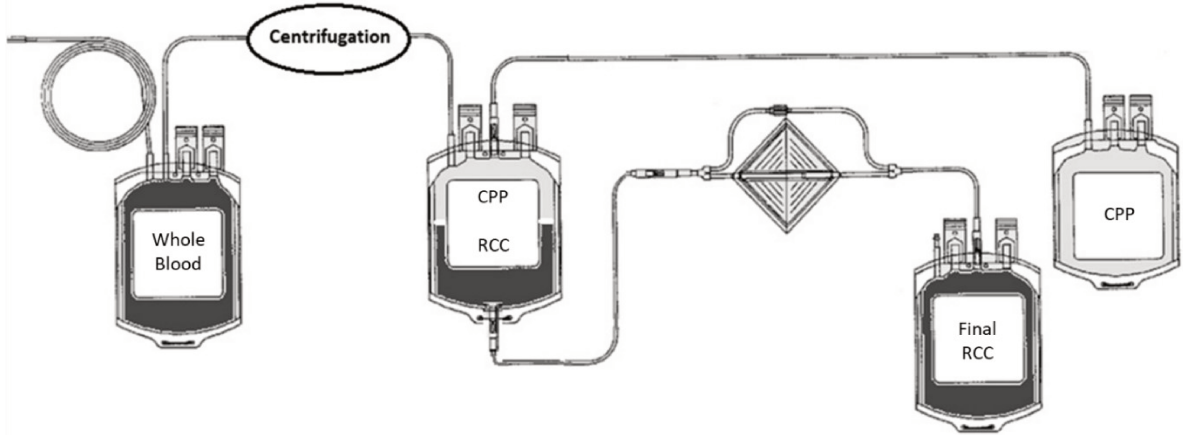
while variations exist at the individual unit level, these differences may not be apparent when considering the overall dataset. Analysis of the ratio of biologically Y-to-O-RBCs across units processed using different manufacturing methods revealed no significant differences. This indicates that while there may be differences in the absolute numbers of Y-RBCs and O-RBCs between units processed via different methods, the relative balance between these subpopulations within each unit remains stable. This finding suggests that the manufacturing method may not have a substantial impact on the overall Y-to-O ratio of RBCs within RCC units.

## **2.5 Conclusion**

The study provides a comprehensive analysis of the density-based distribution of RBC subpopulations within RCCs produced using RCF and WBF methods. Significant differences were observed in various parameters, with RCF-derived RCCs exhibiting lower HCT, Hb, RBC count, and volume compared to WBF-derived RCCs. No significant differences were found in the EMD values of RCCs produced using different methods. Unit-to-unit analysis revealed variability in the proportion of Y- and O-RBC subpopulations, with some units showing consistent differences between processing methods. However, no significant differences were observed in the Y-to-O-RBCs ratio between the two methods, suggesting a stable balance between these subpopulations regardless of the manufacturing method employed. Variations observed in the distribution of RBCs in RCCs may be attributed to donor-related factors such as age and sex rather than the manufacturing method. This highlights the importance of considering donor-related factors when assessing RCC composition. Despite the importance of these findings, it's essential to acknowledge potential limitations, such as errors introduced by the Percoll<sup>®</sup> separation method and manual pipetting in calculating the proportion of RBC subpopulations. Future research should aim to address these limitations and further explore the impact of manufacturing methods on RCC composition by taking into account factors such as the age and sex of donors and the initial composition of whole blood. Additionally, biotin labeling of RBCs at both ends of the spectrum could enhance our understanding by enabling us to trace these subpopulations throughout various manufacturing stages.

## Figure 2-1 Comparison of Red Cell Filtration and Whole Blood Filtration Processing Methods

A. RCF



B. WBF

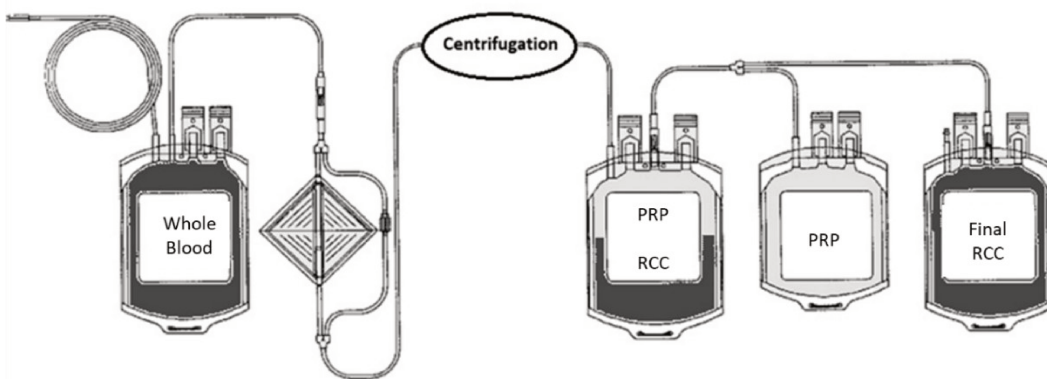


**Figure 2-1:** Figure A illustrates the Red Cell Filtration (RCF) method, starting with the collection of whole blood with CPD-anticoagulant, followed by rapid cooling and centrifugation. The buffy coat and packed RBCs are separated using hard spin centrifugation and semiautomated component separation. Leukoreduction is achieved through filtration, followed by a hold period before leukoreduction. Figure B depicts the Whole Blood Filtration (WBF) method, where whole blood units are collected and cooled, then filtered within 72 hours of the stop-bleeding time. Units undergo centrifugation and platelet-rich plasma (PRP) and packed RBCs are separated using a manual separator. The separated RBCs are transferred into a final bag with SAGM and stored for further analysis.

## Figure 2-2 Preparation of Percoll® Density Gradients for RBC Subpopulation Isolation

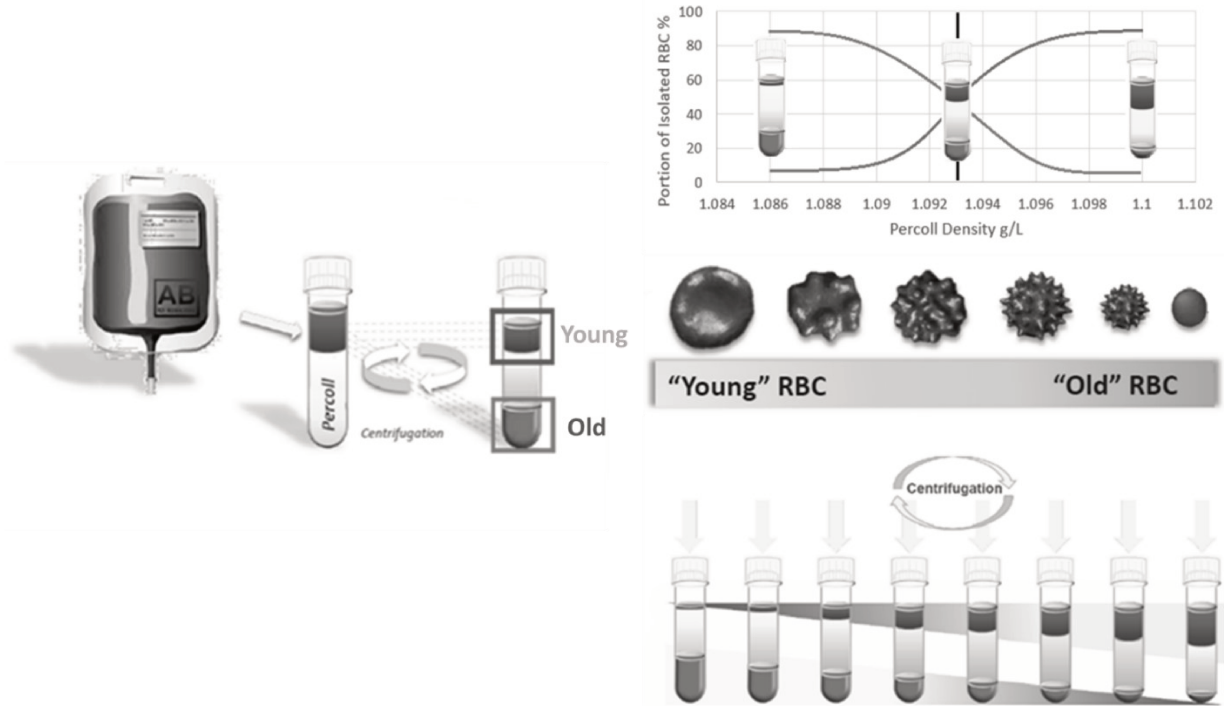


**Figure 2-2:** Percoll® solutions of varying densities were meticulously prepared in round-bottom 5 mL tubes. RBCs were then gently layered onto the Percoll® solutions and subjected to centrifugation. Subsequently, less dense RBCs were carefully isolated from the upper layer of the Percoll® solution, while the denser RBC subpopulation was isolated from the bottom of the tubes. These distinct RBC subpopulations were washed using PBS, and the volume of each subpopulation was measured using a calibrated pipette. RBC indices for each subpopulation were measured using a Coulter counter. The proportion of each RBC subpopulation was then calculated, and the estimated median density was determined.

**Figure 2-3 Comparison of Hemoglobin Levels between RCF and WBF Methods**

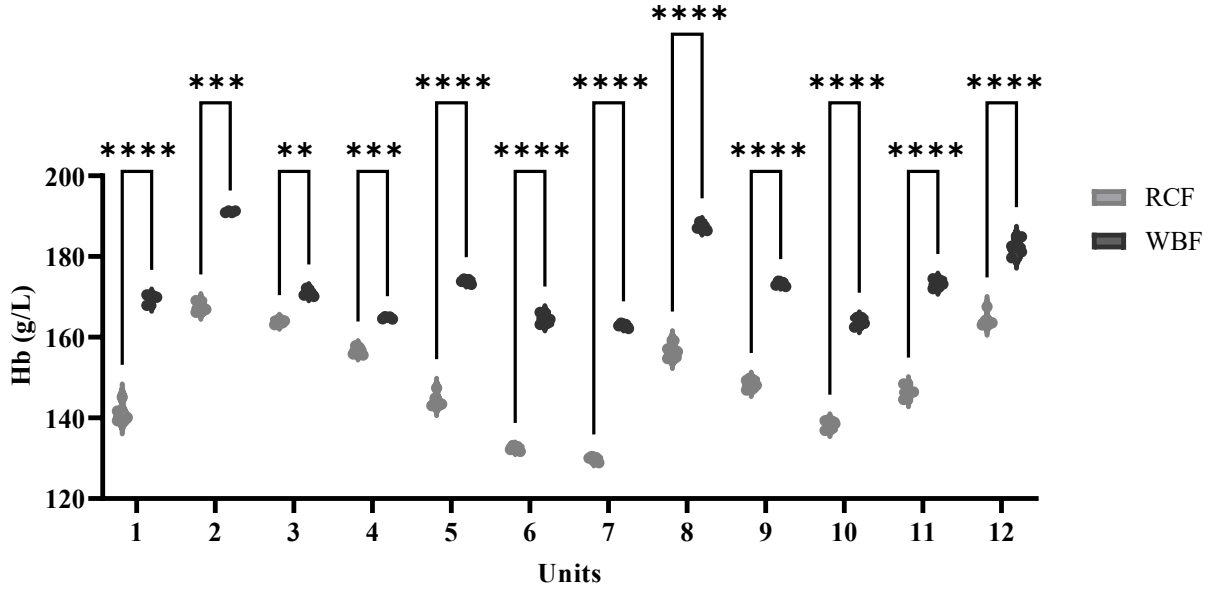


**Figure 2-3:** The figure illustrates significant differences in hemoglobin levels among units processed using different methods, with red cell concentrates produced by the RCF method showing lower hemoglobin levels compared to those processed with the WBF method ( $p < 0.0001$ ). Statistical significance denoted by \*:  $p < 0.05$ , \*\*:  $p < 0.01$ , \*\*\*:  $p < 0.001$ , and \*\*\*\*:  $p < 0.0001$ .

**Figure 2-4 Comparison of Red Blood Cell Counts between RCF and WBF Methods**

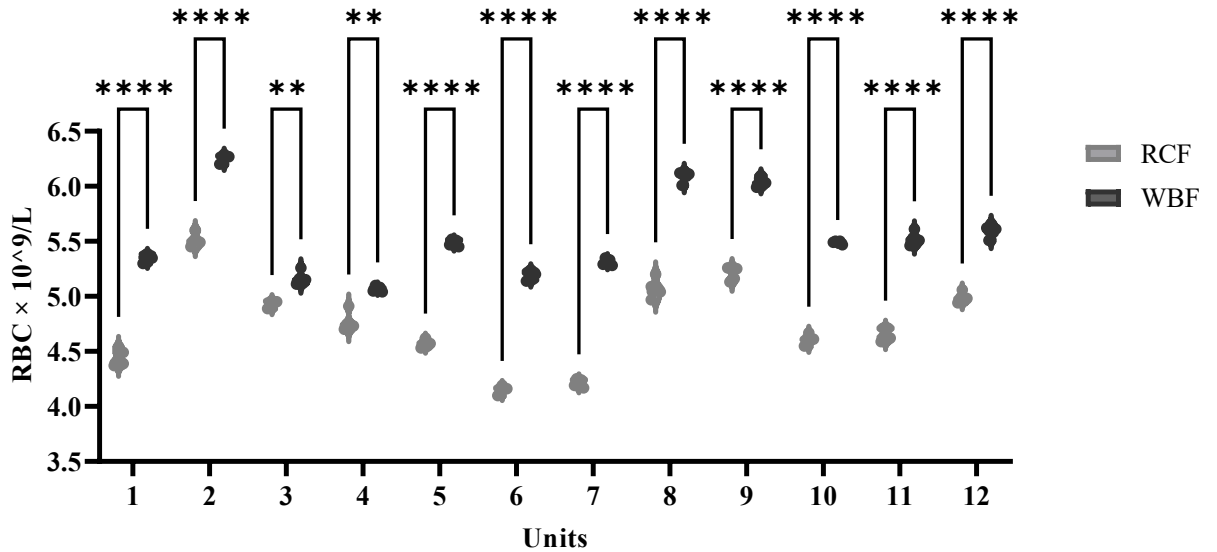


**Figure 2-4:** The figure depicts a significant difference in RBC count among units processed using different methods. Units processed with the WBF method exhibited a significantly higher number of red blood cells compared to those processed with the RCF method ( $p < 0.0001$ ). Statistical significance denoted by \*:  $p < 0.05$ , \*\*:  $p < 0.01$ , \*\*\*:  $p < 0.001$ , and \*\*\*\*:  $p < 0.0001$ .

**Figure 2-5 Comparison of Mean Corpuscular Volume (MCV) between RCF and WBF Methods**

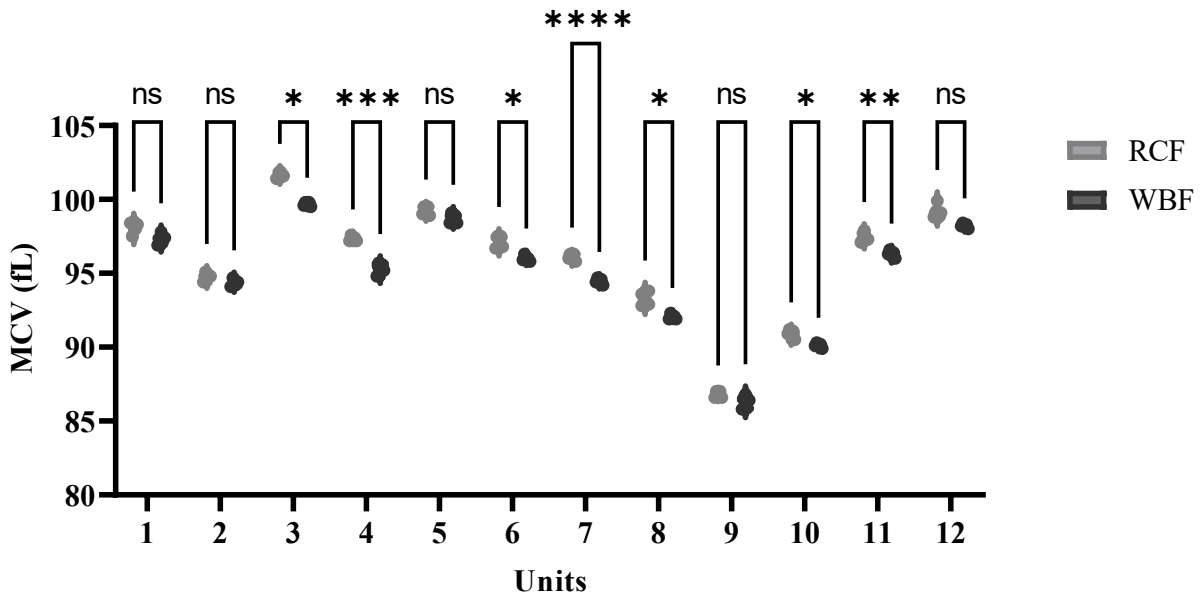


**Figure 2-5:** The figure illustrates significant variations in MCV levels among RCCs processed using distinct methods. Specifically, RCCs subjected to the WBF method exhibited significantly lower MCV values in units 3, 4, 6, 7, 8, 10, and 11 compared to those processed via the RCF method. However, upon analyzing each unit individually, we did not observe significant differences among RCCs produced by different methods in some units, including units 1, 2, 5, 9, and 12. Statistical significance denoted by \*:  $p < 0.05$ , \*\*:  $p < 0.01$ , \*\*\*:  $p < 0.001$ , and \*\*\*\*:  $p < 0.0001$ .

**Figure 2-6 Comparison of Hematocrit (HCT) Levels between RCF and WBF Methods**

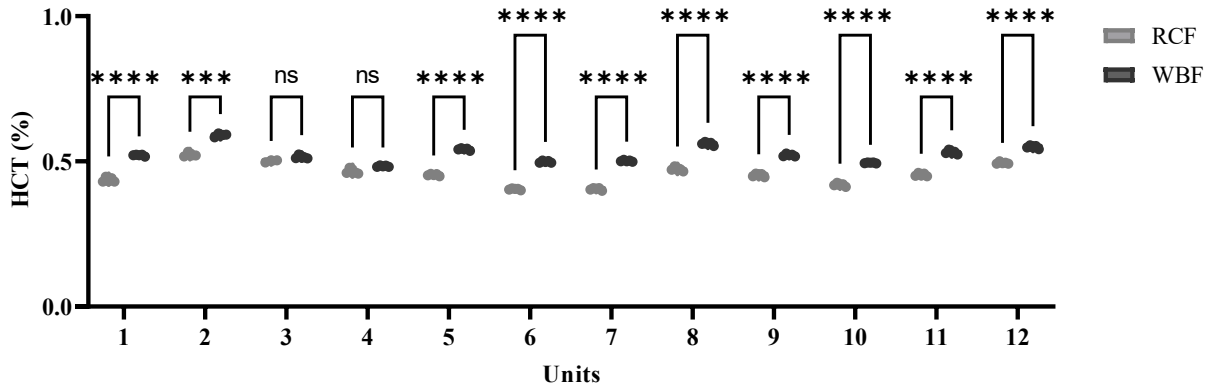


**Figure 2-6:** The figure illustrates significant differences in HCT among units processed using different methods. Units processed with the WBF method displayed significantly higher hematocrit levels compared to those processed with the RCF method ( $p < 0.0001$ ). However, no significant differences were observed in units 3 and 4 between the different processing methods. Statistical significance denoted by \*:  $p < 0.05$ , \*\*:  $p < 0.01$ , \*\*\*:  $p < 0.001$ , and \*\*\*\*:  $p < 0.0001$ .

**Figure 2-7 Comparison of Estimated Median Density between RCF and WBF Methods**

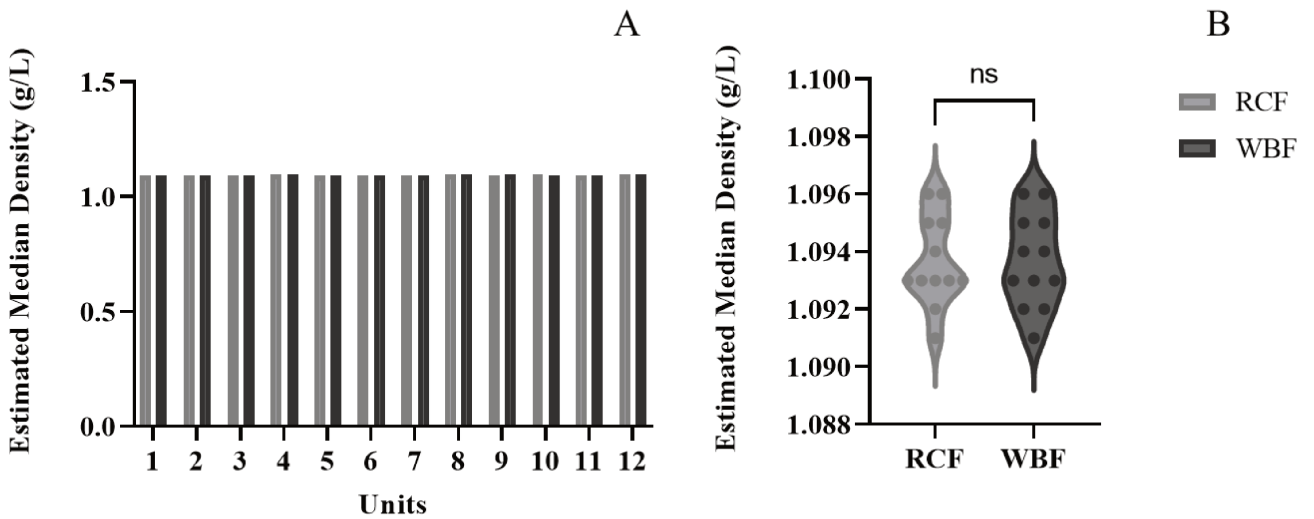


**Figure 2-7:** Figure A illustrates the unit-to-unit comparison of EMD among RCCs processed using different methods. ANOVA analysis revealed no significant differences between units ( $p < 0.9999$ ). In Figure B, the Student's t-test analysis of EMD across RCC units also showed no significant differences in the estimated median density between RCCs produced by the RCF and WBF methods ( $p < 0.9999$ ).

**Figure 2-8 Comparison of Red Cell Distribution Width (RDW) between RCF and WBF Methods**

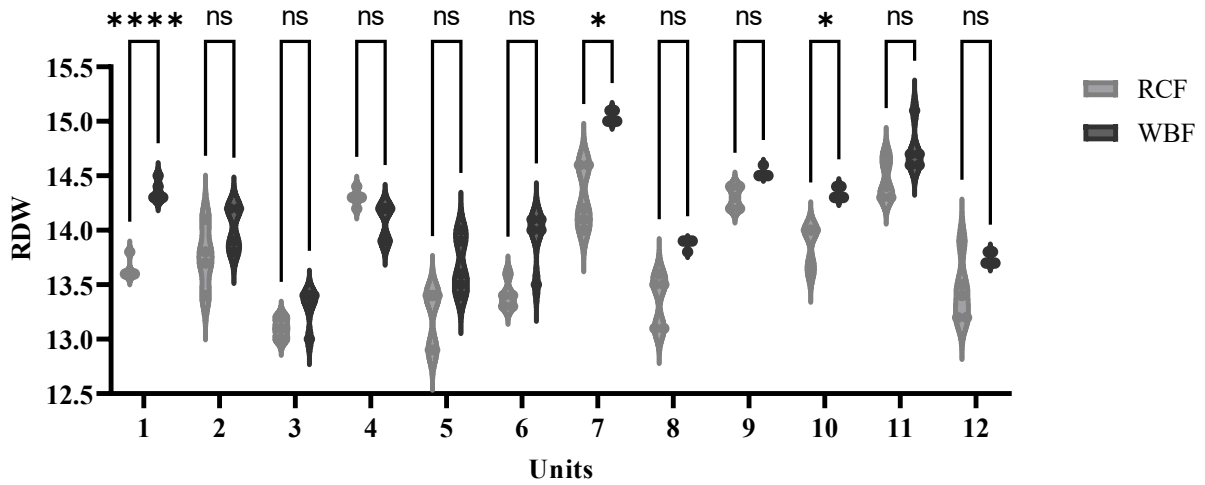


**Figure 2-8:** The graph illustrates significant differences in RDW among units processed using different methods. Units processed with the WBF method exhibited significantly higher RDW values compared to those processed with the RCF method. This difference was more pronounced in some units (1, 7, and 10); however, it did not reach statistically significant levels in other units. Statistical significance denoted by \*:  $p < 0.05$ , \*\*:  $p < 0.01$ , \*\*\*:  $p < 0.001$ , and \*\*\*\*:  $p < 0.0001$ .

**Figure 2-9 Comparison of Mean Corpuscular Hemoglobin Concentration (MCHC) between RCF and WBF Methods**

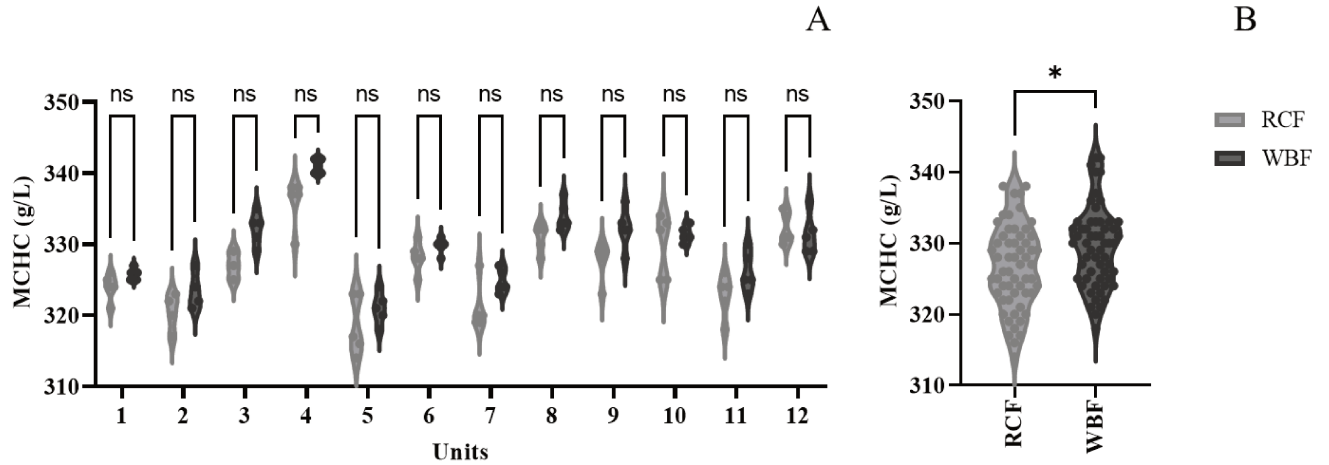


**Figure 2-9:** Figure A illustrates the analysis of Mean Corpuscular Hemoglobin Concentration (MCHC) in RCCs processed using different methods, conducted using ANOVA analysis. The unit-to-unit comparison showed no significant differences in MCHC values among RCCs processed using different methods ( $p > 0.9999$ ). In Figure B, the Student's t-test analysis demonstrated significant differences among units processed using different methods, with the WBF method showing higher MCHC compared to the RCF method ( $p = 0.0107$ ). Statistical significance denoted by \*:  $p < 0.05$ , \*\*:  $p < 0.01$ , \*\*\*:  $p < 0.001$ , and \*\*\*\*:  $p < 0.0001$ .

**Figure 2-10 Comparison of Final Volume Ratios in RCCs Processed with Different Methods**

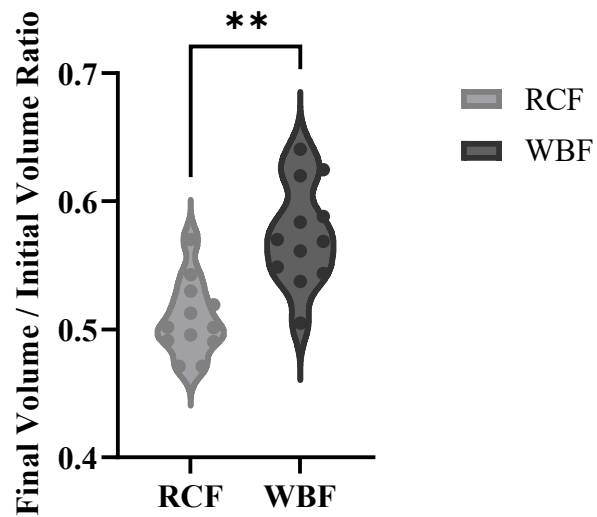


**Figure 2-10:** The figure illustrates the comparison of final volume ratios in RCCs processed using the WBF and RCF methods. Units processed with the WBF method exhibited a significantly higher final volume compared to those processed with the RCF method ( $p=0.0012$ ). Statistical significance denoted by \*:  $p<0.05$ , \*\*:  $p<0.01$ , \*\*\*:  $p<0.001$ , and \*\*\*\*:  $p<0.0001$ .

**Figure 2-11 Unit-to-Unit Comparison of Density-Based Proportion of Red Blood Cells**

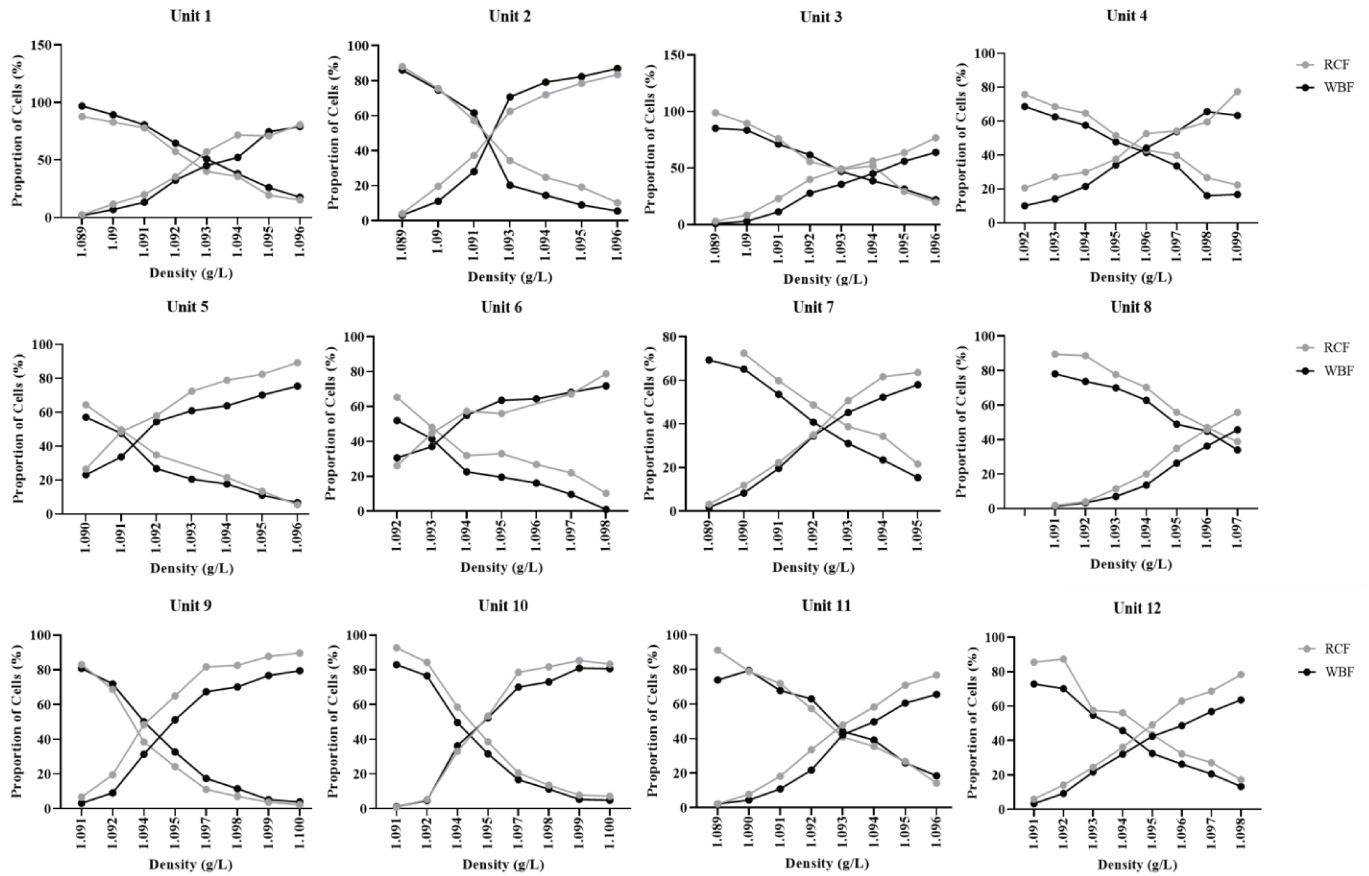


**Figure 2-11:** The figure illustrates the distribution of RBC subpopulations based on their density using different manufacturing methods. In units 1, 2, 6, and 10, no significant differences were observed in the proportion of Y-RBCs among RCCs produced using different manufacturing methods. However, in units 3, 4, 5, 7, 8, 9, 11, and 12, a significantly higher proportion of Y-RBCs was observed at each density in the RCF method compared to the WBF method. No significant differences were observed in the old proportion of RBC subpopulations between RCCs processed using different manufacturing methods, particularly in units 1, 2, 3, 9, and 11. However, units 4, 5, 6, 7, 8, 10, and 12 demonstrate a significantly higher proportion of O-RBCs at each density in the RCF method compared to the WBF method.

**Figure 2-12 Analysis of Young Proportion of RBC Subpopulations in RCCs Processed Using Different Methods**

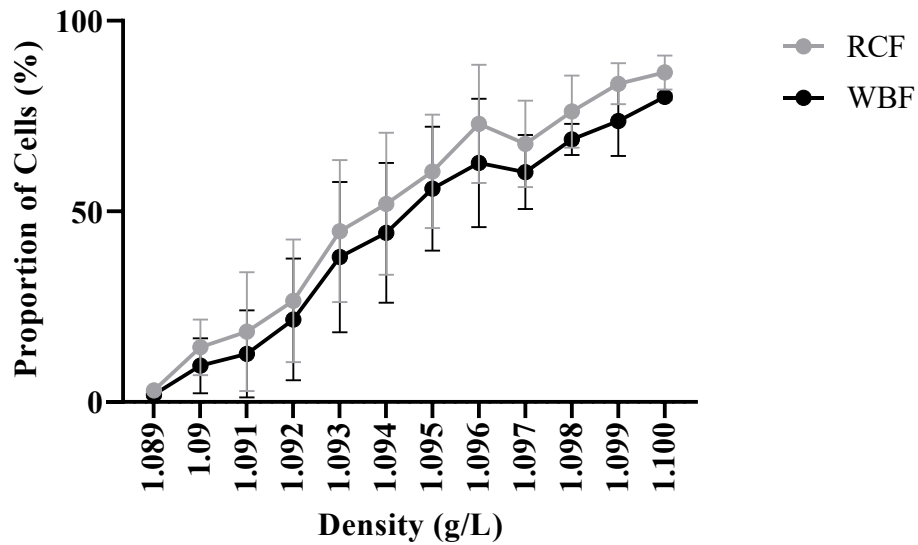


**Figure 2-12:** The figure illustrates the comparison of the young proportion of RBC subpopulations based on their density across units processed using different manufacturing methods. The mixed-effect analysis of the proportion of Y-RBCs in units processed using different methods showed no significant differences across all RCC units ( $p=0.3134$ ).

**Figure 2-13 Analysis of Old Proportion of RBC Subpopulations in RCCs Processed Using Different Methods**

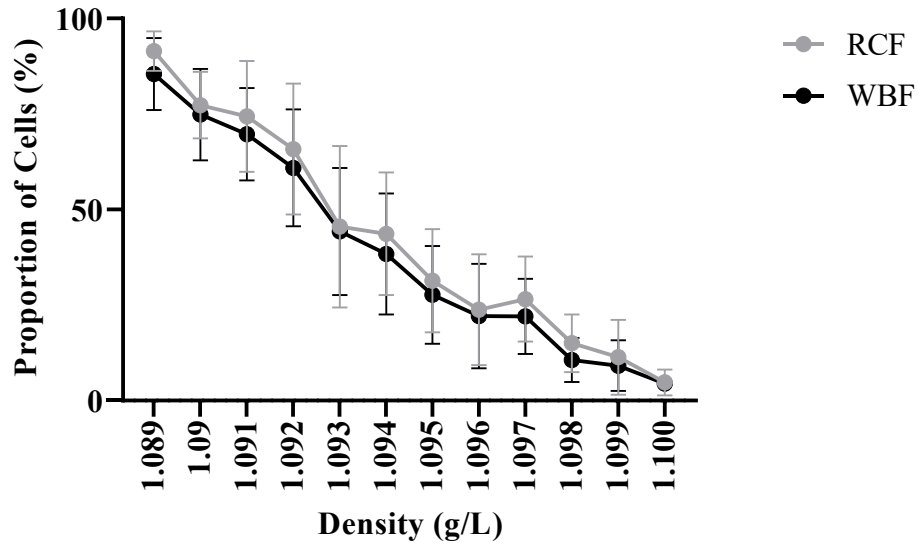


**Figure 2-13:** The figure illustrates the comparison of the old proportion of RBC subpopulations based on their density across units processed using different manufacturing methods. The mixed effect analysis of the proportion of O-RBCs in units processed using different methods showed no significant differences across all RCC units ( $p=0.4967$ ).

**Figure 2-14 Comparative Analysis of Density Distribution of RCCs Processed Using Different Methods**

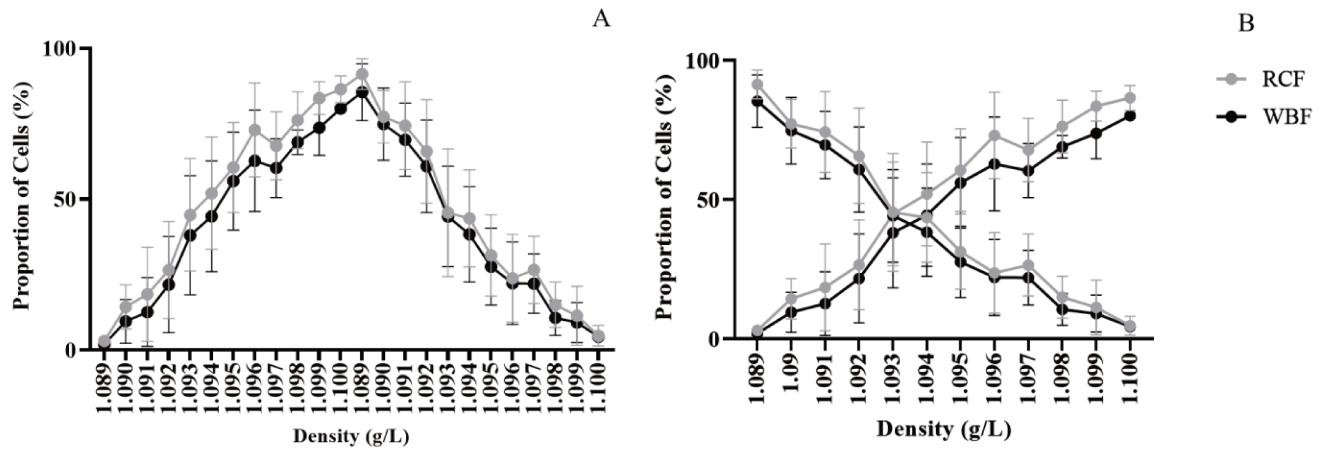


**Figure 2-14:** Figure A presents a cumulative analysis of the data on the distribution of RBCs based on their density. No significant differences are observed between the two manufacturing methods. Figure B illustrates the cumulative data of density distribution and EMD of RCCs processed using two different methods. No significant differences were observed between the methods.

**Figure 2-15 Comparison of Young to Old RBC Ratio across Units Processed Using Different Manufacturing Methods**

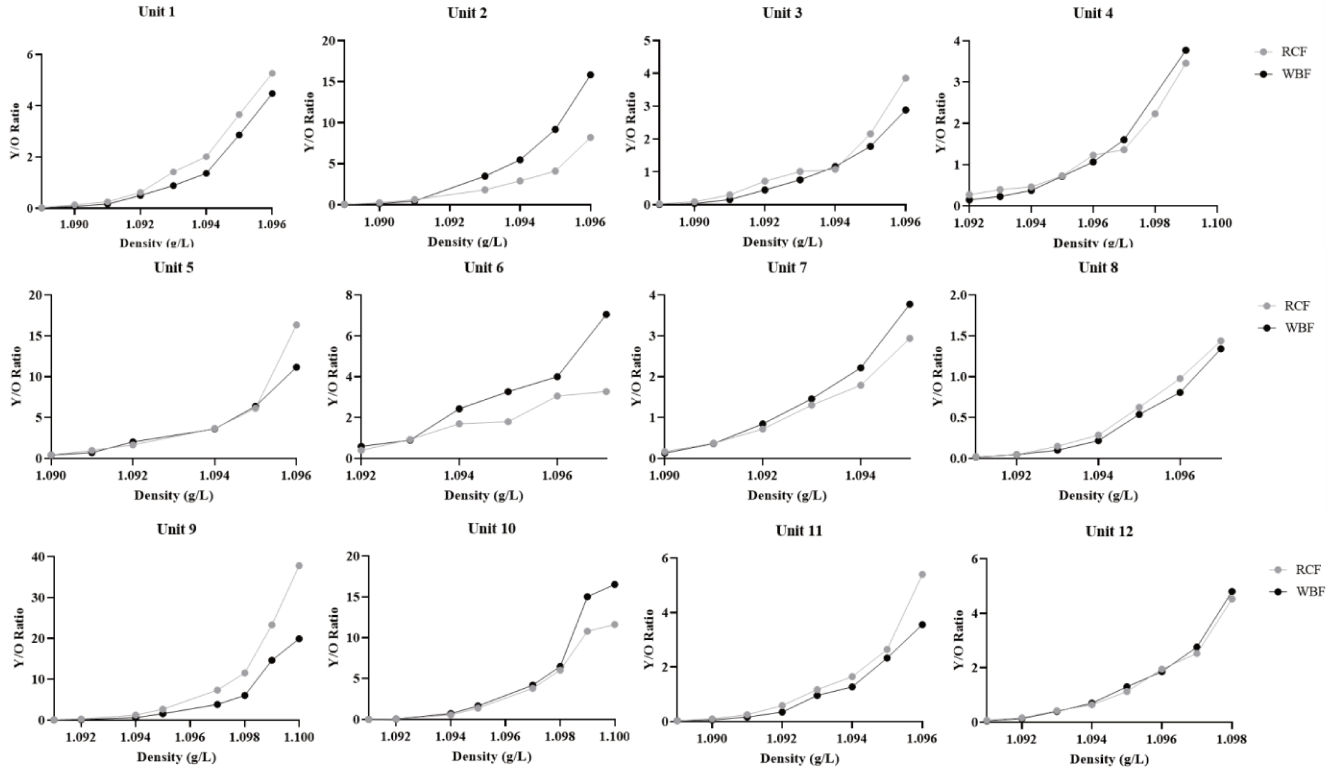


**Figure 2-15:** The figure illustrates the ratio of biological Y-to-O-RBCs in units processed using either the RCF or WBF methods. Across all 12 units, no significant differences were observed in the Y-to-O-RBC ratio between the different processing methods.

**Figure 2-16 Mixed Effect Analysis of Aggregate Data on Young to Old RBC Ratio**

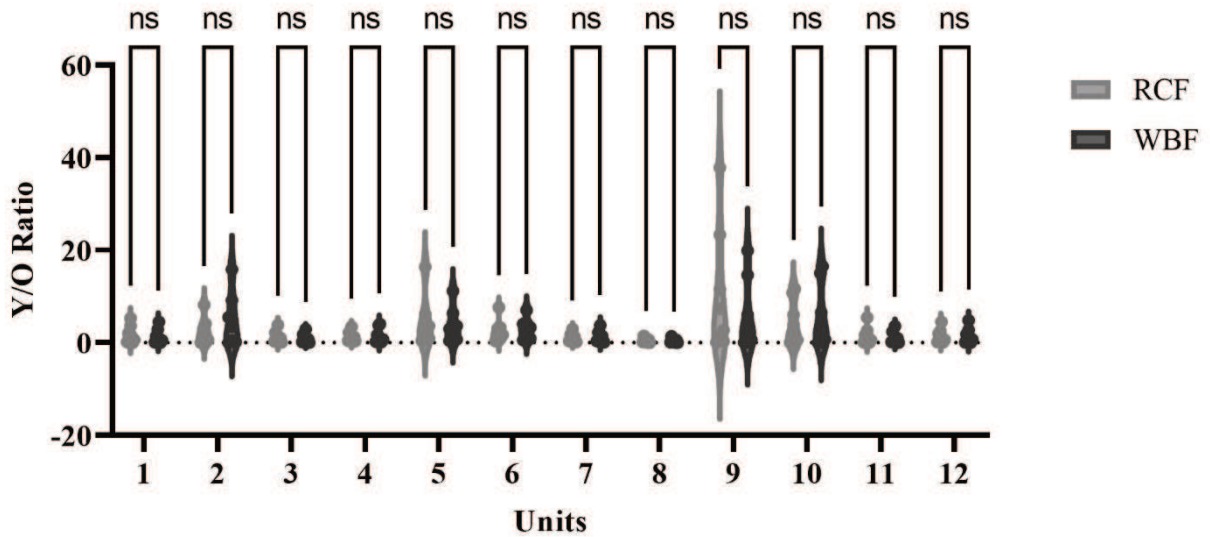


**Figure 2-16:** The figure illustrates the ratio of Y-to-O-RBC across all units. No significant differences were observed in the ratio of Y-to-O- RBCs between units processed using different manufacturing methods.

## 2.6 References

1. Ramirez-Arcos S, Marks DC, Acker JP, Sheffield WP. Quality and Safety of Blood Products. *Journal of Blood Transfusion*. 2016;2016:2482157.
2. Tzounakas VL, Georgatzakou HT, Kriebardis AG, Voulgaridou AI, Stamoulis KE, Foudoulaki-Paparizos LE, et al. Donor variation effect on red blood cell storage lesion: A multivariable, yet consistent, story. *Transfusion (Paris)*. 2016;56(6):1274–86.
3. Jordan A, Chen D, Yi QL, Kaniyas T, Gladwin MT, Acker JP. Assessing the influence of component processing and donor characteristics on quality of red cell concentrates using quality control data. *Vox Sang*. 2016;111(1):8–15.
4. Dumaswala UJ, Dumaswala RU, Levin DS, Greenwalt TJ. Improved red blood cell preservation correlates with decreased loss of bands 3, 4.1, acetylcholinesterase, and lipids in microvesicles. *Blood*. 1996;87(4):1612–6.
5. Turner TR, Lautner L, Hill A, Howell A, Skeate R, Acker JP. Evaluating the quality of red blood cell concentrates irradiated before or after cryopreservation. *Transfusion (Paris)*. 2020;60(1):26–9.
6. Mollison PL. The introduction of citrate as an anticoagulant for transfusion and of glucose as a red cell preservative. *British Journal of Haematology*. 2000;108(1):13–8.
7. Bratosin D, Leszczynski S, Sartiaux C, Fontaine O, Descamps J, Huart JJ, et al. Improved storage of erythrocytes by prior leukodepletion: Flow cytometric evaluation of stored erythrocytes. *Communications in Clinical Cytometry*. 2001;46(6):351–6.
8. Wang D, Sun J, Solomon SB, Klein HG, Natanson C. Transfusion of older stored blood and risk of death: A meta-analysis. *Transfusion (Paris)*. 2012;52(6):1184–95.
9. Hod EA, Spitalnik SL. Harmful effects of transfusion of older stored red blood cells: Iron and inflammation. *Transfusion (Paris)*. 2011;51(4):881–5.
10. Lannan KL, Sahler J, Spinelli SL, Phipps RP, Blumberg N. Transfusion immunomodulation - the case for leukoreduced and (perhaps) washed transfusions. *Blood Cells, Molecules, and Diseases*. 2013;50(1):61–8.
11. Heddle NM, Arnold DM, Acker JP, Liu Y, Barty RL, Eikelboom JW, et al. Red blood cell processing methods and in-hospital mortality: A transfusion registry cohort study. *The Lancet haematology*. 2016;3(5):e246–54.
12. Bakkour S, Acker JP, Chafets DM, Inglis HC, Norris PJ, Lee TH, et al. Manufacturing method affects mitochondrial DNA release and extracellular vesicle composition in stored red blood cells. *Vox Sang*. 2016;111(1):22–32.

13. Hansen AL, Turner TR, Kurach JDR, Acker JP. Quality of red blood cells washed using a second wash sequence on an automated cell processor. *Transfusion (Paris)*. 2015 Oct 1;55(10):2415–21.
14. Acker JP, Hansen AL, Kurach JDR, Turner TR, Croteau I, Jenkins C. A quality monitoring program for red blood cell components: In vitro quality indicators before and after implementation of semiautomated processing. *Transfusion (Paris)*. 2014;54(10):2534–43.
15. Levin E, Jenkins C, Culibrk B, Gyöngyössi-Isa MIC, Serrano K, Devine D V. Development of a quality monitoring program for platelet components: A report of the first four years' experience at Canadian Blood Services. *Transfusion (Paris)*. 2012 Apr;52(4):810–8.
16. Sheffield WP, Bhakta V, Jenkins C, Devine D V. Conversion to the buffy coat method and quality of frozen plasma derived from whole blood donations in Canada. *Transfusion (Paris)*. 2010 May;50(5):1043–9.
17. Hansen AL, Kurach JDR, Turner TR, Jenkins C, Busch MP, Norris PJ, et al. The effect of processing method on the in vitro characteristics of red blood cell products. *Vox Sang*. 2015;108(4):350–8.
18. Radwanski K, Garraud O, Cognasse F, Hamzeh-Cognasse H, Payrat JM, Min K. The effects of red blood cell preparation method on in vitro markers of red blood cell aging and inflammatory response. *Transfusion (Paris)*. 2013;53(12):3128–38.
19. Devine D v., Howe D. Processing of whole blood into cellular components and plasma. *ISBT Science Series*. 2010;5(n1):78–82.
20. Högman CF, Eriksson L, Hedlund K, Wallvik J. The Bottom and Top System: A New Technique for Blood Component Preparation and Storage. *Vox Sang*. 1988;55(4):211–7.
21. Card RT, Mohandas N, Perkins HA, Shohet SB. Deformability of stored red blood cells. *Transfusion (Paris)*. 1982;22(2):96–101.
22. Almizraq RJ, Norris PJ, Inglis H, Menocha S, Wirtz MR, Juffermans N, et al. Blood manufacturing methods affect red blood cell product characteristics and immunomodulatory activity. *Blood Advances*. 2018;2(18):2296–306.
23. Almizraq RJ, Seghatchian J, Acker JP. Extracellular vesicles in transfusion-related immunomodulation and the role of blood component manufacturing. *Transfusion and Apheresis Science*. 2016;55(3):281–91.
24. Almizraq RJ, Holovati JL, Acker JP. Characteristics of Extracellular Vesicles in Red Blood Concentrates Change with Storage Time and Blood Manufacturing Method. *Transfusion Medicine and Hemotherapy*. 2018 May 1;45(3):185–93.

25. D'Alessandro A, Blasi B, D'Amici GM, Marrocco C, Zolla L. Red blood cell subpopulations in freshly drawn blood: Application of proteomics and metabolomics to a decades-long biological issue. *Blood Transfusion*. 2013;11(1):75–87.
26. Bosman GJCGM, Werre JM, Willekens FLA, Novotný VMJ. Erythrocyte ageing in vivo and in vitro: Structural aspects and implications for transfusion. *Transfusion Medicine*. 2008;18(6):335–47.
27. Weisel JW, Litvinov RI. Red blood cells: the forgotten player in hemostasis and thrombosis. *Journal of Thrombosis and Haemostasis*. 2019;17(2):271–82.
28. Kiefer CR, Snyder LM. Oxidation and erythrocyte senescence. *Current Opinion in Hematology*. 2000;7(2):113–6.
29. Kay MMB, Goodman SR, Sorensen K, Whitfield CF, Wong P, Zaki L, et al. Senescent cell antigen is immunologically related to band 3. *Proceedings of the National Academy of Sciences of the United States of America*. 1983;80(6 I):1631–5.
30. Lutz HU, Stammer P, Fasler S. Preferential formation of C3b-IgG complexes in vitro and in vivo from nascent C3b and naturally occurring anti-band 3 antibodies. *Journal of Biological Chemistry*. 1993;268(23):17418–26.
31. Khandelwal S, Saxena RK. A role of phosphatidylserine externalization in clearance of erythrocytes exposed to stress but not in eliminating aging populations of erythrocyte in mice. *Experimental Gerontology*. 2008;43(8):764–70.
32. Snyder LM, Garver F, Liu SC, Leb L, Trainor J, Fortier NL. Demonstration of haemoglobin associated with isolated, purified spectrin from senescent human red cells. *British Journal of Haematology*. 1985;61(3):415–9.
33. Snyder LM, Fortier NL, Trainor J, Jacobs J, Leb L, Lubin B, et al. Effect of hydrogen peroxide exposure on normal human erythrocyte deformability, morphology, surface characteristics, and spectrin-hemoglobin cross-linking. *Journal of Clinical Investigation*. 1985;76(5):1971–7.
34. Snyder LM, Leb L, Piotrowski J, Sauberman N, Liu SC, Fortier NL. Irreversible spectrin-haemoglobin crosslinking in vivo: a marker for red cell senescence. *British Journal of Haematology*. 1983 Mar;53(3):379-84.
35. Samaja M, Rubinacci A, Motterlini R, de Ponti A, Portinaro N. Red cell aging and active calcium transport. *Experimental Gerontology*. 1990;25(3–4):279–86.
36. Giel J.C. G.M. Bosman FLAW and JMW. Erythrocyte aging- a more than superficial.pdf. *Cellular Physiology and Biochemistry*. 2005;16:1–8.
37. Lee TH, Kim SU, Yu SL, Kim SH, Park DS, Moon HB, Dho SH, Kwon KS, Kwon HJ, Han YH, Jeong S, Kang SW, Shin HS, Lee KK, Rhee SG, Yu DY. Peroxiredoxin II is essential for sustaining life span of erythrocytes in mice. *Blood*. 2003 Jun 15;101(12):5033-8.

38. Nagababu E, Chrest FJ, Rifkind JM. Hydrogen-peroxide-induced heme degradation in red blood cells: the protective roles of catalase and glutathione peroxidase. *Biochimica et Biophysica Acta*. 2003 Mar 17;1620(1-3):211-7.
39. Gonzales R, Auclair C, Voisin E, Gautero H, Dhermy D, Boivin P. Superoxide dismutase, catalase, and glutathione peroxidase in red blood cells from patients with malignant diseases. *Cancer Research*. 1984 Sep;44(9):4137-9.
40. Bosch FH, Werre JM, Roerdinkholder-Stoelwinder B, Huls TH, Willekens FLA, Halie MR. Characteristics of red blood cell populations fractionated with a combination of counterflow centrifugation and Percoll separation. *Blood*. 1992;79(1):254–60.
41. Triadou, P., R. Girot, D. Rebibo, D. Lemau, B. Mattlinger, P. Bolo, M. Maier, and L. Barritault. Neocytopenesis: a new approach for the transfusion of patients with thalassaemia major. *European Journal of Pediatrics* (1986) 145: 10–13.
42. Yoshida T, Prudent M, D'alessandro A. Red blood cell storage lesion: causes and potential clinical consequences. *Blood Transfusion*. 2019 Jan;17(1):27-52.
43. Mykhailova O, Olafson C, Turner TR, D'Alessandro A, Acker JP. Donor-dependent aging of young and old red blood cell subpopulations: Metabolic and functional heterogeneity. *Transfusion (Paris)*. 2020;60(11):2633–46.
44. Kanas T, Stone M, Page GP, Guo Y, Endres-Dighe SM, Lanteri MC, et al. Frequent blood donations alter susceptibility of red blood cells to storage- and stress-induced hemolysis. *Transfusion (Paris)*. 2019 Jan 1;59(1):67–78.
45. Zeller MP, Rochweg B, Jamula E, Li N, Hillis C, Acker JP, et al. Sex-mismatched red blood cell transfusions and mortality: A systematic review and meta-analysis. *Vox Sang*. 2019;114(5):505–16.
46. Piomelli S, Seaman C, Reibman J, Tytun A, Graziano J, Tabachnik N, et al. Separation of younger red cells with improved survival in vivo: an approach to chronic transfusion therapy. *Proceedings of the National Academy of Sciences of the United States of America*. 1978;75(7):3474–8.
47. Cohen AR, Schmidt JM, Martin MB, Barnsley W, Schwartz E. Clinical trial of young red cell transfusions. *The Journal of Pediatrics*. 1984;104(6):865–8.
48. Tuo WW, Wang D, Liang WJ, Huang YX. How cell number and cellular properties of blood-banked red blood cells of different cell ages decline during storage. *PLoS One*. 2014 Aug 28;9(8):e105692.
49. Key; JA. Studies On Erythrocytes, With Special Reference To Reticulum, Polychromatophilia And Mitochondria. *Arch, Intern Med*. 1921;28(5):511–49.
50. Hogan VA, Blanchette VS, Rock G. A simple method for preparing neocyte-enriched leukocyte- poor blood for transfusion-dependent patients. *Transfusion (Paris)*. 1986;26(3):253–7.

51. Unit Sampling Protocol. Dr. Jason Acker's laboratory, Version 1.3, Revised 2019-03-01.
52. Mykhailova O, Brandon-Coatham M, Phan C, Yazdanbakhsh M, Olafson C, Yi QL, Kanias T, Acker JP. Red cell concentrates from teen male donors contain poor-quality biologically older cells. *Vox Sang*. 2024 Feb 28.
53. Mykhailova O, Brandon-Coatham M, Durand K, Olafson C, Xu A, Yi QL, Kanias T, Acker JP. Estimated median density identifies donor age and sex differences in red blood cell biological age. *Transfusion*. 2024 Feb 29.
54. Lutz H, Stammler P, Fasler S, Ingold M, Fehr J. Density separation of human red blood cells on self forming Percoll. *Biochimica biophysica acta (G) General subjects*. 1992;1116(1):1–10.
55. Piomelli S, Seaman C. Mechanism of red blood cell aging: Relationship of cell density and cell age. *American Journal of Hematology*. 1993;42(1):46–52.
56. Gulliksson H, Van Der Meer PF. Storage of whole blood overnight in different blood bags preceding preparation of blood components: In vitro effects on red blood cells. *Blood Transfusion*. 2009;7(3):210–5.
57. Eckstein M, Zimmermann R, Roth T, Hauck-Dlimi B, Strasser EF, Xiang W. The effects of an overnight holding of whole blood at room temperature on haemoglobin modification and in vitro markers of red blood cell aging. *Vox Sang*. 2015 May 1;108(4):359–67.

## **Chapter 3**

**Exploring Osmotic Characteristics and Survival of Red Blood Cell Subpopulation  
Extremes Following Cryopreservation: A Biotinylation Approach**

### 3.1 Introduction

Cryopreservation is a long-term storage strategy for maintaining the quality of RBCs for commercial and medical purposes. (1) In 1940, for the first time, Dr. Charles Drew demonstrated that human RBCs can be frozen and later reconstituted. (2) The use of CPAs offers distinct mechanisms of protection against freezing injury. (3,4) In 1950, after Polge and Smith discovered the protective effect of glycerol during the freezing of spermatozoa (5), glycerol was used for RBC cryopreservation. (6) The first successful cryopreserved RBC transfusion was achieved by Mollison and Sloviter in 1951. (7) The standard method for cryopreserving RBCs in the US and Canada is high glycerol–slow cooling. This method involves adding glycerol to RBCs to a final concentration of 40% w/v and cooling at 1 °C/min to <-65 °C. (4,8,9) Cryopreserved RBCs can be stored for up to 10 years, allowing maintenance of a reliable inventory for rare blood types, individuals with adverse alloantibody formation, civil emergencies, and military applications. (10,11) Deglycerolization involves rapid thawing and washing using sodium chloride solutions. (4,8,9) While cryopreservation offers a promising method for preserving RBCs, osmotic stresses during cryoprotectant addition/removal and freezing/thawing can lead to a significant loss of RBCs, estimated at 15-20%. (12) This highlights the need for assessing the osmotic characteristics of RBC subpopulations and their vulnerability to osmotic stress caused by various stages of cryopreservation

#### 3.1.2 Impact of Biological Aging on RBC Membrane Properties

The RBC biological aging process is associated with a decline in metabolic activity, progressive failure of cellular homeostasis, and impaired antioxidant defenses. (13,14) During the biological aging process, RBCs experience a decline in ATP levels and aging-related changes in RBC membrane composition (15,16), disrupting ion homeostasis within RBCs. (17,18) These age-related alterations contribute to decreased functionality of membrane transporter proteins, (19) progressive cell shape transformation (20–38), and reduced deformability in RBCs. (39–44) This reduction in pump activity results in the accumulation of  $\text{Ca}^{2+}$  within RBCs cytoplasm and triggers calcium-sensitive  $\text{K}^+$  channels, resulting in  $\text{K}^+$  leakage and cell shrinkage. *In vitro* studies demonstrate that under non-

isotonic conditions, Y-RBCs exhibit lower hemolysis and rigidity. (20,27,45–48) Mykhailova et al. demonstrated that O-RBCs exhibit the lowest  $O_{\text{hyper}}$  and greater rigidity under osmotic gradients compared to Y-RBCs. (49,50) These findings highlight the intricate alterations in the membrane properties of RBCs as they undergo biological aging, potentially affecting the membrane permeability of distinct RBC subpopulations and their responses to osmotic stress caused by cryopreservation.

### **3.1.3 Variability in RBC Membrane Characteristics: Donor Traits and Manufacturing Methods**

The RBC membrane plays a pivotal role in mediating cellular responses to cryopreservation (51,52) (53–56), regulating osmotically induced changes in the cell volume during freezing by governing the transport of water and solutes between the cytoplasm and the extracellular milieu. (54,57–59) Higgins et al. found that the permeability of the RBC membrane to glycerol varies from cell to cell within a single donor, and prolonged deglycerolization times were observed to reduce hemolysis, suggesting a subpopulation with lower glycerol permeability. (60) Jay and Rowlands observed a wide range of glycerol permeability values in a subpopulation of RBCs within an individual. (61)

Donor-specific traits, including age, sex, and ethnicity, influence the osmotic characteristics of RBCs, with senior blood donors exhibiting higher water permeability in RBCs. (62–65) Besides donor factors, manufacturing methods can also impact the osmotic characteristics of RBCs. Alshalani et al. found that RCCs processed using the WBF manufacturing method exhibited significantly higher membrane water permeability throughout storage compared to units manufactured using the RCF method. (64) Moreover, it has been observed that manufacturing methods can influence the integrity of RBC membranes. Units prepared by the WBF method exhibited higher hemolysis and supernatant  $K^+$  compared to those processed by the RCF method, emphasizing the impact of the manufacturing process on membrane integrity. (66) Additionally, the chronologic age of RBCs is associated with increased  $L_p$ ,  $V_b$ , and  $E_a$ , resulting in higher hemolysis, supernatant  $K^+$ , and reduced deformability. (65)

The average RBC freeze-thaw-wash recovery rate of  $85.2 \pm 5.9\%$  in the high glycerol-slow cooling method with a 24-hour post-transfusion survival of 83%, demonstrating 15-20% of RBCs are lost during the cryopreservation process. (12) These findings suggest that the osmotic characteristics of RBC subpopulations are different and affected by biological age, resulting in a different recovery rate of RBC subpopulations after thawing. The purpose of this chapter was to investigate how variations in osmotic characteristics among RBC subpopulations with different biological ages contribute to their susceptibility to loss during cryopreservation-induced osmotic stress. The study aimed to compare osmotic parameters in Y- and O-RBC subpopulations, such as  $L_p$ ,  $P_s$ ,  $V_b$ ,  $E_a$ ,  $O_{\text{hyper}}$ , and  $EI_{\text{max}}$ , to understand the impact of RBC biological age on these parameters. Additionally, the recovery of Y- and O-BioRBC was examined to explore potential associations between osmotic differences and post-deglycerolization recovery rates of RBC subpopulations. We hypothesize that differences in osmotic characteristics at the cellular level, resulting from RBC biological aging, contribute to the selective loss of O-RBCs during cryopreservation. Understanding the cell-to-cell variability of osmotic characteristics of RBC subpopulations can offer valuable insights for enhancing cryopreservation protocols by considering the distribution of RBC subpopulations present within the RCC and ultimately enhance overall preservation efficiency and ensure the availability of high-quality RBC products for transfusion purposes.

## **3.2 Materials and Methods:**

### **3.2.1 Red Cell Concentrate (RCC) Selection and Pooling**

The RCCs utilized in this study were sourced from the Canadian Blood Services Blood4Research program, collected in Macopharma collection bags (LQT 7291 LX Leucoflex LCR-Diamond quadruple bottom-and-top system, CPD/SAGM 500 mL, MacoPharma, Tourcoing, France), processed via RCF method, and stored in CPD anticoagulant and SAGM at temperatures ranging from 1-6 °C. To maintain optimal integrity, the RCCs used in the experiments were within seven days of their collection. Approval for the study was obtained from both the University of Alberta Health Research Ethics Board (Biomedical Panel; Protocol #PRO00103459) and the Canadian Blood Services Research Ethics Board (Protocol #2020.005).

To minimize the potential impact of donor variations on RBC subpopulation density profiles, a pool-and-split study design was used. Seven ABO / Rh-matched RCCs were collected from available healthy volunteers of different ages and sexes. Four units were from female donors with an average age of  $70.0 \pm 2.6$  (mean  $\pm$  SD), CV: 12% years old, while three units were from male donors with an average age of  $57.6 \pm 5.0$  (mean  $\pm$  SD), CV: 24% years old. Before pooling units, the RBC indices of each RCC were measured using a hematology analyzer. Results are as follows: HCT:  $0.559 \pm 0.01$  (%) (CV: 3.18%), Hgb:  $186.01 \pm 1.63$  (g/dL) (CV: 4.38%), and MCHC:  $332.58 \pm 1.47$  (g/dL) (CV: 2.21%) ([Table 3-1](#)). The units were pooled in a waste bag from the Haemonetics Deglycerolization set (Haemonetics, ACP<sup>®</sup>215, Haemonetics Corporation, Massachusetts, USA The bag capacity is up to 4000 mL). This pooling process involved connecting the tube of the RCC units to the main tube of the waste bag using a sterile connection device. After sequentially transferring all of the RBCs to the pooling bag, the tube connections were detached using sterile sealing. The pooled unit was inverted several times to ensure thorough mixing.

### **3.2.2 Density-Fractionation using Percoll<sup>®</sup> Separation**

Percoll<sup>®</sup> separation, a technique based on density gradient centrifugation, is utilized to investigate the density distribution of RBCs within the pooled unit. A comprehensive explanation of this method can be found in Chapter 2, where all aspects of the technique are discussed in detail. An aliquot of 450 mL from the pooled RCC bag was collected into nine 50 mL conical tubes. A 25 mL aliquot was reserved for density profiling of the pooled unit, while 425 mL was used for extracting sufficient volume of the Y- and O-RBC subpopulations for further experiments. RBC indices were assessed, and the Percoll<sup>®</sup> densities necessary for creating a density panel were estimated. We estimated the Percoll<sup>®</sup> densities using the method proposed by Mykhailova et al., which involves estimating Percoll<sup>®</sup> density based on RBC indices using measurements of MCHC and MCV. (49,50)

Percoll<sup>®</sup> solutions with varying densities were carefully prepared according to predetermined tables using Percoll<sup>®</sup>, NaCl (1.5 M), and distilled H<sub>2</sub>O. Ten round-bottom tubes, each containing a specific density of Percoll<sup>®</sup> solutions (ranging from 1.089 to

1.098 g/mL), were carefully arranged. A 3 mL aliquot of each Percoll<sup>®</sup> solution was distributed into designated tubes, followed by gently layering a 1 mL aliquot of RBCs onto the solutions. The tubes underwent centrifugation, after which the Y-RBCs were extracted into separate tubes while the O-RBC pellet remained undisturbed at the bottom. The RBC subpopulations were washed with PBS, and then the supernatants were carefully removed, leaving PBS covering the packed RBCs to achieve a hematocrit range of 40-55%. The RBC indices for each subpopulation were measured using a hematology analyzer. The volume of each RBC subpopulation was measured using a calibrated adjustable-volume pipette to estimate the proportion of each subpopulation. Two distinct densities were identified and used to isolate extreme subpopulations of Y- and O-RBCs. The density of 1.091 g/mL was chosen for separating Y-RBCs, and 1.098 g/mL was selected for isolating cells with higher density (O-RBCs), constituting  $13.18 \pm 0.07\%$  and  $10.08 \pm 0.07\%$  of the total population respectively. The Percoll<sup>®</sup> separation was repeated with these selected densities (1.091, 1.098) to extract sufficient volumes of Y- and O-RBC subpopulations (with a minimum volume requirement of 20 mL per RBC subpopulation at 50% Hct) for subsequent experiments.

### **3.2.3 Biotinylation of Red Blood Cells**

Mock et al. introduced a standardized biotinylation protocol that provides a safe, reliable, and efficient method for labeling RBCs with biotin, making it suitable for clinical research use and the *in vivo* evaluation of RBC circulation and recovery in humans. (67–69) The biotinylation method was utilized to label the Y- and O-RBCs. To effectively distinguish between Y- and O-RBCs, two distinct concentrations of the biotin reagent (15  $\mu\text{g/mL}$  and 48  $\mu\text{g/mL}$ ) were employed, ensuring optimal fluorescence separation of each subpopulation using standard flow cytometry. The O-RBCs were labeled with a high concentration of biotin solution 48  $\mu\text{g/mL}$ , and Y-RBCs were labeled with a low concentration of biotin 15  $\mu\text{g/mL}$ . In a 50 mL volumetric flask, 0.75 mg of Sulfo-NHS-LC-Biotin was added to 25 mL of saline dextrose solution, including 0.2% dextrose and 0.9% sodium chloride. (Baxter, Deerfield, Illinois, USA). After the Sulfo-NHS-LC-Biotin completely dissolved through swirling on a plate, the volumetric flask was filled to the calibration mark, reaching a final volume of 50 mL using saline dextrose solution. For the

preparation of a 48 µg/L biotin solution, 24 mg of Sulfo-NHS-LC-Biotin was added to the same 50 mL volumetric flask, followed by the addition of 2.5 mL of saline dextrose solution. After thorough mixing, the solutions were sterilized by passing them through a 2 µM filter (DMSO safe, 2 µM Nylon Sterile membrane, Acrodisc® Syringe filters, PALL Corporation, Life Sciences, Hampshire, United Kingdom). (70)

To prepare the RBCs for labeling, 16.5 mL aliquots of both Y- and O-RBC subpopulations were placed into individual 50 mL conical tubes. Subsequently, 33 mL of saline dextrose solution was added to each tube for washing. The tubes were centrifuged at 2560 x g for 10 min at 20 °C with acceleration 6 and deceleration 4 (Eppendorf 5810R—15 Amp Version, Germany). After discarding the supernatants, the pre-washed extreme subpopulations of Y- and O-RBCs were transferred into separate 50 mL conical tubes with appropriate labeling. In the Y-RBC tube, 33 mL of the 15 µL/mL biotinylation solution was added, and in the O-RBC tube, 33 mL of the 48 µL/mL biotinylation solution was introduced. The RBC samples were mixed thoroughly by inverting them ten times and placed on a mixer (SARMIX® GM1, Sarstedt Inc, Newton, NC, USA) (1 cycle/sec) at room temperature for 30 min of incubation with no requirement for darkness during this process. After incubation, the BioRBC tubes were centrifuged for 10 min at 2560 × g at room temperature with acceleration 6 and deceleration 4. The supernatant was discarded as much as possible without disturbing the interface. Then, 40 mL of saline dextrose solution was added to each tube, mixed by inverting until RBCs were suspended, and centrifuged again for 10 min at 2560 x g at room temperature. The supernatant was carefully discarded using a vacuum flask. The washing steps were repeated twice. (70) Finally, saline dextrose solution was added to each conical tube to reach a final volume of 16.5 mL and hematocrit of 40-55%. The RBCs were mixed by inverting until fully suspended, and HCT and Hb were measured using the hematology analyzer to ensure they fell within the desired range. For Y-BioRBCs, the HCT was  $0.41 \pm 0.00\%$  (CV: 0.51%), and Hb was  $130.43 \pm 0.60$  (g/dL) (CV: 0.97%); for O-BioRBCs, the HCT was  $0.50 \pm 0.00\%$  (CV: 0.87%), and Hb was  $177.27 \pm 0.39$  (g/dL) (CV: 0.47%). For Y-RBCs, the HCT was  $0.42 \pm 0.00\%$  (CV: 1.49%), and Hb was  $133.63 \pm 0.55$  (g/dL) (CV: 0.99%); for O-RBCs, the HCT was  $0.59 \pm 0.00\%$  (CV: 0.42%), and Hb was  $212.23 \pm 0.44$  (g/dL)

(CV: 0.44%). The post-biotinylation hemolysis values were measured, and they remained below the baseline hemolysis threshold specified by the CSA standards (<0.8%). Hemolysis measurements are as follows: pooled unit  $0.23 \pm 0.01\%$  (CV: 1.15%), Y-RBCs  $0.21 \pm 0.03\%$  (CV: 6.81%), O-RBCs  $0.29 \pm 0.02\%$  (CV: 4.04%), spiked pooled unit  $0.31 \pm 0.07\%$  (CV: 15.95%), Y-BioRBCs  $0.57 \pm 0.04\%$  (CV: 7.55%), O-BioRBCs  $0.71 \pm 0.06\%$  (CV: 13.61%) ([Table 3-2](#)).

### **3.2.4 Spiking the Pooled Unit with Young and Old Biotin-labelled RBCs**

The biotinylated Y-RBCs and O-RBCs were re-introduced into the original pooled unit to accurately track each subpopulation throughout the cryopreservation process. A 12.5 mL aliquot of each biotinylated subpopulation was re-introduced into the pooled blood unit to attain a final concentration of around 1% for each subpopulation within the pooled unit. A volume of 3.75 mL from each of the Y- and O-BioRBC subpopulations was retained by placing them in a 5 mL round-bottom tube for further experiments and investigation of the impact of biotinylation on the osmotic characteristics of RBCs. After completing the spiking process, the pooled unit was thoroughly mixed by carefully inverting the bag multiple times to guarantee an even distribution of the biotinylated RBC subpopulations within the pooled unit.

The pooled RCC bag was subsequently split into five units with matching weights. Dried RCC collection sets (LQT 7291 LX Leucoflex LCR-Diamond quadruple bottom-and-top system, CPD/SAGM 500 mL, MacoPharma, Tourcoing, France) were connected to the pooled RCC using a sterile connection device. The RCC storage bag was placed on a scale (GSE 574, Scale System, Michigan, USA) and blanked, and blood flowed from the pooled unit until the calculated weight was obtained. The tube was sealed, and the splitting process was repeated for the remaining 4 RCC units.

### **3.2.5 Equilibrium RBC Volume Measurement**

RBCs were categorized into washed unseparated RBCs (U-RBCs), spiked pooled RBCs (SP-RBCs), subpopulations of young/old RBCs (Y/O-RBCs), and young/old-biotinylated RBCs (Y/O-BioRBCs). The equilibrium volume of each group of RBCs in

anisotonic and isotonic NaCl solutions was determined on an electronic particle counter (ZB1, Beckman Coulter Electronics, Inc., Hialeah, FL, USA) equipped with a pulse-height analyzer (The Great Canadian Computer Company, Spruce Grove, AB, Canada). (71) RBCs were diluted in 10 mL of 0.68%, 0.9%, 1.6%, and 3.5% (w/v) NaCl solution to reach a concentration of approximately 20000 cells per mL and were allowed to equilibrate at room temperature for at least 5 min. Current pulses, proportional to cell volumes, were measured as RBCs passed through a 50  $\mu\text{m}$  aperture on the electronic particle counter. The equilibrium volume of each group of RBC was measured in triplicate for each solution. To calibrate the electronic particle counter, 5  $\mu\text{m}$  latex beads (Beckman Coulter, Inc., Fullerton, CA, USA) were added to each NaCl concentration and run on the electronic particle counter. The bead volume was determined using **Eq 3-1** and then divided this calculated volume by the bead volume to derive the calibration factor for each solution. These calibration factors were subsequently applied to convert the instrument's output data into RBC volumes. (72) The calibration factors for each solution are documented in ([Table 3-3](#)).

$$V = \frac{3}{2} \times \pi \times r^3 \quad \text{(Equation 3-1)}$$

Where  $V$  is the volume of the cell,  $\pi$  is the mathematical constant (3.14159), and  $r$  is the radius of the hemisphere (latex beads used in this study,  $r = 5 \mu\text{m}$ ).

### 3.2.6 Preparation of Stopped-Flow Experimental Solutions

NaCl solutions were prepared by diluting a 12% (w/v) NaCl stock solution (Baxter, Deerfield, IL, USA) with distilled water to achieve final concentrations of 0.46, 0.9, 2.3, and 6.1 % (w/v). Additionally, a solution containing 3.5% glycerol (w/v) and 0.99% NaCl (w/v) was prepared by diluting 61 mL of 57 Glycerolyte (57%, Sigma Aldrich, Inc., St. Louis, MO, USA) and 933 mL of 0.9% NaCl solution ([Table 3-4](#)). The osmolality of these experimental solutions was measured using a freezing-point depression osmometer (Osmette, Precision Systems Inc., Natick, Massachusetts) ([Table 3-5](#)). (73) Before each experimental run, the osmometer underwent calibration using a 100, 500, and 1500 mmol/kg standard (Precision Systems Inc., Natick, Massachusetts, USA). After calibration, measurements were taken for controls at three different osmolality levels: 200,

400, and 1000 mOsm/kg (Calibration standard, Advanced Instrument Inc., Norwood, Massachusetts, USA) ([Table 3-6](#)).

### **3.2.7 Stopped-Flow Spectrophotometer Setup and Measurement of RBC Volume Kinetics**

To effectively assess rapid changes in RBC cell volume in response to anisotonic environments, researchers often utilize techniques such as stopped-flow spectroscopy. (74–76) Zhurova et al. developed this method to capture these changes by measuring variations in intrinsic hemoglobin fluorescence intensity. (52)

Rapid kinetics experiments were conducted using an SX20 stopped-flow reaction analyzer (Applied Photophysics, Ltd., Leatherhead, UK). This method involves measuring the osmotically-driven changes in RBC fluorescence by rapidly mixing RBCs with an equal volume of an anisotonic experimental solution. RBC fluorescence intensity was recorded simultaneously as a function of time. Changes in RBC volume upon exposure to different hypo- and hypertonic NaCl solutions were calculated by monitoring changes in intrinsic hemoglobin fluorescence intensity. The RBC suspensions for these experiments were prepared by adding 20  $\mu$ L of RBCs into 1 mL of 0.9% (w/v) NaCl solution (final osmolality of 292 mOsm/kg). Hematocrit measurements were as follows: pooled unit  $0.56 \pm 0.00\%$ , CV: 1.01%, Y-RBCs  $0.42 \pm 0.00\%$  (CV: 1.49%), O-RBCs  $0.59 \pm 0.00\%$  (CV: 0.42%), spiked pooled unit  $0.55 \pm 0.00\%$  (CV: 0.99%), Y-BioRBCs  $0.41 \pm 0.00\%$  (CV: 0.51%), O-BioRBCs  $0.50 \pm 0.00\%$  (CV: 0.87%).

The extracellular NaCl concentrations were adjusted to 0.68%, 0.9%, 1.6%, and 3.5% (w/v) through rapid 1:1 mixing of the RBC suspension (in 0.9% (w/v) NaCl) with 0.46%, 0.9%, 2.3%, and 6.1% (w/v) NaCl, respectively. The final osmolalities of these solutions after mixing with RBC solution were 222.5 mOsm/kg, 292 mOsm/kg, 523 mOsm/kg, and 1140 mOsm/kg, respectively. The autofluorescence of RBCs when exposed to an isotonic 0.9% NaCl (osmotic equilibrium condition) was used as the baseline control. The background fluorescence of buffer solutions without RBCs was measured and subtracted from RBC autofluorescence. The stopped-flow circuit was flushed with the solution of the same osmolality as the test solution before each run to prevent cross-contamination

between experimental solutions and maintain accurate osmolality during each experimental run. The RBC suspension was excited at 280 nm, and the emission of the hemoglobin autofluorescence was measured at 314 nm for all RBC subpopulations. The excitation and emission slit widths were set to 3 nm (equivalent to a wavelength bandwidth of 13.95 nm). The total stopped-flow drive volume was set to approximately 120  $\mu$ L, and 1000 fluorescence data points were collected during the 10 seconds immediately following the mixing event. The 20  $\mu$ L optical cell had a 10 mm path length and a 1 ms dead time (during which mixing occurred). Fluorescence was expressed in volts (V), and data were acquired using the ProData SX software (Applied Photophysics, Ltd., Leatherhead, UK). Based on earlier studies conducted within our team (52), the optimized excitation wavelength ( $\lambda_{\text{ex}}$ ) of 280 nm and an emission wavelength ( $\lambda_{\text{em}}$ ) of 314 nm is ideal for RBCs using the stopped-flow analyzer. These wavelength settings were consistent with the previous research findings, ensuring the reliability and comparability of our data. (52,77) Measurements were made in triplicate for each anisotonic solution.

To determine the Arrhenius activation energy, the kinetics of the osmotically-induced changes in RBC volume were taken at two different temperatures:  $3.8 \pm 0.1^\circ\text{C}$  (within the target 3.5-4.0  $^\circ\text{C}$  range) and  $19.4 \pm 0.1^\circ\text{C}$  (within the 18.6-21.0  $^\circ\text{C}$  target range). An attached water-filled circulator (CH/P temperature control system, Forma Scientific, Marietta, OH, USA) was used to maintain the temperature of the stopped-flow system. Syringes containing RBC samples and experimental solutions were also equilibrated in a water bath to reach the experiment temperature before use.

### **3.2.8 Measurement of Glycerol Permeability**

**Addition of glycerol to RBCs.** RBCs were exposed to a hypertonic concentration of 3.5% (w/v) glycerol. RBCs suspended in 0.9% NaCl solution were mixed 1:1 with 3.5% (w/v) glycerol, which resulted in a concentration of 1.75% (w/v) glycerol. As a control, RBCs were mixed 1:1 with 0.9% NaCl (osmotic equilibrium conditions), and RBC autofluorescence was measured as a function of time. Subsequently, the equilibrium curve was subtracted from the curve obtained with RBCs + 1.75% (w/v) glycerol.

**Removal of glycerol from RBCs.** RBCs were loaded with 3.5% (w/v) glycerol, then mixed 1:1 with 0.9% NaCl solution to cause glycerol efflux from the RBCs down the concentration gradient. As a control, RBCs loaded with 3.5% (w/v) glycerol were mixed 1:1 with 3.5% (w/v) glycerol in 0.9% NaCl (osmotic equilibrium conditions), and the RBC autofluorescence was measured as a function of time. The equilibrium curve was then subtracted from the curve obtained with RBCs in 3.5% (w/v) glycerol + 0.9% NaCl. In both experiments, 1000 data points were collected for 100 seconds immediately following mixing until complete equilibration of glycerol on both sides of the RBC membrane.

### 3.2.9 Conversion from Fluorescence to Volume

Previous studies from our laboratory have shown that there is a strong positive correlation between equilibrium relative cell volume ( $\frac{V}{V_0}$ ) and equilibrium relative cell autofluorescence intensity ( $\frac{F}{F_0}$ ) (52). The relative fluorescence ( $\frac{F}{F_0}$ ) was converted to relative volume ( $\frac{V}{V_0}$ ) using the following linear regression equation:

$$\frac{V}{V_0} = m \frac{F}{F_0} + c \quad \text{(Equation 3-2)}$$

Where  $V$  is the equilibrium RBC volume at an experimental osmolality,  $V_0$  is the isotonic RBC volume,  $F$  is the equilibrium RBC fluorescence at an experimental osmolality, and  $F_0$  is the isotonic RBC fluorescence,  $m$  is the slope, and  $c$  is the y-intercept.

The relative RBC volume was calculated by dividing the RBC volume measured in each experimental NaCl solution by the RBC volume measured in isotonic 0.9% (w/v) NaCl using the Coulter Electronic Particle Counter equipped with a pulse-height analyzer. (71) Two replicate runs for each sample were performed in the experiment to measure the volume of RBCs in isotonic and anisotonic NaCl solution. Additionally, relative RBC autofluorescence was calculated under equilibrium conditions in two steps. First, the mean autofluorescence value was calculated during the last 3 s of stopped-flow autofluorescence data acquisition (at the autofluorescence plateau). Then, the relative RBC

autofluorescence was calculated by dividing RBC autofluorescence in each experimental NaCl solution by RBC autofluorescence in isotonic 0.9% NaCl. To measure the intensity of RBC fluorescence in isotonic and anisotonic solutions, three to five replicates for each sample were collected. Relative cell volume and autofluorescence for different subpopulations of RBCs were fitted into **Eq 3-2** to derive values for  $m$  and  $c$  at 4 and 20 °C. The relation between relative RBC volume and relative RBC autofluorescence was assessed using Pearson's correlation analysis using Excel, 2016. By calculating the  $m$  and  $c$  values, the volume of RBCs at different NaCl solutions was determined by converting the fluorescent intensity to RBC volume using **Eq 3-3**.

$$V = V_0 \times \left( m \left( \frac{F_0}{F} \right) + c \right) \quad \text{(Equation 3-3)}$$

### 3.2.10 Calculating the Osmotically Inactive Fraction of RBC Subpopulations

The osmotically inactive fraction is the total volume of solutes / biological material in the cell cytoplasm that do not participate in osmotic equilibrium and is typically determined through a linear comparison of parameters, specifically the osmolality and cell volume. To determine the osmotically inactive fraction of RBC subpopulations, RBC equilibrium volumes were measured in different hypo- and hypertonic solutions. All measurements were done at room temperature. A Boyle-van't-Hoff plot was created, representing the equilibrium relative RBC volume ( $\frac{V}{V_0}$ ) as a function of inverse relative osmolality ( $\frac{P}{P_0}$ ). (78) The osmotically inactive fraction of RBC subpopulations was determined using the y-intercept of the linear regression line fitted to the following equation:

$$\frac{V}{V_0} = m \frac{P_0}{P} + V_b \quad \text{(Equation 3-4)}$$

Where  $P$  represents the osmolality of the anisotonic solution, while  $P_0$  represents the osmolality of the isotonic solution.  $V$  represents the volume of RBCs in an anisotonic solution, while  $V_0$  represents RBC volume in an isotonic solution. The intercept ( $V_b$ ) of this linear plot is the osmotically inactive fraction of the RBCs. In other words, it is the portion of the cell volume that remains unchanged and unresponsive to osmotic changes.

The  $V_b$  value is a significant parameter for understanding the structural and functional characteristics of RBCs.

### 3.2.11 Calculating the Water Permeability ( $L_p$ ) and Glycerol Permeability ( $P_s$ )

The equation proposed by Jacobs and Stewart, which describes the rate of cell volume change and solute movement across the cell membrane, was used to calculate the water permeability ( $L_p$ ) of RBCs. (79,80) This equation captures the dynamics of cell volume change under anisotonic conditions, incorporating parameters such as cell volume, time, water permeability ( $\mu\text{m}/\text{min}/\text{atm}$ ), cell surface area, gas constant, absolute temperature, and reflection coefficient.

$$\frac{dV}{dt} = L_p A R T (\sigma(C_s^i - C_s^e) + (C_i^i - C_i^e)) \quad \text{(Equation 3-5)}$$

where  $V$  is the cell volume ( $\mu\text{m}^3$ ),  $t$  is the time (min),  $L_p$  is the water permeability ( $\mu\text{m}/\text{min}/\text{atm}$ ),  $A$  is the cell surface area, either constant at a specified value or the area of a sphere with a volume of the cell ( $\mu\text{m}^2$ ),  $R$  is the gas constant (L-atm/mole/K),  $T$  is the absolute temperature (K),  $\sigma$  (sigma) is the reflection coefficient (dimensionless),  $C_s^i$ ,  $C_s^e$  are the intracellular, extracellular concentration of permeant solute (Moles),  $C_i^i$ ,  $C_i^e$  are the intracellular, extracellular concentration of non-permeating solute (Moles).

To quantify solute movement across the RBC membrane over time **Eq 3-6** was employed. The equation involves the number of solute molecules, solute permeability, cell surface area, concentrations of permeating solute, and the conversion factor from L to  $\mu\text{m}^3$ , reflection coefficient, and cell volume. Experimental data on RBC volume kinetics in PBS and glycerol solutions are fitted to these equations using the least squared method in Excel Solver. Assumptions include dilute solutions, a water density of 1, a potentially changing cell surface area with volume variation, and a zero reflection coefficient indicating no interaction between water and glycerol transport. This comprehensive approach facilitates the determination of water permeability under varying experimental conditions.

$$\frac{dS}{dt} = P_s A \frac{(C_s^i - C_s^e)}{10^{15}} + (1 - \sigma) \frac{(C_s^i - C_s^e)}{2} \times \frac{dV}{10^{15}} \quad \text{(Equation 3-6)}$$

where  $S$  is the number of solute molecules (Moles),  $t$  is the time (min),  $P_s$  is the solute permeability ( $\mu\text{m}/\text{min}$ ),  $A$  is the cell surface area, either constant at a specified value or the area of a sphere with a volume of the cell ( $\mu\text{m}^2$ ),  $C_s^i$ ,  $C_s^e$  are the intracellular, extracellular concentration of permeant solute (Moles),  $10^{15}$  is the factor to convert from L to  $\mu\text{m}^3$ ,  $\sigma$  (sigma) is the reflection coefficient (dimensionless), and  $V$  is the cell volume ( $\mu\text{m}^3$ ).

### 3.2.12 Arrhenius Activation Energies

Arrhenius activation energy ( $E_a$ ) describes the temperature dependence of water and solute permeability of the cell membrane.  $E_a$  was determined from the slope of the plot of the natural logarithm of  $L_p$  or  $P_s$  as a function of the inverse temperature ( $\frac{1}{T}$ ) (81,82):

$$E_a \text{ of } L_p \text{ or } P_s = k \times \exp\left(\frac{-E_a}{RT}\right) \quad (\text{Equation 3-7})$$

Where  $L_p$  is the water permeability ( $\mu\text{m}/\text{min}/\text{atm}$ ),  $P_s$  is the solute permeability ( $\mu\text{m}/\text{min}$ ),  $k$  is the fitting constant,  $R$  is the gas constant (kcal/mole/K),  $E_a$  is the activation energy for  $L_p$  or  $P_s$  (kcal/mol), and  $T$  is the absolute temperature (K).

### 3.2.13 RBC Osmotic Deformability Assessment

RBC osmotic deformability was analyzed using ektacytometry on a Laser-Assisted Optical Rotational Cell Analyzer (LORCA, Mechatronics, Zwaag, Netherlands). The LORCA enables the measurement of RBC deformability, either concerning shear stress (**Deformability**) or in response to the osmotic gradient (**Osmoscan; osmotic deformability**) ([Figure 3-1](#)).

In shear-induced deformability, RBCs in an isotonic medium are subjected to varying shear stresses at different rotation speeds, causing RBCs to elongate to different extents. A laser beam refracts upon passing through the RBC suspension, and the diffraction pattern shape enables the determination of **EI<sub>max</sub>** (the maximum theoretical elongation index) and **KEI** (the shear stress required to achieve half of the EI<sub>max</sub>). (42) For the deformability test, a 9  $\mu\text{L}$  aliquot of each RBC subpopulations, including U-RBCs, SP-RBCs, subpopulations of Y- and O-RBCs, and Y- and O-BioRBCs with hematocrit ranging 40-55% were carefully diluted in 1 mL of an isotonic polyvinylpyrrolidone (**PVP**) solution (LORCA,

RR Mechatronics Manufacturing, Zwaag, Netherlands). A thin layer of the RBC solution was subjected to shear stress between two concentric cylinders, transforming RBC oval biconcave disks into elongated shapes. The diffraction pattern produced by a laser beam was measured to calculate the deformability of RBCs expressed as elongation index (**EI**) as a function of shear stress (**SS**). A high  $EI_{max}$  suggests RBCs are highly deformable, whereas a high  $K_{EI}$  means that RBCs are very rigid and, hence, more force needs to be applied for RBCs to elongate. These deformability experiments involved diluting RBCs 1:100 in PVP and were conducted at 37 °C. Deformability data were analyzed using non-linear regression, following the method previously described by Stadnick et al. (43,83)

Deformability also can be measured as a function of osmolality (osmotic deformability). The Osmoscan test characterizes the deformability of RBCs across varying osmotic levels, providing insight into how RBCs respond differently to constant shear stress under osmotic gradients. To assess osmotic deformability, a 200  $\mu$ L aliquot of RBC subpopulations with a hematocrit ranging from 40-55% was diluted in 5 mL of isotonic PVP solution and mixed carefully. The tubes were positioned under the aspirating needle, and an Osmoscan was conducted. The EI of RBCs was measured across extracellular osmolalities of PVP ranging from 100 to 600 mOsm/kg at constant shear stress (30 Pa) and temperature (37 °C). (84) Osmoscan curves were obtained for all RBC subpopulations. The LORCA indices ( $EI_{max}$ ,  $O_{hyper}$ , and  $O(EI_{max})$ ) were determined and assessed for any associations with the biological age of RBCs (density-separated RBCs) and biotinylation. This investigation of RBC deformability before and after biotinylation will provide a comprehensive understanding of how this biochemical modification impacts RBC biomechanical properties.

### **3.2.14 Measurement of Hemolysis**

Hemolysis was determined for U-RBCs, SP-RBCs, Y-RBCs, O-RBCs, Y-BioRBCs, and O-BioRBCs by spectrophotometric measurement of cyanmethemoglobin according to Drabkin method. (85) RBC hemolysis reports the proportion of hemoglobin released from RBCs due to membrane damage and plays a crucial role in assessing blood product quality. The Drabkin method is a reference method for hemoglobin determination. (86)

Initially, 5  $\mu\text{L}$  of each sample was pipetted into appropriately labeled microtubes containing 1 mL of Drabkin reagent. After gentle mixing and incubation at room temperature for 5 min, the total hemoglobin was measured. For supernatant hemoglobin determination, 40  $\mu\text{L}$  of the supernatant obtained after centrifugation of the RBC samples at  $2200 \times g$  for 10 min at 4  $^{\circ}\text{C}$  using microcentrifuge (Eppendorf 5415 R Refrigerated Centrifuge, Germany) was mixed with Drabkin reagent. These microtubes were then vortexed and incubated. Subsequently, 200  $\mu\text{L}$  of each microtube, including controls and samples (total hemoglobin and supernatant hemoglobin), was pipetted into a 96-well EIA/RIA Plate. Additionally, 200  $\mu\text{L}$  of Drabkin reagent was used as a sample blank. The absorbance was measured at 540 nm.

Drabkin reagent converts most forms of hemoglobin into cyanmethemoglobin (HiCN). During this reaction, hemoglobin iron oxidizes from  $\text{Fe}^{2+}$  to  $\text{Fe}^{3+}$  (methemoglobin), and methemoglobin then reacts with cyanide, forming HiCN. HiCN's absorbance is measured on spectrophotometer SPECTRA max PLUS 384 microplate spectrophotometer (Molecular Devices Corporation, Sunnyvale, CA) at 540 nm. Since HiCN absorbance is directly proportional to hemoglobin concentration, hemoglobin concentration was calculated using SoftMax Pro software (Molecular Devices Corporation, Sunnyvale, CA, USA) according to the equation below:

$$C = \frac{A_{540} \times M \times F}{\epsilon_{540} \times l \times 1000} \quad \text{(Equation 3-8)}$$

Where  $C$  is the concentration of hemoglobin (g/L),  $A_{540}$  is the absorbance of the solution at 540 nm,  $M$  is the molecular mass of hemoglobin monomer (16114.5 mg/mmol),  $F$  is the dilution factor,  $\epsilon_{540}$  is the extinction coefficient of HiCN at 540 nm ( $11.0 \text{ cm}^{-1} \cdot \text{mM}^{-1}$ ), and  $l$  is the light path (cm). (85)

The hematocrit of the RBC sample was measured using the micro-hematocrit centrifuge (Hettich, Tuttlingen, Germany) as the ratio of the volume occupied by packed RBCs to the volume of a whole RBC sample. (41,87) After total and supernatant hemoglobin concentrations were determined, percent hemolysis was calculated as follows:

$$\text{Hemolysis}(\%) = \frac{(100-HCT) \times Hbs}{Hbt} \quad (\text{Equation 3-9})$$

Where *Hct* is hematocrit (%), *Hbs* is supernatant hemoglobin concentration (g/L), and *Hbt* is the total hemoglobin concentration (g/L).

A tri-level hemoglobin control (Stanbio Laboratory, Boerne, TX, USA) was used to ensure accurate measurements. This comprehensive approach aided in evaluating the integrity and quality of Y- and O-RBCs before and after biotinylation.

### 3.2.15 Oxidative Hemolysis

The oxidative hemolysis of U-RBCs, Y-RBCs, O-RBCs, SP-RBCs, Y-BioRBCs, and O-BioRBCs were assessed. The sample preparation involved pipetting RBC samples into labeled 1.5 mL tubes and adding PBS, followed by centrifugation at  $1500 \times g$  for 10 min at 18 °C to remove the supernatant. The procedure continues with two additional washes. To investigate the susceptibility of RBCs to oxidative stress, 700  $\mu$ L of pre-washed RBCs were subjected to incubation with 300  $\mu$ L of 150 mM 2,2'-azobis-2-methylpropanimidamide dihydrochloride (AAPH) and a film (VWR<sup>®</sup> Rayon Films for Biological Cultures, adhesive cover for 12-well plate incubation; VWR, 60941-084, Pennsylvania, USA) used to cover the wells at 37 °C for three hours. As a control, RBCs were incubated with PBS under film-covered conditions at 37 °C for three hours, providing a baseline for comparison with the AAPH-exposed RBCs to evaluate their susceptibility to oxidative stress. This process initiates the formation of peroxy radicals, inducing hemolysis through lipid peroxidation, which is subsequently quantified as a percentage to assess cellular damage. Subsequent measurements of samples total and supernatant hemoglobin are conducted in a 96-well plate filled with Drabkin reagent using a spectrophotometer at 540 nm and 700 nm, with quality control ensuring a CV of less than 10%. (88)

### 3.2.16 Osmotic Hemolysis

Osmotic hemolysis was performed to assess the susceptibility of RBC subpopulation extremes to hemolysis under osmotic stress. The sample preparation involves pipetting RBC samples into labeled 1.5 mL tubes and adding PBS, followed by centrifugation at

1500 × g for 10 minutes at 18 °C to remove the supernatant. The procedure continues with two additional washes. 20 µL of washed packed RBCs were sampled in a 1.5 mL microtube treated with 1 mL of pink test buffer and incubated for four hours. To measure the total hemolysis, 40 µL from each sample was added to Drabkin reagent and placed in a dark. After incubation, tubes were centrifuged at 1,500 x g for 10 min at 18 °C. Then, 40 µL of supernatant from each Pink test RBC sample was collected into a Drabkin reagent. The absorbance of total and supernatant hemoglobin was measured at 540 nm using spectrophotometry. Hemoglobin concentration was calculated using SoftMax Pro software (Molecular Devices Corporation, Sunnyvale, CA). The procedure, adapted from previous methods, ensured high reproducibility and quality control. (89) This approach provided insights into how different subpopulations respond to osmotic hemolysis and if biotinylation can influence the osmotic characteristics and fragility of RBCs.

### **3.2.17 Osmotic Fragility**

Osmotic fragility assessment, a pivotal measure of RBC susceptibility to osmotic stress, was conducted by subjecting RBCs to varying concentrations of hypotonic buffered saline solutions. RBCs immersed in these solutions underwent osmotic-induced swelling and subsequent hemolysis, enabling the quantification of fragility. Concentrations of 9.0 to 1.0 g/L buffered saline solutions were employed, and the resulting hemolysis was measured at 540 nm using spectroscopy. The degree of RBC fragility was measured using the concentration of salt required for 50% hemolysis. Accordingly, RBCs are more fragile if a higher salt concentration can cause hemolysis (an osmotic fragility curve shifts to the left from the control curve). If the cells can tolerate more dilute solutions, they are less fragile, and the curve shifts to the right relative to the control curve. The point of 50% hemolysis is termed the mean corpuscular fragility (MCF). (90) This comprehensive analysis provided insights into the adaptive responses of U-RBCs, Y-RBCs, and O-RBCs to osmotic changes, offering valuable insights into RBC adaptive responses to osmotic changes and their implications for physiological stability and function. 10 µL of the samples were dispensed into each of the 12 tubes containing 1 mL of descending saline concentrations (ranging from 9.0 to 1.0 g/L) and gently mixed by inverting the tubes. After a 30-minute incubation, the tubes were centrifuged for 5 minutes at room

temperature ( $2200 \times g$ ). Subsequently, 200  $\mu$ L of each supernatant was transferred from the control and the samples into the 96-well plate to measure the hemolysis level at 540 nm using spectrophotometry.

### **3.2.18 Glycerolization of RCCs**

The process of glycerolization involves preparing RCCs for freezing using an HGM to achieve a final glycerol concentration of 35-40%. RCCs were warmed and equilibrated at a controlled temperature by placing the units in a plastic overwrap bag and submerging them in a circulating water bath for 20-30 minutes (36-38 °C). After warming RCCs, they underwent centrifugation (Thermo Scientific Sorvall RC3BP Plus Refrigerated Centrifuge, CAN NO: 75007533 Germany) using the following settings (Rotor setting HBB-6, 2355 rounds per minute, ACE value  $1.49 \times 10^7$ , Temperature 18-24 °C). The waste bag was sterile-docked to RCCs and excess plasma was extracted using a manual plasma extractor. The supernatant layer was pressed off until RBCs started moving up in the tubing. The bags were separated and the supernatant was discarded within the waste bag. The RCC units were then connected to a glycerolization set (Haemonetics, Haemonetics Corporation, Massachusetts, USA), using a sterile docking procedure, while maintaining tubing length, using a clamp to prevent RBCs from prematurely traveling to the freezing bag. The integrity and alignment of the weld were checked. RBCs were mixed and approximately 280g of RBCs were transferred into a freezing bag. Glycerolization was then carried out using the Haemonetics ACP<sup>®</sup> 215 Automated Cell Processor (Haemonetics, ACP<sup>®</sup>215, Haemonetics Corporation, Massachusetts, USA), with the required Glycerolyte<sup>®</sup> 57 bottle added to the system. Following glycerolization, units underwent centrifugation using the following settings: HBB-6, 2070 rounds per minute, ACE value  $2.88 \times 10^7$ , Temperature 18-24 °C. Excess glycerol was removed using a manual plasma extractor. Glycerolized components were placed in a metal storage container with tubing neatly placed and lying flat under the top of the bag. The metal storage container was laid flat in temperature-controlled storage at below -65 °C. (91)

### **3.2.19 Deglycerolization of RCCs**

Cryopreserved RCCs underwent deglycerolization after storage at  $<-65$  °C for a month. The frozen RCCs were put into a plastic overwrap bag and placed in a circulating water bath with a controlled temperature of 36-38 °C for 7-10 min. The thawed RBCs were transferred from the original freezing bag into a 1000 mL transfer bag. The tubing was heat-sealed and detached while maintaining approximately 35 cm of tubing on the freezing bag, and sterile docked the freezing bag to the waste bag, ensuring weld integrity and alignment were checked.

Units underwent centrifugation using a pre-set program: HBB-6, 2070 rounds per minute, ACE value  $2.88 \times 10^7$ , Temperature 18-24 °C. Following centrifugation, excess glycerol was pressed off using the manual plasma extractor until the RBCs started moving up the tubing. Then the tube was heat-sealed near the tubing dock to maintain the tubing length on the RBC transfer bag. The scale was tarred to 0, and the RBCs were weighed, with the RBC gross weight and calculated RBC net weight. The ACP® 215 Cell Processor was set for deglycerolization by loading the deglycerolization set (Haemonetics, ACP®215, Haemonetics Corporation, Massachusetts, USA), performing line sensor calibration, and confirming the proper installation of the required solutions including 12% sodium chloride (150 mL), 0.2% dextrose with 0.9% sodium chloride (2000 mL), AS-3 additive solution (300 mL), transfer bag (1000 mL), and waste bag (600 mL). Then, the RCCs were subject to the deglycerolization procedure and closely monitored. Deglycerolized RBCs were automatically transferred into the final product bag. The disposable set was removed and discarded. This detailed methodology ensures the proper deglycerolization of RCCs while maintaining sterility and quality standards. (92)

### **3.2.20 Tracing Biotin-labeled RBCs in Cryopreserved RCCs**

Flow cytometry was used to track the spiked Y-BioRBC and O-BioRBC through the RCCs cryopreservation process. Streptavidin-conjugated antibodies (Alexa Fluor 488 conjugate (S32354); Thermo Fisher Scientific Inc, Invitrogen, Waltham, Massachusetts, USA) were used to quantify and categorize biotinylated RBCs using an LSRFortessa X-20 flow cytometer (Becton, Dickinson and Company (BD Bioscience), East Rutherford, New

Jersey, USA). The survival of biotinylated Y- and O-RBCs post-deglycerolization was assessed at three different time points after thawing (1, 7, and 14 days). Controls are essential to ensure the accuracy and reliability of flow cytometry experiments by accounting for non-specific binding and validating staining procedures.

- **Buffer Unstained:** Using PBS as the "Buffer Unstained" control helps evaluate background fluorescence.
- **Buffer Cocktail:** This tube contained our buffer with no cells, helping to establish a baseline for our analysis.
- **Negative Controls**

Unstained BioRBCs: It helped us assess potential false positives

Unlabeled RBCs + Streptavidin: This control involved RBCs without biotin but treated with Streptavidin to gauge any non-specific binding.

- **Positive Control**

Y-BioRBC + Streptavidin: providing a known positive control, helping to gate

O-BioRBC + Streptavidin: offering another known positive control, helping to gate

For the sample preparation process, tubes were labeled based on two dilution stages, namely Dilution 1 (consisting of Control RBC Dil1, BioRBC Dil1, and Unit# Dil1) and Dilution 2 (including Control RBC Dil2, BioRBC Dil2, and Unit# Dil2). Initially, we pipetted samples into the pre-labeled Dilution 1 tube, resulting in a 1/100 dilution of the RBCs. Following this initial dilution step, a precise volume of control and sample solutions was pipetted from the Dilution 1 tubes into their respective designated Dilution 2 tubes. This additional step led to a further dilution of the RBCs, achieving a final dilution factor of 1/1000. The HCT of the samples fell within the range of 45-55%. Customized antibody cocktails, adjusted to a 30% concentration, were prepared for the respective sample sizes and added to Dilution 2 tubes. Following vortex mixing and 15 minutes of dark incubation at room temperature, samples were acquired on the device. Every

parameter, including flow rate, sample order, and other relevant settings, was configured to ensure accurate data acquisition. 100,000 events were acquired for each sample, representing the number of cells recorded during the flow cytometry analysis. Gating is vital to differentiate RBC populations based on their fluorescence intensity. The strategy involves using forward scatter (FSC), side scatter (SSC), and B530 fluorescence intensity to differentiate between different populations of RBCs. By setting specific boundaries on data plots generated by these parameters, RBC subpopulations were effectively isolated and analyzed while excluding irrelevant data points. Unmixed Y-BioRBCs and O-BioRBCs were analyzed to verify that gating settings were accurately calibrated ([Figure 3-2](#)). This systematic approach allowed the precise identification and quantification of biotinylated RBCs within RCCs, providing insights into their recovery rate after deglycerolization. (93)

### 3.2.21 Statistical Analysis

Data was analyzed using GraphPad Prism software. Descriptive statistics (mean, SD, SEM) were calculated. Statistical significance was determined using appropriate tests (t-tests, one-way/two-way ANOVA with post hoc tests). Graphs with error bars (SEM/SD) were generated. Flow cytometry data was analyzed with gating strategies. Results are presented as mean  $\pm$  SEM/SD, with  $p < 0.05$  denoting significance. Osmotic fragility, osmotic hemolysis, and hemolysis data were fitted to ANOVA models for analysis.

## 3.3 Results

### 3.3.1 Correlation Analysis of Relative RBC Volumes and Autofluorescence Across NaCl Concentrations

By utilizing the equilibrium volume of RBCs in various NaCl solutions (w/v) ([Table 3-7](#)) and the fluorescence intensity of RBCs at the last 3 seconds of the equilibrium condition ([Table 3-8](#)), the relative RBC volumes corresponding to relative fluorescence were calculated at different NaCl concentrations. Applying these values to [Eq 3-2](#) enabled the computation of the slope ( $m$ ) and y-intercept ( $c$ ) for various RBC subpopulations. The correlation between relative RBC volume and autofluorescence was assessed using Pearson correlation analysis in Excel 2016 ([Table 3-9](#)). The  $m$  value for U-RBC =  $0.676 \pm$

0.114, Y-RBC=0.722 ± 0.111, and O-RBC=0.626 ± 0.125 and  $c$  value for U-RBC=0.335 ± 0.112, Y-RBC=0.308 ± 0.107, and O-RBC=0.452 ± 0.109 ([Figure 3-3](#)). After determining the values of  $m$  and  $c$ , they were incorporated into [Eq 3-3](#) to convert the fluorescence intensity of RBC subpopulations over a 10-second interval to RBC volume. This allowed for an analysis of the dynamic changes in RBC volumes in response to varying NaCl osmolalities.

### 3.3.2 Osmotically Inactive Fraction ( $V_b$ ) Analysis Reveals Subpopulation Variances

The osmotically inactive fraction of each RBC subpopulation was calculated using the Boyle-van't-Hoff ([Eq 3-4](#)). The osmotically inactive fraction was determined from the y-intercept of the linear regression between the equilibrium relative RBC volume ( $\frac{V}{V_0}$ ) as a function of inverse relative osmolality ( $\frac{P}{P_0}$ ). (78) The results indicate significant differences in  $V_b$  between RBC subpopulations, with O-RBCs demonstrating the lowest osmotically inactive fraction followed by Y-RBCs and U-RBCs demonstrating the highest  $V_b$  ( $p=0.0081$ ). The calculated  $V_b$  values were 0.768 ± 0.035 for U-RBCs, 0.732 ± 0.015 for Y-RBCs, 0.706 ± 0.019 for O-RBCs ([Figure 3-4](#)).

### 3.3.3 Fluorescence Dynamics in Red Blood Cells: Subpopulation Variation and Osmotic Responsiveness

The equilibrium fluorescence intensity of RBCs displayed an inverse relation with the NaCl concentration in which RBCs were suspended ( $p<0.0001$ ). Within the experimental range of NaCl concentrations (0.68% to 3.5% w/v), RBC fluorescence intensity was highest in 0.68% NaCl and lowest in 3.5% NaCl for all RBC subpopulations ([Figure 3-5](#)). Mixing RBCs with a hypotonic NaCl solution causes water influx and cell swelling followed by increased fluorescence intensity, as measured using the stopped-flow analyzer. Conversely, mixing RBCs with a hypertonic solution caused water efflux and cell shrinkage, resulting in decreased autofluorescence attributed to the self-quenching characteristic of hemoglobin ([Figure 3-6](#)). Results demonstrated a positive correlation between the RBC volumes and the intensity of fluorescence at both 4 and 20 °C at different NaCl concentrations ( $p<0.0001$ ). Fluorescence results revealed a negative

correlation between RBC senescent level and fluorescence intensity, with Y-RBCs displaying the highest fluorescence intensity at all NaCl concentrations, followed by U-RBCs. In contrast, O-RBCs exhibited the lowest fluorescence intensity at all NaCl concentrations ( $p < 0.0001$ ) ([Figure 3-7](#)).

During the glycerolization process at 4 °C, RBCs suspended in a 3.5% (w/v) glycerol solution initially demonstrated a decrease in fluorescence intensity and cell volume due to water efflux, followed by an increase with the influx of glycerol. Conversely, when RBCs loaded with 3.5% (w/v) glycerol were rapidly mixed with 0.9% (w/v) NaCl, an initial increase in autofluorescence and cell volume was noted due to water influx, followed by a gradual decrease before ultimately reaching a plateau. In both glycerolization and deglycerolization processes, Y-RBCs exhibit significantly higher fluorescence intensity than O-RBCs across the 100 seconds at both temperatures ([Figure 3-8](#)).

### 3.3.4 Water Permeability of RBC Subpopulations

Analysis of  $L_p$  values revealed noteworthy distinctions among RBC subpopulations, with O-RBCs exhibiting the highest  $L_p$  values, followed by Y-RBCs, and U-RBCs demonstrated the lowest  $L_p$  value across all NaCl solutions ( $p < 0.0001$ ) at both 4 and 20 °C. No substantial differences in  $L_p$  value were observed between Y- and O-RBCs at 0.68% (w/v) NaCl. At 1.6% (w/v) NaCl, O-RBCs displayed the highest  $L_p$  value, with Y-RBCs presenting the smallest  $L_p$  value ( $p = 0.0015$ ). The difference in  $L_p$  value between Y- and O-RBCs intensified at 3.5% (w/v) NaCl at 4 °C ( $p = 0.0010$ ). The  $L_p$  values exhibited an increasing trend with the rise in NaCl concentration at 4 °C; however, these trends were not statistically significant for U- and Y-RBCs. Nevertheless, this increasing trend was more pronounced in O-RBCs ( $p = 0.0010$ ) ([Figure 3-9](#)).

At 20 °C, O-RBCs presented the highest  $L_p$  values, followed by Y-RBCs, and U-RBCs demonstrated the lowest  $L_p$  across all NaCl solutions ([Figure 3-10](#)). Notably, O-RBCs displayed higher  $L_p$  values compared with Y-RBCs across all NaCl solutions. This difference became more pronounced at higher concentrations of NaCl ( $p = 0.0008$ ). Additionally, a positive correlation was identified between the concentration of NaCl and  $L_p$  values.  $L_p$  significantly increased in U-RBCs with the escalating NaCl concentration

( $p < 0.0001$ ). Although the  $L_p$  trend was also increasing for Y- and O-RBCs, it did not reach statistical significance ([Figure 3-10](#)).  $L_p$  values are available in ([Table 3-10](#)).

### **3.3.5 Solute Permeability ( $P_s$ ) and Water Permeability ( $L_p$ ) of RBC Subpopulations During Glycerolization and Deglycerolization**

The calculated  $P_s$  results revealed no significant differences among RBC subpopulations during the glycerolization process at both 4 and 20 °C, indicating similar glycerol influx rates. However, a significant increase in  $P_s$  value was observed across all RBC subpopulations during deglycerolization at both temperatures ( $p < 0.0001$ ), indicating a higher rate of glycerol efflux during deglycerolization. O-RBCs displayed the highest  $P_s$  value during deglycerolization, with this difference being more pronounced at 4 °C ( $p = 0.0020$ ). Nonetheless, this difference was alleviated at 20 °C ([Figure 3-11](#)).

The  $L_p$  value did not show any significant differences between glycerolization and deglycerolization across all RBC subpopulations. Additionally, no significant differences in  $L_p$  were observed between RBC subpopulations during glycerolization and deglycerolization at both temperatures ([Figure 3-12](#)).  $P_s$  and  $L_p$  values related to glycerolization and deglycerolization are available in ([Table 3-11](#)).

### **3.3.6 Arrhenius Energy**

The  $E_a$  values did not exhibit any significant differences among RBC subpopulations across different NaCl solutions, suggesting that in our study, there were no specific temperature-dependent differences between Y- and O-RBCs, indicating that their membrane permeability behaved similarly across different temperature conditions ([Figure 3-13](#)).

### **3.3.7 Rheological and Osmotic Properties of Red Blood Cell Subpopulations**

In terms of deformability, notable distinctions were observed among RBC subpopulations, with Y-RBCs exhibiting the highest elongation deformation, followed by U-RBCs ( $p < 0.0001$ ). Conversely, O-RBCs consistently displayed the lowest  $EI_{max}$  across all shear stress levels. Notably, the elongation of Y-RBCs significantly exceeded that of O-RBCs across a wide range of shear stresses, ranging from 0.30 to 16.87 Pa ([Figure 3-](#)

**14).** The biotinylation process had negligible effects on the deformability of Y-RBCs. In contrast, it improved the deformability of O-RBCs within a specific range of shear stress levels, spanning from 1.69 to 5.33 Pa ( $p=0.0019$ ). However, no significant differences were noted at shear stress levels higher or lower than this range. ([Figure 3-15](#)).

Distinct variations in rigidity ( $K_{EI}$ ) were observed among RBC subpopulations, with O-RBCs exhibiting the highest  $K_{EI}$ , followed by U-RBCs and Y-RBCs ( $p<0.0001$ ) ([Figure 3-16](#)). Biotinylation had no significant impact on the rigidity of Y-RBCs. However, in the case of O-RBCs, biotinylation led to a reduction in  $K_{EI}$  ( $p=0.0106$ ) ([Figure 3-17](#)).

In the realm of osmotic characteristics,  $O_{hyper}$  emerged as a pivotal parameter, revealing significant variations among RBC subpopulations. A noteworthy correlation between  $O_{hyper}$  and the senescent levels of RBCs was observed. O-RBCs exhibited the lowest  $O_{hyper}$  values compared to Y-RBCs and U-RBCs ( $p<0.0001$ ) ([Figure 3-18](#)). Biotinylation had no significant impact on the  $O_{hyper}$  in Y-RBCs. However, biotinylation in O-RBCs led to a decrease in  $O_{hyper}$  ( $p=0.0471$ ) ([Figure 3-19](#)). No significant correlations were observed between different subpopulations and  $O_{min}$ . Additionally, there were no significant correlations between biotinylation and  $O_{min}$ .

A significant correlation was identified between  $EI_{max}$  under osmotic conditions and the senescent level of RBCs. Y-RBCs exhibited the highest  $EI_{max}$  under an osmotic gradient, followed by U-RBCs, while O-RBCs demonstrated the lowest  $EI_{max}$ . The descending order of  $EI_{max}$  values under osmotic gradient was as follows: Y-RBCs > U-RBCs > O-RBCs ( $p<0.0001$ ), emphasizing the superior deformability of Y-RBCs compared to O-RBCs ([Figure 3-20](#)). Biotinylation had no impact on  $EI_{max}$  under osmotic gradient in Y-RBCs. However, in O-RBCs, it led to a decrease in  $EI_{max}$  ( $p=0.0097$ ) ([Figure 3-21](#)). No significant correlations were observed between the area under the curve and RBC subpopulations or biotinylation. Likewise, no significant correlation was found between  $EI_{min}$  and RBC subpopulations or biotinylation.

A significant variation in  $EI_{hyper}$  was observed among RBC subpopulations, with Y-RBCs exhibiting the highest  $EI_{hyper}$ , followed by U-RBCs, and O-RBCs displaying the lowest ( $p<0.0001$ ) ([Figure 3-22](#)). Biotinylation did not impact  $EI_{hyper}$  in Y-RBCs.

However, biotinylation in O-RBCs resulted in a significant decrease in  $EI_{\text{hyper}}$  ( $p=0.0097$ ) ([Figure 3-23](#)). The results indicate a partially significant correlation between the  $O(EI_{\text{max}})$  of Y-RBCs and O-RBCs, with Y-RBCs demonstrating the lowest  $O(EI_{\text{max}})$ , followed by O-RBCs and U-RBCs ( $p=0.0472$ ) ([Figure 3-24](#)). No significant differences were observed between O-RBCs and U-RBCs. Furthermore, there was no significant correlation between biotinylation and  $O(EI_{\text{max}})$  across RBC subpopulations.

### 3.3.8 Hemolytic Variability in Red Blood Cell Subpopulations

No significant differences in the initial hemolysis level were observed following RBC separation between subpopulations. However, the biotinylation process elevated initial hemolysis levels in both Y- and O-RBC subpopulations (Y-RBCs vs. Y-BioRBC,  $p=0.0062$  and O-RBCs vs. O-BioRBC  $p=0.0022$ ) ([Figure 3-25](#)). The results demonstrate a positive correlation between the degree of RBC senescence and an increase in oxidative hemolysis. As RBCs age, they become more susceptible to oxidative damage, leading to higher levels of hemolysis ( $p<0.0001$ ) ([Figure 3-26](#)). The biotinylation process did not impact Y-RBCs; however, it contributed to an increase in oxidative hemolysis in O-RBCs ( $p=0.0269$ ) ([Figure 3-27](#)). Osmotic hemolysis analysis uncovered variations in hemolysis levels among RBC subpopulations, indicating that O-RBCs exhibited the lowest osmotic hemolysis compared to both Y-RBCs and U-RBCs ( $p=0.0189$ ). Additionally, no distinction was found in the levels of osmotic hemolysis between Y-RBCs and U-RBCs ([Figure 3-28](#)).

The osmotic fragility results reveal significant differences among RBC subpopulations. At 0.5% NaCl, a significant difference in hemolysis levels was observed between U-RBCs, Y-RBCs, and O-RBCs. U-RBCs exhibited the highest level of hemolysis compared to Y-RBCs and O-RBCs. At 0.46% NaCl, O-RBCs display the lowest hemolysis, followed by Y-RBCs, with U-RBCs exhibiting the highest hemolysis level ( $p=0.0177$ ), indicating a greater tolerance to hypotonic solutions in O-RBCs. At 0.4% NaCl, O-RBCs demonstrate the lowest hemolysis level, while Y-RBCs display an intermediate level, and U-RBCs exhibit the highest hemolysis ( $p=0.0035$ ). These results illustrate the superior ability of O-RBCs to tolerate hypotonic solutions compared to Y- and U-RBCs ([Figure 3-29](#)).

### 3.3.9 Survival of RBC Subpopulation Post-Deglycerolization

Following deglycerolization, the numbers of both O-BioRBCs and Y-BioRBCs experienced a decrease by day 7 ([Figure 3-30](#)). By day 14 post-deglycerolization, O-BioRBCs demonstrated a more notable reduction in cell count compared to Y-BioRBCs. The decline in Y-BioRBCs exhibited a milder slope of -0.01663, while O-BioRBCs displayed a steeper negative trend with a slope of approximately -0.07683; however, this difference lacks statistical significance. The  $R^2$  values for both datasets are low, indicating that the linear regression lines offer limited explanatory power for the data variability and lack statistical significance.

## 3.4 Discussion

The stopped-flow experiment provided insights into RBC membrane permeability, revealing higher  $L_p$  values in O-RBCs followed by Y-RBCs, with U-RBCs showing the lowest  $L_p$  values across all NaCl solutions at both 4 and 20 °C ( $p < 0.0001$ ) ([Figure 3-9](#), [Figure 3-10](#)). While  $P_s$  values showed no significant differences among subpopulations during glycerolization, O-RBCs displayed higher  $P_s$  values than Y-RBCs during deglycerolization ([Figure 3-11](#)), indicating faster glycerol efflux. Furthermore, Y-RBCs exhibited higher  $O_{\text{hyper}}$ ,  $EI_{\text{max}}$ , and lower rigidity compared to O-RBCs ([Figure 3-14](#), [Figure 3-16](#), [Figure 3-18](#)), suggesting greater shear stress tolerance. Despite these findings, no advantages in Y-RBC post-deglycerolization survival were observed.

### 3.4.1 Fluorescence Intensity Variations and Hemoglobin Concentration in RBC Subpopulations Under Osmotic Stress

The study revealed a significant negative correlation between RBC senescent level and fluorescence intensity ([Figure 3-7](#)), with Y-RBCs exhibiting the highest fluorescence intensity across all NaCl concentrations. This observation can be attributed to the lower concentration of cytoplasmic hemoglobin (MCHC) in Y-RBCs compared to O-RBCs. As RBCs age, the progressive failure of cellular homeostasis leads to the efflux of  $K^+$  ions and the subsequent loss of water from the RBCs, causing them to shrink and increase the MCHC. Higher MCHC results in self-quenching of the hemoglobin auto-fluorescence and

decreased fluorescence intensity in O-RBCs. (94–97) Moreover, the equilibrium fluorescence intensity of RBCs exhibited an inverse relationship with NaCl concentration across all RBC subpopulations ([Figure 3-5](#)), peaking at 0.68% NaCl and reaching the lowest level at 3.5% NaCl, which aligns with previous results from our team. (52) When RBCs are exposed to hypertonic NaCl solutions, water moves out of the cells to balance the osmotic gradient. This efflux of water results in cell shrinkage and increased MCHC. The increased MCHC contributes to a reduction in fluorescence intensity. This effect becomes more pronounced as the concentration of the surrounding medium is elevated, causing more water to exit the cells, further amplifying the cytoplasm Hb concentration and decreasing fluorescence intensity in RBCs. Zhurova et al.'s findings indicate hemoglobin quenches fluorescence at concentrations exceeding 10 g/L. (52) Conversely, when cells are subjected to hypotonic solutions, water enters the cells, leading to a dilution of the Hb and resulting in an increase in fluorescence.

The  $V_b$  results demonstrate significant differences among RBC subpopulations, with O-RBCs exhibiting the lowest level, followed by Y-RBCs, and U-RBCs demonstrating the highest  $V_b$  value ( $p=0.0081$ ) ([Figure 3-4](#)). A lower  $V_b$  in O-RBCs indicates that these cells possess less osmotically inactive volume, suggesting they have a higher volume available to participate in osmosis. Despite their smaller volume (MCV), O-RBCs still maintain a relatively higher proportion of active osmotically responsive volume compared to other RBC subpopulations. This finding suggests that O-RBCs may be more adept at regulating their volume in response to changes in osmotic conditions. This capacity could enhance their resilience to dehydration and other osmotic stresses, potentially impacting their overall function and survival in conditions of osmotic stress.

### **3.4.2 Variations in Red Blood Cell Membrane Permeability Across Subpopulations with Differing Biological Ages**

The stopped-flow experiment yielded noteworthy insights into the membrane permeability of RBC subpopulations, with O-RBCs exhibiting the highest  $L_p$  values, followed by Y-RBCs, and U-RBCs demonstrated the lowest  $L_p$  value across all NaCl solutions ( $p<0.0001$ ) at both 4 and 20 °C ([Figure 3-9](#), [Figure 3-10](#)). The higher  $L_p$  value

in O-RBCs correlates with a more rapid volume change in response to anisotonic conditions compared to Y-RBCs. The distinctions in  $L_p$  value between Y- and O-RBCs become more prominent with the elevation of NaCl concentration at both temperatures. The  $L_p$  values exhibited an increasing trend with the rise in NaCl concentration. During both glycerolization and deglycerolization processes, similar water influx was observed across RBC subpopulations. The  $P_s$  values exhibited no significant differences among RBC subpopulations during the glycerolization process at both temperatures. However, a notable increase in solute permeability was observed during deglycerolization across all RBC subpopulations, indicating a higher rate of glycerol efflux. In the deglycerolization process, O-RBCs demonstrated a higher  $P_s$  value compared to Y-RBCs, suggesting that the O-RBC membrane allows for a faster rate of glycerol efflux. This suggests that RCCs with a higher proportion of O-RBCs might undergo deglycerolization more efficiently due to the enhanced glycerol efflux facilitated by the membrane characteristics of O-RBCs. Membrane remodeling during RBC aging (20–38), driven by oxidative stress, can alter membrane asymmetry, disrupt the organization and stability of membrane proteins (98–104), and may lead to alterations in water permeability. Moreover, Alshalani et al. demonstrated that RBC membrane water permeability markedly escalates with chronological aging, suggesting a significant association between chronological aging and altered membrane properties. (65) Contrary to the traditional belief that fresh RBCs are optimal for cryopreservation, our findings suggest that RCCs with higher biological age may be easier to deglycerolize due to membrane remodeling caused by biological aging. This presents new opportunities for refining cryopreservation procedures by considering the age distribution of RBCs within RCCs.

### **3.4.3 Temperature Dependency of Water Permeability in Biologically Aged RBC Subpopulations**

The  $E_a$  values showed no statistically significant differences across RBC subpopulations, contradicting our initial hypothesis. Research by Elmoazzen et al. suggested that  $E_a$  values correlate with the structure of cell membranes, with cells containing membrane water transporter proteins exhibiting lower  $E_a$  compared to those without such transporters. (105) Considering that RBC senescence level correlates with

the loss of membrane components and subsequent alterations in membrane osmotic properties (106), it was expected that the permeability of RBC membranes would be more temperature-dependent in O-RBCs compared to Y-RBCs. However, our study did not observe any significant differences in  $E_a$  among Y- and O-RBCs, indicating that the temperature dependence of membrane permeability does not vary significantly between these subpopulations. This phenomenon may be attributed to the adaptive mechanisms in O-RBCs, allowing them to maintain their membrane integrity in response to temperature alteration. Further investigation is warranted to comprehensively explore the complex relationships between RBC senescence level and  $E_a$  and elucidate the underlying mechanisms that affect the regulation of temperature-dependent membrane permeability.

#### **3.4.4 Deformability Analysis of Young and Old RBC Subpopulations**

The deformability results revealed that Y-RBCs have higher  $O_{\text{hyper}}$ ,  $E_{\text{I,max}}$ , and lower  $K_{\text{EI}}$  compared to O-RBCs, suggesting that Y-RBCs are better able to withstand shear stress across a broader range of anisotonic gradients. The deformability of RBCs naturally degrades during biological aging due to age-dependent membrane remodeling, morphology changes, and increased viscosity of cytoplasmic content. (107) Previous studies demonstrated that Y-RBCs retained lower rigidity, and higher  $O_{\text{hyper}}$  in anisotonic conditions, while O-RBCs are more susceptible to destruction under a relatively lower level of osmotic gradients and shear stress. (52,108) The RBC membrane cytoskeleton proteins, including spectrin and actin, play a crucial role in maintaining RBC shape and deformability. (99) However, during RBC aging, cytoskeletal proteins alter due to oxidative damage or enzymatic degradation, leading to decreased flexibility and deformability in O-RBCs. (98–100,102–104) Additionally, as RBCs age, they undergo gradual shrinkage and microvesiculation, reducing their surface-to-volume ratio and limiting their capacity to deform. (25,35–39) This gradual loss of water during biological aging leads to increased hemoglobin concentration and reduced deformability. (109) This dehydration process is partly attributed to the loss of  $K^+$  and water channels (aquaporins) from the cell membrane, impairing the cell's ability to adjust its shape in response to external forces. (17) Interestingly, biotinylation appears to enhance the deformability of O-RBCs and reduce their rigidity. This phenomenon may be linked to increased water

influx and cytoplasm dilution during the labeling and washing steps, possibly due to the higher  $L_p$  values in O-RBCs. This observation aligns with previous research by Mohandas et al., which reported a reverse correlation between hemoglobin concentration and RBC deformability. (109)

### **3.4.5 Osmotic Hemolysis and Antioxidant Capacity of Young and Old RBC Subpopulations**

A positive correlation was observed between hemolysis levels and RBC senescence levels, indicating elevated hemolysis in O-RBCs compared to Y-RBCs. This finding is consistent with the results reported by Mykhailova et al. (110) A positive correlation was observed between oxidative hemolysis and RBC senescence levels, with O-RBCs demonstrating higher oxidative hemolysis, suggesting compromised antioxidant systems in O-RBCs. (110) Biotinylation further increased oxidative hemolysis in O-RBCs, highlighting a potential lower antioxidant capacity in O-RBCs to overcome the oxidative stress induced by biotinylation. Notably, O-RBCs exhibit the lowest osmotic hemolysis, surpassing both Y-RBCs and U-RBCs, indicating higher resistance to osmotic stress and superior ability to maintain their membrane integrity under osmotic stress. Osmotic fragility results demonstrated that U-RBCs have the highest hemolysis, followed by Y-RBCs, with O-RBCs having the lowest hemolysis. This observation might be explained by the possibility of elimination of vulnerable RBCs during the Percoll® separation method and washing steps, resulting in lower hemolysis levels in Y- and O-RBCs compared to U-RBCs. In the context of cryopreservation, the lowest osmotic hemolysis in O-RBCs may suggest that they are more resilient to hypotonic conditions. The higher  $L_p$  value in O-RBCs could facilitate water transport across the cell membrane, potentially enhancing the cell's ability to adapt to cryopreservation-induced osmotic changes.

### **3.4.6 Biological Age and Recovery Rate of Biotinylated RBCs**

Following deglycerolization, both Y- and O-BioRBCs experienced a decrease in cell count by day 7. By day 14 post-deglycerolization, O-BioRBCs displayed a more noticeable reduction compared to Y-BioRBCs; however, this disparity lacked statistical significance ([Figure 3-30](#)). Contrary to expectations based on the superior osmotic

characteristics of Y-RBCs over O-RBCs, no significant advantages were observed in their post-deglycerolization survival. This unexpected outcome could be attributed to the high glycerol-slow cooling method that was employed and the higher  $P_s$  value in O-RBCs, providing favorable conditions for O-RBCs in deglycerolization processes, and potentially facilitating the preservation of this subpopulation. Further investigations to understand the impact of the low glycerol-rapid cooling method on Y-RBCs and O-RBCs during glycerolization and deglycerolization processes would provide valuable insights into cryopreservation techniques and their specific impact on various RBC subpopulations, providing supplementary findings that enrich our understanding of this process. Given the reduced glycerol concentration and faster freezing rate, the osmotic stress experienced by RBCs might be more pronounced. Consequently, this could result in varying degrees of post-deglycerolization survival and functionality between Y-RBCs and O-RBCs, with O-RBCs being more vulnerable to loss.

### **3.5 Conclusion**

The study revealed significant variations in osmotic characteristics among RBC subpopulations, with O-RBCs demonstrating higher membrane permeability and lower osmotic deformability parameters compared to Y-RBCs. Despite the superior osmotic characteristics of Y-RBCs, their advantages did not result in improved post-deglycerolization survival. Methodological factors such as the use of a high glycerol-slow cooling method may have favored O-RBC preservation, emphasizing the necessity for further exploration of cryopreservation techniques tailored to specific RBC characteristics. The pooling and splitting of RCCs from diverse donors presents challenges in studying distinct RBC subpopulations due to inherent donor variability. Donor characteristics can influence the density profile of each unit, potentially causing the separation of RBCs with lower density from one donor and O-RBCs from another. For example, RBCs from male donors, recognized for their elevated MCHC levels, may be categorized as O-RBCs. It's important to note that sex-related factors can influence the characteristics of these cells. This variability can affect the characteristics of Y-RBCs and O-RBCs, potentially biasing study outcomes. Future research should address these limitations by considering individual donors and exploring different cryopreservation methods, such as the low

glycerol-rapid cooling method, which could differently impact RBC subpopulations. This study offers significant insights into the osmotic characteristics of both Y- and O-RBCs and their responses to osmotic stress. In vivo, monitoring of post-transfusion survival of Y-BioRBCs and O-BioRBCs can further provide a comprehensive assessment of the recovery of RBC subpopulation extremes post-deglycerolization and the feasibility of cryopreserving BioRBCs for tracing studies in human and their functionality and viability post-thawing.

**Table 3-1 RBC Indices Measured for RCCs**

	<b>Average</b>	<b>SD</b>	<b>CV</b>	<b>SE</b>
<b>Unit1</b>				
<b>Hb (g/L)</b>	194.97	2.56	1.31	1.21
<b>HCT (%)</b>	0.58	0.00	0.65	0.00
<b>MCV (fL)</b>	96.80	0.10	0.10	0.05
<b>MCHC (g/L)</b>	335.67	4.04	1.20	1.90
<b>Unit2</b>				
<b>Hb (g/L)</b>	196.23	0.81	0.41	0.38
<b>HCT (%)</b>	0.57	0.00	0.79	0.00
<b>MCV (fL)</b>	89.40	0.10	0.11	0.05
<b>MCHC (g/L)</b>	342.67	2.89	0.84	1.36
<b>Unit3</b>				
<b>Hb (g/L)</b>	178.23	0.38	0.21	0.18
<b>HCT (%)</b>	0.54	0.00	0.84	0.00
<b>MCV (fL)</b>	93.83	0.15	0.16	0.07
<b>MCHC (g/L)</b>	330.67	3.05	0.92	1.44
<b>Unit4</b>				
<b>Hb (g/L)</b>	181.67	1.04	0.57	0.49
<b>HCT (%)</b>	0.54	0.01	1.02	0.00
<b>MCV (fL)</b>	98.10	0.17	0.18	0.08
<b>MCHC (g/L)</b>	334.67	3.79	1.13	1.78
<b>Unit5</b>				
<b>Hb (g/L)</b>	174.60	0.36	0.21	0.17
<b>HCT (%)</b>	0.54	0.00	0.42	0.00
<b>MCV (fL)</b>	93.70	0.20	0.21	0.09
<b>MCHC (g/L)</b>	321.00	1.00	0.31	0.47
<b>Unit6</b>				
<b>Hb (g/L)</b>	193.03	0.67	0.34	0.31
<b>HCT (%)</b>	0.57	0.00	0.67	0.00
<b>MCV (fL)</b>	92.17	0.11	0.12	0.05
<b>MCHC (g/L)</b>	340.33	3.21	0.94	1.51
<b>Unit7</b>				
<b>Hb (g/L)</b>	189.93	0.50	0.26	0.24
<b>HCT (%)</b>	0.58	0.00	0.17	0.24
<b>MCV (fL)</b>	88.53	0.23	0.26	0.11
<b>MCHC (g/L)</b>	326.33	0.58	0.18	0.27

**Table 3-2 RBC Indices for Subpopulation Extremes**

	<b>Average</b>	<b>SD</b>	<b>CV</b>	<b>SE</b>
<b>Y-BioRBC</b>				
<b>Hb (g/L)</b>	130.43	1.27	0.97	0.60
<b>HCT (%)</b>	0.41	0.00	0.51	0.00
<b>MCV (fL)</b>	96.17	0.11	0.12	0.05
<b>MCHC (g/L)</b>	318.67	3.21	1.01	1.51
<b>O-BioRBC</b>				
<b>Hb (g/L)</b>	177.27	0.83	0.47	0.39
<b>HCT (%)</b>	0.50	0.00	0.87	0.00
<b>MCV (fL)</b>	90.83	0.21	0.23	0.10
<b>MCHC (g/L)</b>	356.00	1.73	0.49	0.82
<b>Y-RBC</b>				
<b>Hb (g/L)</b>	133.63	1.04	0.78	0.49
<b>HCT (%)</b>	0.42	0.01	1.49	0.00
<b>MCV (fL)</b>	95.67	0.15	0.16	0.07
<b>MCHC (g/L)</b>	318.33	4.04	1.27	1.90
<b>O-RBC</b>				
<b>Hb (g/L)</b>	212.23	0.93	0.44	0.44
<b>HCT (%)</b>	0.59	0.00	0.42	0.00
<b>MCV (fL)</b>	88.07	0.35	0.40	0.17
<b>MCHC (g/L)</b>	358.00	3.00	0.84	1.41
<b>Pooled Unit</b>				
<b>Hb (g/L)</b>	188.23	1.46	0.78	0.69
<b>HCT (%)</b>	0.56	0.01	1.01	0.00
<b>MCV (fL)</b>	92.63	0.46	0.50	0.22
<b>MCHC (g/L)</b>	335.33	1.15	0.34	0.54
<b>Spiked Pooled Unit</b>				
<b>Hb (g/L)</b>	186.53	1.00	0.54	0.47
<b>HCT (%)</b>	0.55	0.01	1.00	0.00
<b>MCV (fL)</b>	93.30	0.35	0.37	0.16
<b>MCHC (g/L)</b>	337.67	2.52	0.74	1.19

**Table 3-3 Calibration Factors for Coulter Counter-Based Measurement of RBC Volumes**

	<b>Diameter of Bead (<math>\mu\text{m}</math>)</b>	<b>Calculated Bead Volume (fL)</b>	<b>Calibration Factor</b>
<b>0.68% NaCl</b>	44.79	65.42	1.46
<b>0.90% NaCl</b>	47.37	65.42	1.40
<b>1.60% NaCl</b>	43.47	65.42	1.50
<b>3.50% NaCl</b>	43.94	65.42	1.49
<b>1.75% Gly</b>	45.88	65.42	1.43
<b>3.5% Gly</b>	42.83	65.42	1.53

**Table 3-4 Stopped-Flow Experimental Solutions**

<b>Solution ID:</b>	<b>0.9 % Saline</b>			
<b>Component</b>	<b>Manufacturer</b>	<b>Catalogue #</b>	<b>Lot #</b>	<b>Volume</b>
12 % Saline	Baxter	4B7874Q	Y285882	75 mL
dH <sub>2</sub> O	In-House	N/A	N/A	925 mL
<b>Solution ID:</b>	<b>0.46 % Saline</b>			
<b>Component</b>	<b>Manufacturer</b>	<b>Catalogue #</b>	<b>Lot #</b>	<b>Volume</b>
12 % Saline	Baxter	4B7874Q	Y285882	75 mL
dH <sub>2</sub> O	In-House	N/A	N/A	925 mL
<b>Solution ID:</b>	<b>2.3 % Saline</b>			
<b>Component</b>	<b>Manufacturer</b>	<b>Catalogue #</b>	<b>Lot #</b>	<b>Volume</b>
12 % Saline	Baxter	4B7874Q	Y285882	192 mL
dH <sub>2</sub> O	In-House	N/A	N/A	808 mL
<b>Solution ID:</b>	<b>6.1 % Saline</b>			
<b>Component</b>	<b>Manufacturer</b>	<b>Catalogue #</b>	<b>Lot #</b>	<b>Volume</b>
12 % Saline	Baxter	4B7874Q	Y285882	508 mL
dH <sub>2</sub> O	In-House	N/A	N/A	492 mL
<b>Solution ID:</b>	<b>3.5 % Glycerol</b>			
<b>Component</b>	<b>Manufacturer</b>	<b>Catalogue #</b>	<b>Lot #</b>	<b>Volume</b>
57 Glycerolyte	Sigma Aldrich	4A7831	G113993	61 mL
Saline 0.9%	Baxter	4B7878	Y282939	933 mL

**Table 3-5 Experimental Solutions Osmolality Measurements**

<b>Solutions</b>	<b>Target Osmolality (mOsm/kg)</b>	<b>Actual Osmolality (mOsm/kg)</b>
<b>Saline 0.9%</b>	0.308	0.292
<b>Saline 0.46%</b>	0.157	0.153
<b>Saline 1.6%</b>	0.787	0.753
<b>Saline 3.5%</b>	2.087	1.987
<b>Glycerol 3.5%</b>	0.688	0.701
<b>Mixed Solution</b>	<b>Target Osmolality</b>	<b>Actual Osmolality</b>
<b>Saline 0.68%</b>	0.233	0.222
<b>Saline 1.6%</b>	0.547	0.523
<b>Saline 3.5%</b>	1.198	1.140
<b>Glycerol 1.75%</b>	0.498	0.496

**Table 3-6 Osmometer Control Data**

<b>Control</b>	<b>Lot Number</b>	<b>Expiry Date</b>	<b>Measured Osmolality (mOsm/kg)</b>
<b>Advanced Instruments 200 mOsm/kg Standard Cat#3MA020</b>	16914	2024-02-29	187
<b>Advanced Instruments 400 mOsm/kg Standard Cat#3MA040</b>	16915	2024-02-29	388
<b>Advanced Instruments 1000 mOsm/kg Standard Cat#3MA010</b>	17609	2024-11-30	981
<b>dH<sub>2</sub>O(0 mOsm/kg)</b>	In House	NA	0

**Table 3-7 Equilibrium RBC Volume in Various NaCl Solutions**

<b>Osmolality</b>	<b>Equilibrium Cell Volume (fL)</b>		
	<b>U-RBC</b>	<b>Y-RBC</b>	<b>O-RBC</b>
<b>NaCl 0.68%</b>	73.00	75.92	70.08
	68.62	71.54	65.70
	73.00	74.46	73.00
	73.00	73.00	68.62
<b>NaCl 0.90%</b>	61.60	63.0	56.00
	56.00	61.60	56.00
	60.20	58.80	60.20
	54.60	61.60	57.40
<b>NaCl 1.60%</b>	52.50	60.00	51.00
	54.00	54.00	57.00
	55.50	61.50	54.00
	54.00	57.00	55.50
<b>NaCl 3.50%</b>	44.70	49.17	46.19
	43.21	49.17	40.23
	43.21	49.17	44.70
	49.17	52.15	44.70

**Table 3-8 Fluorescence Intensity of RBCs at Equilibrium's Final 3 Seconds**

Osmolality	Fluorescence Intensity (AU)		
	U-RBC	Y-RBC	O-RBC
NaCl 0.68%	1.442	3.504	1.027
	1.613	3.222	1.580
	3.319	3.265	0.968
	94.874	2.263	3.603
NaCl 0.9%	1.190	3.300	0.949
	1.178	2.894	1.377
	3.200	1.069	0.906
	1.469	95.885	2.636
NaCl 1.6%	1.116	2.627	0.534
	1.338	2.259	1.020
	3.355	2.411	0.985
	63.131	1.541	3.906
NaCl 3.5%	0.841	2.492	0.592
	1.068	2.115	1.096
	3.267	2.060	0.741
	67.978	1.463	3.867

**Table 3-9 The Correlation Between Relative RBC Volume and Autofluorescence**

	U-RBC		Y-RBC		O-RBC	
Osmolality	V/V0	F/F0	V/V0	F/F0	V/V0	F/F0
NaCl 0.68%	1.23761	1.21179	1.20376	1.06153	1.20819	1.08198
NaCl 0.68%	1.23761	1.36974	1.20376	1.11359	1.20819	1.14695
NaCl 0.68%	1.23761	1.08028	1.20376	1.24311	1.20819	1.00830
NaCl 0.68%	1.23761	1.19860	1.20376	1.16842	1.20819	1.04565
NaCl 0.9%	1.00000	1.00000	1.00000	1.00000	1.00000	1.00000
NaCl 0.9%	1.00000	1.00000	1.00000	1.00000	1.00000	1.00000
NaCl 0.9%	1.00000	1.00000	1.00000	1.00000	1.00000	1.00000
NaCl 0.9%	1.00000	1.00000	1.00000	1.00000	1.00000	1.00000
NaCl 1.6%	0.92943	0.93789	0.94898	0.79598	0.94730	0.56305
NaCl 1.6%	0.92943	1.13571	0.94898	1.13571	0.94730	0.74067
NaCl 1.6%	0.92943	0.69145	0.94898	0.81391	0.94730	0.61963
NaCl 1.6%	0.92943	0.89110	0.94898	0.87929	0.94730	0.67850
NaCl 3.5%	0.77577	0.70664	0.81494	0.75493	0.76577	0.62355
NaCl 3.5%	0.77577	0.90691	0.81494	0.73092	0.76577	0.79544
NaCl 3.5%	0.77577	0.59700	0.81494	0.79374	0.76577	0.60128
NaCl 3.5%	0.77577	0.68028	0.81494	0.67454	0.76577	0.60080
Corellation	0.84506		0.86726		0.79955	
Slope	0.6755126429		0.7219672373		0.6255510543	
Intercept	0.3352107476		0.3075990666		0.4522781261	

**Table 3-10  $L_p$  Values Among RBC Subpopulations in Various NaCl Solutions**

Osmolality	$L_p$ ( $\mu\text{m}/\text{min}/\text{atm}$ ) U-RBCs															
	22 °C										4 °C					
<b>0.68%</b>	4.817	3.62	3.563	4.312	4.39		3.309	1.626	4.113	2.976	1.752	2.319	2.591	3.22	2.658	1.942
<b>1.6%</b>	2.459	2.495	2.524	1.907	1.557	2.104	3.124	2.582	2.629	2.37	2.393	2.341	2.154	2.324	2.467	2.774
<b>3.5%</b>	7.345	6.002	7.768	6.525	6.676	6.09	7.393	5.831	6.386	7.226	2.185	2.308	2.874	3.887	2.738	2.565
	$L_p$ ( $\mu\text{m}/\text{min}/\text{atm}$ ) Y-RBCs															
	22 °C										4 °C					
<b>0.68%</b>	7.33	4.55	5.66	7.32	5.79	10.294	5.398	6.917	7.067	5.055	5.09	4.01	4.59	4.289	4.503	4.744
<b>1.6%</b>	4.723	4.667	4.535	4.661	5.334	7.777	7.154	7.078	6.852	8.162	2.993	2.432	3.203	3.141	3.352	3.272
<b>3.5%</b>	7.97	7.72	7.873	8.246	8.324	8.099	8.213	7.61	7.664	8.254	5.866	5.263	4.538	3.224	3.545	3.05
	$L_p$ ( $\mu\text{m}/\text{min}/\text{atm}$ ) O-RBCs															
	22 °C										4 °C					
<b>0.68%</b>	5.327	12.36	8.798	15.20	6.312	15.3326	16.57	12.045		14.79	4.953	4.27	5.734	4.7539	6.223	4.369
<b>1.6%</b>			5.735	8.592	5.025	20.905	14.43	11.843	12.992	13.941	4.775	4.766	4.104	5.514	4.501	3.834
<b>3.5%</b>	9.267	8.987	8.559	9.064	9.162	8.697	9.249	9.04	7.587	9.007	7.707	7.532	8.464	7.171	7.34	6.846

**Table 3-11  $L_p$  and  $P_s$  Values Across RBC Subpopulations during Glycerolization and Deglycerolization**

	$P_s$ $\mu\text{m}/\text{min}/\text{atm}$										$L_p$ $\mu\text{m}/\text{min}/\text{atm}$									
	<b>U-RBC</b>																			
	20 °C					4 °C					20 °C					4 °C				
<b>Gly</b>	0.2857	0.3231	0.3065	0.482	0.488	0.512	0.3442	0.3774	0.292	0.279	2.714	2.7041	3.226	3.057	3.077	2.755	3.0136	3.0866	3.268	2.836
<b>Degly</b>	2.129	2.313		2.325	2.28		1.823	1.86	1.914	1.884	4.074	5.682		5.785	4.379		3.385	2.204	6.997	3.418
	<b>Y-RBC</b>																			
	20 °C					4 °C					20 °C					4 °C				
<b>Gly</b>	0.2393	0.2609	0.2228	0.27	0.211	0.172	0		0.604	0.463	3.0786	3.0722	2.871	3.002	3.317	3.272	3.5501		3.745	3.118
<b>Degly</b>	2.49	3.4389		2.921	3.13		1.918	1.9149	1.912	1.901	4.391	3.4598		3.401	3.541		2.843	2.8295	3.095	2.534
	<b>O-RBC</b>																			
	20 °C					4 °C					20 °C					4 °C				
<b>Gly</b>	0.133	0.386	0.267	0.203	0.255	0.255	0.261	0.286	0.302	0.237	3.908	3.099	3.47	3.432	3.675	3.675	3.835	4.29	4.324	3.383
<b>Degly</b>	2.563	3.121		3.071	2.975		2.418	2.391	2.236	2.096	5.69	7.409		3.002	3.424		4.456	2.67	2.585	2.224

**Figure 3-1 Osmoscan Curve and LORCA Indices**

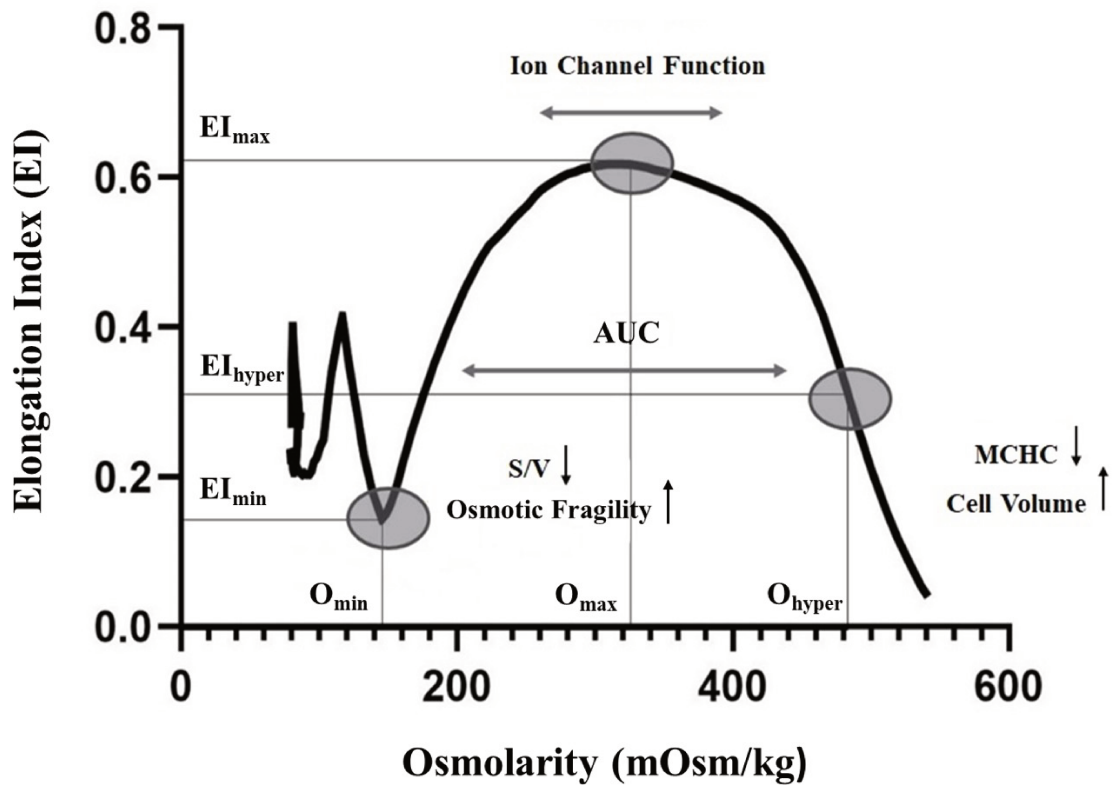


**Figure 3-1:**  $EI_{max}$ : Maximal deformability at isotonic osmolality,  $O_{min}$ : Osmolality where 50% of RBC lyse, minimum osmolality,  $O_{hyper}$ : Hypertonic osmolality where 50% of max EI is achieved, **Area under curve:** AUC defined between  $O_{min}$  and the osmolality point of 500 mOsm/kg,  $EI_{min}$ : Elongation index at hypotonic osmolality ( $O_{min}$ ),  $EI_{hyper}$ : Elongation index (1/2 of  $EI_{max}$ ) at hypertonic osmolality,  $O(EI_{max})$ : Osmolality where maximal EI is achieved.

### Figure 3-2 Gate Selection for Cell Population Identification

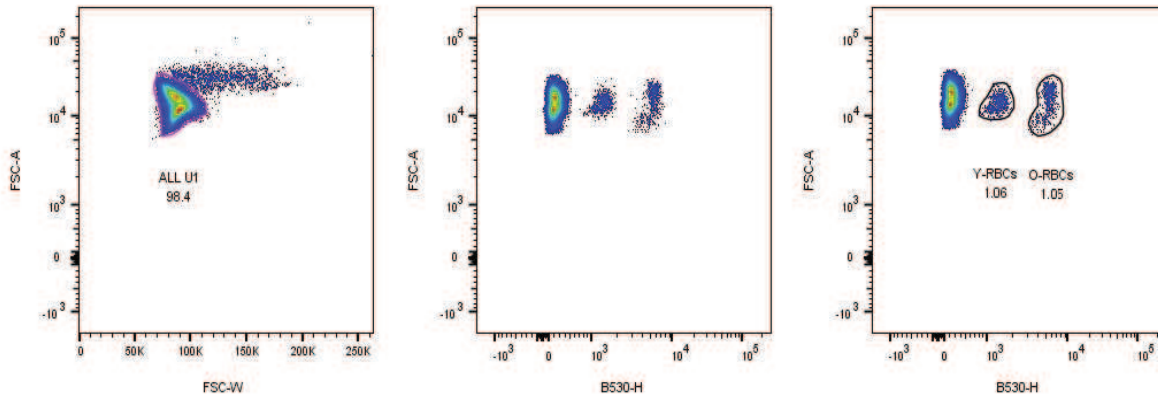


**Figure 3-2: Flow cytometry gating.** Y- and O-BioRBCs were accurately gated using FlowJo, Version 10, and ensuring precise analysis. The gating strategy, demonstrated in the accompanying image, was applied consistently across all units for accurate calculation of the BioRBC number. Graphs based on FSC-A and B530-A depict BioRBCs' survival.

### Figure 3-3 Linear Regression Analysis of Relative Equilibrium Volume ( $V/V_0$ ) and Fluorescence ( $F/F_0$ )

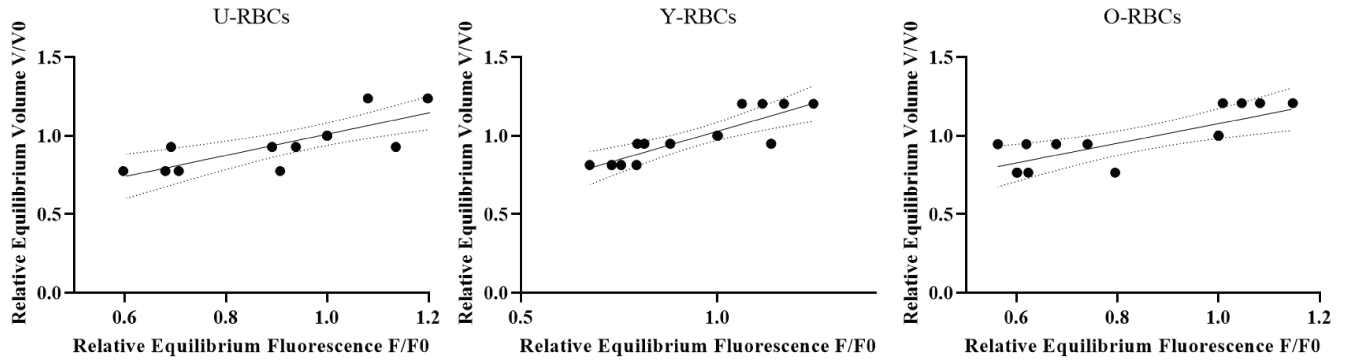


**Figure 3-3:** The graph displays the calculated relative RBC volumes correlated with relative fluorescence at different NaCl concentrations. The slope ( $m$ ) and y-intercept ( $c$ ) values for various RBC subpopulations, including U-RBC ( $m=0.676$ ,  $c=0.335$ ), Y-RBC ( $m=0.722$ ,  $c=0.308$ ), and O-RBC ( $m=0.626$ ,  $c=0.452$ ), were determined using Pearson's correlation analysis.

### Figure 3-4 Boyle-van't-Hoff Equation: $V_b$ Calculation in RBC Subpopulations

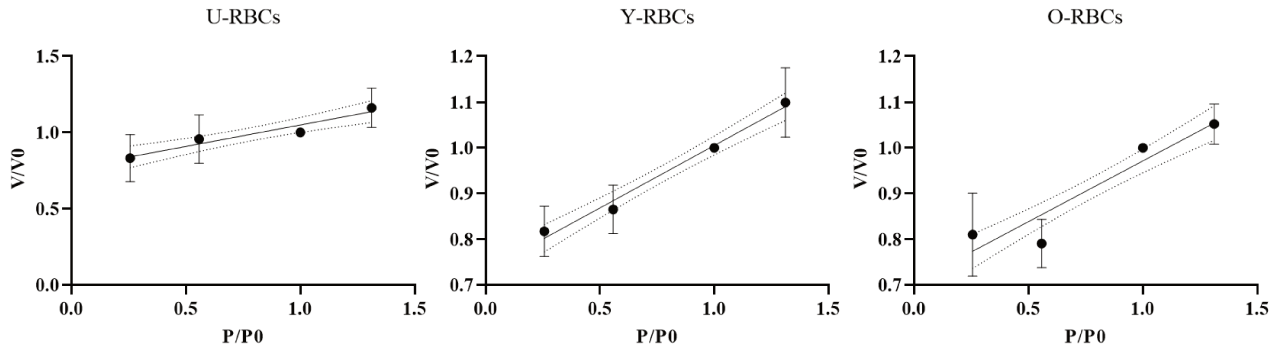


**Figure 3-4:** The graph illustrates the equilibrium relative RBC volume ( $V/V_0$ ) as a function of inverse relative osmolality ( $P/P_0$ ). The calculated  $V_b$  values are 0.768 for U-RBCs, 0.732 for Y-RBCs, and 0.706 for O-RBCs. Significant differences in  $V_b$  were observed among the various RBC subpopulations, with O-RBCs demonstrated the lowest  $V_b$  ( $p=0.0081$ ).

### Figure 3-5 Effect of NaCl Concentration on Fluorescence Intensity of RBC Subpopulations at Different Temperatures

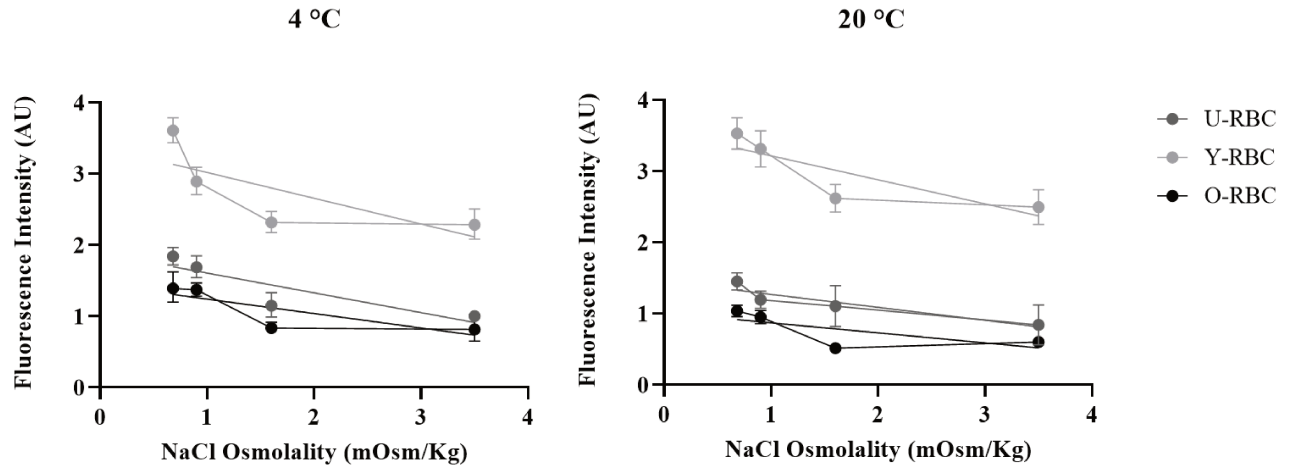


**Figure 3-5:** In the graph, the x-axis represents NaCl Osmolality, while the y-axis represents Fluorescence Intensity. This graph illustrates the inverse correlation between NaCl concentration and fluorescence intensity across RBC subpopulations (Y-RBCs, U-RBCs, and O-RBCs) at different temperatures (4 °C and 20 °C). As NaCl concentration increases, fluorescence intensity decreases. Y-RBCs consistently demonstrate the highest fluorescence intensity across all NaCl concentrations, whereas U-RBCs and O-RBCs exhibit the lowest fluorescence intensity levels ( $p < 0.0001$ ).

**Figure 3-6 RBC Responses to NaCl: Volume and Autofluorescence**

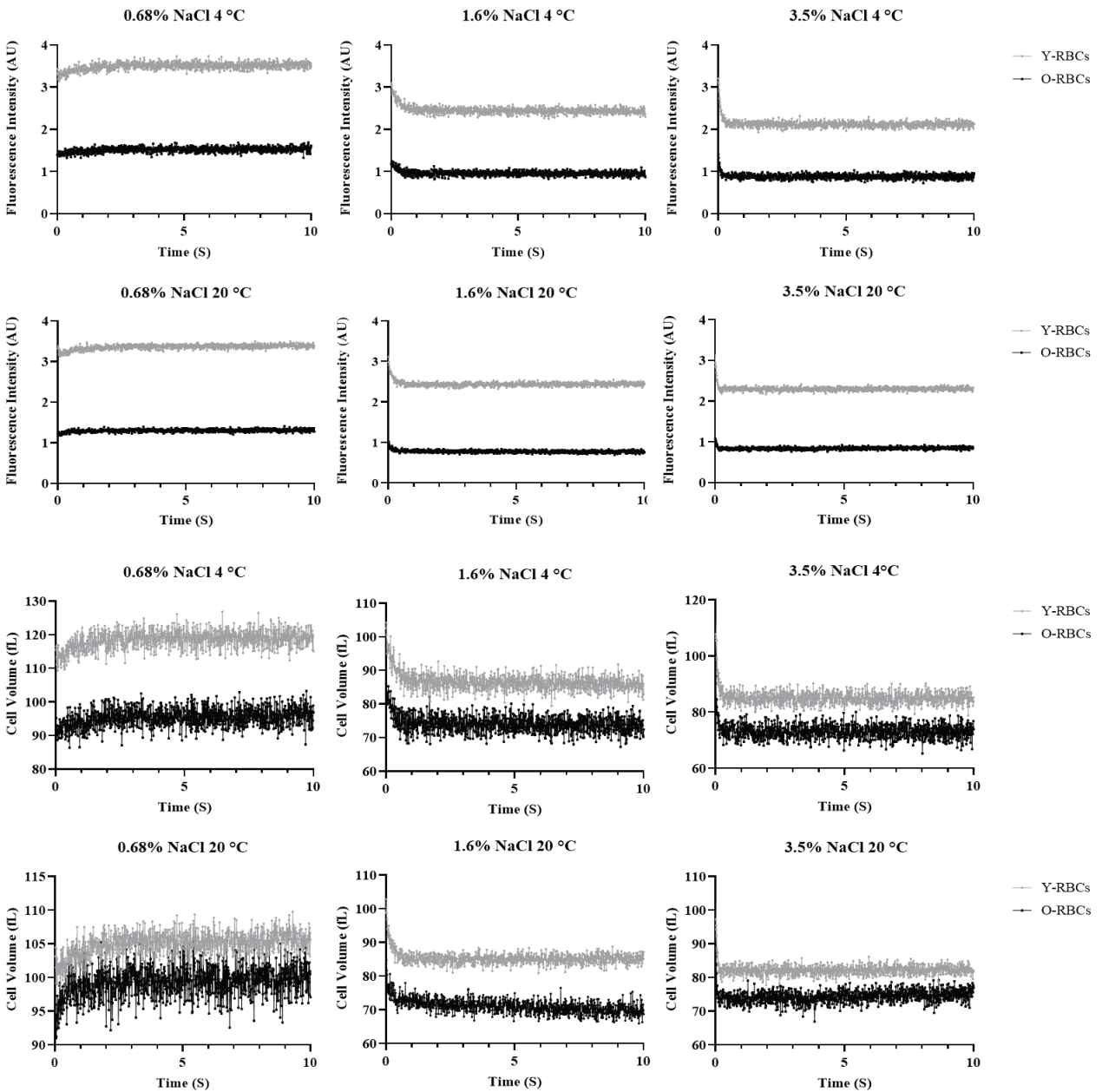


**Figure 3-6:** The graphs in section **A** depict the fluorescence intensity response of RBCs over 10 seconds following mixing with different NaCl concentrations. Hypotonic solutions lead to increased fluorescence, whereas hypertonic solutions result in decreased autofluorescence. RBCs reach equilibrium fluorescence levels within approximately 3 seconds. In section **B**, the graphs illustrate the volume changes of RBCs in reaction to varying NaCl concentrations at both 4 °C and 20 °C. RBCs exposed to hypotonic solutions undergo swelling, while those in hypertonic solutions experience cell shrinkage.

**Figure 3-7 Correlation between RBC Volume and Fluorescence Intensity in Different RBC Subpopulations**

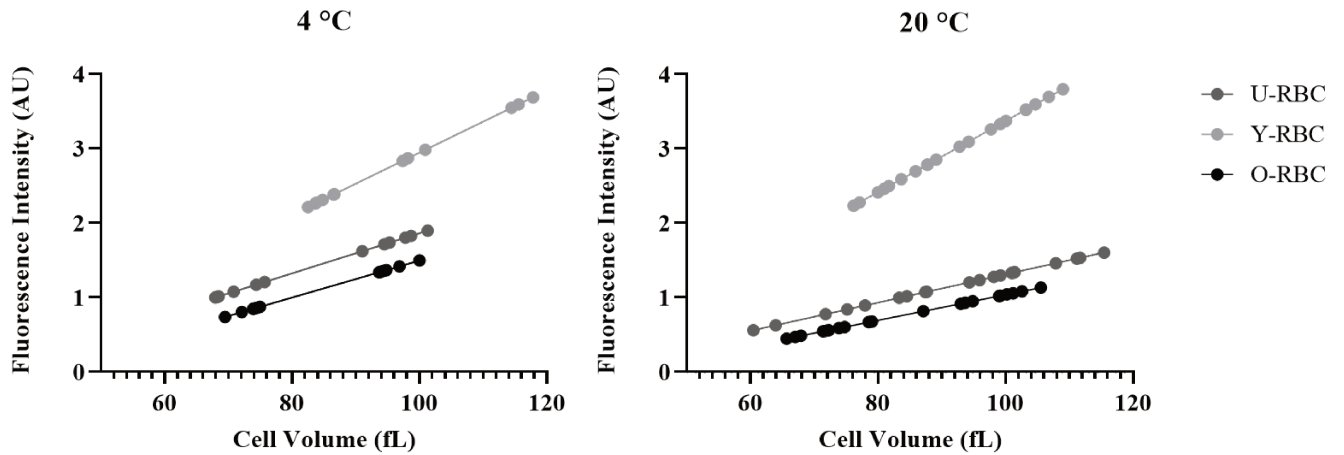


**Figure 3-7:** This graph depicts the relationship between RBC fluorescence intensity and volume across various RBC subpopulations. There is a positive correlation between RBC volumes and fluorescence intensity at 4 and 20 °C. Y-RBCs exhibit the highest fluorescence intensity and volume, followed by U-RBCs, while O-RBCs display the lowest fluorescence intensity at every time point ( $p < 0.0001$ ).

### Figure 3-8 Dynamics of RBC Fluorescence and Volume During Glycerolization and Deglycerolization Processes

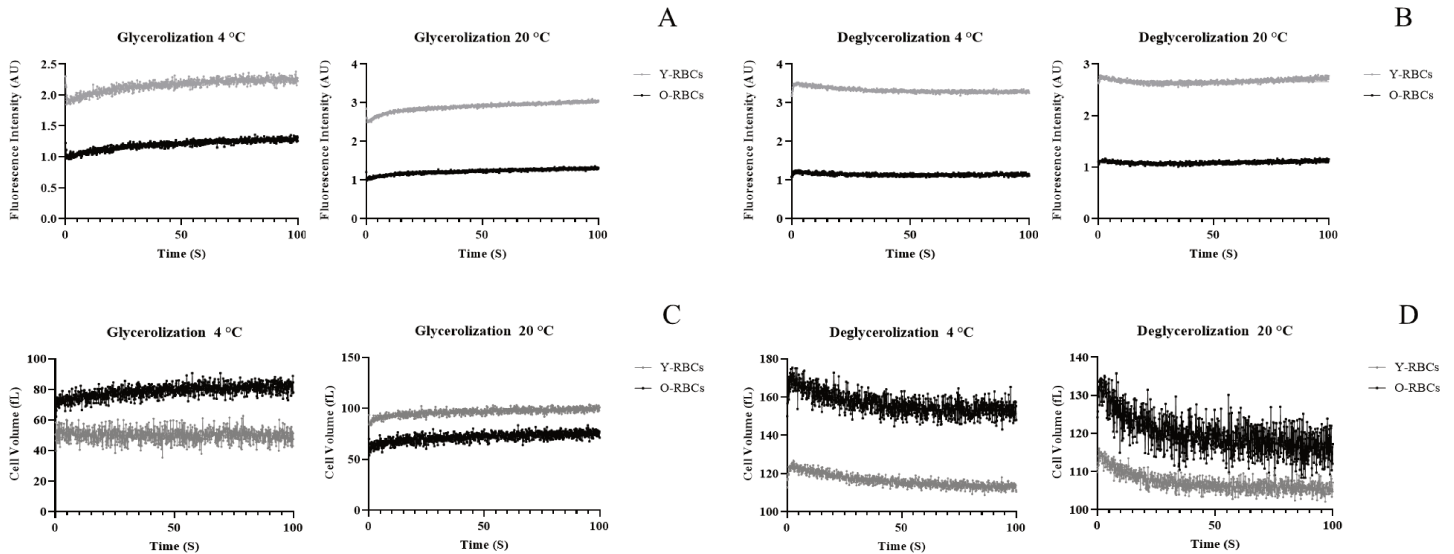


**Figure 3-8:** In section A, the fluorescence intensity of RBCs during glycerolization shows an initial decrease followed by an increase. Conversely, in section B, during deglycerolization, there is an initial surge in autofluorescence followed by a gradual decrease before reaching a plateau. Throughout both processes, Y-RBCs consistently exhibit significantly higher fluorescence intensity than O-RBCs across the 100-second duration at both 4 °C and 20 °C. Section C depicts the change in RBC volume over time at 4 °C and 20 °C during glycerolization. Initially, cell volume decreases before increasing. In contrast, section D illustrates the deglycerolization process, where cell volume initially increases followed by a decrease and stabilization. Similar to fluorescence intensity, Y-RBCs consistently demonstrate significantly higher volumes than O-RBCs across the 100-second duration and at both temperatures.

**Figure 3-9 Analysis of  $L_p$  Values of RBC Subpopulations Across NaCl Solutions at 4 °C**

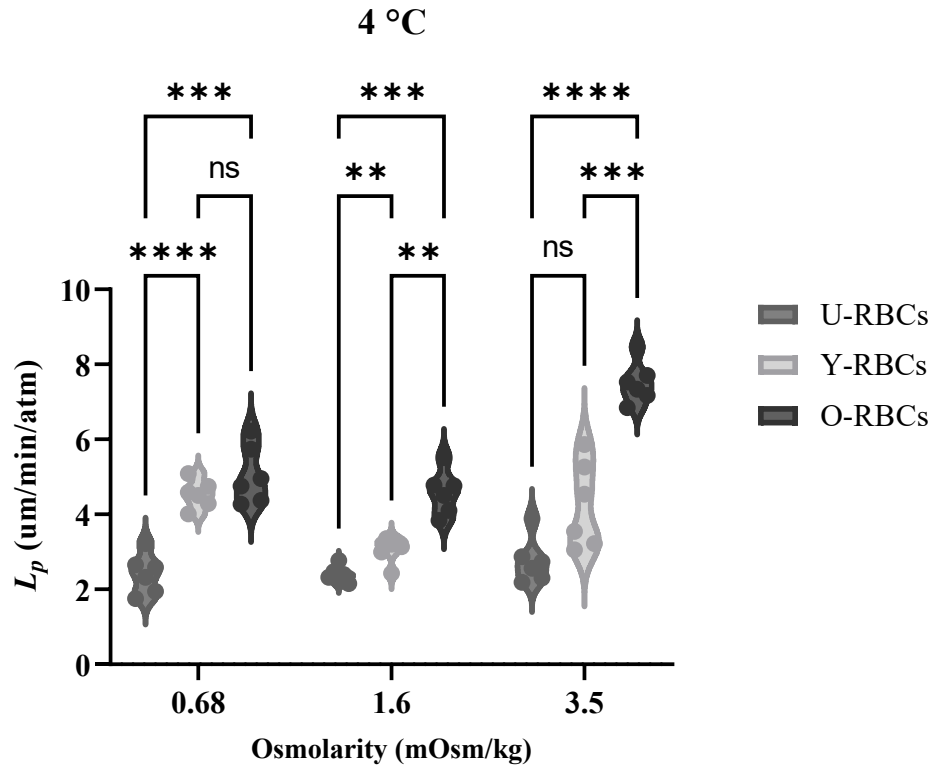


**Figure 3-9:** The figure depicts the analysis of RBC subpopulation  $L_p$  values across various NaCl solutions. Significant differences were observed among RBC subpopulations ( $p < 0.0001$ ), with O-RBCs showing the highest  $L_p$  values, followed by Y-RBCs, and U-RBCs displaying the lowest  $L_p$  values across all NaCl concentrations ( $p < 0.0001$ ). At 0.68% (w/v) NaCl, no substantial differences in  $L_p$  values were observed between Y- and O-RBCs. However, at higher NaCl concentrations, particularly at 1.6% and 3.5% (w/v) NaCl, significant differences were noted. The increasing trend of  $L_p$  values with higher NaCl concentrations was more pronounced in O-RBCs ( $p = 0.0010$ ). Statistical significance denoted by \*:  $p < 0.05$ , \*\*:  $p < 0.01$ , \*\*\*:  $p < 0.001$ , and \*\*\*\*:  $p < 0.0001$ .

**Figure 3-10 Analysis of  $L_p$  Values of RBC Subpopulations Across NaCl Solutions at 20 °C**

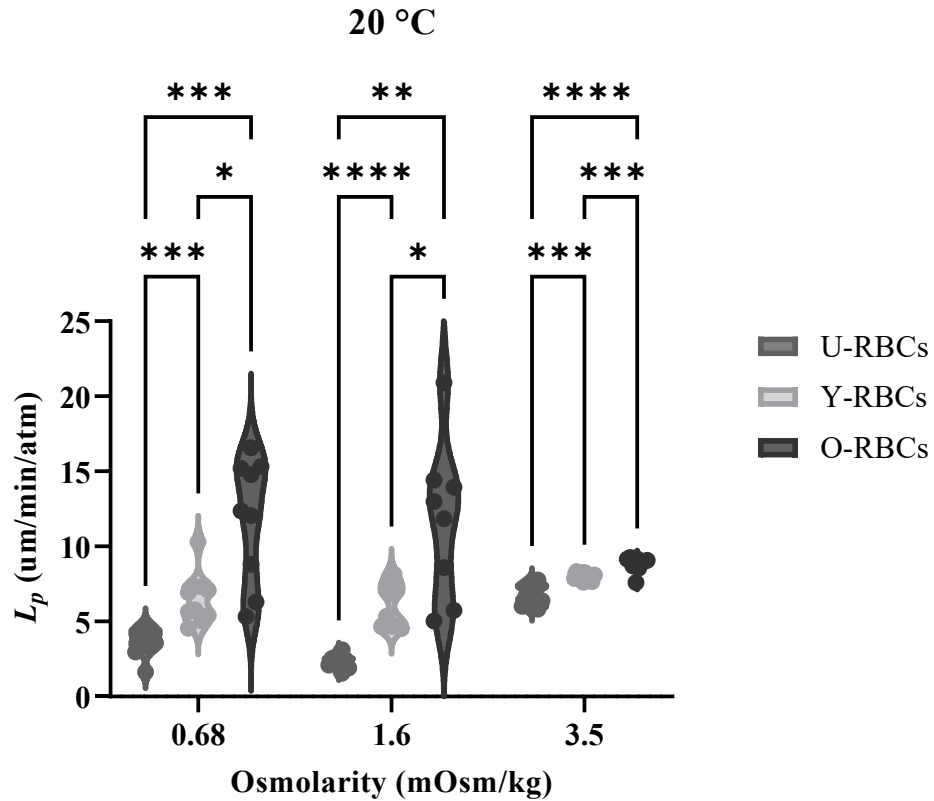


**Figure 3-10:** The graph illustrates significant differences in  $L_p$  values among RBC subpopulations ( $p < 0.0001$ ). O-RBCs presented the highest  $L_p$  values, followed by Y-RBCs, and U-RBCs demonstrated the lowest  $L_p$  values across all NaCl solutions. O-RBCs displayed higher  $L_p$  values compared with Y-RBCs across all NaCl solutions. This difference became more pronounced at higher concentrations of NaCl ( $p = 0.0008$ ). Additionally, a positive correlation was identified between the concentration of NaCl and  $L_p$  values.  $L_p$  values significantly increased in U-RBCs with the escalating NaCl concentration ( $p < 0.0001$ ). Statistical significance denoted by \*:  $p < 0.05$ , \*\*:  $p < 0.01$ , \*\*\*:  $p < 0.001$ , and \*\*\*\*:  $p < 0.0001$ .

**Figure 3-11 Analysis of RBC Subpopulation  $P_s$  Values During Glycerolization and Deglycerolization Processes**

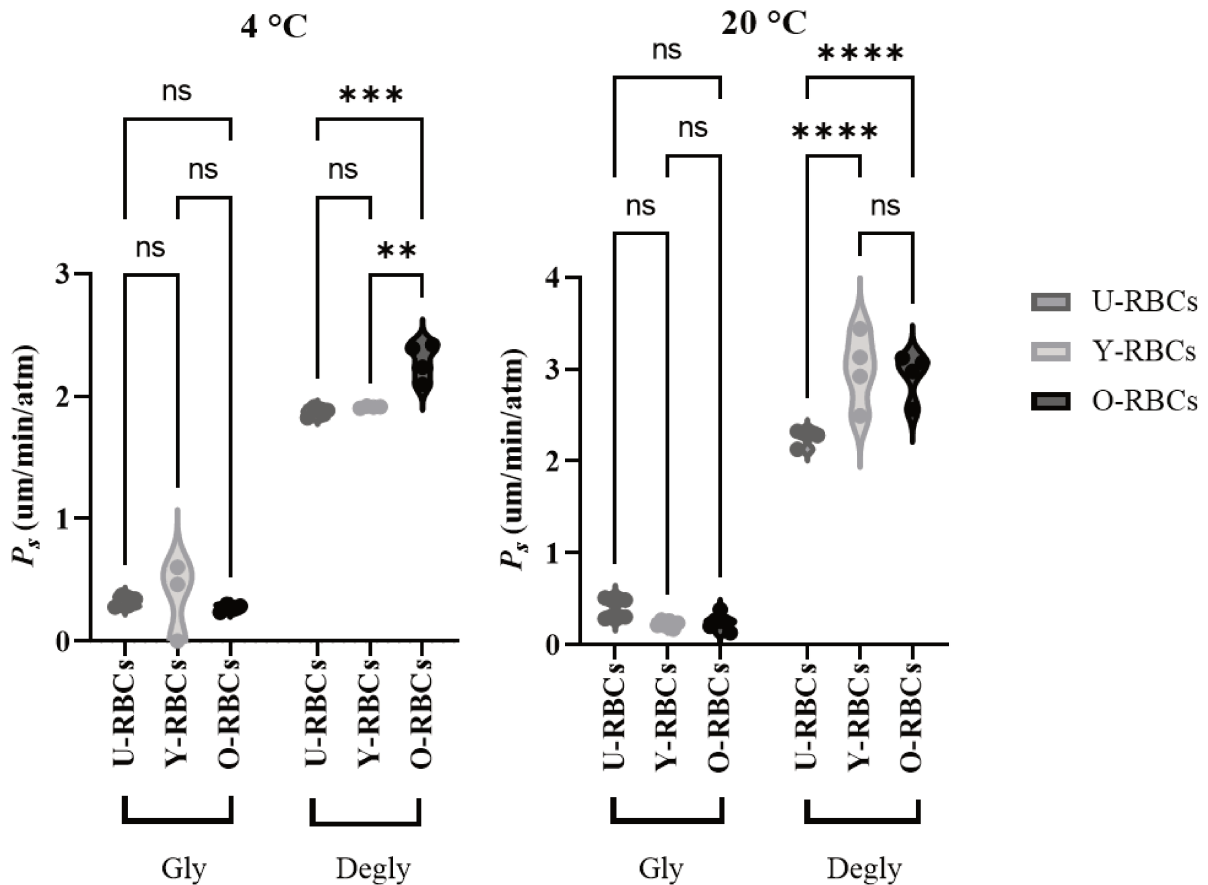


**Figure 3-11:** The graph presents the analysis of  $P_s$  values across RBC subpopulations during glycerolization and deglycerolization processes. No significant differences were observed among RBC subpopulations during glycerolization at both temperatures. However, a significant increase in  $P_s$  value was noted across all RBC subpopulations during deglycerolization ( $p < 0.0001$ ). O-RBCs exhibited the highest  $P_s$  value during deglycerolization, particularly pronounced at 4 °C ( $p = 0.0020$ ). Nevertheless, this difference was attenuated at 20 °C. Statistical significance denoted by \*:  $p < 0.05$ , \*\*:  $p < 0.01$ , \*\*\*:  $p < 0.001$ , and \*\*\*\*:  $p < 0.0001$ .

**Figure 3-12 Comparison of RBC Subpopulation  $L_p$  Values During Glycerolization and Deglycerolization Processes**

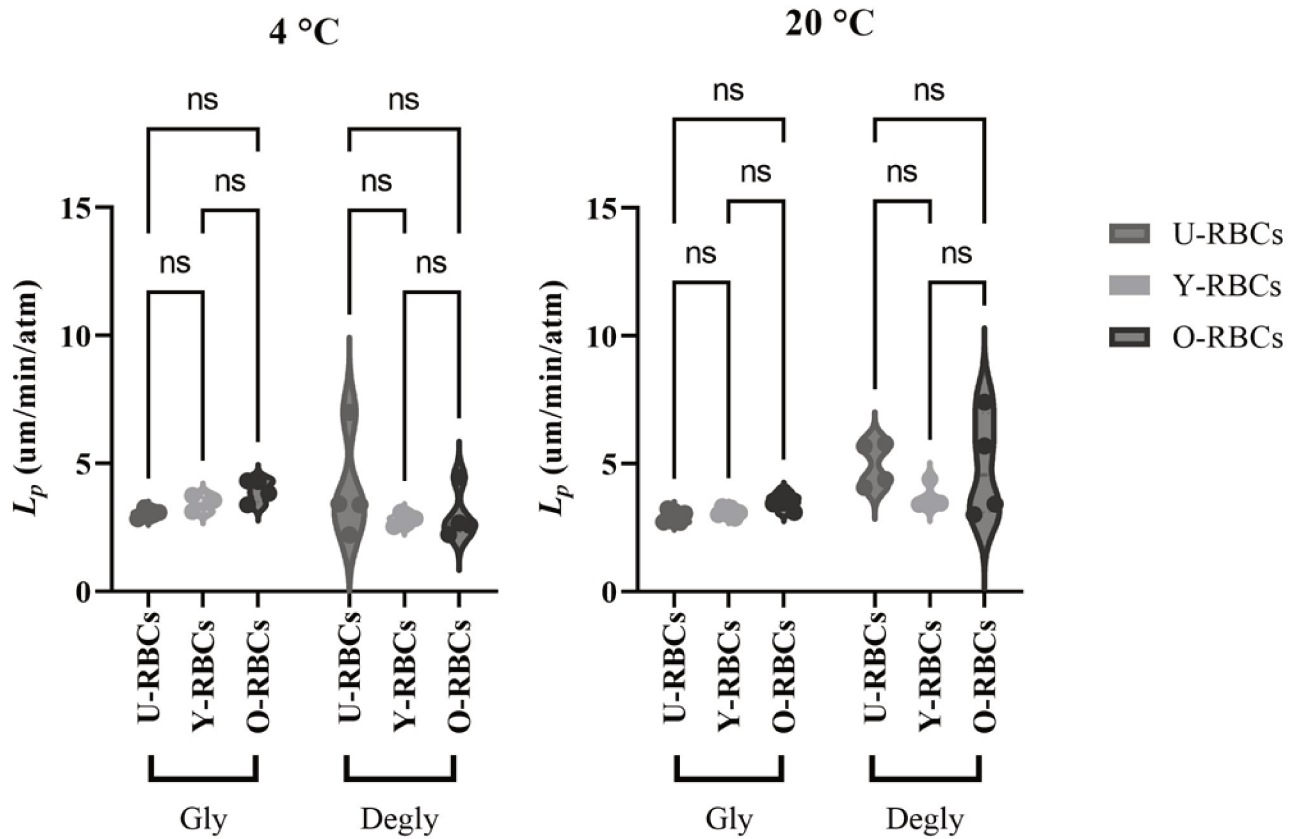


**Figure 3-12:** The graph illustrates the comparison of RBC subpopulation  $L_p$  values during glycerolization and deglycerolization processes. No significant differences were detected in  $L_p$  values during glycerolization and deglycerolization across all RBC subpopulations. Furthermore, no significant differences in  $L_p$  values were observed between RBC subpopulations during both glycerolization and deglycerolization at both temperatures.

**Figure 3-13 Analysis of RBC Subpopulation  $E_a$  Values Across NaCl Solutions**

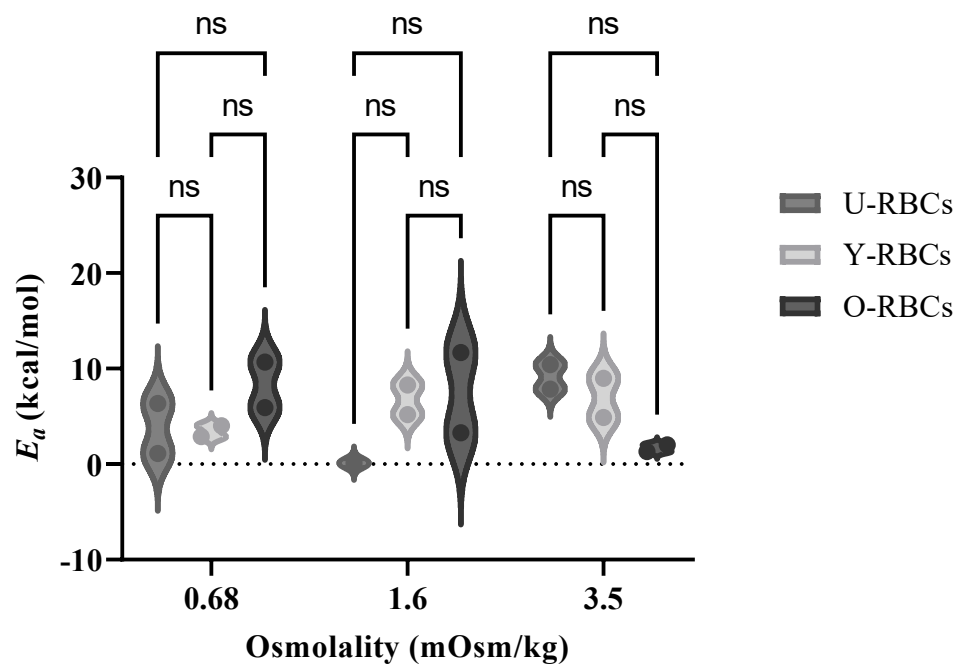


**Figure 3-13:** The graph presents the analysis of RBC subpopulation  $E_a$  values across different NaCl solutions. No significant differences were observed among RBC subpopulations across the various NaCl concentrations.

**Figure 3-14 Elongation Analysis of RBC Subpopulations as a Function of Shear Stress**

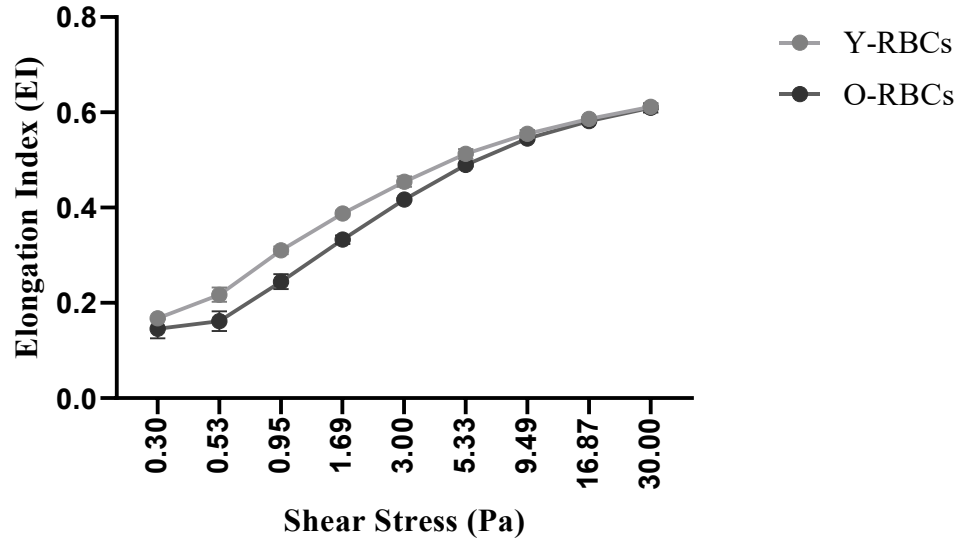


**Figure 3-14:** The graph depicts the analysis of elongation among RBC subpopulations under varying shear stress levels. Y-RBCs show the highest elongation, followed by U-RBCs ( $p < 0.0001$ ), while O-RBCs consistently exhibit the lowest elongation across all shear stress levels.

**Figure 3-15 Impact of Biotinylation on RBC Elongation**

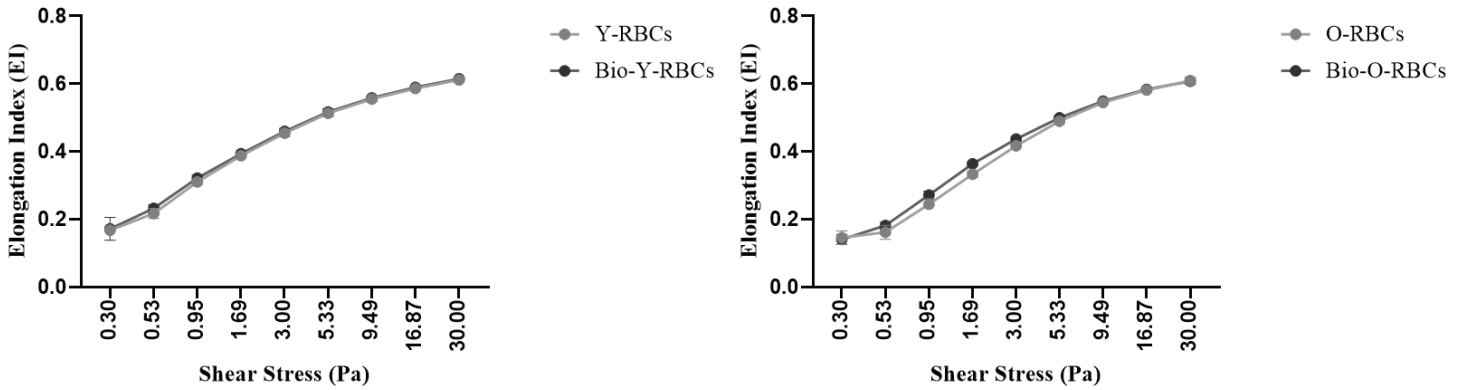


**Figure 3-15:** The graph illustrates the effect of biotinylation on the deformability of RBC subpopulations. Biotinylation did not significantly affect the elongation of Y-RBCs. However, it was found to enhance the elongation of O-RBCs at specific shear stress levels, ranging from 1.69 to 5.33 Pa ( $p=0.0019$ ). No significant differences were detected at higher and lower shear stress levels.

**Figure 3-16 Comparison of RBC Rigidity ( $K_{EI}$ ) Among Subpopulations**

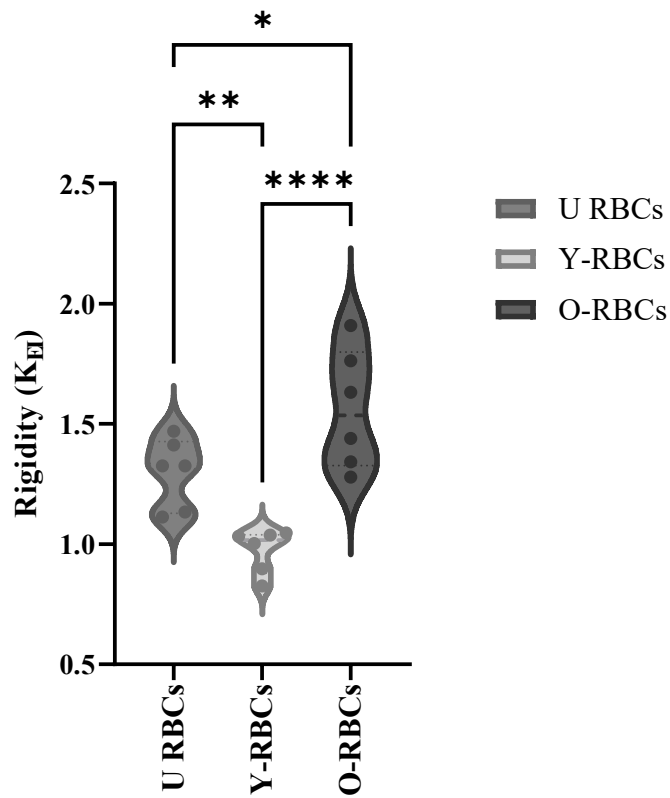


**Figure 3-16:** The graph shows the comparison of RBC rigidity ( $K_{EI}$ ) among subpopulations. O-RBCs display the highest rigidity, followed by U-RBCs and Y-RBCs ( $p<0.0001$ ). Statistical significance denoted by \*:  $p<0.05$ , \*\*:  $p<0.01$ , \*\*\*\*:  $p<0.0001$ , and \*\*\*\*\*:  $p<0.0001$ .

**Figure 3-17 Effect of Biotinylation on RBC Rigidity ( $K_{EI}$ )**

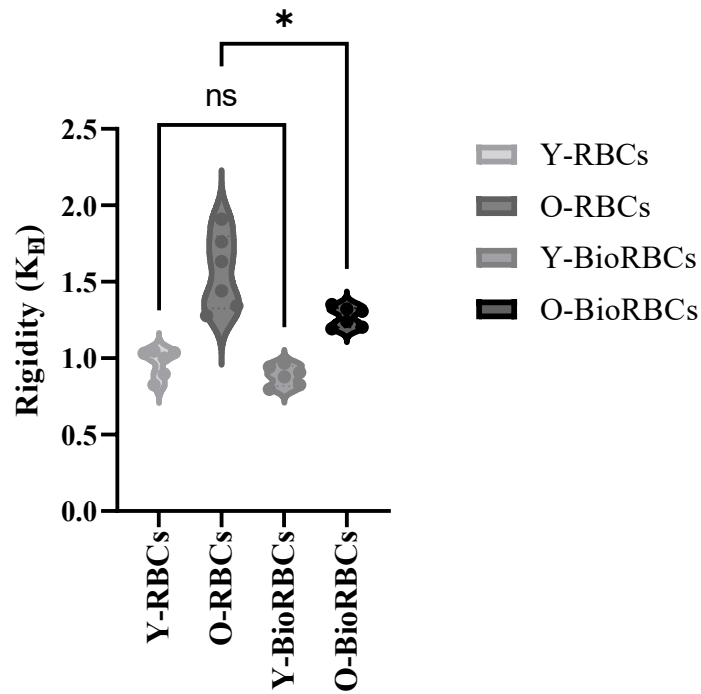


**Figure 3-17:** The graph depicts the impact of biotinylation on the rigidity of RBC subpopulations. Biotinylation did not significantly affect the rigidity of Y-RBCs. However, it reduced the rigidity of O-RBCs ( $p=0.0106$ ). Statistical significance denoted by \*:  $p<0.05$ , \*\*:  $p<0.01$ , \*\*\*:  $p<0.001$ , and \*\*\*\*:  $p<0.0001$ .

**Figure 3-18 Analysis of  $O_{\text{hyper}}$  Values among RBC Subpopulations**

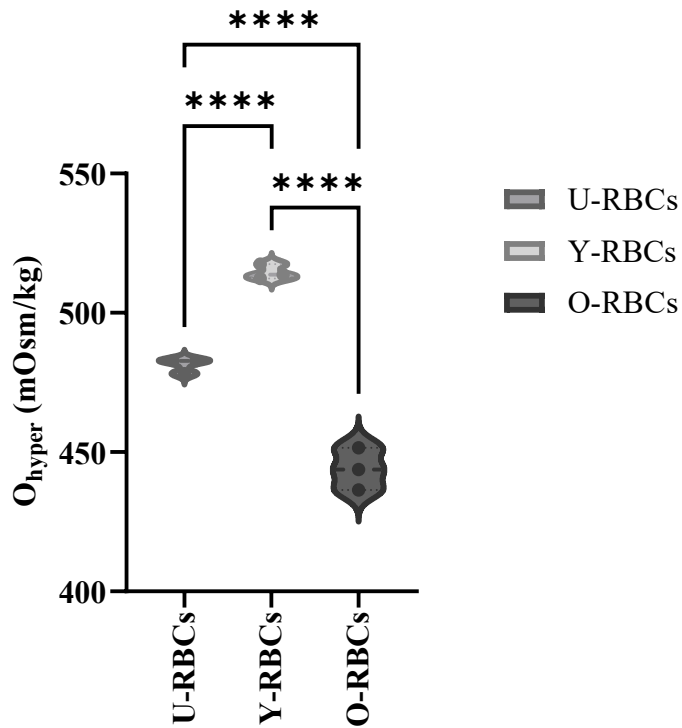


**Figure 3-18:** The figure illustrates the analysis of  $O_{\text{hyper}}$  values among RBC subpopulations. O-RBCs displayed the lowest  $O_{\text{hyper}}$  values, followed by U-RBCs with Y-RBCs exhibiting the highest  $O_{\text{hyper}}$ . ( $p < 0.0001$ ) Statistical significance denoted by \*:  $p < 0.05$ , \*\*:  $p < 0.01$ , \*\*\*:  $p < 0.001$ , and \*\*\*\*:  $p < 0.0001$ .

**Figure 3-19 Effect of Biotinylation on  $O_{\text{hyper}}$  Values in RBC Subpopulations**

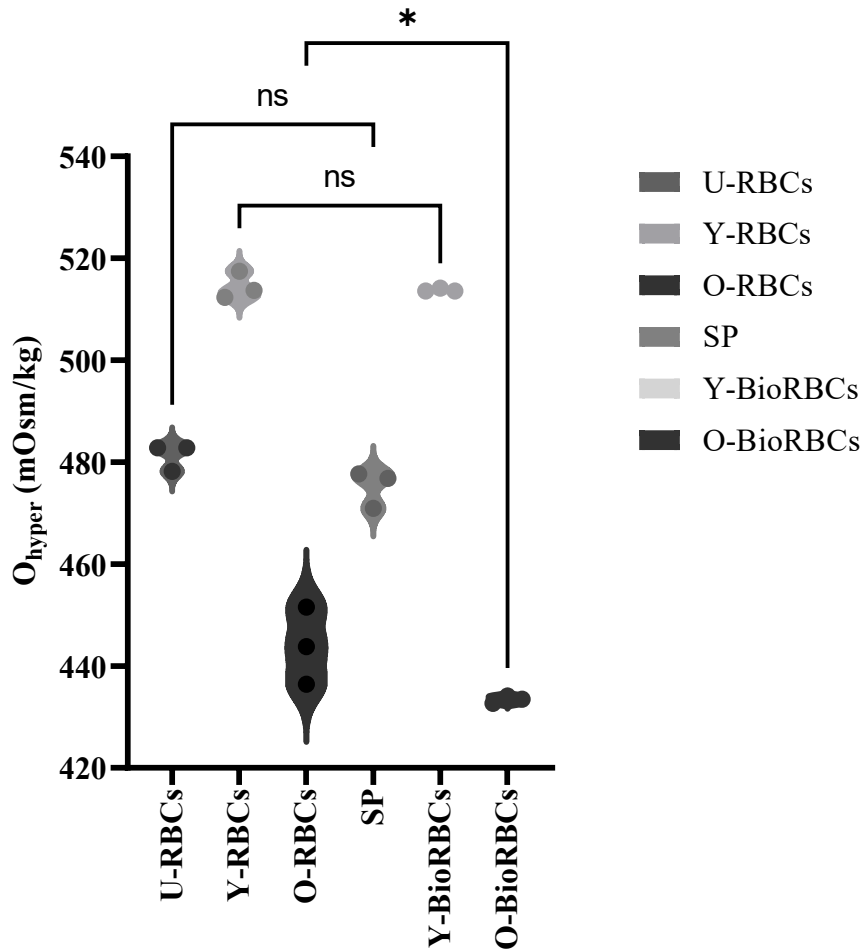


**Figure 3-19:** The figure demonstrates the impact of biotinylation on  $O_{\text{hyper}}$  values in RBC subpopulations. Biotinylation did not lead to a significant alteration of  $O_{\text{hyper}}$  in Y-RBCs. However, biotinylation resulted in a reduction in  $O_{\text{hyper}}$  in O-RBCs ( $p=0.0471$ ). Statistical significance denoted by \*:  $p<0.05$ , \*\*:  $p<0.01$ , \*\*\*:  $p<0.001$ , and \*\*\*\*:  $p<0.0001$ .

**Figure 3-20 Comparison of Maximum Elongation Index ( $EI_{max}$ ) Among RBC Subpopulations**

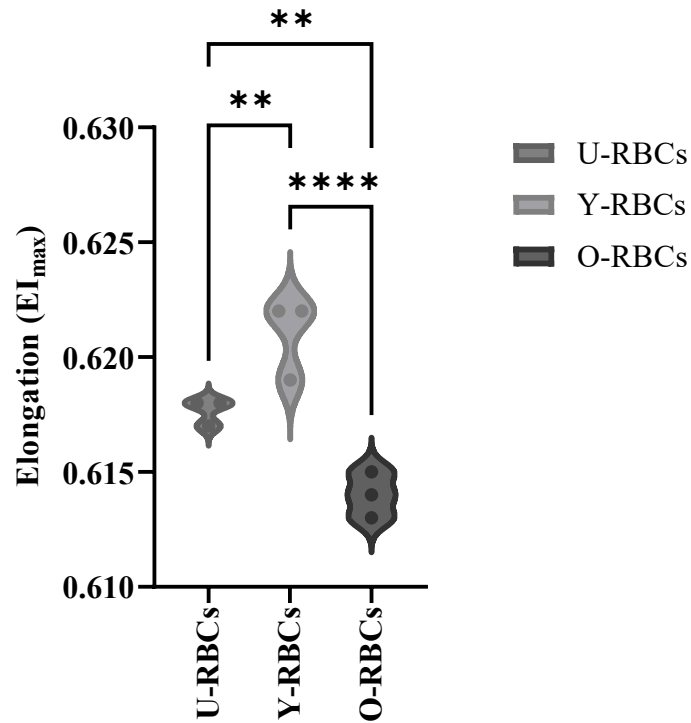


**Figure 3-20:** The figure illustrates the comparison of  $EI_{max}$  among RBC subpopulations. Y-RBCs displayed the highest  $EI_{max}$ , followed by U-RBCs, while O-RBCs demonstrated the lowest  $EI_{max}$  ( $p < 0.0001$ ). Statistical significance denoted by \*:  $p < 0.05$ , \*\*:  $p < 0.01$ , \*\*\*:  $p < 0.001$ , and \*\*\*\*:  $p < 0.0001$ .

**Figure 3-21 Impact of Biotinylation on Maximum Elongation Index ( $EI_{max}$ ) in RBC Subpopulations**

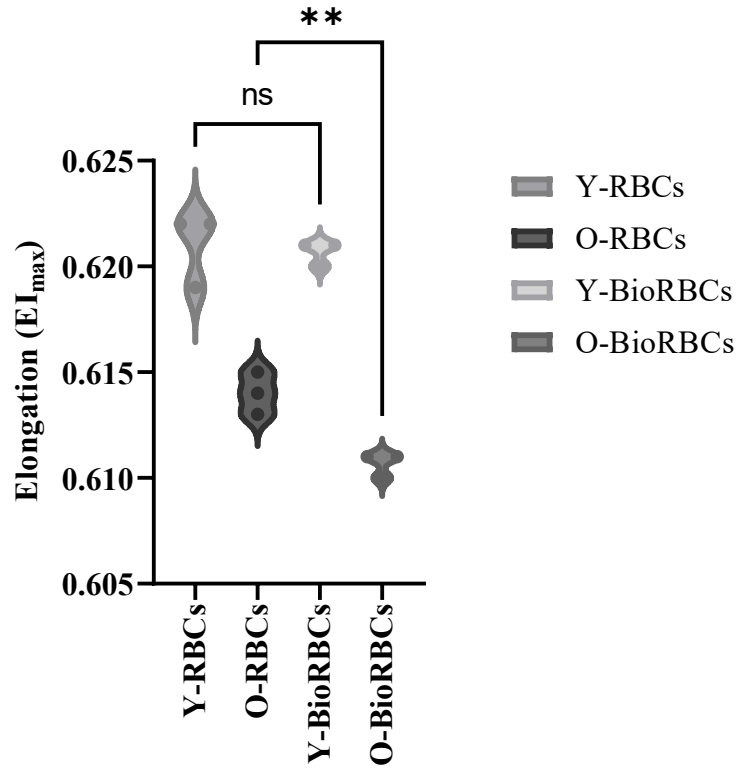


**Figure 3-21:** The figure depicts the influence of biotinylation on  $EI_{max}$  in RBC subpopulations. Biotinylation did not influence  $EI_{max}$  in Y-RBCs, while in O-RBCs, it resulted in a decrease in  $EI_{max}$ . O-BioRBCs demonstrated a lower  $EI_{max}$  compared to O-RBCs ( $p=0.0097$ ). Statistical significance denoted by \*:  $p<0.05$ , \*\*:  $p<0.01$ , \*\*\*:  $p<0.001$ , and \*\*\*\*:  $p<0.0001$ .

**Figure 3-22 Comparison of Elongation Index at Hypertonic Osmolality ( $EI_{\text{hyper}}$ ) Among RBC Subpopulations**

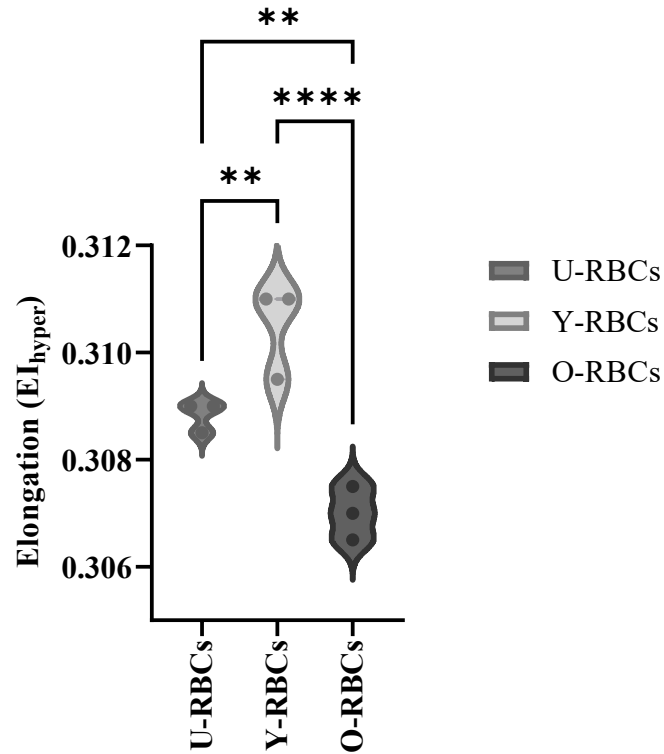


**Figure 3-22:** The figure illustrates the comparison of  $EI_{\text{hyper}}$  among RBC subpopulations. Y-RBCs showed the highest  $EI_{\text{hyper}}$ , followed by U-RBCs, while O-RBCs exhibited the lowest ( $p < 0.0001$ ). Statistical significance denoted by \*:  $p < 0.05$ , \*\*:  $p < 0.01$ , \*\*\*:  $p < 0.001$ , and \*\*\*\*:  $p < 0.0001$ .

**Figure 3-23 Impact of Biotinylation on Elongation Index at Hypertonic Osmolality ( $EI_{\text{hyper}}$ ) in RBC Subpopulations**

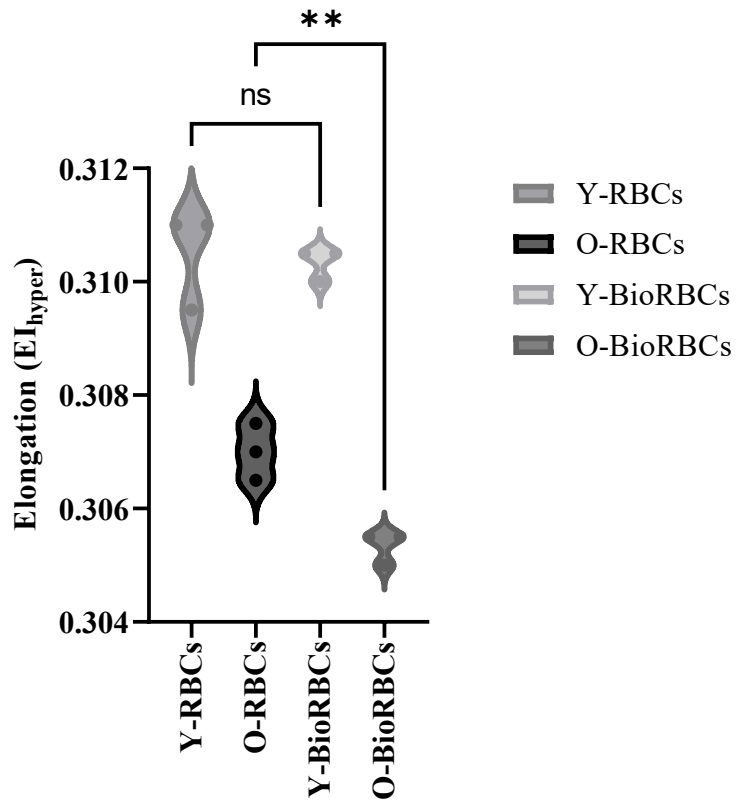


**Figure 3-23:** The figure depicts the effect of biotinylation on the Elongation Index at hypertonic osmolality ( $EI_{\text{hyper}}$ ) across RBC subpopulations. Biotinylation did not affect  $EI_{\text{hyper}}$  in Y-RBCs, while it resulted in a significant reduction in  $EI_{\text{hyper}}$  in O-RBCs ( $p=0.0097$ ). Statistical significance denoted by \*:  $p<0.05$ , \*\*:  $p<0.01$ , \*\*\*:  $p<0.001$ , and \*\*\*\*:  $p<0.0001$ .

**Figure 3-24 Comparison of Osmolality for Maximum Elongation Index ( $O(EI_{max})$ ) among RBC Subpopulations**

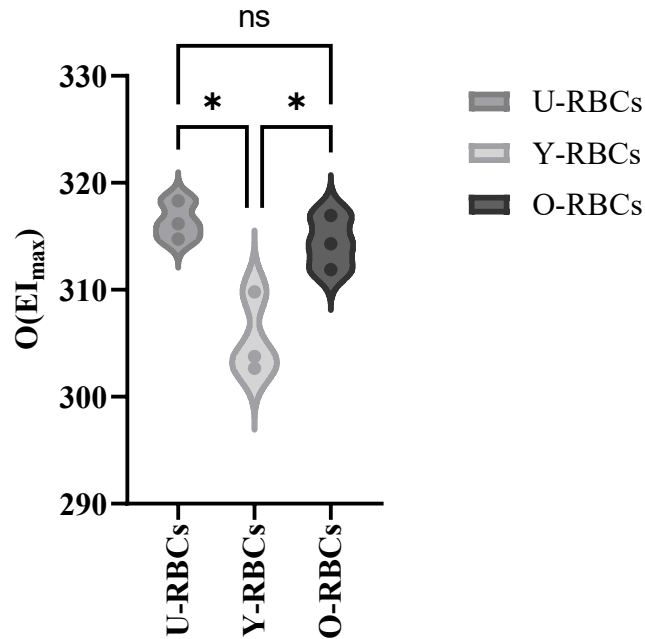


**Figure 3-24:** The figure illustrates the comparison of  $O(EI_{max})$  among RBC subpopulations. Y-RBCs exhibit the lowest  $O(EI_{max})$ , followed by O-RBCs and U-RBCs ( $p=0.0472$ ). Statistical significance denoted by \*:  $p<0.05$ , \*\*:  $p<0.01$ , \*\*\*:  $p<0.001$ , and \*\*\*\*:  $p<0.0001$ .

**Figure 3-25 Comparison of Initial Hemolysis Levels Post-RBC Separation among Subpopulations**

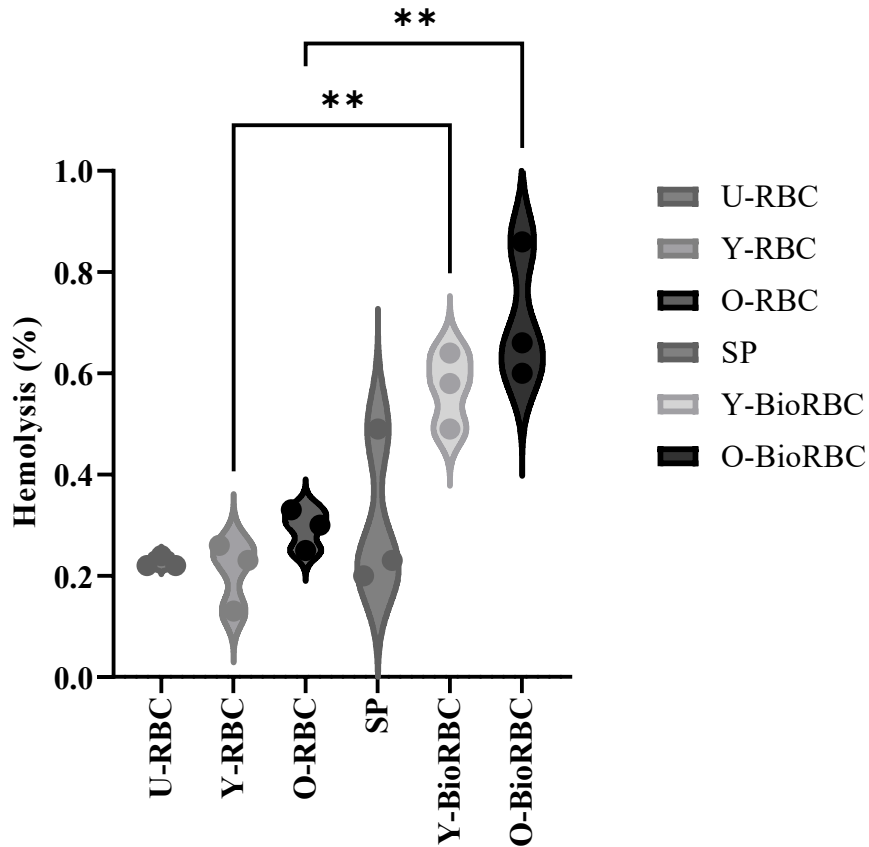


**Figure 3-25:** The graph presents the analysis of initial hemolysis levels post-RBC separation among subpopulations. No significant differences were observed initially among RBC subpopulations. However, the biotinylation process correlated with increased initial hemolysis levels in both Y- and O-RBC subpopulations (Y-RBCs vs. Y-BioRBC,  $p=0.0062$ ; O-RBCs vs. O-BioRBC,  $p=0.0022$ ). Statistical significance denoted by \*:  $p<0.05$ , \*\*:  $p<0.01$ , \*\*\*:  $p<0.001$ , and \*\*\*\*:  $p<0.0001$ .

**Figure 3-26 Comparison of Oxidative Hemolysis Levels Across RBC Subpopulations**

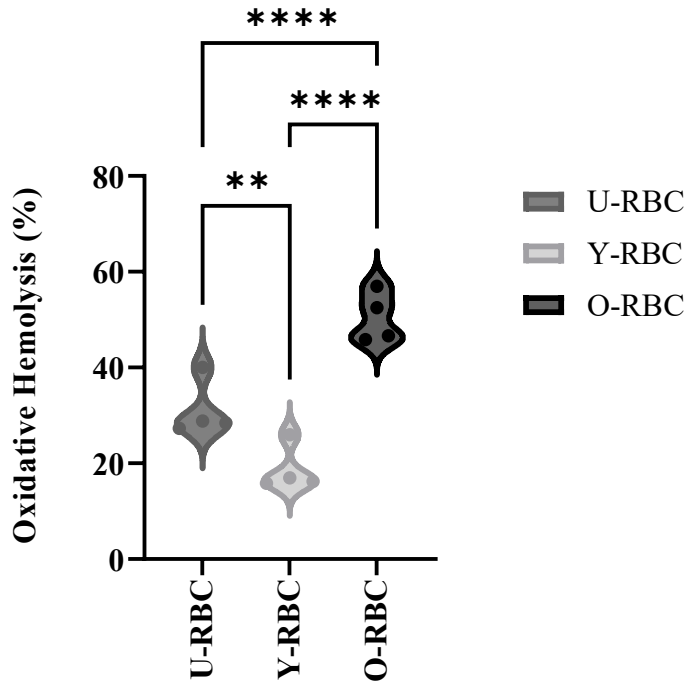


**Figure 3-26:** The figure illustrates the comparison of oxidative hemolysis levels among RBC Subpopulations. Y-RBCs displayed the lowest oxidative hemolysis, followed by U-RBCs, and O-RBCs exhibited the highest levels ( $p < 0.0001$ ). Statistical significance denoted by \*:  $p < 0.05$ , \*\*:  $p < 0.01$ , \*\*\*:  $p < 0.001$ , and \*\*\*\*:  $p < 0.0001$ .

**Figure 3-27 Effect of Biotinylation on Oxidative Hemolysis in RBC Subpopulations**

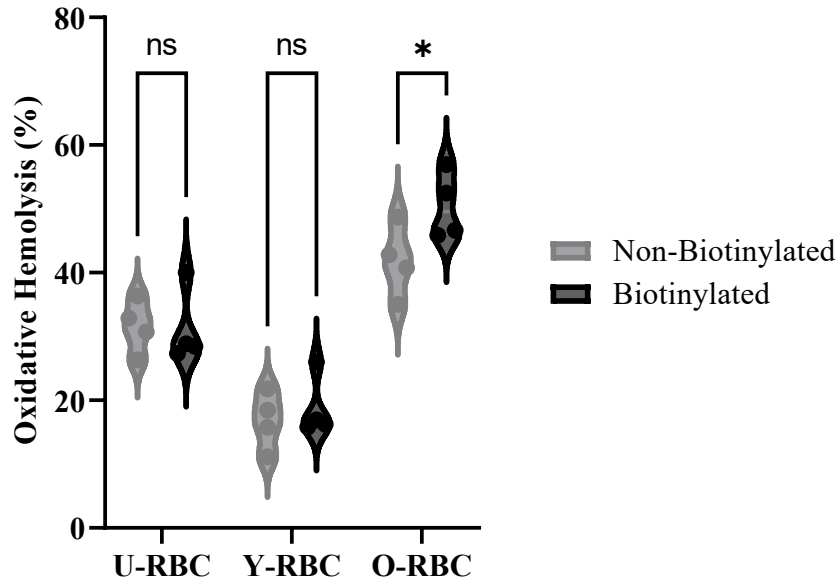


**Figure 3-27:** The figure illustrates the impact of biotinylation on oxidative hemolysis in RBC subpopulations. Biotinylation did not affect the oxidative hemolysis of Y-RBCs; however, it correlated with an upsurge in oxidative hemolysis in O-RBCs ( $p=0.0269$ ). Statistical significance denoted by \*:  $p<0.05$ , \*\*:  $p<0.01$ , \*\*\*:  $p<0.001$ , and \*\*\*\*:  $p<0.0001$ .

**Figure 3-28 Comparison of Osmotic Hemolysis Among RBC Subpopulations**

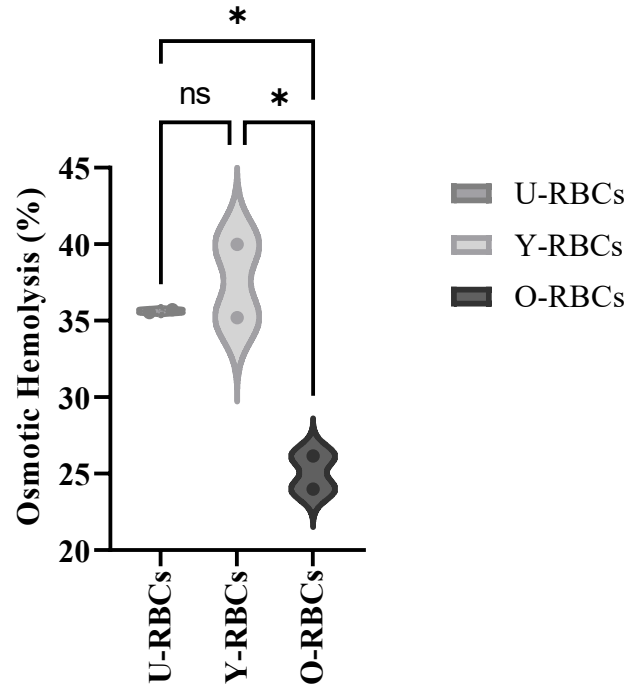


**Figure 3-28:** The figure illustrates the comparison of osmotic hemolysis among RBC subpopulations. O-RBCs demonstrate the lowest osmotic hemolysis compared to Y-RBCs and U-RBCs ( $p=0.0189$ ). Statistical significance denoted by \*:  $p<0.05$ , \*\*:  $p<0.01$ , \*\*\*:  $p<0.001$ , and \*\*\*\*:  $p<0.0001$ .

**Figure 3-29 Comparison of Osmotic Fragility Among RBC Subpopulations**

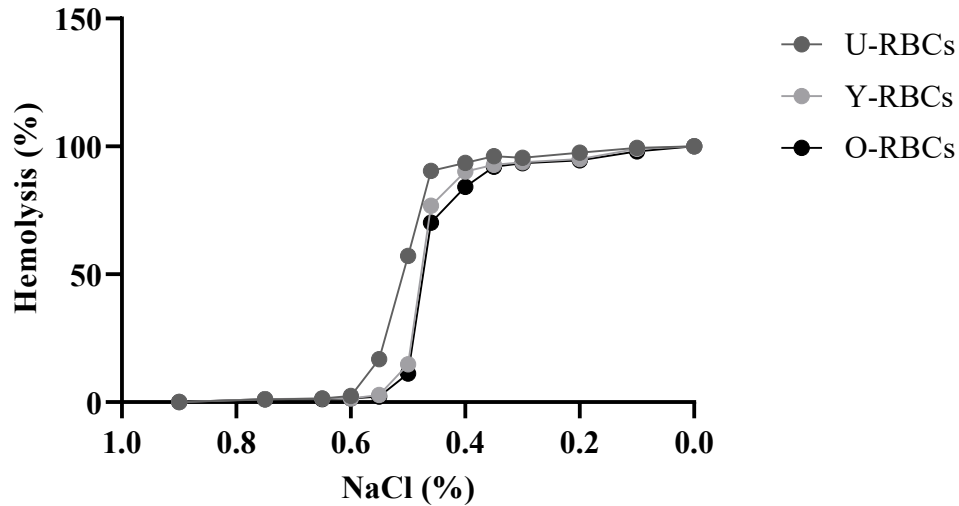


**Figure 3-29:** The graph illustrates the osmotic fragility results, indicating significant variations among RBC subpopulations. At 0.5% NaCl, U-RBCs exhibit higher hemolysis compared to Y-RBCs and O-RBCs. At 0.46% NaCl, O-RBCs displayed the lowest hemolysis, followed by Y-RBCs, with U-RBCs showing the highest hemolysis level ( $p=0.0177$ ). Similarly, at 0.4% NaCl, O-RBCs demonstrate the lowest hemolysis, Y-RBCs exhibit an intermediate level, and U-RBCs display the highest hemolysis ( $p=0.0035$ ).

**Figure 3-30 Tracking Changes in the Numbers of Biolabeled RBC Subpopulations Post-Deglycerolization**

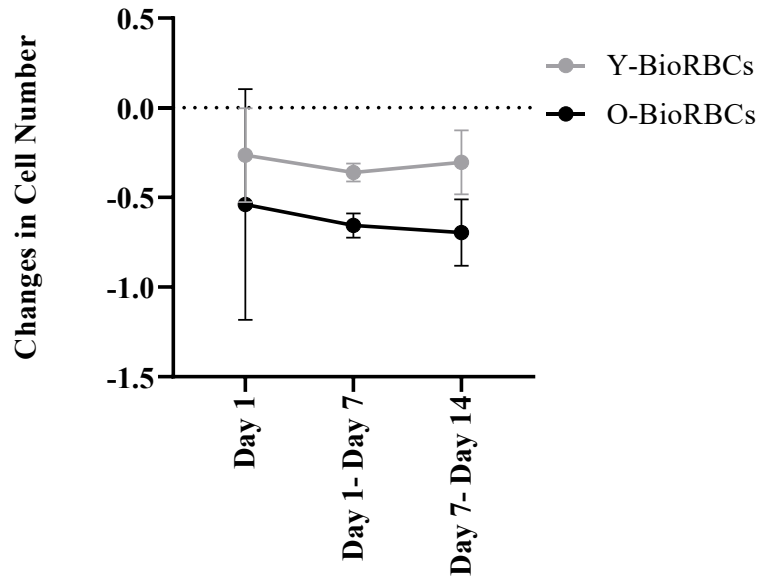


**Figure 3-30:** The graph illustrates the dynamic shifts in cell counts over the specified time points. Following deglycerolization and hypothermic storage, both Y- and O-BioRBCs experienced a decrease in cell numbers. There were no significant differences in the reduction trends between Y- and O-BioRBCs.

### 3.6 References

1. Sputtek A, Sputtek R. Cryopreservation in Transfusion Medicine and Hematology. In: Life in the Frozen State. CRC Press; 2004. p. 483–504.
2. BloodBook.com. (2024, March 4). Blood banking. Retrieved March 4, 2024, from <http://www.bloodbook.com/banking.html>
3. McGann LE. Differing actions of penetrating and nonpenetrating cryoprotective agents. *Cryobiology*. 1978 Aug;15(4):382-90.
4. Scott KL, Lecak J, Acker JP. Biopreservation of red blood cells: Past, present, and future. *Transfusion Medicine Reviews*. 2005;19(2):127–42.
5. Polge C, Smith AU, Parkes A. Revival of spermatozoa after vitrification and dehydration. Vol. 164, *Nature (London)*. 1949. p. 666.
6. A.U. Smith. Prevention Of Haemolysis During Freezing And Thawing Of Red Blood-Cells. *The Lancet*. 1950;256(6644):910–1.
7. P L Mollison, H A Sloviter. Successful transfusion of previously frozen human red cells. *The Lancet*. 1951;258(6689):862–4.
8. Meryman HT, Hornblower M. A method for freezing and washing red blood cells using a high glycerol concentration. *Transfusion (Paris)*. 1972;12(3):145–56.
9. Sputtek A, Kühnl P, Rowe AW. Cryopreservation of erythrocytes, thrombocytes, and lymphocytes. Vol. 34, *Transfusion Medicine and Hemotherapy*. 2007. p. 262–7.
10. Hess JR. Red cell freezing and its impact on the supply chain. *Transfusion Medicine*. 2004 Feb;14(1):1-8. DIO:10.1111/j.0958-7578.2004.00472.
11. Sputtek A. Cryopreservation of red blood cells and platelets. *Methods in Molecular Biology*. 2007;368:283-301.
12. Robert Valeri C, Ragno G, Pivacek LE, Srey R, Hess JR, Lippert LE, et al. A multicenter study of in vitro and in vivo values in human RBCs frozen with 40-percent (wt/vol) glycerol and stored after deglycerolization for 15 days at 4°C in AS-3: Assessment of RBC processing in the ACP® 215. *Transfusion (Paris)*. 2001;41(7):933–9.
13. N Mohandas, J A Chasis. Red blood cell deformability, membrane material properties and shape: regulation by transmembrane, skeletal and cytosolic proteins and lipids. *Seminars in Hematology*. 1993 Jun;30(3):171–92.
14. Weed RI, Laceille PL, Gael Craib M, Ann Gregory M, Fred Karch M, Franges Pickens M. Metabolic Dependence of Red Cell Deformability. *The journal of Clinical Investigation*, Vol. 48, 1969, 795-809.

15. Boas FE, Forman L, Beutler E. Phosphatidylserine exposure and red cell viability in red cell aging and in hemolytic anemia. *Proceedings of the National Academy of Sciences of the United States of America*. 1998 Mar 17;95(6):3077-81.
16. Gifford SC, Derganc J, Shevkoplyas SS, Yoshida T, Bitensky MW. A detailed study of time-dependent changes in human red blood cells: From reticulocyte maturation to erythrocyte senescence. *British Journal of Haematology*. 2006 Nov;135(3):395–404.
17. Lew VL, Tiffert T. On the Mechanism of Human Red Blood Cell Longevity: Roles of Calcium, the Sodium Pump, PIEZO1, and Gardos Channels. *Frontiers in Physiology*. 2017 Dec 12;8:977.
18. D'Alessandro A, Blasi B, D'Amici GM, Marrocco C, Zolla L. Red blood cell subpopulations in freshly drawn blood: Application of proteomics and metabolomics to a decades-long biological issue. *Blood Transfusion*. 2013;11(1):75–87.
19. An X, Mohandas N. Disorders of red cell membrane. In: *British Journal of Haematology*. 2008. p. 367–75.
20. Bosman GJCGM, Werre JM, Willekens FLA, Novotný VMJ. Erythrocyte ageing in vivo and in vitro: Structural aspects and implications for transfusion. *Transfusion Medicine*. 2008;18(6):335–47.
21. Kiefer CR, Snyder LM. Oxidation and erythrocyte senescence. *Current Opinion in Hematology*. 2000;7(2):113–6.
22. Kay MMB, Goodman SR, Sorensen K, Whitfield CF, Wong P, Zaki L, et al. Senescent cell antigen is immunologically related to band 3. *Proceedings of the National Academy of Sciences of the United States of America*. 1983;80(6 D):1631–5.
23. Lutz HU, Stammler P, Fasler S. Preferential formation of C3b-IgG complexes in vitro and in vivo from nascent C3b and naturally occurring anti-band 3 antibodies. *Journal of Biological Chemistry*. 1993;268(23):17418–26.
24. Khandelwal S, Saxena RK. A role of phosphatidylserine externalization in clearance of erythrocytes exposed to stress but not in eliminating aging populations of erythrocyte in mice. *Experimental Gerontology*. 2008;43(8):764–70.
25. Bosman GJCGM, Lasonder E, Groenen-Döpp YAM, Willekens FLA, Werre JM, Novotný VMJ. Comparative proteomics of erythrocyte aging in vivo and in vitro. *Journal of Proteomics*. 2010;73(3):396–402.
26. Willekens FLA, Roerdinkholder-Stoelwinder B, Groenen-Döpp YAM, Bos HJ, Bosman GJCGM, van den Bos AG, et al. Hemoglobin loss from erythrocytes in vivo results from spleen-facilitated vesiculation. *Blood*. 2003;101(2):747–51.
27. Piomelli S, Seaman C. Mechanism of red blood cell aging: Relationship of cell density and cell age. *American Journal of Hematology*. 1993;42(1):46–52.

28. Bosch FH, Werre JM, Roerdinkholder-Stoelwinder B, Huls TH, Willekens FLA, Halie MR. Characteristics of red blood cell populations fractionated with a combination of counterflow centrifugation and Percoll separation. *Blood*. 1992;79(1):254–60.
29. Mueller TJ, Jackson CW, Dockter ME, Morrison M. Membrane skeletal alterations during in vivo mouse red cell aging. Increase in the band 4.1a:4.1b ratio. *Journal of Clinical Investigation*. 1987;79(2):492–9.
30. Lutz H, Stammler P, Fasler S, Ingold M, Fehr J. Density separation of human red blood cells on self forming Percoll. *Biochimica biophysica acta (G) General subjects*. 1992;1116(1):1–10.
31. Rettig MP, Low Philip S. PS, Gimm JA, Mohandas N, Wang J, Christian JA. Evaluation of biochemical changes during in vivo erythrocyte senescence in the dog. *Blood*. 1999;93(1):376–84.
32. Ando K, Beppu M, Kikugawa K, Nagai R, Horiuchi S. Membrane proteins of human erythrocytes are modified by advanced glycation end products during aging in the circulation. *Biochemical and Biophysical Research Communications*. 1999;258(1):123–7.
33. Almizraq RJ, Seghatchian J, Acker JP. Extracellular vesicles in transfusion-related immunomodulation and the role of blood component manufacturing. *Transfusion and Apheresis Science*. 2016;55(3):281–91.
34. Weisel JW, Litvinov RI. Red blood cells: the forgotten player in hemostasis and thrombosis. *Journal of Thrombosis and Haemostasis*. 2019;17(2):271–82.
35. Blasi B, D'Alessandro A, Ramundo N, Zolla L. Red blood cell storage and cell morphology. *Transfusion Medicine*. 2012;22(2):90–6.
36. D'Alessandro A, D'Amici GM, Vaglio S, Zolla L. Time-course investigation of sgm-stored leukocyte-filtered red blood cell concentrates: From metabolism to proteomics. *Haematologica*. 2012;97(1):107–15.
37. Malka R, Delgado FF, Manalis SR, Higgins JM. In Vivo Volume and Hemoglobin Dynamics of Human Red Blood Cells. *PLoS Computational Biology*. 2014;10(10).
38. Kameneva M V., Garrett KO, Watach MJ, Borovetz HS. Red blood cell aging and risk of cardiovascular diseases. *Clinical Hemorheology and Microcirculation*. 1998;18(1):67–74.
39. Simak J, Gelderman MP. Cell membrane microparticles in blood and blood products: potentially pathogenic agents and diagnostic markers. *Transfusion Medicine Reviews*. 2006 Jan;20(1):1-26.
40. Greenwalt TJ. The how and why of exocytic vesicles. *Transfusion*. 2006 Jan;46(1):143-52.

41. Denise Harmening. Clinical hematology and fundamentals of hemostasis. 2024 Sixth edition. Denise Harmening, LeAnne M. Hutson, editors. F.A. Davis Co., Philadelphia, PA, ©2009; 2002.
42. Hardeman MR, Dobbe JG, Ince C. The Laser-assisted Optical Rotational Cell Analyzer (LORCA) as red blood cell aggregometer. *Clinical Hemorheology and Microcirculation*. 2001;25(1):1–11.
43. Stadnick H, Onell R, Acker JP, Holovati JL. Eadie-Hofstee analysis of red blood cell deformability. *Clinical Hemorheology and Microcirculation*. 2011;47(3):229–39.
44. Franco RS, Puchulu-Campanella ME, Barber LA, Palascak MB, Joiner CH, Low PS, et al. Changes in the properties of normal human red blood cells during in vivo aging. *American Journal of Hematology*. 2013 Jan;88(1):44–51.
45. Orbach A, Zelig O, Yedgar S, Barshtein G. Biophysical and Biochemical Markers of Red Blood Cell Fragility. *Transfusion Medicine and Hemotherapy*. 2017;44(3):183–7.
46. Cohen AR, Schmidt JM, Martin MB, Barnsley W, Schwartz E. Clinical trial of young red cell transfusions. *The Journal of Pediatrics*. 1984;104(6):865–8.
47. Acker JP, Hansen AL, Kurach JDR, Turner TR, Croteau I, Jenkins C. A quality monitoring program for red blood cell components: In vitro quality indicators before and after implementation of semiautomated processing. *Transfusion (Paris)*. 2014;54(10):2534–43.
48. Bruil A, Beugeling T, Feijen J, van Aken WG. The mechanisms of leukocyte removal by filtration. *Transfusion Medicine Reviews*. 1995;9(2):145–66.
49. Mykhailova O, Brandon-Coatham M, Phan C, Yazdanbakhsh M, Olafson C, Yi QL, Kanas T, Acker JP. Red cell concentrates from teen male donors contain poor-quality biologically older cells. *Vox Sang*. 2024 Feb 28.
50. Mykhailova O, Brandon-Coatham M, Durand K, Olafson C, Xu A, Yi QL, Kanas T, Acker JP. Estimated median density identifies donor age and sex differences in red blood cell biological age. *Transfusion*. 2024 Feb 29.
51. Zhurova M, McGann LE, Acker JP. Osmotic parameters of red blood cells from umbilical cord blood. *Cryobiology*. 2014;68(3):379–88.
52. Zhurova M, Olivieri A, Holt A, Acker JP. A method to measure permeability of red blood cell membrane to water and solutes using intrinsic fluorescence. *Clinica Chimica Acta*. 2014;431:103–10.
53. Mazur P, Leibo SP, Chu EH. A two-factor hypothesis of freezing injury. Evidence from Chinese hamster tissue-culture cells. *Experimental Cell Research*. 1972;71(2):345–55.

54. Mazur P. The Role Of Cell Membranes In The Freezing Of Yeast And Other Single Cells. *Annals of the New York Academy of Sciences*. 1965;125(2):658–76.
55. Nagashima H, Kashiwazaki N, Ashman RJ, Grupen CG, Seamark RF, Nottle MB. Removal of cytoplasmic lipid enhances the tolerance of porcine embryos to chilling. *Biology of Reproduction*. 1994 Oct;51(4):618-22.
56. J E Lovelock. The denaturation of lipid-protein complexes as a cause of damage by freezing. *Proceedings of the Royal Society B: Biological Sciences*. 1957 Dec 17;17(147(929)):427–33.
57. Hall, John E. *Guyton and Hall Textbook of Medical Physiology*. 13th ed., W B Saunders, 2015
58. Benga G, Borza T. Diffusional water permeability of mammalian red blood cells. *Comparative Biochemistry and Physiology Part B: Biochemistry & Molecular Biology*. 1995 Dec;112(4):653-9.
59. Ross-Rodriguez LU, Elliott JAW, McGann LE. Investigating cryoinjury using simulations and experiments. 1: TF-1 cells during two-step freezing (rapid cooling interrupted with a hold time). *Cryobiology*. 2010 Aug;61(1):38–45.
60. Lahmann JM, Sanchez CC, Benson JD, Acker JP, Higgins AZ. Implications of variability in cell membrane permeability for design of methods to remove glycerol from frozen-thawed erythrocytes. *Cryobiology*. 2020 Feb 1;92:168–79.
61. Jay AW, Rowlands S. The stages of osmotic haemolysis. *The Journal of Physiology*. 1975 Nov;252(3):817-32.
62. Jordan A, Chen D, Yi QL, Kanas T, Gladwin MT, Acker JP. Assessing the influence of component processing and donor characteristics on quality of red cell concentrates using quality control data. *Vox Sang*. 2016;111(1):8–15.
63. Kanas T, Sinchar D, Osei-Hwedieh D, Baust JJ, Jordan A, Zimring JC, et al. Testosterone-dependent sex differences in red blood cell hemolysis in storage, stress, and disease. *Transfusion (Paris)*. 2016;56(10):2571–83.
64. Alshalani A, Howell A, Acker JP. Impact of blood manufacturing and donor characteristics on membrane water permeability and in vitro quality parameters during hypothermic storage of red blood cells. *Cryobiology*. 2018 Feb 1;80:30–7.
65. Alshalani A, Acker JP. Red blood cell membrane water permeability increases with length of ex vivo storage. *Cryobiology*. 2017 Jun 1;76:51–8.
66. Hansen AL, Kurach JDR, Turner TR, Jenkins C, Busch MP, Norris PJ, et al. The effect of processing method on the in vitro characteristics of red blood cell products. *Vox Sang*. 2015;108(4):350–8.

67. de Back DZ, Vlaar R, Beuger B, Daal B, Lagerberg J, Vlaar APJ, et al. A method for red blood cell biotinylation in a closed system. *Transfusion (Paris)*. 2018 Apr 1;58(4):896–904.
68. Mock DM, Matthews NI, Zhu S, Burmeister LF, Zimmerman MB, Strauss RG, et al. Red blood cell (RBC) volume can be independently determined in vivo in humans using RBCs labeled at different densities of biotin. *Transfusion (Paris)*. 2011 Jan;51(1):148–57.
69. Mock DM, Matthews NI, Zhu S, Strauss RG, Schmidt RL, Nalbant D, et al. Red blood cell (RBC) survival determined in humans using RBCs labeled at multiple biotin densities. *Transfusion (Paris)*. 2011 May;51(5):1047–57.
70. Protocol for Biotinylation of Red Blood Cells. Dr. Jason Acker’s laboratory, Version 1.2, Revised 2023-01-10.
71. McGann LE, Turner AR, Turc JM. Microcomputer interface for rapid measurements of average volume using an electronic particle counter. *Medical and Biological Engineering and Computing*. 1982 Jan;20(1):117-20.
72. Ross-Rodriguez LU, Elliott JAW, McGann LE. Characterization of cryobiological responses in TF-1 cells using interrupted freezing procedures. *Cryobiology*. 2010 Apr;60(2):106–16.
73. Protocol Micro Osmette 5004 Osmometer. Dr. Jason Acker’s laboratory, Version 0.3, Revised 2022-08-19.
74. Chen PY, Pearce D, Verkman AS. Membrane water and solute permeability determined quantitatively by self-quenching of an entrapped fluorophore. *Biochemistry*. 1988 Jul 26;27(15):5713-8.
75. Agre P, Smith B L, Baumgarten R, Preston G M, Pressman E, Wilson P, Illum N, Anstee D J, Lande M B, Zeidel M L. Human Red Cell Aquaporin CHIP 11. Expression during Normal Fetal Development and in a Novel Form of Congenital Dyserythropoietic Anemia. *Journal of Clinical Investigation*. 1994;94(3):1050-1058.
76. Mariia Zhurova. Cryobiological characteristics of red blood cells from human umbilical cord blood. University of Alberta; 2013.
77. Hirsch RE, Zukin RS, Nagel RL. Intrinsic fluorescence emission of intact oxy hemoglobins. *Biochemical and Biophysical Research Communications*. 1980 Mar 28;93(2):432-9.
78. Prickett RC, Elliott JAW, Hakda S, McGann LE. A non-ideal replacement for the Boyle van’t Hoff equation. *Cryobiology*. 2008 Oct;57(2):130–6.
79. Jacobs MH. The simultaneous measurement of cell permeability to water and to dissolved substances. *Journal of Cellular Physiology*. 1933 Feb;2(4):427–44.

80. Jacobs MH, Stewart DR. A simple method for the quantitative measurement of cell permeability. *Journal of Cellular Physiology*. 1932 Feb;1(1):71–82.
81. Ebertz SL, McGann LE. Cryoprotectant permeability parameters for cells used in a bioengineered human corneal equivalent and applications for cryopreservation. *Cryobiology*. 2004 Oct;49(2):169–80.
82. Ross-Rodriguez LU, Elliott JAW, McGann LE. Characterization of cryobiological responses in TF-1 cells using interrupted freezing procedures. *Cryobiology*. 2010 Apr;60(2):106–16.
83. Protocol for Determining RBC Deformability using the LORCA (Laser Optical Rotational Red Cell Analyzer). Dr. Jason Acker's laboratory, Version 1.0, Created 2019-01-03.
84. Protocol for Osmoscan using the LORCA (Laser Optical Rotational Red Cell Analyzer). Dr. Jason Acker's laboratory, Version 1.0, Created 2019-01-04.
85. Protocol for determining % hemolysis. Dr. Jason Acker's laboratory, version 4.5, revised 2008-12-16.
86. Recommendations for reference method for haemoglobinometry in human blood (ICSH standard 1995) and specifications for international haemoglobinocyanide standard (4th edition) International Council for Standardisation in Haematology: Expert Panel on Haemoglobinometry Introduction Scientific symposia.
87. Protocol for Determining Microhematocrit. Dr. Jason Acker's laboratory, Version 4.2, revised 2015-10-28.
88. Protocol for AAPH-induced oxidative hemolysis. Dr. Jason Acker's laboratory, Version 1.3. Revised 2021-08-05.
89. Protocol for Osmotic Hemolysis. Dr. Jason Acker's laboratory, Version 0.2, Revised 2022-08-05.
90. Protocol for Determining Osmotic Fragility. Dr. Jason Acker's laboratory, Version 1.0, Created 2007-06-07.
91. ACP<sup>®</sup> 215 Preparation of Frozen Red Cells. Canadian Blood Service, WI# 02 180 Revision #2.
92. ACP<sup>®</sup> 215 Preparation of Deglycerolized Red Cells. Canadian Blood Service, WI# 02 181 Revision #3.
93. A flow cytometric method to quantify biotinylated red blood cells. Dr. Jason Acker's laboratory, Version 1.2, Revised 2023-01-05.
94. Nash GB, Meiselman HJ. Red cell and ghost viscoelasticity. Effects of hemoglobin concentration and in vivo aging. *Biophysical Journal*. 1983;43(1):63–73.

95. Bocci V. Determinants Of Erythr Ocyte Ageing: A Reappraisal. *British Journal of Haematology*. 1981;48(4):515–22.
96. Linderkamp O, Meiselman HJ. Geometric, osmotic, and membrane mechanical properties of density-separated human red cells. *Blood*. 1982 Jun;59(6):1121-7.
97. Sutura SP, Gardner RA, Boylan CW, Carroll GL, Chang KC, Marvel JS, Kilo C, Gonen B, Williamson JR. Age-related changes in deformability of human erythrocytes. *Blood*. 1985 Feb;65(2):275-82.
98. Bogdanova A, Petrushanko IY, Hernansanz-Agustín P, Martínez-Ruiz A. "Oxygen Sensing" by Na,K-ATPase: These Miraculous Thiols. *Frontiers in Physiology*. 2016 Aug 2;7:314.
99. Chu H, Puchulu-Campanella E, Galan JA, Tao WA, Low PS, Hoffman JF. Identification of cytoskeletal elements enclosing the ATP pools that fuel human red blood cell membrane cation pumps. *Proceedings of the National Academy of Sciences of the United States of America*. 2012 Jul 31;109(31):12794–9.
100. Kuo MS, Chuang CH, Cheng HC, Lin HR, Wang JS, Hsu K. Different Involvement of Band 3 in Red Cell Deformability and Osmotic Fragility-A Comparative GP.Mur Erythrocyte Study. *Cells*. 2021 Nov 30;10(12):3369.
101. Lew VL, Daw N, Etzion Z, Tiffert T, Muoma A, Vanagas L, Bookchin RM. Effects of age-dependent membrane transport changes on the homeostasis of senescent human red blood cells. *Blood*. 2007 Aug 15;110(4):1334-42.
102. Keller MA, Piedrafita G, Ralser M. The widespread role of non-enzymatic reactions in cellular metabolism. *Current Opinion in Biotechnology*. 2015 Aug;34:153-61.
103. Piedrafita G, Keller MA, Ralser M. The Impact of Non-Enzymatic Reactions and Enzyme Promiscuity on Cellular Metabolism during (Oxidative) Stress Conditions. *Biomolecules*. 2015 Sep 10;5(3):2101-22.
104. González Flecha FL, Castello PR, Gagliardino JJ, Rossi JP. Molecular characterization of the glycated plasma membrane calcium pump. *The Journal of Membrane Biology*. 1999 Sep 1;171(1):25-34. 105.
105. Elmoazzen HY, Elliott JA, McGann LE. The effect of temperature on membrane hydraulic conductivity. *Cryobiology*. 2002 Aug;45(1):68-79.
106. Verkman AS, van Hoek AN, Ma T, Frigeri A, Skach WR, Mitra A, Tamarappoo BK, Farinas J. Water transport across mammalian cell membranes. *American Journal of Physiology*. 1996 Jan;270(1 Pt 1):C12-30.
107. Tillmann W, Levin C, Prindull G, Schröter W. Rheological properties of young and aged human erythrocytes. *Wiener klinische Wochenschrift*. 1980 Jun 2;58(11):569-74.

108. Mykhailova O, Olafson C, Turner TR, D'Alessandro A, Acker JP. Donor-dependent aging of young and old red blood cell subpopulations: Metabolic and functional heterogeneity. *Transfusion (Paris)*. 2020;60(11):2633–46.
109. N Mohandas, S B Shohet. Control of red cell deformability and shape. *Current Topics in Hematology* . 1978;1:75–125.
110. Mykhailova O, Olafson C, Turner TR, D'Alessandro A, Acker JP. Donor-dependent aging of young and old red blood cell subpopulations: Metabolic and functional heterogeneity. *Transfusion (Paris)*. 2020;60(11):2633–46.

## **Chapter 4**

### **Exploring the Impact of Gamma Irradiation on Biologically Young and Old Subpopulations of Red Blood Cells**

## 4.1 Introduction

Gamma irradiation of RCCs is utilized to prevent TA-GVHD, a rare but often fatal complication for high-risk recipients, by preventing DNA replication in donor T-lymphocytes that may be present in the RCCs. (1) Irradiation of leukoreduced RCCs is the standard care for patients at risk of GVHD, including patients with immune deficiencies, intrauterine transfusions, and allogeneic stem cell recipients. (2) The Association for Advancement of Blood & Biotherapies (AABB) and Canadian Standards Association (CSA) have suggested that irradiation can be performed at any time during storage (up to day 42) and that the irradiated RCCs can be stored for up to 28 days, not exceeding the original expiry date. (3,4) In the United States and Canada, a minimum dose of 25 grays (Gy) to the midpoint of the component and of 15 Gy to the entire component is required. (3,4)

### 4.1.1 Impact of Gamma-Irradiation on Red Blood Cells

Gamma-irradiation through different mechanisms accelerates storage lesions (5), causing predominantly biochemical changes and altering RBC metabolism. (6–8) Radiation induces oxidative stress that compromises RBC membrane integrity, leading to membrane destabilization, protein denaturation, hemolysis, and impaired oxygen delivery. (9–13) Gamma-irradiation affects the homeostasis of RBCs, disrupting the function of ion transporters and channels on the RBC membrane. (14–16) Radiation-induced oxidative stress affects the metabolomics of RBCs by targeting enzymes involved in glycolysis and the Krebs cycle, disrupting ATP production. The impaired metabolomics system of RBCs affects its homeostasis by disrupting the function of ion transporters and channels that rely on ATP. (9–12) This disruption can change the intracellular ion concentrations, increasing the cytosolic  $\text{Ca}^{2+}$  concentration (9–12,17), and triggering microvesiculation and  $\text{K}^+$  leakage by activation of calcium-sensitive  $\text{K}^+$  channels. (18–25) Irradiation also disrupts the integrity of RBC membranes and associated proteins, leading to the release of Hb and lactate dehydrogenase (LDH), which accelerates aging processes. (18–21) Previous studies have demonstrated that the elevation in supernatant  $\text{K}^+$  and hemolysis levels becomes more pronounced with extended post-irradiation storage duration. (26–28) This considerable elevation in  $\text{K}^+$  levels and hemolysis increases the risk of post-transfusion hyperkalemia and subsequent cardiac complications, particularly in neonates or patients undergoing massive transfusions.

(21,23,28,29) Additionally, decreased ATP levels impede the progression through the Ruperport-Leubering shunt, leading to lower levels of 2,3-DPG (30), enhanced O<sub>2</sub> affinity, and impaired O<sub>2</sub> delivery post-transfusion. (31)

#### **4.1.2 RBC Biological Aging**

RCCs consist of different subpopulations of RBCs with varying biological age, including Y-RBC and O-RBC. (32–34) The biological aging of RBCs is characterized by changes in RBC properties. (32) Metabolomic analysis reveals unique metabolic signatures within Y- and O-RBCs, indicating that the capacity to cope with oxidant stress decreases with RBC aging. (34) Additionally, the biological aging of RBCs leads to a rapid depletion of ATP and 2,3-DPG, disrupting energy-dependent activities within RBCs. (32,35) Different studies revealed that transfusion of RCCs containing a higher presence of O-RBCs within the RCCs is associated with a higher level of storage hemolysis and impaired oxygen delivery post-transfusion. (34,36–38) Given the compromised function of membrane proteins and reduced antioxidant defense in O-RBCs (34,37), these cells are more likely to be susceptible to oxidative stress induced by irradiation. Therefore, it is hypothesized that O-RBCs, with their compromised membrane and antioxidant defense mechanisms, may contribute significantly to the observed increase in hemolysis, supernatant potassium levels in RCCs, and impaired RBC oxygen delivery post-irradiation.

This study aims to investigate the impact of gamma irradiation on Y- and O-RBC subpopulations. The study involved a comparison of oxidative stress, p50, and supernatant K<sup>+</sup> levels in Y- and O-RBCs before and after gamma irradiation. These parameters were monitored throughout hypothermic storage for up to 14 days post-irradiation. Anticipated outcomes include higher supernatant K<sup>+</sup> levels and increased hemolysis in O-RBCs due to compromised membrane function, alongside elevated O<sub>2</sub> affinity possibly attributed to decreased 2,3-DPG concentration and increased methemoglobin concentration post-irradiation. Biotinylation will be utilized to evaluate the post-irradiation recovery of Y- and O-BioRBCs, with an expectation of higher recovery rates in Y-BioRBCs compared to O-BioRBCs. The investigation aims to optimize irradiation strategies by aiming for a

favorable Y- to O-RBC ratio in RCCs designated for irradiation, thereby improving their quality and effectiveness for transfusion purposes, particularly in vulnerable patient populations.

## **4.2 Method and Material**

### **4.2.1 Red Cell Concentrate (RCC) Selection and Pooling**

The Canadian Blood Services Blood4Research provided the RCCs from healthy donors and collected in Macopharma collection bags, processed via the RCF method, and stored in CPD and SAGM at temperatures ranging from 1-6 °C. To maintain optimal integrity, the RCCs used in the experiments were within seven days of their collection. Approval for the study was obtained from both the University of Alberta Health Research Ethics Board (Biomedical Panel; Protocol #PRO00103459) and the Canadian Blood Services Research Ethics Board (Protocol #2020.005).

To mitigate the potential influence of donor variability on RBC subpopulation density profiles, six ABO/Rh-matched RCCs were pooled. Four units were from female donors with an average age of  $54 \pm 14.5$  years old, while two units were from male donors with an average age of  $32 \pm 1$  years old. The RBC indices for each unit were measured using a cell counter. The RBC parameters within our dataset are as follows: HCT:  $0.571 \pm 0.004$  (%) (CV: 3.38%), Hb:  $186.39 \pm 1.90$  (g/dL) (CV: 4.45%), MCHC:  $326.61 \pm 3.5$  (g/dL) (CV: 4.68%), and MCV:  $87.86 \pm 2.65$  (fL) (CV: 132.15%) ([Table 4-1](#)). The units were pooled in a waste bag from the Haemonetics Deglycerolization set (LN 236; capacity of up to 4000 mL). In Chapter 3, the pooling process have been described in detail.

### **4.2.2 Density-Fractionation using Percoll® Separation**

The Percoll® separation was utilized to investigate the density distribution of RBCs within the pooled unit. A comprehensive explanation of this method can be found in Chapter 2, where all aspects of the technique are discussed in detail. To isolate sufficient volumes of Y- and O-RBCs, an aliquot of 450 mL from the pooled unit was collected into nine 50 mL conical tubes. A 25 mL aliquot was reserved for density profiling of the pooled unit, while 425 mL was used for extracting sufficient volume of the Y- and O-RBC

subpopulations for further experiments. RBC indices were assessed using a hematology analyzer, and the Percoll<sup>®</sup> densities necessary for creating a density panel were estimated using the method proposed by Mykhailova et al., which involves estimating Percoll<sup>®</sup> density based on RBC indices using measurements of MCHC and MCV. (39,40)

Percoll<sup>®</sup> solutions with varying densities were carefully prepared, ranging from 1.087 to 1.099 g/mL. A 3 mL aliquot of each Percoll<sup>®</sup> solution was distributed into designated tubes, followed by gently layering a 1 mL aliquot of RBCs onto the solutions. The tubes underwent centrifugation, after which the Y-RBCs were isolated into separate tubes while the O-RBC pellet remained undisturbed at the bottom. The RBC subpopulations were washed with PBS, and then the supernatants were carefully removed, leaving PBS covering the packed RBCs to achieve a hematocrit range of 40-55%. The RBC indices for each subpopulation were measured using a hematology analyzer. The volume of each RBC subpopulation was measured using a calibrated adjustable-volume pipette to estimate the proportion of each subpopulation. A density of 1.088 g/mL was chosen for separating Y-RBCs, while 1.099 g/mL was selected for isolating O-RBCs, constituting  $13.8 \pm 0.07\%$  and  $18.5 \pm 0.07\%$  of the total population, respectively. The Percoll<sup>®</sup> separation was repeated with these selected densities (1.088, 1.099) to extract a sufficient volume of Y- and O-RBC subpopulations (with a minimum volume requirement of 20 mL per RBC subpopulation at 50% HCT).

#### **4.2.3 Biotinylation of Red Blood Cell**

Two concentrations of the biotin reagent (15  $\mu\text{g/mL}$  and 48  $\mu\text{g/mL}$ ) were prepared for optimal fluorescence separation of Y- and O-RBCs using standard flow cytometry. A higher concentration of biotin (48  $\mu\text{g/mL}$ ) was used for O-RBCs, while a lower concentration (15  $\mu\text{g/mL}$ ) was used for Y-RBCs. Pre-washed RBCs were mixed with the respective biotin solutions and incubated for 30 minutes. After incubation, RBCs were washed twice with a dextrose-saline solution. (41) The biotinylation method is thoroughly explained in Chapter 3. The RBC indices, including HCT and Hb were measured using the hematology analyzer. For Y-BioRBCs, the HCT was  $0.551 \pm 0.004$  (%) (CV: 1.41%), and Hb was  $160.53 \pm 0.47$  (g/dL) (CV: 1.51%); for O-BioRBCs, the HCT was  $0.561 \pm$

0.001(%) (CV: 0.45%), and Hb was  $195.60 \pm 0.73$  (g/dL) (CV: 0.79%) ([Table 4-2](#)). The hemolysis levels before and after labeling were measured and did not exceed the baseline (0.8%) except for O-BioRBCs. Hemolysis measurements are as follow: Pooled unit  $0.24 \pm 0.03\%$  (CV: 23.57%), Y-RBCs  $0.35 \pm 0.05\%$  (CV: 29.88%), O-RBCs  $0.20 \pm 0.00\%$  (CV: 3.45%), spiked pooled unit  $0.18 \pm 0.00\%$  (CV: 15.94%), Y-BioRBCs  $0.54 \pm 0.00\%$  (CV: 1.3 %), O-BioRBCs  $1.0 \pm 0.12\%$  (CV: 12.73%).

#### **4.2.4 Spiking the Pooled Unit with Young and Old Biotin-Labeled RBCs**

Spiking and splitting the pooled unit have been described in detail in Chapter 3. A 12.5 mL aliquot of each biotinylated subpopulation was reintroduced into the pooled unit to attain a final concentration of around 1% for each biotin-labeled RBC subpopulation within the pooled unit. After completing the spiking process, the pooled unit was mixed by carefully inverting the bag multiple times and split into five separate units of matched blood weight.

#### **4.2.5 Blood Component Irradiation Procedure:**

A small aliquot (10 mL) from each RBC subpopulation (unlabeled and labeled) was stored in 5 mL round-bottom tubes at 4 °C. These aliquots were used to assess K<sup>+</sup> leakage, p50, oxidative hemolysis, and storage hemolysis at three specific time points following irradiation (day 1, day 7, and day 14). Both RCC units and small aliquots of RBC subpopulations were irradiated with a minimum dose of 25 Gy using the Canadian Blood Service Irradiation Protocol. (42)

Four out of five units and 25 sets of 5 mL tubes containing RBC subpopulations were delivered to the Distribution Staff at the Canadian Blood Service in Edmonton for gamma irradiation, with one unit serving as an unirradiated control. The irradiation cycle was initiated by recording essential batch information (F040557 and F800049 forms, Irradiated Blood Components Record Forms). Irradiation indicators were carefully applied following labeling guidelines, and the components were loaded into a Gammacell Irradiator to initiate the irradiation cycle (Gammacell<sup>®</sup> 3000, Elan, Best Medical International, Virginia, USA). Units underwent irradiation in two separate cycles (1st cycle: 3 units, 2nd cycle: 1 unit, and 25 tubes) as per Canadian Blood Service instructions. Tube irradiation

involved applying three irradiation indicators on the tubes, with one placed on the outer tubes and two on the inner tubes ([Figure 4-1](#)). The tubes, arranged in a group and secured with an elastic band, were positioned upright in the middle of the irradiation container, and the distribution staff proceeded with the irradiation cycle, following the protocol typically used for an RCC unit. (42) After each cycle, components were removed, and the exposure time was verified either by an independent backup timer or the irradiation setting time. Irradiation indicators were subsequently examined for the absence of "NOT". The disappearance of the word "NOT" indicated that it had received the minimum irradiation dose of 15 Gy. The entire process adhered to CBS guidelines, incorporating comprehensive checks and documentation at each step to ensure the quality and safety of irradiated blood components. (42)

#### **4.2.6 Measurement of Hemolysis**

As thoroughly explained in Chapter 3, hemolysis assessment was conducted for various RBC subpopulations, including U-RBCs, Y-RBCs, O-RBCs, SP-RBCs, Y-BioRBCs, and O-BioRBCs, utilizing cyanmethemoglobin spectrophotometric measurement based on Drabkin method. (43) In summary, 5  $\mu\text{L}$  of each sample was mixed with 1 mL of Drabkin reagent and incubated for 5 minutes to measure total hemoglobin. For supernatant hemoglobin determination, 40  $\mu\text{L}$  of the supernatant obtained after centrifugation was mixed with Drabkin reagent, followed by vortexing and incubation. Subsequently, 200  $\mu\text{L}$  of each mixture was pipetted into a 96-well EIA/RIA Plate, along with 200  $\mu\text{L}$  of Drabkin reagent as a sample blank. Absorbance was measured at 540 nm, and hemoglobin concentration was calculated accordingly.

The oxidative hemolysis of RBC subpopulations was evaluated, as explained in Chapter 3 in detail. The procedure involved pipetting RBC samples into labeled tubes, washing them with PBS, and incubating them with AAPH to induce oxidative stress. Controls were incubated with PBS to establish a baseline. Hemolysis was quantified using spectrophotometry. Quality control measures ensured reliable results with a CV of less than 10%. (44)

#### 4.2.7 Measurement of Supernatant Potassium (K<sup>+</sup>)

Supernatant K<sup>+</sup> levels were measured in U-RBCs, Y-RBCs, O-RBCs, SP-RBCs, Y-BioRBCs, and O-BioRBCs as well as in all five units. Measurements were taken before irradiation, immediately after irradiation, and on days 7 and 14 post-irradiation during hypertonic storage. 1 mL of each sample was dispensed into 1.5 mL microtubes and centrifuged using a microcentrifuge at a speed of  $2200 \times g$  for 10 min at 4 °C (acceleration: 9, brake: 3). After centrifugation, 0.5 mL of supernatant was carefully removed and placed in the corresponding microtube. The supernatant tubes, accompanied by the necessary forms, were dispatched to Alberta Precision Laboratories (APL). Supernatant K<sup>+</sup> levels were analyzed using a chemistry analyzer (Roche Cobas c503, Roche Diagnostics, Basel, Switzerland). (45)

#### 4.2.8 p50 Measurement

Accurate measurement of hemoglobin oxygen saturation (pO<sub>2</sub>) and 50% saturation levels (p50) is vital for evaluating the quality of RBCs. The Hemox™ analyzer (TCS Scientific Corp., Pennsylvania, USA) was employed to measure p50 values, which reflect hemoglobin's affinity for oxygen, providing a critical assessment of RBCs' oxygen-carrying capacity. The method involves generating a de-oxygenation curve by fully oxygenating RBC samples with compressed O<sub>2</sub> gas and subsequently de-oxygenating them with compressed nitrogen (N<sub>2</sub>). The p50 value is extrapolated from this curve, offering insights into the oxygen saturation point. The process incorporates various reagents, equipment, and calculations to ensure precise measurements.

The p50 levels in U-RBCs, Y-RBCs, and O-RBCs were evaluated at three distinct time points (day 1, day 7, and day 14). For p50 measurement, 5000 uL of Hemox Buffer (TCS Scientific Corp., Pennsylvania, USA), 10 uL of anti-foaming agent (TCS Scientific Corp., Pennsylvania, USA), and 20 uL of 22% Bovine Serum Albumin (Sigma-Aldrich, St. Louise, MD, USA), and 50 uL of samples were added to the dilution vial. For the oxygenation process, samples were fully oxygenated by flipping the gas selector to O<sub>2</sub>, opening the release valve on the tubing to the compressed air tank, and allowing the sample to warm up and oxygenate for approximately 15-20 min. Subsequently, for

deoxygenation, the gas selector was switched to N<sub>2</sub>, ensuring that the valve on the tubing connected to the compressed N<sub>2</sub> tank was opened. The deoxygenation occurs over approximately 20-40 minutes until the pressure reaches the predetermined stop value. (46)

#### **4.2.9 Tracing Biotin-labeled RBC Subpopulations in Irradiated RCCs**

Flow cytometry was employed to assess the recovery of spiked Y-BioRBC and O-BioRBC post-irradiation during hypothermic storage. Streptavidin-conjugated antibodies were utilized for quantifying and categorizing biotinylated RBC subpopulations. Necessary controls were included to ensure accuracy and reliability. Samples underwent dilution stages and were analyzed using appropriate gating parameters to distinguish RBC populations based on fluorescence intensity. This systematic approach facilitated the precise identification and quantification of biotinylated RBCs within irradiated RCCs. (47) Detailed methodology is outlined in Chapter 3.

#### **4.2.10 Statistical Analysis**

Statistical analyses were performed using GraphPad Prism software (version 9.5.0, GraphPad Software, San Diego, CA, USA). Descriptive statistics (mean, SD, SEM) were calculated. Statistical significance was determined using appropriate tests (t-tests, one-way/two-way ANOVA with post hoc tests). Graphs with error bars (SEM/SD) were generated. Flow cytometry data was analyzed with gating strategies. Results are presented as mean ± SEM/SD, with  $p < 0.05$  denoting significance.

### **4.3 Results**

#### **4.3.1 Hemolytic Variability in Red Blood Cell Subpopulations**

The results demonstrate a significant increase in hemolysis levels following gamma irradiation during hypothermic storage across all RBC subpopulations ( $p < 0.0001$ ) ([Figure 4-2](#)). Comparatively, both Y- and O-RBCs consistently exhibited higher hemolysis levels than U-RBCs at all observed time points ( $p < 0.0001$ ); however, no significant differences were observed between Y- and O-RBCs during hypothermic storage after irradiation ( $p = 0.1410$ ) ([Figure 4-3](#)). Biotinylation displayed a positive correlation with increased

hemolysis levels. This correlation appears to be more pronounced in O-RBCs than in Y-RBCs (Y-RBCs vs. Y-BioRBCs,  $p=0.010$ ; O-RBCs vs. O-BioRBCs,  $p<0.0001$ ) ([Figure 4-4](#)). Furthermore, irradiated units demonstrated higher hemolysis levels compared to non-irradiated units at every time point, with this difference becoming more pronounced at day 14 post-irradiation ( $p=0.0005$ ) ([Figure 4-5](#)).

The results revealed a significant positive correlation between RBC senescent level and oxidative hemolysis. O-RBCs consistently demonstrated higher levels of oxidative hemolysis at all observed time points, followed by U-RBCs, while Y-RBCs exhibited the lowest oxidative hemolysis levels ( $p<0.0001$ ) ([Figure 4-6](#)). Oxidative hemolysis exhibited an increase by day 14 following irradiation across all subpopulation groups ( $p=0.0188$ ) ([Figure 4-7](#)). While irradiation did not exacerbate the escalation of oxidative hemolysis in Y-RBCs during hypothermic storage ( $p=0.2608$ ), it did contribute to an increasing trend of oxidative hemolysis in O-RBCs ( $p=0.0110$ ) ([Figure 4-8](#)). Furthermore, the biotinylation process was found to be correlated with an increase in oxidative hemolysis in O-RBCs ( $p=0.0269$ ) ([Figure 4-9](#)).

#### 4.3.2 Measurement of Supernatant $K^+$ in RBC Subpopulations

The results reveal a substantial increase in supernatant  $K^+$  levels during hypothermic storage following irradiation across all RBC subpopulations ( $p<0.0001$ ) ([Figure 4-10](#)). Comparison of  $K^+$  levels between RBC subpopulations demonstrated significant differences, with U-RBCs demonstrating the highest  $K^+$  levels at all time points, followed by O-RBCs and Y-RBCs having the lowest supernatant  $K^+$  levels ( $p=0.0006$ ). However, no significant differences were observed between Y- and O-RBCs across hypothermic storage ( $p=0.9994$ ) ([Figure 4-11](#)). Analysis of  $K^+$  levels in irradiated and non-irradiated RBC subpopulations in 5 mL tubes revealed a significant correlation between irradiation and supernatant  $K^+$  levels in Y-RBCs and U-RBCs during hypothermic storage ( $p<0.0001$ ), while no significant differences were observed in  $K^+$  levels between irradiated and non-irradiated O-RBCs during the hypothermic storage ( $p=0.0762$ ) ([Figure 4-12](#)). Additionally, a comparison of  $K^+$  levels in irradiated units and non-irradiated unit demonstrated a significant difference, with the non-irradiated unit demonstrating the

lowest  $K^+$  levels across all testing time points ( $p < 0.0001$ ) ([Figure 4-13](#)). The biotinylation process did not exert a significant impact on supernatant  $K^+$  levels in both Y- and O-RBCs ( $p = 0.0682$ ).

#### 4.3.3 Dynamic Changes in p50 Values across RBC Subpopulations

The analysis of p50 values during hypothermic storage following irradiation revealed a significant decrease across all RBC subpopulations ( $p < 0.0001$ ). Dynamic changes were observed in p50 values, with Y-RBCs initially exhibiting the highest values, followed by a decline at day 7 post-irradiation, which persisted until day 14. In contrast, O-RBCs and U-RBCs showed a notably lower baseline p50 level, which remained constant after 7 days post-irradiation and decreased by day 14. Analysis of irradiation impact on various RBC subpopulations revealed a significant decline in U-RBCs from day 1 to day 14 ( $p = 0.0224$ ). Additionally, a significant decrease in p50 levels was observed in Y-RBCs between days 7 and 14 post-irradiation ( $p = 0.0065$ ). However, no significant differences were observed in p50 value in O-RBCs over the hypothermic storage period ( $p = 0.8600$ ) ([Figure 4-14](#)). Evaluating the impact of irradiation, no significant differences were observed in the p50 values between irradiated and non-irradiated RBC subpopulations ([Figure 4-15](#)). This suggests that hypothermic storage has a more significant impact on p50 levels compared to irradiation.

#### 4.3.4 RBC Survival Post-Irradiation

The examination of post-irradiation survival dynamics in different RBC subpopulations revealed a decreasing trend in both subpopulations during hypothermic storage, with Y-BioRBCs exhibiting a notable decrease by day 14 ( $p < 0.0001$ ). The delta changes in Y-BioRBCs showed a decreasing slope (slope=0.0006571) from day 1 to day 14 post-irradiation. The delta change of O-BioRBCs did not demonstrate any significant decrease over the 14 days of hypothermic storage (slope=0.0009528). Moreover, there were no significant differences in the survival of RBC subpopulations following irradiation during hypothermic storage ( $p = 0.5341$ ) ([Figure 4-16](#)).

## 4.4 Discussion

This study investigated the impact of gamma irradiation and subsequent hypothermic storage on different RBC subpopulations. The results of this study demonstrated a significant increase in hemolysis levels post-irradiation across all RBC subpopulations ([Figure 4-2](#)), with Y- and O-RBCs consistently exhibiting higher levels compared to U-RBCs ([Figure 4-3](#)). Additionally, a positive correlation was noted between biotinylation and increased hemolysis, particularly pronounced in O-RBCs ([Figure 4-4](#)). Oxidative hemolysis results demonstrated that O-RBCs consistently exhibited higher levels of oxidative hemolysis than Y-RBCs and U-RBCs ([Figure 4-6](#)). Following irradiation, oxidative hemolysis increased across all subpopulations, with O-RBCs showing a more pronounced trend compared to Y-RBCs ([Figure 4-8](#)). Supernatant K<sup>+</sup> levels displayed a substantial increase during hypothermic storage, with U-RBCs consistently exhibiting the highest levels ([Figure 4-10](#)). Furthermore, analysis of p50 values revealed a significant decrease across all RBC subpopulations post-irradiation. Initially, Y-RBCs exhibited the highest values, which then declined, while O- and U-RBCs consistently displayed lower baseline levels that decreased over time ([Figure 4-14](#)). Post-irradiation survival dynamics exhibited decreasing trends in both Y- and O-BioRBC during hypothermic storage. The trend was notably more pronounced in Y-RBCs; however, we did not observe any significant differences in survival between Y- and O-RBC subpopulations ([Figure 4-16](#)).

### 4.4.1 Impact of Irradiation on Hemolysis Levels in RBC Subpopulations

The observed increase in hemolysis following irradiation during hypothermic storage underscores the role of irradiation in exacerbating hemolysis during storage. This difference becomes more pronounced by day 14 post-irradiation ( $p=0.0005$ ), aligning with findings from previous studies indicating an elevation in hemolysis after gamma-irradiation. (23,24,48) Hauk et al. demonstrated a significant rise in hemolysis rates post-irradiation, with a significant difference between irradiated and non-irradiated units by day +28 onwards. (23) Serrano et al. revealed a progressive increase in hemolysis with storage time, both before and after irradiation, with predictors including male gender, greater donor age, and storage duration post-irradiation. (24) Mykhailova et al. demonstrate a strong association between RBC hemolysis and hypothermic storage time regardless of

donor groups. (34) Comparison of hemolysis levels between RBC subpopulations showed that Y- and O-RBCs exhibited higher hemolysis levels compared to U-RBCs across all testing time points. This finding can be attributed to mechanical and osmotic stress induced by Percoll<sup>®</sup> separation, leading to membrane damage and subsequent hemoglobin leakage. Previous studies, such as Masalunga et al., have demonstrated that the mechanical manipulation of RBCs, including centrifugation and saline washing, increases the osmotic fragility of RBC membranes, consequently leading to enhanced hemolysis. (49) Additionally, O'Leary et al. found an immediate increase in hemolysis and free Hb levels following RBC washing. (50) Biotinylation was found to contribute to hemolysis level, with a more pronounced correlation observed in O-RBCs compared to Y-RBCs. This phenomenon can be attributed to the biological age-dependent remodeling of the RBC membrane, which gradually impairs membrane function and properties over time. (51–56) Consequently, O-RBCs might be more susceptible to damage during the biotinylation process and subsequent washing steps.

#### **4.4.2 Impact of Irradiation on Oxidative Hemolysis Levels in RBC Subpopulations**

The study observed a positive correlation between oxidative hemolysis and RBC senescence levels, with O-RBCs consistently exhibiting higher levels of oxidative hemolysis at all testing time points, followed by U-RBCs, with Y-RBCs displaying the lowest oxidative hemolysis levels. The accumulation of ROS during RBC aging, along with the metabolic differences between Y- and O-RBC subpopulations, highlights variations in their capacity to manage oxidative stress. Specifically, O-RBCs exhibit a lower capacity to cope with oxidative hemolysis compared to Y-RBCs. (34) This aligns with our results, demonstrating that while irradiation did not significantly exacerbate the oxidative hemolysis in Y-RBCs post-irradiation ( $p=0.2608$ ), it did contribute to an increasing trend of oxidative hemolysis in O-RBCs during hypothermic storage ( $p=0.0110$ ). As ATP levels decline during the biological aging process of RBCs, their antioxidant system undergoes progressive impairment, leading to an elevation in methemoglobin concentration. (33) Consequently, O-RBCs become more vulnerable to oxidative stress induced by gamma irradiation, while Y-RBCs are capable to withstand oxidative stress following irradiation. Additionally, a positive correlation was observed

between oxidative hemolysis level and hypothermic storage time. Serrano et al. demonstrated that RCCs with higher chronological age have higher oxidative hemolysis levels, suggesting the reduced antioxidant protective capacity of RBC during storage. (24) These results are in alignment with Katharia et al. findings, demonstrating a progressive and significant increase in markers of oxidative injury during the 28 days of RBC storage. These changes were more pronounced in irradiated RBCs compared to non-irradiated ones. (6) The role of biotinylation in oxidative hemolysis introduced a potential link between biotinylation and oxidative damage, with this correlation being more pronounced in O-RBCs. This association could be attributed to the impaired antioxidant capacity of O-RBCs (51–56), rendering them more susceptible to potential oxidative stress induced by the biotinylation process.

#### **4.4.3 Effect of Gamma Irradiation on Supernatant K<sup>+</sup> Levels in RBC Subpopulations**

The study results indicate an association between the duration of hypothermic storage and increased extracellular K<sup>+</sup>. The K<sup>+</sup> level in the stored RCCs increases over time due to the gradual leakage of K<sup>+</sup> out of the cell. (57) Irradiation was correlated with elevated supernatant K<sup>+</sup> levels during hypothermic storage across all RBC subpopulations, with U-RBCs demonstrating the highest K<sup>+</sup> level at every testing time point. Serrano et al. demonstrated that K<sup>+</sup> levels increased rapidly following gamma irradiation, with storage time before and after irradiation, male gender, and older donor age being predictive factors for K<sup>+</sup> concentration. (6,24,58) Additionally, previous investigations demonstrated that gamma irradiation inhibits 40% of the Na<sup>+</sup>/K<sup>+</sup> pump by day 14 after irradiation, disrupting ion balance and membrane functionality. (12) During hypothermic storage, supernatant K<sup>+</sup> concentration increases in all RBC subpopulations, with Y-RBCs displaying the lowest levels, followed by O-RBCs and U-RBCs. The lower K<sup>+</sup> levels observed in Y- and O-RBCs compared to U-RBCs could be attributed to the effect of washing on the supernatant K<sup>+</sup> concentration. This process involves the removal of supernatant, leading to decreased levels of K<sup>+</sup> in Y- and O-RBCs. Swindell et al. demonstrated that the supernatant K<sup>+</sup> concentration decreases after washing RBCs for neonatal patients. (59) Similarly, previous studies show that washing RBCs reduces supernatant K<sup>+</sup> concentration. (60,61) The discrepancy between the higher K<sup>+</sup> levels in U-

RBCs compared to O- and Y-RBCs and the elevated hemolysis levels observed in O-RBCs and Y-RBCs relative to U-RBCs poses an intriguing question. This disparity could potentially be attributed to the dilution of samples before measuring  $K^+$  levels, necessitated by the high  $K^+$  concentration in the samples. However, it is important to note that the dilution process itself may introduce errors in the results, thus warranting further investigation into this discrepancy.

Analysis of  $K^+$  levels in irradiated and non-irradiated RBC subpopulations in 5 mL tubes revealed a significant correlation between irradiation and supernatant  $K^+$  levels in Y-RBCs and U-RBCs during hypothermic storage ( $p < 0.0001$ ), while no significant differences were observed in  $K^+$  levels between irradiated and non-irradiated O-RBCs during the hypothermic storage ( $p = 0.0762$ ). One potential explanation for this phenomenon is associated with the fact that RBC aging is associated with impaired functionality of membrane transporter proteins and  $K^+$  leakage. (32,35) Consequently, the initial concentration of intracellular  $K^+$  might be lower in O-RBCs compared to Y-RBCs, so irradiation cannot significantly intensify the release of  $K^+$  in O-RBCs. Further investigations are required to validate this hypothesis by measuring intracellular  $K^+$  levels in RBC subpopulations. The biotinylation process did not significantly impact supernatant  $K^+$  levels in both Y- and O-RBCs ( $p = 0.0682$ ).

#### **4.4.4 Effects of Irradiation on p50 Values and Post-Irradiation Survival of RBC Subpopulations**

Analysis of p50 values during hypothermic storage post-irradiation revealed a significant decrease across all RBC subpopulations ( $p < 0.0001$ ), indicating increased hemoglobin affinity for oxygen and decreased oxygen release in tissues. These findings are consistent with previous clinical trials, which demonstrated that hypothermic storage following irradiation can compromise the oxygen delivery capacity of RBCs. (62) The decline in 2,3-DPG levels in RBCs following chronological aging post-irradiation leads to impaired oxygen release function of the RBCs. (63–65) This study found no significant differences in p50 values among O-RBCs over the hypothermic storage period ( $p = 0.8600$ ) ([Figure 4-14](#)). One explanation might be related to the lower initial p50 value in O-RBCs,

suggesting that further degradation during hypothermic storage may not be significant in this subpopulation. Comparing p50 values in both irradiated and non-irradiated RBC subpopulations, there was a decrease regardless of irradiation, indicating a significant impact of hypothermic storage on p50 levels compared to irradiation alone ([Figure 4-15](#)).

The investigation into post-irradiation survival revealed a decrease in the numbers of both Y-BioRBCs and O-BioRBCs during hypothermic storage, with Y-BioRBCs showing a more pronounced decrease by day 14 ([Figure 4-16](#)). Previous studies have suggested that transfusion of RCCs containing predominantly Y-RBCs can prolong post-transfusion survival, whereas a higher presence of O-RBCs within the RCCs is associated with increased storage hemolysis,  $K^+$  leakage, and impaired oxygen delivery post-transfusion. (34,36–38) Although initial observations indicated potential benefits of Y-RBCs, including lower  $K^+$  and hemoglobin leakage, lower oxidative hemolysis, and higher p50 values, these advantages did not translate into significant outperformance in post-irradiation recovery rate compared to O-RBCs during hypothermic storage. One possible factor contributing to this outcome could be related to the pooling and splitting method. When pooling RCCs, there is a risk of segregating RBC subpopulations from individual donors with distinct characteristics, potentially affecting the results. Analysis revealed that the classified fraction as Y-RBCs may have originated from a donor exhibiting microcytosis and lower MCHC, indicating potential iron deficiency. Iron-deficient RBCs have lower antioxidant capacity (66,67), reduced deformability, and increased rigidity. (67–73) To validate our findings, two additional units were separately analyzed, with Y- and O-RBCs separated from each unit, using a density-based age profiling pattern. Biotinylation was used to label Y- and O-RBCs, which were then spiked back into a small volume of RBCs and subjected to irradiation. Additionally, 10 mL aliquots of Y- and O-RBCs were separated and irradiated, and all tests were repeated to ensure consistency and verify that mixing did not impact the results. The supplementary data validated our initial findings, showcasing consistent results.

## 4.5 Conclusion

In conclusion, this study aimed to assess the effects of gamma irradiation and subsequent hypothermic storage on various subpopulations of RBCs. Our findings

revealed a significant increase in hemolysis levels post-irradiation across all RBC subpopulations, with Y- and O-RBCs displaying higher levels compared to U-RBCs. Additionally, oxidative hemolysis was more pronounced in O-RBCs, suggesting their increased vulnerability to oxidative stress. Analysis of supernatant  $K^+$  levels indicated a substantial increase during hypothermic storage, with U-RBCs consistently exhibiting the highest levels. Furthermore, a significant decrease in p50 values across all RBC subpopulations post-irradiation was observed, indicating reduced hemoglobin affinity for oxygen. Interestingly, while Y-RBCs initially exhibited higher p50 values, they experienced a decline over time, while O- and U-RBCs displayed lower baseline levels that decreased further during storage. The lack of significant differences in RBC survival across the subpopulations underscores the ongoing necessity for extensive research to enhance our understanding of the intricate factors that impact the behavior of RBC subpopulations both post-irradiation and during hypothermic storage. This understanding ultimately contributes to clinical practice optimization.

**Table 4-1 RBC Indices Measured for RCCs**

	<b>Average</b>	<b>SD</b>	<b>CV</b>	<b>SE</b>
<b>Unit1</b>				
<b>Hb (g/dL)</b>	186.067	2.926	1.573	1.379
<b>HCT (%)</b>	0.554	0.008	1.433	0.004
<b>MCV (fL)</b>	94.633	0.058	0.061	0.027
<b>MCHC (g/dL)</b>	335.667	0.577	0.172	0.272
<b>Unit2</b>				
<b>Hb (g/dL)</b>	192.433	1.361	0.707	0.642
<b>HCT (%)</b>	0.583	0.004	0.693	0.002
<b>MCV (fL)</b>	93.367	0.306	0.327	0.144
<b>MCHC (g/dL)</b>	330.000	0.000	0.000	0.000
<b>Unit3</b>				
<b>Hb (g/dL)</b>	185.400	1.418	0.765	0.668
<b>HCT (%)</b>	0.568	0.006	0.970	0.003
<b>MCV (fL)</b>	87.433	0.006	0.006	0.003
<b>MCHC (g/dL)</b>	326.333	2.082	0.638	0.981
<b>Unit4</b>				
<b>Hb (g/dL)</b>	198.967	1.501	0.754	0.708
<b>HCT (%)</b>	0.589	0.005	0.854	0.002
<b>MCV (fL)</b>	91.200	0.100	0.110	0.047
<b>MCHC (g/dL)</b>	337.667	0.577	0.171	0.272
<b>Unit5</b>				
<b>Hb (g/dL)</b>	173.767	1.950	1.122	0.919
<b>HCT (%)</b>	0.590	0.006	1.031	0.003
<b>MCV (fL)</b>	63.633	0.058	0.091	0.027
<b>MCHC (g/dL)</b>	294.667	2.309	0.784	1.089
<b>Unit6</b>				
<b>Hb (g/dL)</b>	181.733	0.702	0.386	0.331
<b>HCT (%)</b>	0.542	0.004	0.738	0.002
<b>MCV (fL)</b>	96.900	0.200	0.206	0.094
<b>MCHC (g/dL)</b>	335.333	2.082	0.621	0.981

**Table 4-2 RBC Indices for Subpopulation Extremes**

	<b>Average</b>	<b>SD</b>	<b>CV</b>	<b>SE</b>
<b>Y-RBC</b>				
<b>Hb (g/dL)</b>	161.900	3.158	1.950	1.488
<b>HCT (%)</b>	0.565	0.013	2.381	0.006
<b>MCV (fL)</b>	65.867	0.321	0.488	0.152
<b>MCHC (g/dL)</b>	286.667	3.215	1.121	1.515
<b>Y-BioRBC</b>				
<b>Hb (g/dL)</b>	160.53	2.419	1.507	0.466
<b>HCT (%)</b>	0.55	0.008	1.408	0.004
<b>MCV (fL)</b>	66.53	0.058	0.087	0.011
<b>MCHC (g/dL)</b>	291.00	0.000	0.000	0.000
<b>O-RBC</b>				
<b>Hb (g/dL)</b>	202.367	0.503	0.249	0.237
<b>HCT (%)</b>	0.577	0.005	0.800	0.002
<b>MCV (fL)</b>	87.167	0.231	0.265	0.109
<b>MCHC (g/dL)</b>	350.667	3.786	1.080	1.785
<b>O-BioRBC</b>				
<b>Hb (g/dL)</b>	195.60	1.539	0.787	0.726
<b>HCT (%)</b>	0.56	0.003	0.448	0.001
<b>MCV (fL)</b>	89.47	0.153	0.171	0.072
<b>MCHC (g/dL)</b>	348.67	2.082	0.597	0.981

**Figure 4-1 Arrangement of Tubes and Placement of Radsure Stickers for Irradiation**



**Figure 4-1:** The figure demonstrated tube arrangement for irradiation with the suggested placement of Radsure stickers.

**Figure 4-2 Hemolysis Levels Post-irradiation in Different RBC Subpopulations**

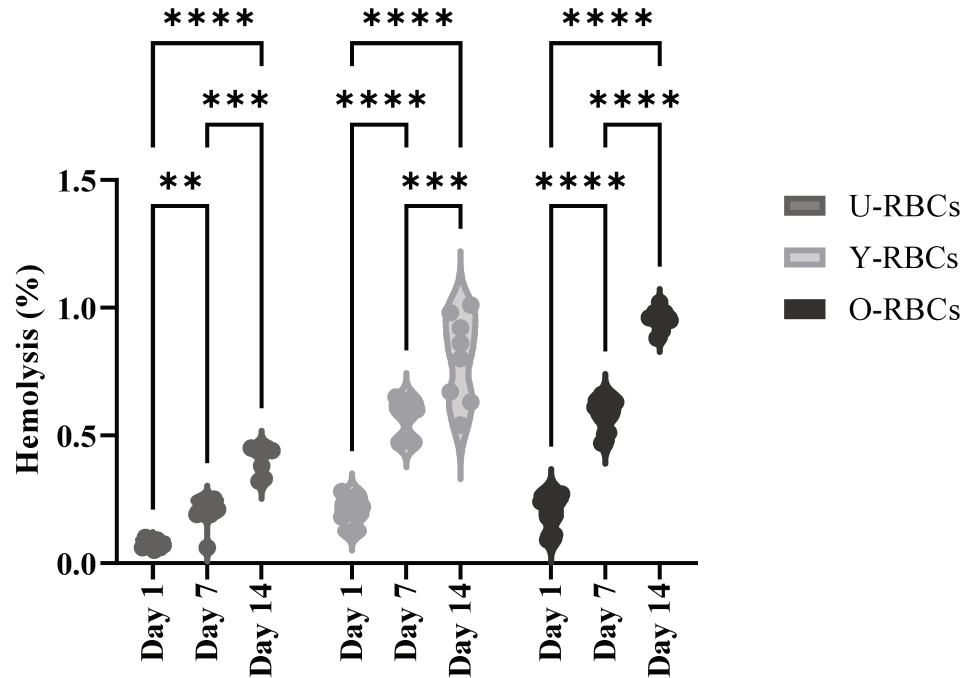


**Figure 4-2:** The figure illustrates a significant increase in hemolysis levels post-irradiation during hypothermic storage across all experimental groups ( $p < 0.0001$ ). Hemolysis increases after 7 days post-irradiation, which was further intensified by day 14 post-irradiation across all RBC subpopulations. Statistical significance denoted by \*:  $p < 0.05$ , \*\*:  $p < 0.01$ , \*\*\*:  $p < 0.001$ , and \*\*\*\*:  $p < 0.0001$ .

**Figure 4-3 Comparative Hemolysis Levels in Young and Old RBC Subpopulations**

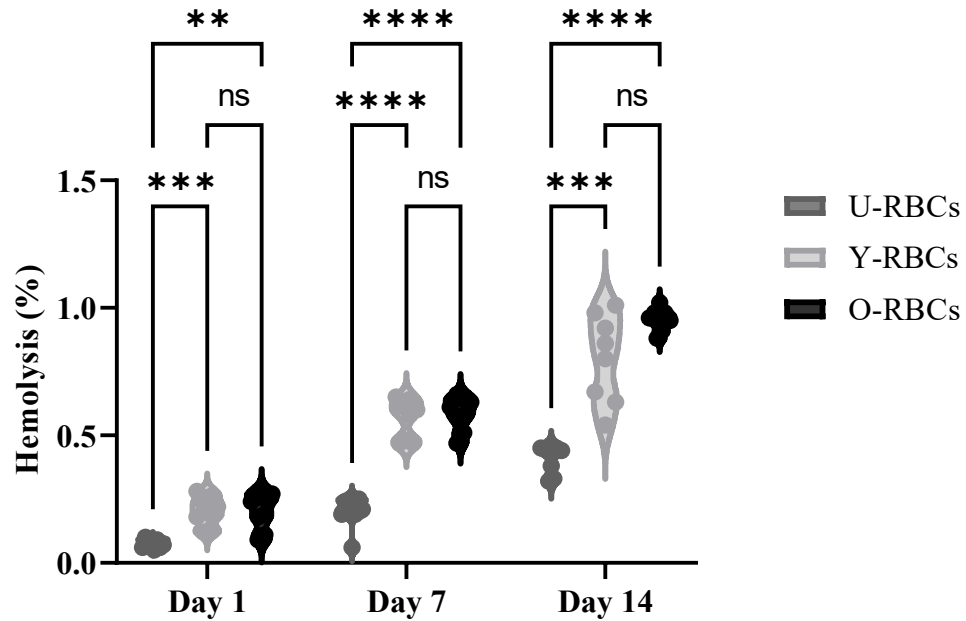


**Figure 4-3:** This figure illustrates the varying levels of hemolysis observed across different red blood cell subpopulations during hypothermic storage following irradiation. O-RBCs consistently exhibited the highest hemolysis levels throughout the storage period, followed by Y-RBCs, while U-RBCs showed the lowest hemolysis levels at each time point post-irradiation. No significant differences between O-RBCs and Y-RBCs across all observed time points ( $p=0.1410$ ). Statistical significance denoted by \*:  $p<0.05$ , \*\*:  $p<0.01$ , \*\*\*:  $p<0.001$ , and \*\*\*\*:  $p<0.0001$ .

**Figure 4-4 Correlation between Biotinylation and Hemolysis**

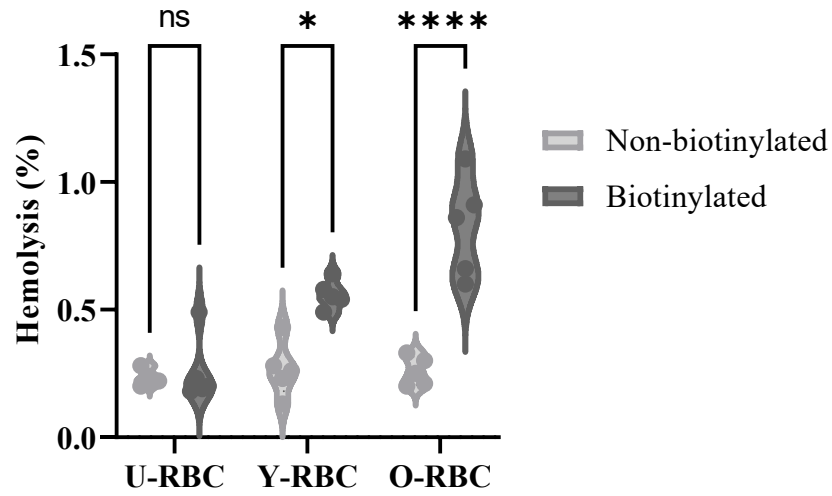


**Figure 4-4:** This figure depicts a positive correlation between biotin and hemolysis levels in Y- and O-RBC subpopulations. Biotinylation accentuates hemolysis levels in both Y- and O-RBCs ( $p=0.0101$ ,  $p<0.0001$ ), with O-BioRBCs exhibiting higher hemolysis levels compared to Y-BioRBCs. Additionally, the impact of biotinylation on hemolysis level appears to be more pronounced in O-RBCs than in Y-RBCs. Statistical significance denoted by \*:  $p<0.05$ , \*\*:  $p<0.01$ , \*\*\*:  $p<0.001$ , and \*\*\*\*:  $p<0.0001$ .

**Figure 4-5 Comparison of Hemolysis Levels between Irradiated and Non-irradiated RCCs**

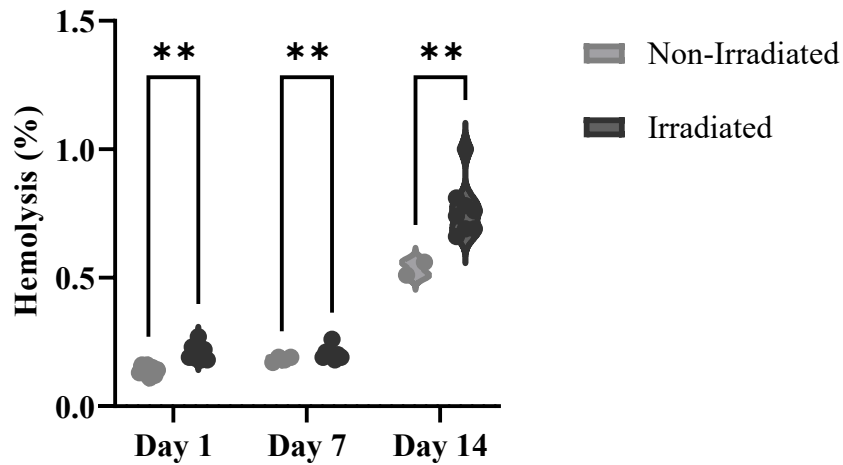


**Figure 4-5:** This figure compares hemolysis levels between irradiated and non-irradiated red blood cell units at various time points during hypothermic storage. Irradiated units consistently demonstrate higher hemolysis levels compared to non-irradiated units at every time point, with a more pronounced difference at day 14 post-irradiation ( $p=0.0005$ ). Statistical significance denoted by \*:  $p<0.05$ , \*\*:  $p<0.01$ , \*\*\*:  $p<0.001$ , and \*\*\*\*:  $p<0.0001$ .

**Figure 4-6 Correlation Between RBC Senescence and Oxidative Hemolysis**

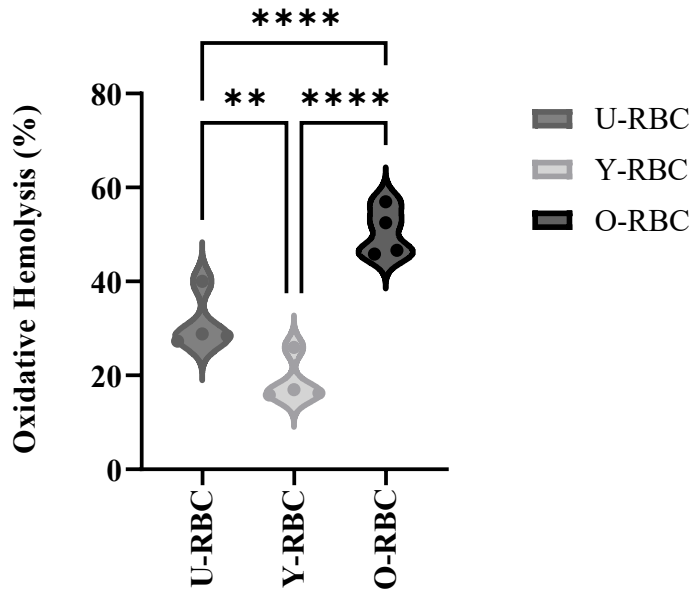


**Figure 4-6:** The graph illustrates oxidative hemolysis levels among Y-RBC, O-RBC, and U-RBC subpopulations. A significant positive correlation was observed between RBC senescent level and oxidative hemolysis. O-RBCs consistently demonstrated higher levels of oxidative hemolysis at all observed time points, followed by U-RBCs, while Y-RBCs exhibited the lowest oxidative hemolysis levels ( $p < 0.0001$ ). Statistical significance denoted by \*:  $p < 0.05$ , \*\*:  $p < 0.01$ , \*\*\*:  $p < 0.001$ , and \*\*\*\*:  $p < 0.0001$ .

**Figure 4-7 Impact of Irradiation on Oxidative Hemolysis Levels during Hypothermic Storage**

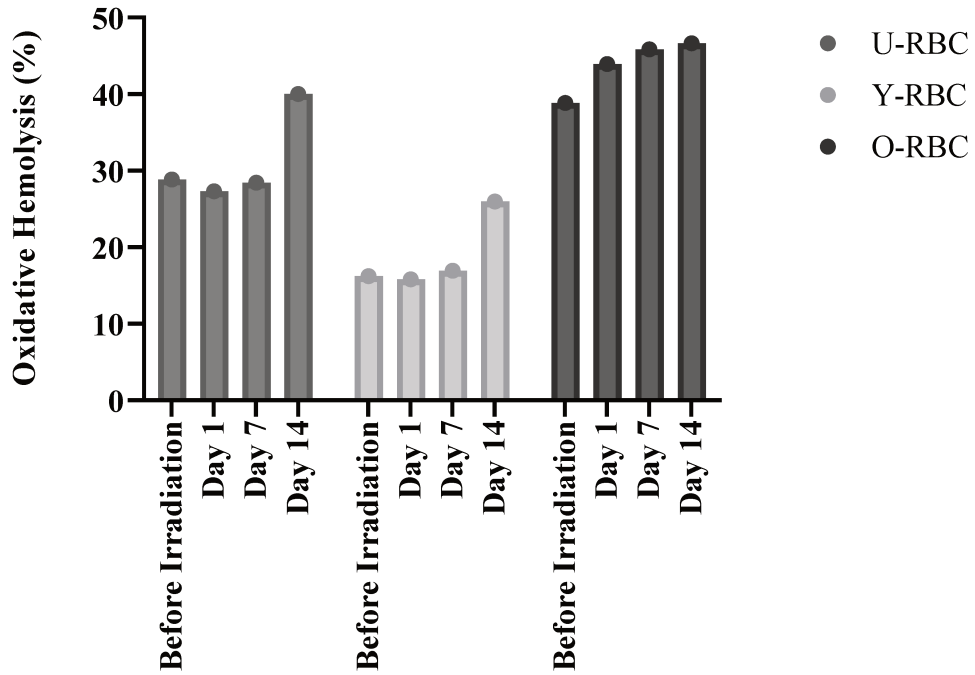


**Figure 4-7:** The figure illustrates the impact of irradiation on oxidative hemolysis levels across all testing time points. There is a significant increase in oxidative hemolysis by day 14 following irradiation across all red blood cell subpopulation groups (p=0.0188)

### Figure 4-8 Impact of Irradiation on Oxidative Hemolysis in RBC Subpopulations

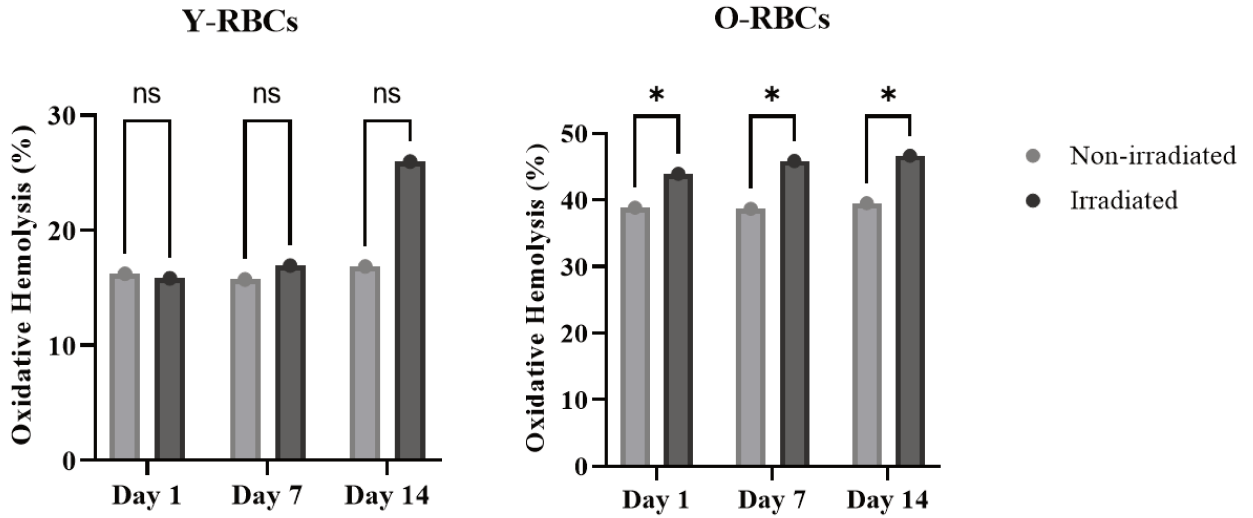


**Figure 4-8:** The figure illustrates the impact of irradiation on the trend of oxidative hemolysis in Y-RBC and O-RBC subpopulations during hypothermic storage. While irradiation did not exacerbate the escalation of oxidative hemolysis in Y-RBCs ( $p=0.2608$ ), it contributed to an increasing trend in O-RBCs ( $p=0.0110$ ). Statistical significance denoted by \*:  $p<0.05$ , \*\*:  $p<0.01$ , \*\*\*:  $p<0.001$ , and \*\*\*\*:  $p<0.0001$ .

**Figure 4-9 Correlation Between Biotinylation and Oxidative Hemolysis Levels in RBC Subpopulations**

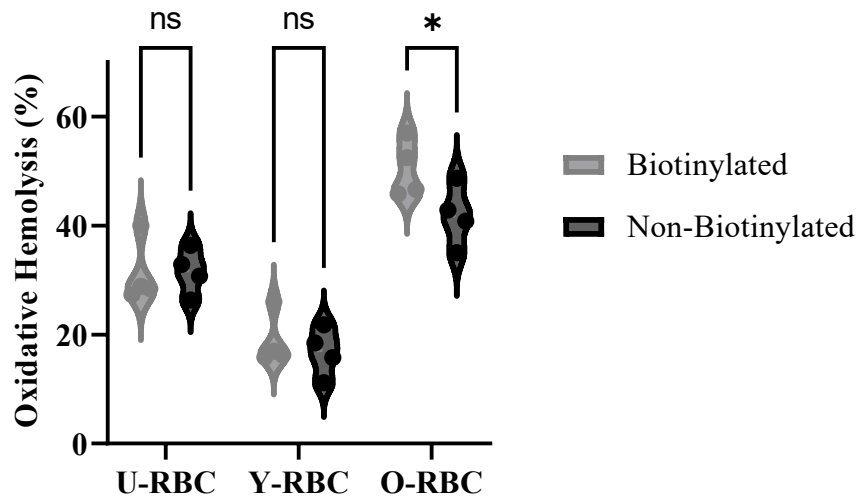


**Figure 4-9:** The figure depicts the correlation between biotinylation and oxidative hemolysis levels across RBC subpopulations. Specifically, the biotinylation process was associated with an increase in oxidative hemolysis in O-RBCs ( $p=0.0269$ ). Statistical significance denoted by \*:  $p<0.05$ , \*\*:  $p<0.01$ , \*\*\*:  $p<0.001$ , and \*\*\*\*:  $p<0.0001$ .

**Figure 4-10 Comparison of Supernatant K<sup>+</sup> Levels during Hypothermic Storage after Irradiation**

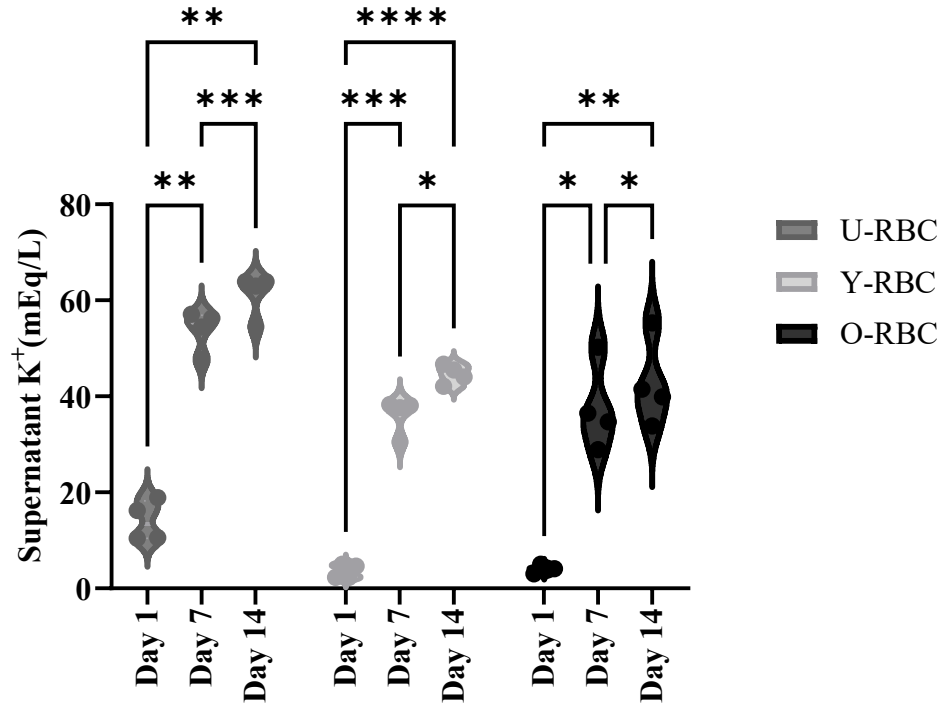


**Figure 4-10:** The graph illustrates the comparison of supernatant K<sup>+</sup> levels across RBC subpopulations during hypothermic storage following irradiation. A significant increase in supernatant K<sup>+</sup> levels was observed across all RBC subpopulations during hypothermic storage ( $p<0.0001$ ). Statistical significance denoted by \*:  $p<0.05$ , \*\*:  $p<0.01$ , \*\*\*:  $p<0.001$ , and \*\*\*\*:  $p<0.0001$ .

**Figure 4-11 Comparison of Supernatant K<sup>+</sup> Levels Across RBC Subpopulation After Irradiation**

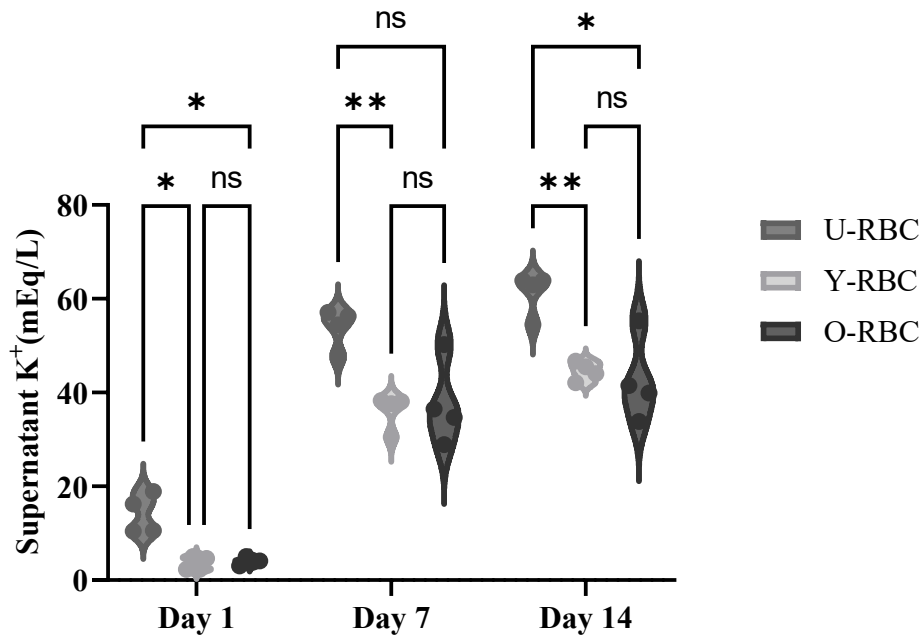


**Figure 4-11:** The figure illustrates a comparison of K<sup>+</sup> levels between Y-RBCs, O-RBCs, and U-RBCs during hypothermic storage after irradiation. U-RBCs exhibit the highest K<sup>+</sup> levels consistently at all time points (p=0.0006). No significant differences were observed between Y- and O-RBCs across all testing time points (p=0.9994). Statistical significance denoted by \*: p<0.05, \*\*: p<0.01, \*\*\*: p<0.001, and \*\*\*\*: p<0.0001.

## Figure 4-12 Analysis of K<sup>+</sup> Levels in Irradiated and Non-irradiated RBC Subpopulations

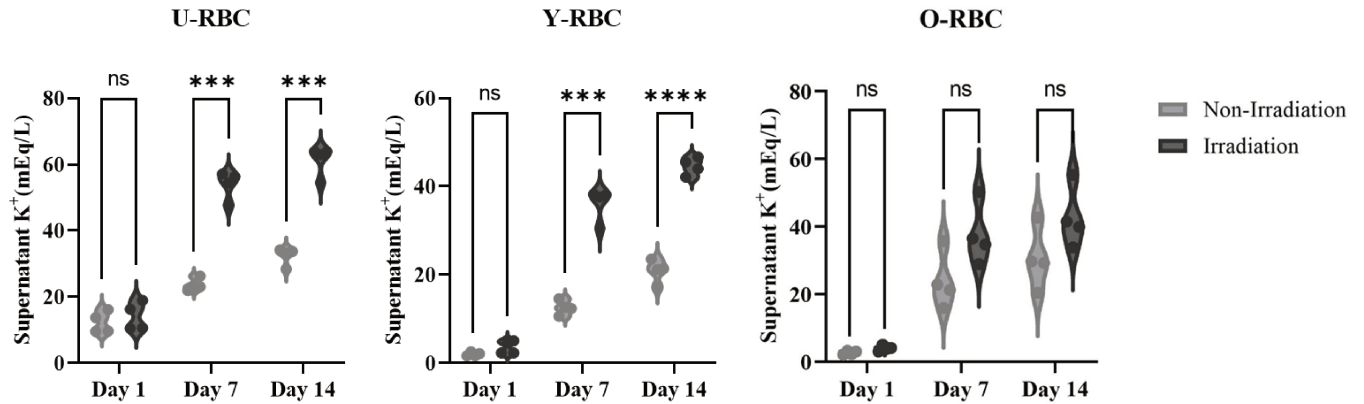


**Figure 4-12:** The figure illustrates the K<sup>+</sup> level in both irradiated and non-irradiated subpopulations of RBC in 5 mL tubes. Significant correlations were observed between irradiation and supernatant K<sup>+</sup> levels in Y-RBCs and U-RBCs ( $p < 0.0001$ ), while no significant differences were found in K<sup>+</sup> levels between irradiated and non-irradiated O-RBCs ( $p = 0.0762$ ). Statistical significance denoted by \*:  $p < 0.05$ , \*\*:  $p < 0.01$ , \*\*\*:  $p < 0.001$ , and \*\*\*\*:  $p < 0.0001$ .

**Figure 4-13 Comparison of K<sup>+</sup> Levels Between Irradiated and Non-Irradiated RCCs**

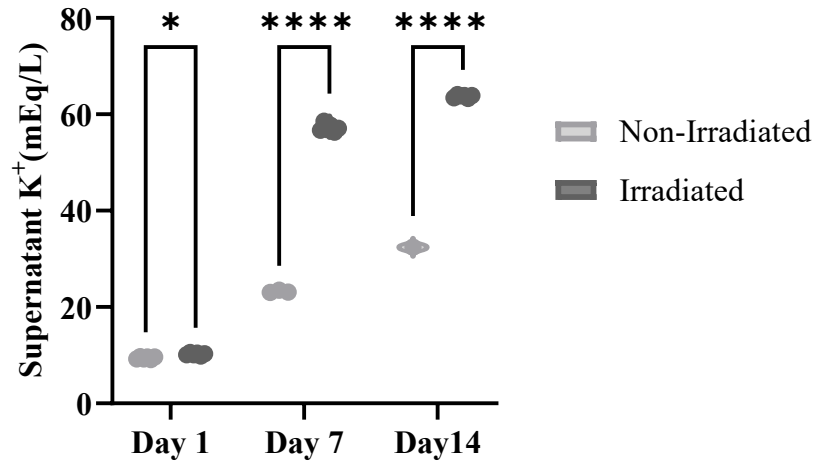


**Figure 4-13:** The figure illustrates the comparison of K<sup>+</sup> levels between irradiated units and non-irradiated unit across all testing time points. Non-irradiated unit demonstrated the lowest K<sup>+</sup> levels compared to irradiated units across all testing time points (p<0.0001). Statistical significance denoted by \*: p<0.05, \*\*: p<0.01, \*\*\*: p<0.001, and \*\*\*\*: p<0.0001.

**Figure 4-14 Dynamic Changes in p50 Values Across RBC Subpopulations Following Irradiation**

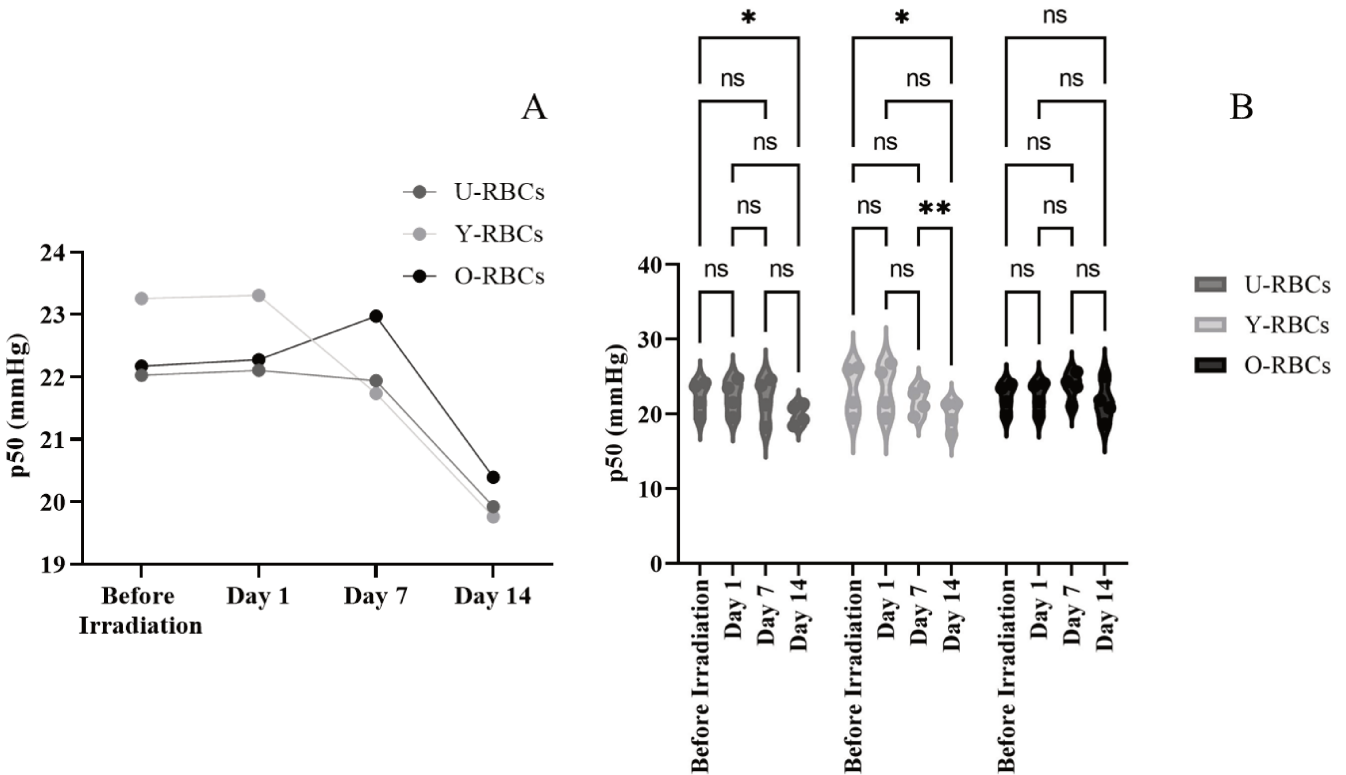


**Figure 4-14:** Graph A depicts a significant reduction in p50 values across all RBC subpopulations after irradiation during hypothermic storage ( $p < 0.0001$ ). Y-RBCs initially exhibit the highest values, followed by a decline at day 7 post-irradiation. O-RBCs and U-RBCs show lower baseline p50 levels, remaining constant after 7 days post-irradiation and decreasing by day 14. The p50 values continued to decrease by day 14 across all subpopulations. Figure B demonstrates the p50 value across RBC subpopulations. While significant decreases in p50 values were observed in Y-RBCs between day 7 and day 14 post-irradiation ( $p = 0.0065$ ) and in U-RBCs from day 1 to day 14 ( $p = 0.0224$ ), no significant differences were found in p50 values after irradiation during hypothermic storage ( $p = 0.8600$ ). Statistical significance denoted by \*:  $p < 0.05$ , \*\*:  $p < 0.01$ , \*\*\*:  $p < 0.001$ , and \*\*\*\*:  $p < 0.0001$ .

**Figure 4-15 Comparison of p50 Values Between Irradiated and Non-Irradiated RBC Subpopulations**

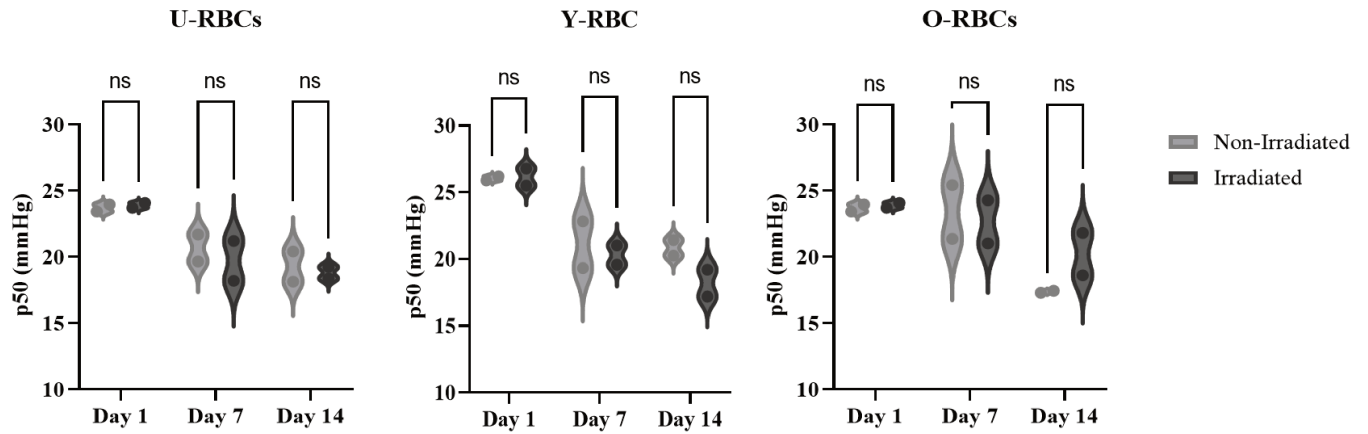


**Figure 4-15:** The figure illustrates the comparison of p50 values between irradiated and non-irradiated RBC subpopulations. No significant differences were observed in p50 value between irradiated and non-irradiated RBC subpopulations.

**Figure 4-16 Post-Irradiation Survival Dynamics of Different RBC Subpopulations**

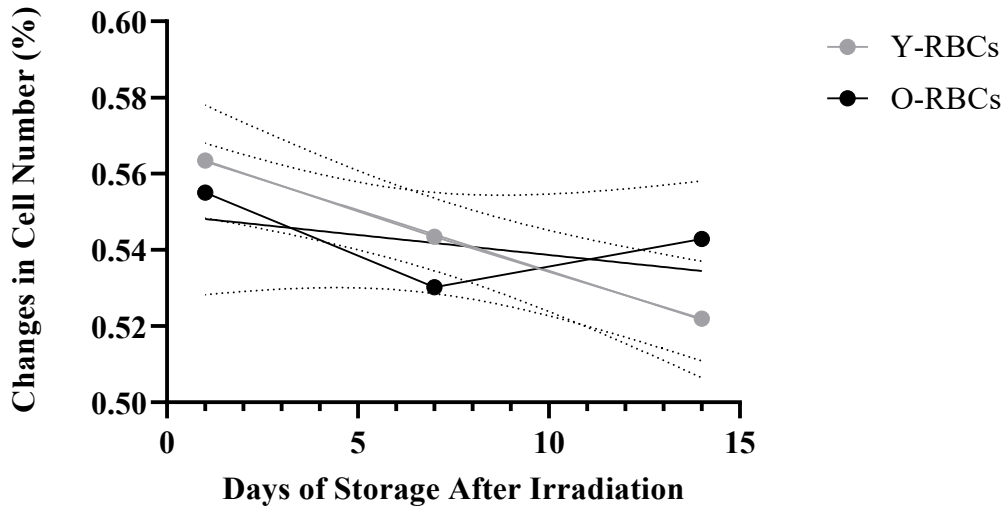


**Figure 4-16:** The figure illustrates the trends in post-irradiation survival dynamics of Y-BioRBCs and O-BioRBCs during hypothermic storage. Y-BioRBCs exhibit a significant decrease by day 14 ( $p < 0.0001$ ), whereas O-RBCs show no significant decrease over the 14-day storage period. No significant differences in survival are observed between the RBC subpopulations following irradiation ( $p = 0.5341$ ).

## 4.6 References

1. Moroff G, Luban NLC. The irradiation of blood and blood components to prevent graft-versus-host disease: Technical issues and guidelines. *Transfusion Medicine Reviews*. 1997;11(1):15–26.
2. Treleaven J, Gennery A, Marsh J, Norfolk D, Page L, Parker A, et al. Guidelines on the use of irradiated blood components prepared by the British Committee for Standards in Haematology Blood Transfusion task force. *British Journal of Haematology*. 2011;152(1):35–51.
3. Gammon R. Standards for blood banks and transfusion services. Bethesda M, editor. Association for the Advancement of Blood & Biotherapies (AABB); 2020.
4. Canadian Standards Association. CAN/CSA-Z902:20 Blood and blood components. . Toronto, ON; 2020.
5. de Korte D, Thibault L, Handke W, Harm SK, Morrison A, Fitzpatrick A, et al. Timing of gamma irradiation and blood donor sex influences in vitro characteristics of red blood cells. *Transfusion (Paris)*. 2018;58(4):917–26.
6. Katharia R, Chaudhary R, Agarwal P. Prestorage gamma irradiation induces oxidative injury to red cells. *Transfusion and Apheresis Science*. 2013 Feb;48(1):39–43.
7. Relevy H, Koshkaryev A, Manny N, Yedgar S, Barshtein G. Blood banking-induced alteration of red blood cell flow properties. *Transfusion*. 2008 Jan;48(1):136-46.
8. Patel RM, Roback JD, Uppal K, Yu T, Jones DP, Josephson CD. Metabolomics profile comparisons of irradiated and nonirradiated stored donor red blood cells. *Transfusion (Paris)*. 2015;55(3):544–52.
9. Brugnara C, Churchill WH. Effect of irradiation on red cell cation content and transport. *Transfusion (Paris)*. 1992;32(3):246–52.
10. Pribush A, Agam G, Yermiahu T, Dvilansky A, Meyerstein D, Meyerstein N. Radiation damage to the erythrocyte membrane: The effects of medium and cell concentrations. *Free Radical Research*. 1994;21(3):135–46.
11. Weinmann M, Hoffmann W, Rodegerdts E, Bamberg M. Biological effects of ionizing radiation on human blood compounds ex vivo. *Journal of Cancer Research and Clinical Oncology*. 2000 Oct;126(10):584-8.
12. Moreira OC, Oliveira VH, Benedicto LBF, Nogueira CM, Mignaco JA, Fontes CFL, et al. Effects of  $\gamma$ -irradiation on the membrane ATPases of human erythrocytes from transfusional blood concentrates. *Annals of Hematology*. 2008 Feb;87(2):113–9.

13. Apell HJ, Nelson MT, Marcus MM, Lauger P. Effects of the ATP, ADP and inorganic phosphate on the transport rate of the Na<sup>+</sup>,K<sup>+</sup>-pump. *Biochimica et Biophysica Acta*. 1986 May 9;857(1):105-15.
14. El Kenz H, Corazza F, Van Der Linden P, Chabab S, Vandenvelde C. Potassium content of irradiated packed red blood cells in different storage media: Is there a need for additive solution-dependent recommendations for infant transfusion? *Transfusion and Apheresis Science*. 2013;49(2):249–53.
15. Xu D, Peng M, Zhang Z, Dong G, Zhang Y, Yu H. Study of damage to red blood cells exposed to different doses of  $\gamma$ -ray irradiation. *Blood Transfusion*. 2012;10(3):321–30.
16. Axelsen KB, Palmgren MG. Evolution of substrate specificities in the P-type ATPase superfamily. *Journal of Molecular Evolution*. 1998 Jan;46(1):84-101.
17. Emanuel E Strehler, Marek Treiman. Calcium pumps of plasma membrane and cell interior. *Current Molecular Medicine* . 2004 May;4(3):323–35.
18. Zimmermann R, Schoetz AM, Frisch A, Hauck B, Weiss D, Strobel J, et al. Influence of late irradiation on the in vitro RBC storage variables of leucoreduced RBCs in SAGM additive solution. *Vox Sang*. 2011 Apr;100(3):279–84.
19. P Agarwal, V L Ray, N Choudhury, R K Chaudhary. Effect of pre-storage gamma irradiation on red blood cells. *Indian Journal of Medical Research*. 2005 Nov;122(5):385–7.
20. Patidar GK, Joshi A, Marwaha N, Prasad R, Malhotra P, Sharma RR, et al. Serial assessment of biochemical changes in irradiated red blood cells. *Transfusion and Apheresis Science*. 2014;50(3):479–87.
21. Harm SK, Raval JS, Cramer J, Waters JH, Yazer MH. Haemolysis and sublethal injury of RBCs after routine blood bank manipulations. *Transfusion Medicine*. 2012;22(3):181–5.
22. Winter KM, Johnson L, Webb RG, Marks DC. Gamma-irradiation of deglycerolized red cells does not significantly affect in vitro quality. *Vox Sang*. 2015 Oct 1;109(3):231–8.
23. Hauck B, Oremek D, Zimmermann R, Ruppel R, Troester B, Eckstein R. Influence of irradiation on in vitro red-blood-cell (RBC) storage variables of leucoreduced RBCs in additive solution PAGGS-M. *Vox Sang*. 2011 Jul;101(1):21–7.
24. Serrano K, Chen D, Hansen AL, Levin E, Turner TR, Kurach JDR, et al. The effect of timing of gamma-irradiation on hemolysis and potassium release in leukoreduced red cell concentrates stored in SAGM. *Vox Sang*. 2014;106(4):379–81.
25. Moroff G, Luban NLC. The influence of gamma irradiation on red cell and platelet properties. *Transfusion Science*. 1994;15(2):141–8.

26. Rühl H, Bein G, Sachs UJH. Transfusion-Associated Graft-Versus-Host Disease. Vol. 23, *Transfusion Medicine Reviews*. 2009. p. 62–71.
27. McCoy NC, Yu M, Sullivan Ja, Spiegel Dm, Leitman Sf. The effect of prestorage irradiation red cell survival on posttransfusion. *Transfusion (Paris)*. 1992;32(6):525–8.
28. Vraets A, Lin Y, Callum JL. Transfusion-associated hyperkalemia. *Transfusion Medicine Reviews*. 2011 Jul;25(3):184–96.
29. Lee AC, Reduque LL, Luban NLC, Ness PM, Anton B, Heitmiller ES. Transfusion-associated hyperkalemic cardiac arrest in pediatric patients receiving massive transfusion. *Transfusion (Paris)*. 2014 Jan;54(1):244–54.
30. F A Oski. The unique fetal red cell and its function. E. Mead Johnson Award address. *Pediatrics*. 1973 Mar;51(3):494–500.
31. Högman CF, Löf H, Meryman HT. Storage of red blood cells with improved maintenance of 2,3-bisphosphoglycerate. *Transfusion (Paris)*. 2006 Sep;46(9):1543–52.
32. D’Alessandro A, Blasi B, D’Amici GM, Marrocco C, Zolla L. Red blood cell subpopulations in freshly drawn blood: Application of proteomics and metabolomics to a decades-long biological issue. *Blood Transfusion*. 2013;11(1):75–87.
33. Bosman GJCGM, Werre JM, Willekens FLA, Novotný VMJ. Erythrocyte ageing in vivo and in vitro: Structural aspects and implications for transfusion. *Transfusion Medicine*. 2008;18(6):335–47.
34. Mykhailova O, Olafson C, Turner TR, D’Alessandro A, Acker JP. Donor-dependent aging of young and old red blood cell subpopulations: Metabolic and functional heterogeneity. *Transfusion (Paris)*. 2020;60(11):2633–46.
35. An X, Mohandas N. Disorders of red cell membrane. *British Journal of Haematology*. 2008 May;141(3):367-75.
36. Cohen AR, Schmidt JM, Martin MB, Barnsley W, Schwartz E. Clinical trial of young red cell transfusions. *The Journal of Pediatrics*. 1984;104(6):865–8.
37. Triadou, P., R. Girot, D. Rebibo, D. Lemau, B. Mattlinger, P. Bolo, M. Maier, and L. Barritault. Neocytopenesis: a new approach for the transfusion of patients with thalassaemia major. *European Journal of Pediatrics* (1986) 145: 10–13.
38. Tuo WW, Wang D, Liang WJ, Huang YX. How cell number and cellular properties of blood-banked red blood cells of different cell ages decline during storage. *PLoS One*. 2014 Aug 28;9(8):e105692.
39. Mykhailova O, Brandon-Coatham M, Durand K, Olafson C, Xu A, Yi QL, Kanas T, Acker JP. Estimated median density identifies donor age and sex differences in red blood cell biological age. *Transfusion*. 2024 Apr;64(4):705-715.

40. Mykhailova O, Brandon-Coatham M, Phan C, Yazdanbakhsh M, Olafson C, Yi QL, Kanas T, Acker JP. Red cell concentrates from teen male donors contain poor-quality biologically older cells. *Vox Sang*. 2024 Feb 28.
41. Protocol for Biotinylation of Red Blood Cells. Dr. Jason Acker's laboratory, Version 1.2, Revised 2023-01-10.
42. Irradiation Of Blood Components, Canadian Blood Service, WI Number 02-146, Revision Number 18.
43. Protocol for determining % hemolysis. Dr. Jason Acker's laboratory, version 4.5, revised 2008-12-16.
44. Protocol for AAPH-induced oxidative hemolysis. Dr. Jason Acker's laboratory, Version 1.3. Revised 2021-08-05.
45. Protocol for Preparing and Sending Supernatants for Sodium and Potassium Analysis, Acker Lab: Research and Development Operating Procedure Version 1.3 2021-02-03 .
46. Protocol for Determining p50 using the Hemox Analyzer, Dr. Jason Acker's laboratory, Version 5.0, Created 2017-02-14.
47. A flow cytometric method to quantify biotinylated red blood cells. Dr. Jason Acker's laboratory, Version 1.2, Revised 2023-01-05.
48. Antosik A, Czubak K, Gajek A, Marczak A, Glowacki R, Borowczyk K, et al. Influence of pre-storage irradiation on the oxidative stress markers, membrane integrity, size and shape of the cold stored red blood cells. *Transfusion Medicine and Hemotherapy*. 2015 Jun 15;42(3):140–8.
49. Masalunga C, Cruz M, Porter B, Roseff S, Chui B, Mainali E. Increased hemolysis from saline pre-washing RBCs or centrifugal pumps in neonatal ECMO. *Journal of Perinatology*. 2007 Jun;27(6):380–4.
50. O'Leary MF, Szklarski P, Klein TM, Young PP. Hemolysis of red blood cells after cell washing with different automated technologies: Clinical implications in a neonatal cardiac surgery population. *Transfusion (Paris)*. 2011 May;51(5):955–60.
51. Bosman GJCGM, Lasonder E, Groenen-Döpp YAM, Willekens FLA, Werre JM, Novotný VMJ. Comparative proteomics of erythrocyte aging in vivo and in vitro. *Journal of Proteomics*. 2010;73(3):396–402.
52. D'Alessandro A, D'Amici GM, Vaglio S, Zolla L. Time-course investigation of sgm-stored leukocyte-filtered red blood cell concentrates: From metabolism to proteomics. *Haematologica*. 2012;97(1):107–15.

53. Malka R, Delgado FF, Manalis SR, Higgins JM. In Vivo Volume and Hemoglobin Dynamics of Human Red Blood Cells. *PLoS Computational Biology*. 2014;10(10).
54. Kameneva M V., Garrett KO, Watach MJ, Borovetz HS. Red blood cell aging and risk of cardiovascular diseases. *Clinical Hemorheology and Microcirculation*. 1998;18(1):67–74.
55. Blasi B, D'Alessandro A, Ramundo N, Zolla L. Red blood cell storage and cell morphology. *Transfusion Medicine*. 2012;22(2):90–6.
56. Simak J, Gelderman MP. Cell membrane microparticles in blood and blood products: potentially pathogenic agents and diagnostic markers. *Transfusion Medicine Reviews*. 2006 Jan;20(1):1-26.
57. Vraets A, Lin Y, Callum JL. Transfusion-associated hyperkalemia. *Transfusion Medicine Reviews*. 2011 Jul;25(3):184–96.
58. McCoy NC, Yu M, Sullivan JA, Spiegel DM, Leitman SF. The effect of prestorage irradiation red cell survival on posttransfusion. *Transfusion (Paris)*. 1992;32(6):525–8.
59. Swindell CG, Barker TA, McGuirk SP, Jones TJ, Barron DJ, Brawn WJ, et al. Washing of irradiated red blood cells prevents hyperkalaemia during cardiopulmonary bypass in neonates and infants undergoing surgery for complex congenital heart disease. *European Journal of Cardio-thoracic Surgery*. 2007 Apr;31(4):659–64.
60. Weiskopf RB, Schnapp S, Rouine-Rapp K, Bostrom A, Toy P. Extracellular potassium concentrations in red blood cell suspensions after irradiation and washing. *Transfusion (Paris)*. 2005 Aug;45(8):1295–301.
61. Bansal I, Calhoun BW, Joseph C, Pothiawala M, Baron BW. A comparative study of reducing the extracellular potassium concentration in red blood cells by washing and by reduction of additive solution. *Transfusion (Paris)*. 2007 Feb;47(2):248–50.
62. Saito-Benz M, Murphy WG, Tzeng YC, Atkinson G, Berry MJ. Storage after gamma irradiation affects in vivo oxygen delivery capacity of transfused red blood cells in preterm infants. *Transfusion*. 2018 Sep;58(9):2108-2112.
63. Puchała M, Szweda-Lewandowska Z, Kiefer J. The influence of radiation quality on radiation-induced hemolysis and hemoglobin oxidation of human erythrocytes. *Journal of Radiation Research*. 2004 Jun;45(2):275-9.
64. Eshghifar N, Maghsudlu M, Amini Kafi-Abad S. The Effect of Pre-Storage Irradiation Blood on Quality of Red Blood Cells. *International Journal of Hematology-Oncology and Stem Cell Research*. 2021 Jan 1;15(1):1-6.

65. Thiriot C, Kergonou JF, Allary M, Saint-Blancard J, Rocquet G. Effects of whole-body gamma irradiation on oxygen transport by rat erythrocytes. *Biochimie*. 1982 Jan;64(1):79-83.
66. M.B., Ch.B., D.C.H. Lorna G. Macdougall. Red cell metabolism in iron deficiency anemia: III. The relationship between glutathione peroxidase, catalase, serum vitamin E, and susceptibility of iron-deficient red cells to oxidative hemolysis. *The Journal of Pediatrics*. 1972;80(5):774.
67. M.B., Ch.B., Lorna G. Macdougall. Red cell metabolism in iron deficiency anemia. II. The relationship between red cell survival and alterations in red cell metabolism. *The Journal of Pediatrics*. 1970 May;76(5):660–75.
68. Farid Z, Nichols JH, Schulert AR, Bassily S. Chromium51 red cell half-life in severe iron deficiency anemia. *American Journal of Tropical Medicine and Hygiene*. 1965;14(4):605–9.
69. Diez-Ewald M, Layrisse M. Mechanisms of hemolysis in iron deficiency anemia. Further studies. *Blood*. 1968 Dec;32(6):884-94.
70. Miguel Layrisse, Jesus Linares, Marcel Roche. Excess Hemolysis in Subjects with Severe Iron Deficiency Anemia Associated and Nonassociated with Hookworm Infection. *Blood*. 1965 Jan;25(1):73–91.
71. Safeukui I, Buffet PA, Deplaine G, Perrot S, Brousse V, Sauvanet A, et al. Sensing of red blood cells with decreased membrane deformability by the human spleen. *Blood Advances*. 2018 Oct 23;2(20):2581–7.
72. Kanas T, Stone M, Page GP, Guo Y, Endres-Dighe SM, Lanteri MC, et al. Frequent blood donations alter susceptibility of red blood cells to storage- and stress-induced hemolysis. *Transfusion (Paris)*. 2019 Jan 1;59(1):67–78.
73. R Yip, N Mohandas, M R Clark, S Jain, S B Shohet, P R Dallman. Red cell membrane stiffness in iron deficiency. *Blood*. 1983 Jul;62(1):99–106.

## **Chapter 5**

### **General Discussion and Concluding Remarks**

## **5.1 Assessing the Impact of Manufacturing Methods on the Distribution of RBC Subpopulations in Red Cell Concentrates**

The effectiveness of RCCs in transfusion medicine is subject to various factors, including but not limited to storage duration, manufacturing techniques, donor-related variables, and the proportion of different RBC subpopulations within the RCC. Previous studies revealed that transfusion of RCCs containing predominantly Y-RBCs prolongs post-transfusion survival, and the higher presence of O-RBCs within the RCCs is associated with a higher level of storage hemolysis, accumulation of side products of biological aging, and impaired oxygen delivery post-transfusion. (1,2) Previous studies demonstrated that the post-transfusion survival of Y-RBCs is significantly greater than O-RBCs, using a  $^{51}\text{Cr}$  labeling method (3,4), and the average transfusion requirement to sustain hemoglobin levels among splenectomized thalassemia patients who exclusively receive Y-RBCs, significantly decrease. (5) Hence, assessing the effectiveness of RCCs necessitates determining the proportions of Y- and O-RBCs within them, as an increased presence of O-RBCs may degrade RCC quality. (2) This thesis investigated the impact of pre-transfusion processing methods used in transfusion medicine, including component manufacturing methods, cryopreservation, and irradiation, on the distribution of RBC subpopulations with diverse biological ages. The various steps involved in different manufacturing methods lead to the isolation of distinct subpopulations of RBCs. Previous investigations have illuminated substantial disparities in the characteristics of RBCs within an RCC resulting from various manufacturing methods. (6) The results of Chapter 2 align with previous research, emphasizing the significant influence of manufacturing methods on the composition of RCCs. RCF-derived RCCs demonstrated lower HCT, Hb, RBC count, and volume compared to WBF-derived RCCs. This phenomenon could potentially be explained by the loss of RBCs associated with the buffy coat removal step, resulting in the loss of RBCs.

Moreover, the consistency of EMD across RCCs processed using different methods may be attributed to the Gaussian distribution curve of RBC density, with EMD acting as a threshold ensuring equal partitioning along the spectrum. Thus, while EMD remains consistent, the composition of RBCs at each end of the spectrum may differ. Analysis of RBC subpopulation distribution based on density revealed variations among units processed using different methods. This finding may be related to donor-related factors, including donor sex, age, and donation frequency. Remarkably, the sex of donors was found to be significantly associated with the

distribution of RBCs, with RCC units from male donors containing denser RBCs compared to their female counterparts. (7,8)

## **5.2 Comparative Analysis of Osmotic Characteristics and Post-Deglycerolization Survival in Red Blood Cell Subpopulations**

This thesis further elucidated significant correlations between RBC senescence level and fluorescence intensity, with Y-RBCs exhibiting higher intensity attributed to lower cytoplasmic hemoglobin concentration. Higher MCHC results in self-quenching of the hemoglobin auto-fluorescence and decreased fluorescence intensity in O-RBCs. (9–12) Moreover, the equilibrium fluorescence intensity of RBCs exhibited an inverse relationship with NaCl concentration across all RBC subpopulations, peaking at 0.68% NaCl and reaching the lowest level at 3.5% NaCl, which aligns with previous results from our team. (13) Stopped-flow experiments (Chapter 3) yielded noteworthy insights into the membrane permeability of RBC subpopulations with O-RBCs exhibiting the highest  $L_p$  values, leading to a more rapid volume change in response to anisotonic conditions compared to Y-RBCs. The distinctions in  $L_p$  value between Y- and O-RBCs become more prominent with the elevation of NaCl concentration at both temperatures. Additionally, during deglycerolization, O-RBCs demonstrated a higher  $P_s$  value compared to Y-RBCs, suggesting that the O-RBC membrane allows for a faster rate of glycerol efflux. This suggests that RCCs with a higher proportion of O-RBCs might undergo deglycerolization more efficiently due to the enhanced glycerol efflux. This presents new opportunities for refining cryopreservation procedures by considering the age distribution of RBCs within RCCs.

Additionally, Y-RBCs exhibited higher deformability and lower rigidity compared to O-RBCs, indicating their greater ability to withstand shear stress under various anisotonic conditions. The gradual decline in RBC deformability during biological aging is attributed to membrane alterations, morphological shifts, and heightened cytoplasmic viscosity. (1,13,14) The correlation between hemolysis and RBC senescence was consistent, with O-RBCs showing elevated hemolysis. This extends to oxidative hemolysis, highlighting compromised antioxidant systems in O-RBCs. In terms of osmotic hemolysis, O-RBCs exhibited the lowest levels, indicating superior resistance to rupturing under osmotic stress. This could be attributed to their higher  $L_p$  value, which facilitates water transport across the cell membrane and results in faster adaptation to osmotic changes.

Following deglycerolization, the number of both Y- and O-BioRBCs decreased by day 14. Surprisingly, despite the superior osmotic characteristics of Y-RBCs, no significant advantages were observed in their post-deglycerolization survival compared to O-RBCs. This unexpected outcome may be attributed to the high glycerol-slow cooling method, which favored the preservation of O-RBCs. Additionally, the higher  $L_p$  and  $P_s$  values in O-RBCs facilitated the movement of water and glycerol across the RBC membrane. Further investigations into the effects of various glycerolization and deglycerolization methods on Y-RBCs and O-RBCs would offer supplementary data regarding the influence of different levels of freezing and osmotic stress caused by these methods on the survival of RBC subpopulations. This assessment would evaluate their capacity to withstand such stresses induced by different methods. The reduced glycerol concentration and faster freezing rate could exacerbate osmotic stress, potentially leading to varying degrees of post-deglycerolization survival and functionality between Y-RBCs and O-RBCs.

The biological aging of RBCs is associated with decreased ATP and 2,3-DPG levels, impairing the function of ion pumps, antioxidant capacity, and oxygen affinity of RBCs. (1,4,15) Irradiation disrupts cell hemostasis, membrane integrity, and cellular functionality (16), leading to gradual Hb and  $K^+$  leakage (17–20), posing risks of post-transfusion complications, particularly in vulnerable patients. (21–23) Results in Chapter 4 demonstrated that hemolysis levels increased significantly in both irradiated and non-irradiated RCCs during hypothermic storage, with irradiated RCCs exhibiting higher levels of hemolysis at all testing time points. This difference became more pronounced between irradiated and non-irradiated units by day 14 ( $p=0.0005$ ). These results are consistent with findings from previous studies. (19) Comparison of hemolysis levels between RBC subpopulations showed that Y- and O-RBCs exhibited higher hemolysis levels compared to U-RBCs across all testing time points. This finding can be attributed to mechanical and osmotic stress induced by Percoll<sup>®</sup> separation, leading to membrane damage and subsequent hemoglobin leakage. Previous studies have demonstrated that osmotic and mechanical manipulation of RBCs, including centrifugation and saline washing, leads to enhanced hemolysis. (24,25)

The study found a positive correlation between oxidative hemolysis and RBC senescence level, with O-RBCs consistently displaying higher levels of oxidative hemolysis compared to Y-RBCs and U-RBCs. During the biological aging process of RBCs, the accumulation of ROS in

O-RBC, coupled with their impaired antioxidant system (1,19,23,26,27), renders them more susceptible to oxidative hemolysis induced by gamma-irradiation, while Y-RBCs demonstrate greater resilience to oxidative stress following irradiation. This aligns with our results, demonstrating that irradiation did not exacerbate the oxidative hemolysis level in Y-RBCs during hypothermic storage; however, it did contribute to an increasing trend of oxidative hemolysis in O-RBCs ( $p=0.0110$ ).

The supernatant  $K^+$  levels increased significantly in both irradiated and non-irradiated RCCs during hypothermic storage, with irradiated RCCs exhibiting higher levels of supernatant  $K^+$  at all testing time points. Irradiation was found to correlate with elevated supernatant  $K^+$  levels across all RBC subpopulations. U-RBCs exhibited the highest supernatant  $K^+$  levels at each testing time point, followed by O-RBCs, while Y-RBCs had the lowest levels. These results may be attributed to the washing steps of the Percoll<sup>®</sup> separation method, which likely contribute to lower  $K^+$  levels in Y- and O-RBCs by reducing the concentration of supernatant  $K^+$ . (28–30) (15,31) The correlation between irradiation and supernatant  $K^+$  levels was significant in Y-RBCs and U-RBCs, but not in O-RBCs, possibly due to differences in initial intracellular  $K^+$  concentrations. Further investigations are required to measure intracellular  $K^+$  levels in RBC subpopulations. p50 values significantly decrease across all RBC subpopulations during hypothermic storage post-irradiation ( $p<0.0001$ ). This aligns with previous trials showing compromised oxygen delivery capacity of RBCs after hypothermic storage following irradiation. (32) This study revealed no significant differences in the p50 value in O-RBCs over the hypothermic storage ( $p=0.8600$ ). Comparing p50 values between irradiated and non-irradiated RBC subpopulations demonstrated a decrease in p50 values regardless of irradiation, indicating that hypothermic storage has a more pronounced effect on p50 levels than irradiation alone.

The investigation into post-irradiation survival revealed a decrease in the number of both Y- and O-BioRBCs during hypothermic storage, with Y-BioRBCs showing a more pronounced decrease by day 14. Despite initial observations suggesting potential advantages of Y-RBCs in terms of lower  $K^+$  and hemoglobin leakage, lower oxidative hemolysis, and higher p50, our study did not find significant advantages in survival of Y-RBCs compared to O-RBCs during hypothermic storage post-irradiation. These outcomes might be influenced by the pooling and splitting method, where units from different donors with unique characteristics are combined,

potentially affecting the results. However, our validation with two additional units subjected to the same study confirms that this factor did not impact the results. Despite this, the absence of notable differences in RBC survival among subpopulations underscores the ongoing necessity for comprehensive research to comprehend the intricate factors affecting RBC behavior post-irradiation and during hypothermic storage.

#### **5.4 Effects of Biotinylation on Red Blood Cell Properties**

Biotinylation, a process used to label RBCs, has multifaceted effects on RBC properties. Biotinylation was found to enhance the deformability in O-RBCs and reduce the rigidity. This phenomenon can be attributed to the elevated  $L_p$  value in O-RBCs, primarily linked to water influx during the labeling and washing steps. This process leads to cytoplasm dilution, potentially enhancing deformability indices. This is in agreement with Mohandas et al. findings reporting a reverse correlation between the hemoglobin concentration and deformability of RBCs. (33) Additionally, biotinylation further contributes to increased oxidative hemolysis in O-RBCs, highlighting a potential lower antioxidant capacity in O-RBCs to overcome the oxidative stress induced by biotinylation. Interestingly, the impact of biotinylation on hemolysis levels is more pronounced in O-RBCs compared to Y-RBCs.

#### **5.5 Conclusion**

This thesis provides a comprehensive analysis of the density-based distribution of RBC subpopulations using RCF and WBF processing methods. Although WBF-derived RCCs exhibited higher levels of HCT, Hb, RBC counts, and volume, the distribution of Y- and O-RBCs in RCCs was not significantly influenced by manufacturing methods, as evidenced by consistent Y-to-O-RBC ratios across all units. This suggests that the centrifugation settings used in these processing methods might not generate sufficient centrifugal force to establish a density-based gradient of RBCs within the centrifuged bag. Moreover, observed variations in RBC distribution within some RCCs are likely attributed to donor-related factors such as age and sex rather than the manufacturing method itself. This donor-specific variation in the density-based distribution of RBC subpopulations can significantly impact the outcomes of studies examining the effects of different manufacturing processes on RBC subpopulations. These findings underscore the critical importance of considering donor-related factors when assessing RCC composition. The significance of this work lies in its potential to impact transfusion medicine by

providing a deeper understanding of how manufacturing methods affect the distribution of RBC subpopulations with varying biological ages. Future research should focus on tailoring the choice of RCCs based on the donor's profile and the recipient's needs. For instance, transfusing Y-RBCs might be beneficial for chronic blood recipients to reduce the frequency of transfusions and the total amount of blood required.

Despite Y-RBCs having superior osmotic characteristics, these advantages did not result in improved survival after deglycerolization. The use of a high glycerol/slow-cooling method may have favored the preservation of O-RBCs instead. Alternatively, the higher water and solute permeability of O-RBCs could facilitate osmotic adaptation and glycerol removal, potentially enhancing their survival. Additionally, O-RBCs' lower osmotically inactive volume might enable them to better regulate their volume in response to osmotic changes. The significant variations in osmotic characteristics among RBC subpopulations lay the foundation for future research on cryopreservation and post-transfusion survival. Emphasizing these differences highlights O-RBCs as more suitable for deglycerolization due to their higher solute permeability. This research underscores the importance of tailoring cryopreservation protocols based on the distribution of these subpopulations within RCC units to maximize final product quality. Furthermore, assessing the impact of different cryopreservation techniques on various RBC subpopulations could provide additional insights into the effects of cryoprotectant concentration and cooling rate on biologically aged RBC subpopulations. Biotinylation studies also offer valuable insights into the cryopreservation of bio-labeled RBCs for tracing studies in humans, potentially offering deeper insights into RBC lifespan and function post-transfusion.

Assessing the effects of gamma irradiation on various subpopulations of RBCs revealed that hemolysis and supernatant increased in Y- and O-RBCs following irradiation, suggesting comparable membrane damage. The impaired antioxidant capacity of O-RBCs leads to a more pronounced increase in oxidative hemolysis post-gamma irradiation. This suggests that units containing a higher proportion of O-RBCs may be less effective for oxygen delivery due to their impaired ability to withstand oxidative stress after irradiation, leading to a higher affinity for oxygen and reduced oxygenation capability. Moreover, irradiation studies have shown that Y-RBCs exhibit higher potassium efflux. Therefore, for patients at risk of hyperkalemia, units with a higher proportion of Y-RBCs might pose a risk.

A primary limitation of this study lies in the inherent variability within the Gaussian-shaped distribution of RBCs. The same density may represent Y-RBCs in one donor and O-RBCs in another, complicating result comparison and interpretation. Moreover, the separation and biotin labeling processes tend to eliminate the most vulnerable cells, biasing the sample towards the strongest Y- and O-RBC populations. Consequently, the surviving cells may display enhanced characteristics due to their resilience, rendering them non-representative of the average Y and O cells within the original RCC. This selection bias emphasizes the importance of cautious interpretation and necessitates methodologies that can mitigate these biases.

Furthermore, this thesis provides a foundational framework for future advancements in strategically selecting RCCs based on donor-related factors and pre-transfusion manipulations tailored to recipient clinical conditions and requirements. By advancing these methodologies, we can ultimately pave the way for more effective and safer transfusion therapies.

## 5.6 References

1. Mykhailova O, Olafson C, Turner TR, D'Alessandro A, Acker JP. Donor-dependent aging of young and old red blood cell subpopulations: Metabolic and functional heterogeneity. *Transfusion (Paris)*. 2020;60(11):2633–46.
2. Tuo WW, Wang D, Liang WJ, Huang YX. How cell number and cellular properties of blood-banked red blood cells of different cell ages decline during storage. *PLoS One*. 2014;9(8):1–8.
3. Piomelli S, Seaman C, Reibman J, Tytun A, Graziano J, Tabachnik N, et al. Separation of younger red cells with improved survival in vivo: an approach to chronic transfusion therapy. *Proceedings of the National Academy of Sciences of the United States of America*. 1978;75(7):3474–8.
4. Triadou, P., R. Girot, D. Rebibo, D. Lemau, B. Mattlinger, P. Bolo, M. Maier, and L. Barritault. Neocytopheresis: a new approach for the transfusion of patients with thalassaemia major. *Eur The Journal of Pediatrics* (1986) 145: 10–13.
5. Cohen AR, Schmidt JM, Martin MB, Barnsley W, Schwartz E. Clinical trial of young red cell transfusions. *The Journal of Pediatrics*. 1984;104(6):865–8.
6. Acker JP, Hansen AL, Kurach JDR, Turner TR, Croteau I, Jenkins C. A quality monitoring program for red blood cell components: In vitro quality indicators before and after implementation of semiautomated processing. *Transfusion (Paris)*. 2014;54(10):2534–43.
7. Mykhailova O, Brandon-Coatham M, Durand K, Olafson C, Xu A, Yi QL, Kanas T, Acker JP. Estimated median density identifies donor age and sex differences in red blood cell biological age. *Transfusion*. 2024 Feb 29.
8. Mykhailova O, Brandon-Coatham M, Phan C, Yazdanbakhsh M, Olafson C, Yi QL, Kanas T, Acker JP. Red cell concentrates from teen male donors contain poor-quality biologically older cells. *Vox Sang*. 2024 Feb 28.
9. Nash GB, Meiselman HJ. Red cell and ghost viscoelasticity. Effects of hemoglobin concentration and in vivo aging. *Biophysical Journal*. 1983;43(1):63–73.
10. Bocci V. Determinants Of Erythr Ocyte Ageing: A Reappraisal. *British Journal of Haematology*. 1981;48(4):515–22.
11. Linderkamp O, Meiselman HJ. Geometric, Osmotic, and Membrane Mechanical Properties of Density-Separated Human Red Cells. Vol. 59, *Blood*. 1982.
12. Sutura SP, Gardner RA, Boylan CW, Carroll GL, Chang KC, Marvel JS, et al. Age-Related Changes in Deformability of Human Erythrocytes. Vol. 65, *Blood*. 1985.

13. Zhurova M, Olivieri A, Holt A, Acker JP. A method to measure permeability of red blood cell membrane to water and solutes using intrinsic fluorescence. *Clinica Chimica Acta*. 2014;431:103–10.
14. Tillmann W, Levin C, Prindull G, Schr W. *Klinische Wochen-schrift Rheological Properties of Young and Aged Human Erythrocytes*. Vol. 58. 1980.
15. D'Alessandro A, Blasi B, D'Amici GM, Marrocco C, Zolla L. Red blood cell subpopulations in freshly drawn blood: Application of proteomics and metabolomics to a decades-long biological issue. *Blood Transfusion*. 2013;11(1):75–87.
16. Moreira OC, Oliveira VH, Benedicto LBF, Nogueira CM, Mignaco JA, Fontes CFL, et al. Effects of  $\gamma$ -irradiation on the membrane ATPases of human erythrocytes from transfusional blood concentrates. *Annals of Hematology*. 2008 Feb;87(2):113–9.
17. McCoy NC, Yu M, Sullivan JA, Spiegel DM, Leitman SF. The effect of prestorage irradiation red cell survival on posttransfusion. *Transfusion (Paris)*. 1992;32(6):525–8.
18. Katharia R, Chaudhary R, Agarwal P. Prestorage gamma irradiation induces oxidative injury to red cells. *Transfusion and Apheresis Science*. 2013 Feb;48(1):39–43.
19. Serrano K, Chen D, Hansen AL, Levin E, Turner TR, Kurach JDR, et al. The effect of timing of gamma-irradiation on hemolysis and potassium release in leukoreduced red cell concentrates stored in SAGM. *Vox Sang*. 2014;106(4):379–81.
20. Vraets A, Lin Y, Callum JL. Transfusion-associated hyperkalemia. *Transfusion Medicine Reviews*. 2011 Jul;25(3):184–96.
21. Harm SK, Raval JS, Cramer J, Waters JH, Yazer MH. Haemolysis and sublethal injury of RBCs after routine blood bank manipulations. *Transfusion Medicine*. 2012;22(3):181–5.
22. Lee AC, Reduque LL, Luban NLC, Ness PM, Anton B, Heitmiller ES. Transfusion-associated hyperkalemic cardiac arrest in pediatric patients receiving massive transfusion. *Transfusion (Paris)*. 2014 Jan;54(1):244–54.
23. Hauck B, Oremek D, Zimmermann R, Ruppel R, Troester B, Eckstein R. Influence of irradiation on in vitro red-blood-cell (RBC) storage variables of leucoreduced RBCs in additive solution PAGGS-M. *Vox Sang*. 2011 Jul;101(1):21–7.
24. Masalunga C, Cruz M, Porter B, Roseff S, Chui B, Mainali E. Increased hemolysis from saline pre-washing RBCs or centrifugal pumps in neonatal ECMO. *Journal of Perinatology*. 2007 Jun;27(6):380–4.
25. O'Leary MF, Szklarski P, Klein TM, Young PP. Hemolysis of red blood cells after cell washing with different automated technologies: Clinical implications in a neonatal cardiac surgery population. *Transfusion (Paris)*. 2011 May;51(5):955–60.

26. Antosik A, Czubak K, Gajek A, Marczak A, Glowacki R, Borowczyk K, et al. Influence of pre-storage irradiation on the oxidative stress markers, membrane integrity, size and shape of the cold stored red blood cells. *Transfusion Medicine and Hemotherapy*. 2015 Jun 15;42(3):140–8.
27. Bosman GJCGM, Werre JM, Willekens FLA, Novotný VMJ. Erythrocyte ageing in vivo and in vitro: Structural aspects and implications for transfusion. *Transfusion Medicine*. 2008;18(6):335–47.
28. Weiskopf RB, Schnapp S, Rouine-Rapp K, Bostrom A, Toy P. Extracellular potassium concentrations in red blood cell suspensions after irradiation and washing. *Transfusion (Paris)*. 2005 Aug;45(8):1295–301.
29. Bansal I, Calhoun BW, Joseph C, Pothiawala M, Baron BW. A comparative study of reducing the extracellular potassium concentration in red blood cells by washing and by reduction of additive solution. *Transfusion (Paris)*. 2007 Feb;47(2):248–50.
30. Swindell CG, Barker TA, McGuirk SP, Jones TJ, Barron DJ, Brawn WJ, et al. Washing of irradiated red blood cells prevents hyperkalaemia during cardiopulmonary bypass in neonates and infants undergoing surgery for complex congenital heart disease. *European Journal of Cardio-thoracic Surgery*. 2007 Apr;31(4):659–64.
31. An X, Mohandas N. Disorders of red cell membrane. *British Journal of Haematology*. 2008 May;141(3):367-75.
32. Saito-Benz M, Murphy WG, Tzeng YC, Atkinson G, Berry MJ. Storage after gamma irradiation affects in vivo oxygen delivery capacity of transfused red blood cells in preterm infants. *Transfusion*. 2018 Sep;58(9):2108-2112.
33. N Mohandas, S B Shohet. Control of red cell deformability and shape. *Current Topics in Hematology*. 1978;1:75–125.

## **Bibliography**

Abramsson-Zetterberg, Lilianne, Rickard Carlsson, and Salomon Sand. 2013. The Use of Immunomagnetic Separation of Erythrocytes in the in Vivo Flow Cytometer-Based Micronucleus Assay. *Mutation Research - Genetic Toxicology and Environmental Mutagenesis* 752(1–2):8–13.

Acker, Jason P., Adele L. Hansen, Jayme D. R. Kurach, Tracey R. Turner, Ioana Croteau, and Craig Jenkins. 2014a. A Quality Monitoring Program for Red Blood Cell Components: In Vitro Quality Indicators before and after Implementation of Semiautomated Processing. *Transfusion* 54(10):2534–43.

Agarwal P, Ray VL, Choudhury N, Chaudhary RK. Effect of pre-storage gamma irradiation on red blood cells. *Indian Journal of Medical Research*. 2005 Nov; 122(5):385-7.

Agre P, Smith B L, Baumgarten R, Preston G M, Pressman E, Wilson P, Illum N, Anstee D J, Lande M B, Zeidel M L. Human Red Cell Aquaporin CHIP 11. Expression during Normal Fetal Development and in a Novel Form of Congenital Dyserythropoietic Anemia. *Journal of Clinical Investigation*. 1994; 94(3):1050-1058.

Almizraq, Ruqayyah J., Jelena L. Holovati, and Jason P. Acker. 2018. Characteristics of Extracellular Vesicles in Red Blood Concentrates Change with Storage Time and Blood Manufacturing Method. *Transfusion Medicine and Hemotherapy* 45(3):185–93.

Almizraq, Ruqayyah J., Philip J. Norris, Heather Inglis, Somaang Menocha, Mathijs R. Wirtz, Nicole Juffermans, Suchitra Pandey, Philip C. Spinella, Jason P. Acker, and Jennifer A. Muszynski. 2018a. Blood Manufacturing Methods Affect Red Blood Cell Product Characteristics and Immunomodulatory Activity. *Blood Advances* 2(18):2296–2306.

Almizraq, Ruqayyah J., Jerard Seghatchian, and Jason P. Acker. 2016. Extracellular Vesicles in Transfusion-Related Immunomodulation and the Role of Blood Component Manufacturing. *Transfusion and Apheresis Science* 55(3):281–91.

- Alshalani, Abdulrahman, and Jason P. Acker. 2017. Red Blood Cell Membrane Water Permeability Increases with Length of Ex Vivo Storage. *Cryobiology* 76:51–58.
- Alshalani, Abdulrahman, Anita Howell, and Jason P. Acker. 2018. Impact of Blood Manufacturing and Donor Characteristics on Membrane Water Permeability and in Vitro Quality Parameters during Hypothermic Storage of Red Blood Cells. *Cryobiology* 80:30–37.
- Ando, Ken, Masatoshi Beppu, Kiyomi Kikugawa, Ryoji Nagai, and Seikoh Horiuchi. 1999. Membrane Proteins of Human Erythrocytes Are Modified by Advanced Glycation End Products during Aging in the Circulation. *Biochemical and Biophysical Research Communications* 258(1):123–27.
- Annis AM, Sparrow RL. Expression of CD47 (integrin-associated protein) decreases on red blood cells during storage. *Transfusion and Apheresis Science*. 2002 Dec; 27(3):233-8.
- ACP® 215 Preparation of Deglycerolized Red Cells. Canadian Blood Service, WI# 02 181 Revision #3.
- ACP® 215 Preparation of Frozen Red Cells. Canadian Blood Service, WI# 02 180 Revision #2.
- A Flow Cytometric Method to Quantify Biotinylated Red Blood Cells. Dr. Jason Acker's Laboratory, Version 1.2, Revised 2023-01-05.
- Antosik, Adam, Kamila Czubak, Arkadiusz Gajek, Agnieszka Marczak, Rafal Glowacki, Kamila Borowczyk, and Halina Malgorzata Zbikowska. 2015. Influence of Pre-Storage Irradiation on the Oxidative Stress Markers, Membrane Integrity, Size and Shape of the Cold Stored Red Blood Cells. *Transfusion Medicine and Hemotherapy* 42(3):140–48.
- An X, Mohandas N. Disorders of red cell membrane. *British Journal of Haematology*. 2008 May; 141(3):367-75.

- An X, Chen L. Flow Cytometry (FCM) Analysis and Fluorescence-Activated Cell Sorting (FACS) of Erythroid Cells. *Methods in Molecular Biology* (Clifton, N.J.). 2018; 1698:153-174.
- Apell HJ, Nelson MT, Marcus MM, Läuger P. Effects of the ATP, ADP and inorganic phosphate on the transport rate of the Na<sup>+</sup>, K<sup>+</sup>-pump. *Biochimica et Biophysica Acta*. 1986 May 9; 857(1):105-15..
- Arese P, Turrini F, Schwarzer E. Band 3/complement-mediated recognition and removal of normally senescent and pathological human erythrocytes. *Cellular Physiology and Biochemistry*. 2005; 16(4-6):133-46.
- Arthur W. Rowe, E. Eyster, and A. Kellner. 1968. Liquid Nitrogen Preservation of Red Blood Cells for Transfusion: A Low Glycerol — Rapid Freeze Procedure. *Cryobiology* 5(2):119–28.
- Axelsen KB, Palmgren MG. Evolution of substrate specificities in the P-type ATPase superfamily. *Journal of Molecular Evolution*. 1998 Jan; 46(1):84-101.
- de Back DZ, Vlaar R, Beuger B, Daal B, Lagerberg J, Vlaar APJ, de Korte D, van Kraaij M, van Bruggen R. A method for red blood cell biotinylation in a closed system. *Transfusion*. 2018 Apr; 58(4):896-904.
- Bakkour, S., J. P. Acker, D. M. Chafets, H. C. Inglis, P. J. Norris, T. H. Lee, and M. P. Busch. 2016. Manufacturing Method Affects Mitochondrial DNA Release and Extracellular Vesicle Composition in Stored Red Blood Cells. *Vox Sanguinis* 111(1):22–32.
- Bandarenko, Nicholas, Shauna N. Hay, Jerry Holmberg, Pam Whitley, Harry L. Taylor, Gary Moroff, Leslie Rose, Richard Kowalsky, Marla Brumit, Michael Rose, Sherrie Sawyer, Adrienne Johnson, Deanna McNeil, and Mark A. Popovsky. 2004. “Extended Storage of AS-1 and AS-3 Leukoreduced Red Blood Cells for 15 Days after Deglycerolization and Resuspension in AS-3 Using an Automated Closed System.” *Transfusion* 44(11):1656–62.

- Bansal, Ila, Beverly W. Calhoun, Cherilyn Joseph, Mohammad Pothiwala, and Beverly W. Baron. 2007. A Comparative Study of Reducing the Extracellular Potassium Concentration in Red Blood Cells by Washing and by Reduction of Additive Solution. *Transfusion* 47(2):248–50.
- Barshtein, Gregory, Alexander Gural, Orly Zelig, Dan Arbell, and Saul Yedgar. 2020. Preparation of Packed Red Blood Cell Units in the Blood Bank: Alteration in Red Blood Cell Deformability. *Transfusion and Apheresis Science* 59(3).
- Béné, M. C. 2017. Microfluidics in Flow Cytometry and Related Techniques. *International Journal of Laboratory Hematology* 39:93–97.
- Benga G, Borza T. Diffusional water permeability of mammalian red blood cells. *Comparative Biochemistry and Physiology Part B: Biochemistry & Molecular Biology*. 1995 Dec; 112(4):653-9.
- Benson, James D., Anthony J. Kearsley, and Adam Z. Higgins. 2012. Mathematical Optimization of Procedures for Cryoprotectant Equilibration Using a Toxicity Cost Function. *Cryobiology* 64(3):144–51.
- Blasi, B., A. D'Alessandro, N. Ramundo, and L. Zolla. 2012. Red Blood Cell Storage and Cell Morphology. *Transfusion Medicine* 22(2):90–96.
- BloodBook.com. (2024, March 4). Blood banking. Retrieved March 4, 2024, from <http://www.bloodbook.com/banking.html>.
- Boas FE, Forman L, Beutler E. Phosphatidylserine exposure and red cell viability in red cell aging and in hemolytic anemia. *Proceedings of the National Academy of Sciences of the United States of America*. 1998 Mar 17; 95(6):3077-81.
- Bocci V. Determinants of erythrocyte ageing: a reappraisal. *British Journal of Haematology*. 1981 Aug; 48(4):515-22.

- Bosch FH, Werre JM, Roerdinkholder-Stoelwinder B, Huls TH, Willekens FL, Halie MR. Characteristics of red blood cell populations fractionated with a combination of counterflow centrifugation and Percoll separation. *Blood*. 1992 Jan 1; 79(1):254-60.
- Bosch, F. H., J. M. Werre, B. Roerdinkholder-Stoelwinder, T. H. Huls, F. L. A. Willekens, and M. R. Halie. 1992. Characteristics of Red Blood Cell Populations Fractionated with a Combination of Counterflow Centrifugation and Percoll Separation. *Blood* 79(1):254–60.
- Bosman GJ, Willekens FL, Werre JM. Erythrocyte aging: a more than superficial resemblance to apoptosis? *Cellular Physiology and Biochemistry*. 2005; 16(1-3):1-8.
- Bosman GJ. Survival of red blood cells after transfusion: processes and consequences. *Frontiers in Physiology*. 2013 Dec 18; 4:376.
- Bosman, G. J. C. G. M., E. Lasonder, Y. A. M. Groenen-Döpp, F. L. A. Willekens, J. M. Werre, and V. M. J. Novotný. 2010. Comparative Proteomics of Erythrocyte Aging in Vivo and in Vitro. *Journal of Proteomics* 73(3):396–402.
- Bosman, G. J. C. G. M., J. M. Werre, F. L. A. Willekens, and V. M. J. Novotný. 2008. Erythrocyte Ageing in Vivo and in Vitro: Structural Aspects and Implications for Transfusion. *Transfusion Medicine* 18(6):335–47.
- Bratosin D, Mazurier J, Tissier JP, Estaquier J, Huart JJ, Ameisen JC, Aminoff D, Montreuil J. Cellular and molecular mechanisms of senescent erythrocyte phagocytosis by macrophages. A review. *Biochimie*. 1998 Feb; 80(2):173-95.
- Brugnara, C., and W. H. Churchill. 1992. Effect of Irradiation on Red Cell Cation Content and Transport. *Transfusion* 32(3):246–52.
- Bruil A, Beugeling T, Feijen J, van Aken WG. The mechanisms of leukocyte removal by filtration. *Transfusion Medicine Reviews*. 1995 Apr; 9(2):145-66.

- Campos E, Moura TF, Oliva A, Leandro P, Soveral G. Lack of Aquaporin 3 in bovine erythrocyte membranes correlates with low glycerol permeation. *Biochemical and Biophysical Research Communications*. 2011 May 13; 408(3):477-81.
- Canadian Standards Association. 2020. CAN/CSA-Z902:20 Blood and Blood Components. Toronto, ON.
- Card, R. T., N. Mohandas, H. A. Perkins, and S. B. Shoheit. 1982. Deformability of Stored Red Blood Cells. *Transfusion* 22(2):96–101.
- Carlsen, Anders, and Jens Otto Wieth. 1976. Glycerol Transport in Human Red Cells. *Acta Physiologica Scandinavica* 97(4):501–13. DIO:10.1111/j.1748-1716.1976.tb10290.
- Chassé M, Tinmouth A, English SW, et al. Association of Blood Donor Age and Sex With Recipient Survival After Red Blood Cell Transfusion. *JAMA Internal Medicine*. 2016; 176(9):1307–1314.
- Chen PY, Pearce D, Verkman AS. Membrane water and solute permeability determined quantitatively by self-quenching of an entrapped fluorophore. *Biochemistry*. 1988 Jul 26; 27(15):5713-8.
- Cloutier M, Cognasse F, Yokoyama APH, Hazegh K, Mykhailova O, Brandon-Coatham M, Hamzeh-Cognasse H, Kutner JM, Acker JP, Kanias T; Biomedical Excellence for Safer Transfusion (BEST) Collaborative. Quality assessment of red blood cell concentrates from blood donors at the extremes of the age spectrum: The BEST collaborative study. *Transfusion*. 2023 Aug; 63(8):1506-1518.
- Cohen, Alan R., Joanne M. Schmidt, Marie B. Martin, William Barnsley, and Elias Schwartz. 1984. Clinical Trial of Young Red Cell Transfusions. *The Journal of Pediatrics* 104(6):865–68.
- Cohen-Maslaton S, Barnea I, Taieb A, Shaked NT. Cell and nucleus refractive-index mapping by interferometric phase microscopy and rapid confocal fluorescence microscopy. *Journal of Biophotonics*. 2020 Sep; 13(9):e202000117.

- van Cromvoirt AM, Fenk S, Sadafi A, Melnikova EV, Lagutkin DA, Dey K, Petrushanko IY, Hegemann I, Goede JS, Bogdanova A. Donor Age and Red Cell Age Contribute to the Variance in LORCA Indices in Healthy Donors for Next Generation Ektacytometry: A Pilot Study. *Frontiers in Physiology*. 2021 Mar 2; 12:639722.
- D'Alessandro A, Blasi B, D'Amici GM, Marrocco C, Zolla L. Red blood cell subpopulations in freshly drawn blood: application of proteomics and metabolomics to a decades-long biological issue. *Blood Transfusion*. 2013 Jan; 11(1):75-87.
- D'Alessandro A, D'Amici GM, Vaglio S, Zolla L. Time-course investigation of SAGM-stored leukocyte-filtered red blood cell concentrates: from metabolism to proteomics. *Haematologica*. 2012 Jan; 97(1):107-15.
- D'Alessandro A, Anastasiadi AT, Tzounakas VL, Nemkov T, Reisz JA, Kriebardis AG, Zimring JC, Spitalnik SL, Busch MP. Red Blood Cell Metabolism In Vivo and In Vitro. *Metabolites*. 2023 Jun 27; 13(7):793.
- Daly A, Raval JS, Waters JH, Yazer MH, Kameneva MV. Effect of blood bank storage on the rheological properties of male and female donor red blood cells. *Clinical Hemorheology and Microcirculation*. 2014; 56(4):337-45.
- Davidson AF, Benson JD, Higgins AZ. Mathematically optimized cryoprotectant equilibration procedures for cryopreservation of human oocytes. *Theoretical Biology and Medical Modelling*. 2014 Mar 20; 11:13.
- De Gier J, Mandersloot JG, Hupkes JV, McElhaney RN, Van Beek WP. On the mechanism of non-electrolyte permeation through lipid bilayers and through biomembranes. *Biochimica et Biophysica Acta*. 1971 Jun 1; 233(3):610-8.
- Denise Harmening. 2002. *Clinical Hematology and Fundamentals of Hemostasis*. 2024 Sixth edition. Edited by Denise Harmening and LeAnne M. Hutson. F.A. Davis Co., Philadelphia, PA, ©2009.

- Dern RJ, Gwinn RP, Wiorkowski JJ. Studies on the preservation of human blood. I. Variability in erythrocyte storage characteristics among healthy donors. *Journal of Laboratory and Clinical Medicine*. 1966 Jun; 67(6):955-65.
- Devine, D. v., and D. Howe. 2010. Processing of Whole Blood into Cellular Components and Plasma. *ISBT Science Series* 5(n1):78–82.
- Diez-Ewald M, Layrisse M. Mechanisms of hemolysis in iron deficiency anemia. Further studies. *Blood*. 1968 Dec; 32(6):884-94.
- Dumaswala, U. J., R. U. Dumaswala, D. S. Levin, and T. J. Greenwalt. 1996. Improved Red Blood Cell Preservation Correlates with Decreased Loss of Bands 3, 4.1, Acetylcholinesterase, and Lipids in Microvesicles. *Blood* 87(4):1612–16.
- Ebertz, S. L., and L. E. McGann. 2004a. Cryoprotectant Permeability Parameters for Cells Used in a Bioengineered Human Corneal Equivalent and Applications for Cryopreservation. *Cryobiology* 49(2):169–80.
- Ebertz, S. L., and L. E. McGann. 2004b. Cryoprotectant Permeability Parameters for Cells Used in a Bioengineered Human Corneal Equivalent and Applications for Cryopreservation. *Cryobiology* 49(2):169–80.
- Eckstein, M., R. Zimmermann, T. Roth, B. Hauck-Dlimi, E. F. Strasser, and W. Xiang. 2015. The Effects of an Overnight Holding of Whole Blood at Room Temperature on Haemoglobin Modification and in Vitro Markers of Red Blood Cell Aging. *Vox Sanguinis* 108(4):359–67.
- Edgren G, Ullum H, Rostgaard K, Erikstrup C, Sartipy U, Holzmann MJ, Nyrén O, Hjalgrim H. Association of Donor Age and Sex With Survival of Patients Receiving Transfusions. *JAMA Internal Medicine*. 2017 Jun 1; 177(6):854-860..
- Elmoazzen HY, Elliott JA, McGann LE. The effect of temperature on membrane hydraulic conductivity. *Cryobiology*. 2002 Aug; 45(1):68-79.

- European Directorate for the Quality of Medicines and Health Care. Guide to the Preparation, Use and Quality Assurance of Blood Components. 20th ed. 2020. Strasbourg, France: Council of Europe Publishing.
- Strehler EE, Treiman M. Calcium pumps of plasma membrane and cell interior. *Current Molecular Medicine*. 2004 May; 4(3):323-35.
- Eshghifar N, Maghsudlu M, Amini Kafi-Abad S. The Effect of Pre-Storage Irradiation Blood on Quality of Red Blood Cells. *International Journal of Hematology-Oncology and Stem Cell Research*. 2021 Jan 1; 15(1):1-6.
- Oski FA. The unique fetal red cell and its function. E. Mead Johnson Award address. *Pediatrics*. 1973 Mar; 51(3):494-500.
- Farid Z., Nichols J. H., Schulert A. R., and Bassily S. 1965. Chromium51 Red Cell Half-Life in Severe Iron Deficiency Anemia. *American Journal of Tropical Medicine and Hygiene* 14(4):605–9.
- Fergusson DA, Chassé M, Tinmouth A, Acker JP, English S, Forster AJ, Hawken S, Shehata N, Thavorn K, Wilson K, Tuttle A, Perelman I, Cober N, Maddison H, Tokessy M. Pragmatic, double-blind, randomised trial evaluating the impact of red blood cell donor sex on recipient mortality in an academic hospital population: the innovative Trial Assessing Donor Sex (iTADS) protocol. *BMJ Open*. 2021 Feb 23; 11(2):e049598.
- Franco RS, Puchulu-Campanella ME, Barber LA, Palascak MB, Joiner CH, Low PS, Cohen RM. Changes in the properties of normal human red blood cells during in vivo aging. *American Journal of Hematology*. 2013 Jan; 88(1):44-51.
- Gammon R. 2020. Standards for Blood Banks and Transfusion Services. 33<sup>rd</sup> edition, April 1, 2022, dited by M. Bethesda. Association for the Advancement of Blood & Biotherapies (AABB).
- Garraud O, Tissot JD. Blood and Blood Components: From Similarities to Differences. *Frontiers in Medicine (Lausanne)*. 2018 Apr 9; 5:84.

- Gifford, Sean C., Jure Derganc, Sergey S. Shevkoplyas, Tatsuro Yoshida, and Mark W. Bitensky. 2006. A Detailed Study of Time-Dependent Changes in Human Red Blood Cells: From Reticulocyte Maturation to Erythrocyte Senescence. *British Journal of Haematology* 135(3):395–404.
- Girshovitz P, Shaked NT. Generalized cell morphological parameters based on interferometric phase microscopy and their application to cell life cycle characterization. *Biomedical Optics Express*. 2012 Aug 1; 3(8):1757-73.
- Gonzales, R., Auclair, C., Voisin, E.M., Gautero, H., Dhermy, D., & Boivin, P. (1984). Superoxide dismutase, catalase, and glutathione peroxidase in red blood cells from patients with malignant diseases. *Cancer Research*, 44 9, 4137-9.
- González Flecha FL, Castello PR, Gagliardino JJ, Rossi JP. Molecular characterization of the glycated plasma membrane calcium pump. *The Journal of Membrane Biology*. 1999 Sep 1; 171(1):25-34.
- Grant, Joseph L., Melvin C. Britton, and Thomas E. Kurtz. 1960. Measurement of Red Blood Cell Volume with the Electronic Cell Counter. *American Journal of Clinical Pathology*. Vol. 33, No. 2, February, 1960, pp. 138-143.
- Greenwalt TJ. The how and why of exocytic vesicles. *Transfusion*. 2006 Jan; 46(1):143-52.
- Gulliksson H, van der Meer PF. Storage of whole blood overnight in different blood bags preceding preparation of blood components: in vitro effects on red blood cells. *Blood Transfusion*. 2009 Jul; 7(3):210-5.
- Hall, John E. *Guyton and Hall Textbook of Medical Physiology*. 13th ed., W B Saunders, 2015.
- Hansen AL, Turner TR, Kurach JD, Acker JP. Quality of red blood cells washed using a second wash sequence on an automated cell processor. *Transfusion*. 2015 Oct; 55(10):2415-21.

- Hansen AL, Turner TR, Kurach JD, Acker JP. Quality of red blood cells washed using a second wash sequence on an automated cell processor. *Transfusion*. 2015 Oct; 55(10):2415-21.
- Hansen AL, Kurach JD, Turner TR, Jenkins C, Busch MP, Norris PJ, Dugger J, Tomasulo PA, Devine DV, Acker JP. The effect of processing method on the in vitro characteristics of red blood cell products. *Vox Sang*. 2015 May; 108(4):350-8.
- Hardeman MR, Dobbe JG, Ince C. The Laser-assisted Optical Rotational Cell Analyzer (LORCA) as red blood cell aggregometer. *Clinical Hemorheology and Microcirculation*. 2001; 25(1):1-11.
- Harm SK, Raval JS, Cramer J, Waters JH, Yazer MH. Haemolysis and sublethal injury of RBCs after routine blood bank manipulations. *Transfusion Medicine*. 2012 Jun; 22(3):181-5.
- Hauck, B., D. Oremek, R. Zimmermann, R. Ruppel, B. Troester, and R. Eckstein. 2011. Influence of Irradiation on in Vitro Red-Blood-Cell (RBC) Storage Variables of Leucoreduced RBCs in Additive Solution PAGGS-M. *Vox Sanguinis* 101(1):21–27.
- Hazegh K, Fang F, Bravo MD, Tran JQ, Muench MO, Jackman RP, Roubinian N, Bertolone L, D'Alessandro A, Dumont L, Page GP, Kanas T. Blood donor obesity is associated with changes in red blood cell metabolism and susceptibility to hemolysis in cold storage and in response to osmotic and oxidative stress. *Transfusion*. 2021 Feb; 61(2):435-448.
- Heddle NM, Arnold DM, Acker JP, Liu Y, Barty RL, Eikelboom JW, Webert KE, Hsia CC, O'Brien SF, Cook RJ. Red blood cell processing methods and in-hospital mortality: a transfusion registry cohort study. *The Lancet haematology*. 2016 May; 3(5):e246-54.
- Heddle NM, Cook RJ, Liu Y, Zeller M, Barty R, Acker JP, Eikelboom J, Arnold DM. The association between blood donor sex and age and transfusion recipient mortality: an exploratory analysis. *Transfusion*. 2019 Feb; 59(2):482-491.

- Heitzer E, Auer M, Gasch C, Pichler M, Ulz P, Hoffmann EM, Lax S, Waldispuehl-Geigl J, Mauermann O, Lackner C, Höfler G, Eisner F, Sill H, Samonigg H, Pantel K, Riethdorf S, Bauernhofer T, Geigl JB, Speicher MR. Complex tumor genomes inferred from single circulating tumor cells by array-CGH and next-generation sequencing. *Cancer Research*. 2013 May 15; 73(10):2965-75.
- Hess JR. Red cell freezing and its impact on the supply chain. *Transfusion Medicine*. 2004 Feb; 14(1):1-8.
- Hess JR. Red cell storage. *Journal of Proteomics*. 2010 Jan 3; 73(3):368-73.
- Hirsch RE, Zukin RS, Nagel RL. Intrinsic fluorescence emission of intact oxy hemoglobins. *Biochemical and Biophysical Research Communications*. 1980 Mar 28; 93(2):432-9.
- Hod EA, Spitalnik SL. Harmful effects of transfusion of older stored red blood cells: iron and inflammation. *Transfusion*. 2011 Apr; 51(4):881-5.
- Hogan VA, Blanchette VS, Rock G. A simple method for preparing neocyte-enriched leukocyte-poor blood for transfusion-dependent patients. *Transfusion*. 1986 May-Jun; 26(3):253-7.
- Högman CF, Eriksson L, Hedlund K, Wallvik J. The bottom and top system: a new technique for blood component preparation and storage. *Vox Sang*. 1988; 55(4):211-7.
- Högman CF, Löf H, Meryman HT. Storage of red blood cells with improved maintenance of 2,3-bisphosphoglycerate. *Transfusion*. 2006 Sep; 46(9):1543-52.
- Holovati JL, Wong KA, Webster JM, Acker JP. The effects of cryopreservation on red blood cell microvesiculation, phosphatidylserine externalization, and CD47 expression. *Transfusion*. 2008 Aug; 48(8):1658-68.
- Honrado C, Bisegna P, Swami NS, Caselli F. Single-cell microfluidic impedance cytometry: from raw signals to cell phenotypes using data analytics. *Lab on a Chip Journal*. 2021 Jan 5; 21(1):22-54.

- Horn EP, Sputtek A, Standl T, Rudolf B, Kühnl P, Schulte am Esch J. Transfusion of autologous, hydroxyethyl starch-cryopreserved red blood cells. *Anesthesia & Analgesia*. 1997 Oct; 85(4):739-45.
- Huggins CE. Reversible agglomeraton used to remove dimethylsulfoxide from large volumes of frozen blood. *Science*. 1963 Feb 8; 139(3554):504-5.
- I Chin-Yee, and M. S. d'Almeida N Arya. 1997. The Red Cell Storage Lesion and Its Implication for Transfusion. *Transfusion Science* 18(3):447–58.
- Irradiation Of Blood Components, The Canadian Blood Service PWI Number 02-146,Revision Number 18.
- Jacobs, M. H. 1933. The Simultaneous Measurement of Cell Permeability to Water and to Dissolved Substances. *Journal of Cellular and Comparative Physiology* 2(4):427–44.
- Jacobs, M. H., and Dorothy R. Stewart. 1932. A Simple Method for the Quantitative Measurement of Cell Permeability. *Journal of Cellular and Comparative Physiology* 1(1):71–82.
- Jang Y, Jang J, Park Y. Dynamic spectroscopic phase microscopy for quantifying hemoglobin concentration and dynamic membrane fluctuation in red blood cells. *Optics Express*. 2012 Apr 23; 20(9):9673-81.
- Jay AW, Rowlands S. The stages of osmotic haemolysis. *The Journal of Physiology*. 1975 Nov; 252(3):817-32.
- Lovelock JE. The denaturation of lipid-protein complexes as a cause of damage by freezing. *Proceedings of the Royal Society B: Biological Sciences*. 1957 Dec 17; 147(929):427-33.
- Jordan, A., D. Chen, Q. L. Yi, T. Kaniyas, M. T. Gladwin, and J. P. Acker. 2016. Assessing the Influence of Component Processing and Donor Characteristics on Quality of Red Cell Concentrates Using Quality Control Data. *Vox Sanguinis* 111(1):8–15.

Kameneva MV, Garrett KO, Watach MJ, Borovetz HS. Red blood cell aging and risk of cardiovascular diseases. *Clinical Hemorheology and Microcirculation*. 1998 Apr; 18(1):67-74.

Kanias, Tamir, Marion C. Lanteri, Grier P. Page, Yuelong Guo, Stacy M. Endres, Mars Stone, Sheila Keating, Alan E. Mast, Ritchard G. Cable, Darrell J. Triulzi, Joseph E. Kiss, Edward L. Murphy, Steve Kleinman, Michael P. Busch, Mark T. Gladwin, J. L. Gottschall, W. Bialkowski, L. Anderson, J. Miller, A. Hall, Z. Udee, V. Johnson, P. A. D'Andrea, A. M. Guiltinan, B. R. Spencer, S. T. Johnson, D. J. Brambilla, M. T. Sullivan, N. Haywood, D. Ringer, B. C. Siege, S. H. Kleinman, S. A. Glynn, K. B. Malkin, and A. M. Cristman. 2017. Ethnicity, Sex, and Age Are Determinants of Red Blood Cell Storage and Stress Hemolysis: Results of the REDS-III RBC-Omics Study. *Blood Advances* 1(15):1132–41.

Kanias, Tamir, Derek Sinchar, David Osei-Hwedieh, Jeffrey J. Baust, Andrew Jordan, James C. Zimring, Hayley R. Waterman, Karen S. de Wolski, Jason P. Acker, and Mark T. Gladwin. 2016. Testosterone-Dependent Sex Differences in Red Blood Cell Hemolysis in Storage, Stress, and Disease. *Transfusion* 56(10):2571–83.

Kanias, Tamir, Mars Stone, Grier P. Page, Yuelong Guo, Stacy M. Endres-Dighe, Marion C. Lanteri, Bryan R. Spencer, Ritchard G. Cable, Darrell J. Triulzi, Joseph E. Kiss, Edward L. Murphy, Steve Kleinman, Mark T. Gladwin, Michael P. Busch, and Alan E. Mast. 2019a. Frequent Blood Donations Alter Susceptibility of Red Blood Cells to Storage- and Stress-Induced Hemolysis. *Transfusion* 59(1):67–78.

Kanias, Tamir, Mars Stone, Grier P. Page, Yuelong Guo, Stacy M. Endres-Dighe, Marion C. Lanteri, Bryan R. Spencer, Ritchard G. Cable, Darrell J. Triulzi, Joseph E. Kiss, Edward L. Murphy, Steve Kleinman, Mark T. Gladwin, Michael P. Busch, and Alan E. Mast. 2019b. Frequent Blood Donations Alter Susceptibility of Red Blood Cells to Storage- and Stress-Induced Hemolysis. *Transfusion* 59(1):67–78.

- Karlsson, Jens O. M., Abdelmoneim I. Younis, Anthony W. S. Chan, Kenneth G. Gould, and Ali Eroglu. 2009. Permeability of the Rhesus Monkey Oocyte Membrane to Water and Common Cryoprotectants. *Molecular Reproduction and Development* 76(4):321–33.
- Katharia, Rahul, Rajendra Chaudhary, and Prashant Agarwal. 2013. Prestorage Gamma Irradiation Induces Oxidative Injury to Red Cells. *Transfusion and Apheresis Science* 48(1):39–43.
- Kay, M. M. B., S. R. Goodman, K. Sorensen, C. F. Whitfield, P. Wong, L. Zaki, and V. Rudloff. 1983. Senescent Cell Antigen Is Immunologically Related to Band 3. *Proceedings of the National Academy of Sciences of the United States of America* 80(6 I):1631–35.
- Kedem O, Katchalsky A. Thermodynamic analysis of the permeability of biological membranes to non-electrolytes. *Biochimica et Biophysica Acta*. 1958 Feb; 27(2):229-46.
- Kedem O, Katchalsky A. A physical interpretation of the phenomenological coefficients of membrane permeability. *The Journal of General Physiology*. 1961 Sep; 45(1):143-79.
- Keller MA, Piedrafita G, Ralser M. The widespread role of non-enzymatic reactions in cellular metabolism. *Current Opinion in Biotechnology*. 2015 Aug; 34:153-61.
- El Kenz, H., F. Corazza, P. Van Der Linden, S. Chabab, and C. Vandenvelde. 2013. Potassium Content of Irradiated Packed Red Blood Cells in Different Storage Media: Is There a Need for Additive Solution-Dependent Recommendations for Infant Transfusion? *Transfusion and Apheresis Science* 49(2):249–53.
- Key, J. Albert. 1921. Studies on Erythrocytes, With Special Reference to Reticulum, Polychromatophilia And Mitochondria. *Arch, Intern.Med* 28(5):511–49.
- Khandelwal, Sanjay, and Rajiv K. Saxena. 2008. A Role of Phosphatidylserine Externalization in Clearance of Erythrocytes Exposed to Stress but Not in Eliminating Aging Populations of Erythrocyte in Mice. *Experimental Gerontology* 43(8):764–70.

- Kiefer, Charles R., and L. Michael Snyder. 2000. Oxidation and Erythrocyte Senescence. *Current Opinion in Hematology* 7(2):113–16.
- Kleinhans FW. Membrane permeability modeling: Kedem-Katchalsky vs a two-parameter formalism. *Cryobiology*. 1998 Dec; 37(4):271-89.
- de Korte, Dirk, Louis Thibault, Wiebke Handke, Sarah K. Harm, Alex Morrison, Aine Fitzpatrick, Denese C. Marks, Qi Long Yi, and Jason P. Acker. 2018. Timing of Gamma Irradiation and Blood Donor Sex Influences in Vitro Characteristics of Red Blood Cells. *Transfusion* 58(4):917–26.
- Lagerberg, Johan W. M., Rosa Truijens-De Lange, Dirk De Korte, and Arthur J. Verhoeven. 2007. Altered Processing of Thawed Red Cells to Improve the in Vitro Quality during Postthaw Storage at 4°C. *Transfusion* 47(12):2242–49.
- Lahmann JM, Benson JD, Higgins AZ. Concentration dependence of the cell membrane permeability to cryoprotectant and water and implications for design of methods for post-thaw washing of human erythrocytes. *Cryobiology*. 2018 Feb; 80:1-11.
- Lahmann, John M., Cynthia Cruz Sanchez, James D. Benson, Jason P. Acker, and Adam Z. Higgins. 2020. Implications of Variability in Cell Membrane Permeability for Design of Methods to Remove Glycerol from Frozen-Thawed Erythrocytes. *Cryobiology* 92:168–79.
- Lannan, Katie L., Julie Sahler, Sherry L. Spinelli, Richard P. Phipps, and Neil Blumberg. 2013. Transfusion Immunomodulation - the Case for Leukoreduced and (Perhaps) Washed Transfusions. *Blood Cells, Molecules, and Diseases* 50(1):61–68.
- Layrisse M, Linares J, Roche M. Excess Hemolysis in Subjects with Severe Iron Deficiency Anemia Associated And Nonassociated With Hookworm Infection. *Blood*. 1965 Jan; 25:73-91.
- Lecak, J., K. Scott, C. Young, J. Hannon, and Jason P. Acker. 2004. Evaluation of Red Blood Cells Stored at -80°C in Excess of 10 Years. *Transfusion* 44(9):1306–13.

- Lee, Angela C., Leila L. Reduque, Naomi L. C. Luban, Paul M. Ness, Blair Anton, and Eugenie S. Heitmiller. 2014. Transfusion-Associated Hyperkalemic Cardiac Arrest in Pediatric Patients Receiving Massive Transfusion. *Transfusion* 54(1):244–54.
- Lee, Tae-hoon, Sun-uk Kim, Seong-lan Yu, Sue Hee Kim, Do Sim Park, Hyung-bae Moon, So Hee Dho, Ki-sun Kwon, and Hyun Jeong Kwon. 2003. Peroxiredoxin II Is Essential for Sustaining Life Span of Erythrocytes in Mice. 101(12):5033–38.
- Levin, Elena, Craig Jenkins, Brankica Culibrk, Maria I. C. Gyöngyössi-Issa, Katherine Serrano, and Dana V. Devine. 2012. Development of a Quality Monitoring Program for Platelet Components: A Report of the First Four Years' Experience at Canadian Blood Services. *Transfusion* 52(4):810–18.
- Lew VL, Daw N, Etzion Z, Tiffert T, Muoma A, Vanagas L, Bookchin RM. Effects of age-dependent membrane transport changes on the homeostasis of senescent human red blood cells. *Blood*. 2007 Aug 15; 110(4):1334-42.
- Lew VL, Tiffert T. On the Mechanism of Human Red Blood Cell Longevity: Roles of Calcium, the Sodium Pump, PIEZO1, and Gardos Channels. *Frontiers in Physiology*. 2017 Dec 12; 8:977.
- Linderkamp O, Meiselman HJ. Geometric, osmotic, and membrane mechanical properties of density-separated human red cells. *Blood*. 1982 Jun; 59(6):1121-7.
- Liu, Jun, Steve Mullen, Qinggang Meng, John Critser, and Andras Dinnyes. 2009. Determination of Oocyte Membrane Permeability Coefficients and Their Application to Cryopreservation in a Rabbit Model. *Cryobiology* 59(2):127–34.
- Lorna G. Macdougall, Janifer M. Judisch, Silloo B. Mistry, Red cell metabolism in iron deficiency anemia. II. The relationship between red cell survival and alterations in red cell metabolism, *The Journal of Pediatrics*, Volume 76, Issue 5, 1970, Pages 660-675,
- Lovelock JE. The haemolysis of human red blood-cells by freezing and thawing. *Biochimica et Biophysica Acta*. 1953 Mar; 10(3):414-26.

- Lusianti, Ratih E., James D. Benson, Jason P. Acker, and Adam Z. Higgins. 2013. Rapid Removal of Glycerol from Frozen-Thawed Red Blood Cells. *Biotechnology Progress* 29(3):609–20.
- Lusianti RE, Higgins AZ. Continuous removal of glycerol from frozen-thawed red blood cells in a microfluidic membrane device. *Biomicrofluidics*. 2014 Oct 28; 8(5):054124.
- Lutz, Hans U. 2012. Naturally Occurring Anti-Band 3 Antibodies in Clearance of Senescent and Oxidatively Stressed Human Red Blood Cells. *Transfusion Medicine and Hemotherapy* 39(5):321–27.
- Lutz HU, Bogdanova A. Mechanisms tagging senescent red blood cells for clearance in healthy humans. *Frontiers in Physiology*. 2013 Dec 25; 4:387.
- Lutz, H., P. Stammler, S. Fasler, M. Ingold, and J. Fehr. 1992. Density Separation of Human Red Blood Cells on Self Forming Percoll. *Biochimica et Biophysica Acta (G). General Subjects* 1116(1):1–10.
- Lutz, H. U., P. Stammler, and S. Fasler. 1993. Preferential Formation of C3b-IgG Complexes in Vitro and in Vivo from Nascent C3b and Naturally Occurring Anti-Band 3 Antibodies. *Journal of Biological Chemistry* 268(23):17418–26.
- Malka, Roy, Francisco Feijó Delgado, Scott R. Manalis, and John M. Higgins. 2014. In Vivo Volume and Hemoglobin Dynamics of Human Red Blood Cells. *PLoS Computational Biology* 10(10).
- Maria, M.S., Chandra, T.S. & Sen, A.K. Capillary flow-driven blood plasma separation and on-chip analyte detection in microfluidic devices. *Microfluid Nanofluid* 21, 72 (2017).
- Masalunga, C., M. Cruz, B. Porter, S. Roseff, B. Chui, and E. Mainali. 2007. Increased Hemolysis from Saline Pre-Washing RBCs or Centrifugal Pumps in Neonatal ECMO. *Journal of Perinatology* 27(6):380–84.

- Mazur P. The role of cell membranes in the freezing of yeast and other single cells. *Annals of the New York Academy of Sciences*. 1965 Oct 13; 125(2):658-76.
- Mazur P, Miller RH. Permeability of the human erythrocyte to glycerol in 1 and 2 M solutions at 0 or 20 degrees C. *Cryobiology*. 1976 Oct; 13(5):507-22.
- Mazur P. Kinetics of Water Loss from Cells At Subzero Temperatures And The Likelihood Of Intracellular Freezing. *The Journal of General Physiology*. 1963 Nov; 47(2):347-69.
- Mazur P, Cole KW. Roles of unfrozen fraction, salt concentration, and changes in cell volume in the survival of frozen human erythrocytes. *Cryobiology*. 1989 Feb; 26(1):1-29.
- Mazur P, Leibo SP, Chu EH. A two-factor hypothesis of freezing injury. Evidence from Chinese hamster tissue-culture cells. *Experimental Cell Research*. 1972; 71(2):345-55.
- Macdougall LG. Red cell metabolism in iron deficiency anemia. 3. The relationship between glutathione peroxidase, catalase, serum vitamin E, and susceptibility of iron-deficient red cells to oxidative hemolysis. *The Journal of Pediatrics*. 1972 May; 80(5):775-82.
- McGann LE. Differing actions of penetrating and nonpenetrating cryoprotective agents. *Cryobiology*. 1978 Aug; 15(4):382-90. DIO:10.1016/0011-2240(78)90056-1.
- McCoy, N. C., M. Yu, J. A. Sullivan, D. M. Spiegel, and S. F. Leitman. 1992b. The Effect of Prestorage Irradiation Red Cell Survival on Posttransfusion. *Transfusion* 32(6):525–28.
- McGann LE, Turner AR, Turc JM. Microcomputer interface for rapid measurements of average volume using an electronic particle counter. *Medical and Biological Engineering and Computing*. 1982 Jan; 20(1):117-20.
- McGann LE, Ebertz SL, and Elliott JAW. 2002. Optimal Cooling Rates from Osmotic Simulation of Cellular Low Temperature Responses. *Cryobiology* 45(3):255.

- McGann LE, and Elliott JAW. 2003. Optimization of Cryopreservation Protocols Using Computer Simulations. *Cryobiology* 47(3):255.
- Melzak, Kathryn A., John L. Spouge, Clemens Boecker, Frank Kirschhöfer, Gerald Brenner-Weiss, and Karen Bieback. 2021. Hemolysis Pathways during Storage of Erythrocytes and Inter-Donor Variability in Erythrocyte Morphology. *Transfusion Medicine and Hemotherapy* 48(1):39–47.
- Meryman, HT., and M. Hornblower. 1972. A Method for Freezing and Washing Red Blood Cells Using a High Glycerol Concentration. *Transfusion* 12(3):145–56.
- Meryman HT. Modified model for the mechanism of freezing injury in erythrocytes. *Nature*. 1968 Apr 27; 218(5139):333-6.
- Mir, Mustafa, Zhuo Wang, Krishnarao Tangella, and Gabriel Popescu. Diffraction Phase Cytometry: blood on a CD-ROM. Optical Society of America. 16 February 2009 / Vol. 17, No. 4.
- Mock, Donald M., Gary L. Lankford, John A. Widness, Leon F. Burmeister, Daniel Kahn, and Ronald G. Strauss. 1999. Measurement of Red Cell Survival Using Biotin-Labeled Red Cells: Validation against <sup>51</sup>Cr-Labeled Red Cells. *Transfusion* 39(2):156–62.
- Mock, Donald M., Gary L. Lankford, John A. Widness, Leon F. Burmeister, Daniel Kahn, and Ronald G. Strauss. 2004. RBCs Labeled at Two Biotin Densities Permit Simultaneous and Repeated Measurements of Circulating RBC Volume. *Transfusion* 44(3):431–37.
- Mock, Donald M., Nell I. Matthews, Shan Zhu, Leon F. Burmeister, M. Bridget Zimmerman, Ronald G. Strauss, Robert L. Schmidt, Demet Nalbant, Gretchen A. Cress, and John A. Widness. 2011. Red Blood Cell (RBC) Volume Can Be Independently Determined in Vivo in Humans Using RBCs Labeled at Different Densities of Biotin. *Transfusion* 51(1):148–57.
- Mock, Donald M., Nell I. Matthews, Shan Zhu, Ronald G. Strauss, Robert L. Schmidt, Demet Nalbant, Gretchen A. Cress, and John A. Widness. 2011. Red Blood Cell (RBC)

Survival Determined in Humans Using RBCs Labeled at Multiple Biotin Densities. *Transfusion* 51(5):1047–57.

Mock, Donald M., Demet Nalbant, Svetlana V. Kyosseva, Robert L. Schmidt, Guohua An, Nell I. Matthews, Alexander P. J. Vlaar, Robin van Bruggen, Dirk de Korte, Ronald G. Strauss, José A. Cancelas, Robert S. Franco, Peter Veng-Pedersen, and John A. Widness. 2018. Development, Validation, and Potential Applications of Biotinylated Red Blood Cells for Posttransfusion Kinetics and Other Physiological Studies: Evidenced-Based Analysis and Recommendations. *Transfusion* 58(8):2068–81.

Mohandas N, Chasis JA. Red blood cell deformability, membrane material properties and shape: regulation by transmembrane, skeletal and cytosolic proteins and lipids. *Seminars in Hematology*. 1993 Jul; 30(3):171-92.

Mohandas N, Shohet SB. Control of red cell deformability and shape. *Current Topics in Hematology*. 1978; 1:71-125.

Mollison, P. L. 2000. The Introduction of Citrate as an Anticoagulant for Transfusion and of Glucose as a Red Cell Preservative. *British Journal of Haematology* 108(1):13–18.

Mollison PL, Sloviter HA. Successful transfusion of previously frozen human red cells. *The Lancet*. 1951 Nov 10; 2(6689):862-4.

Moreira, Otacilio C., Vanessa H. Oliveira, Luíza B. F. Benedicto, Carmem M. Nogueira, Julio A. Mignaco, Carlos Frederico L. Fontes, and Leandro A. Barbosa. 2008. Effects of  $\gamma$ -Irradiation on the Membrane ATPases of Human Erythrocytes from Transfusional Blood Concentrates. *Annals of Hematology* 87(2):113–19.

Moroff G, George VM, Siegl AM, Luban NL. The influence of irradiation on stored platelets. *Transfusion*. 1986 Sep-Oct; 26(5):453-6.

Moroff, G., and N. L. C. Luban. 1997. The Irradiation of Blood and Blood Components to Prevent Graft-versus-Host Disease: Technical Issues and Guidelines. *Transfusion Medicine Reviews* 11(1):15–26.

- Moss GS, Valeri CR, Brodine CE. Clinical experience with the use of frozen blood in combat casualties. *The New England Journal of Medicine*. 1968 Apr 4; 278(14):747-52.
- Mueller, T. J., C. W. Jackson, M. E. Dockter, and M. Morrison. 1987. Membrane Skeletal Alterations during in Vivo Mouse Red Cell Aging. Increase in the Band 4.1a:4.1b Ratio. *Journal of Clinical Investigation* 79(2):492–99.
- Mykhailova, Olga, Carly Olafson, Tracey R. Turner, Angelo D’Alessandro, and Jason P. Acker. 2020a. Donor-Dependent Aging of Young and Old Red Blood Cell Subpopulations: Metabolic and Functional Heterogeneity. *Transfusion* 60(11):2633–46.
- Mykhailova O, Brandon-Coatham M, Phan C, Yazdanbakhsh M, Olafson C, Yi QL, Kanas T, Acker JP. Red cell concentrates from teen male donors contain poor-quality biologically older cells. *Vox Sang*. 2024 Feb 28.
- Mykhailova O, Brandon-Coatham M, Durand K, Olafson C, Xu A, Yi QL, Kanas T, Acker JP. Estimated median density identifies donor age and sex differences in red blood cell biological age. *Transfusion*. 2024 Feb 29.
- Nagababu, Enika, Francis J. Chrest, and Joseph M. Rifkind. 2003. Hydrogen-Peroxide-Induced Heme Degradation in Red Blood Cells : The Protective Roles of Catalase and Glutathione Peroxidase. 1620:211–17.
- Nagashima H, Kashiwazaki N, Ashman RJ, Grupen CG, Seamark RF, Nottle MB. Removal of cytoplasmic lipid enhances the tolerance of porcine embryos to chilling. *Biology of Reproduction*. 1994 Oct; 51(4):618-22.
- Nash, G. B., and H. J. Meiselman. 1983. Red Cell and Ghost Viscoelasticity. Effects of Hemoglobin Concentration and in Vivo Aging. *Biophysical Journal* 43(1):63–73.
- O'brien TG, Haynes LL, Hering AC, Tullis JL, Watkins E JR. The use of glycerolized frozen blood in vascular surgery and extracorporeal circulation. *Surgery*. 1961 Jan; 49:109-29.

- O'Leary, Mandy Flannery, Penny Szklarski, Thomas M. Klein, and Pampee Paul Young. 2011. Hemolysis of Red Blood Cells after Cell Washing with Different Automated Technologies: Clinical Implications in a Neonatal Cardiac Surgery Population. *Transfusion* 51(5):955–60.
- Orbach A, Zelig O, Yedgar S, Barshtein G. Biophysical and Biochemical Markers of Red Blood Cell Fragility. *Transfusion Medicine and Hemotherapy*. 2017 Jun; 44(3):183-187.
- Owen Charles S., Sykes Norman L., Magnetic labeling and cell sorting, *Journal of Immunological Methods*, Volume 73, Issue 1, 1984, Pages 41-48.
- Owen JD, Eyring EM. Reflection coefficients of permeant molecules in human red cell suspensions. *The Journal of General Physiology*. 1975 Aug; 66(2):251-65.
- Pal N, Dev Verma S, Singh MK, Sen S. Fluorescence correlation spectroscopy: an efficient tool for measuring size, size-distribution and polydispersity of microemulsion droplets in solution. *Analytical Chemistry*. 2011 Oct 15; 83(20):7736-44.
- Patel, Ravi M., John D. Roback, Karan Uppal, Tianwei Yu, Dean P. Jones, and Cassandra D. Josephson. 2015. Metabolomics Profile Comparisons of Irradiated and Nonirradiated Stored Donor Red Blood Cells. *Transfusion* 55(3):544–52.
- Patidar, Gopal Kumar, Aparna Joshi, Neelam Marwaha, Rajendra Prasad, Pankaj Malhotra, Ratti Ram Sharma, and Hari Krishan Dhawan. 2014. Serial Assessment of Biochemical Changes in Irradiated Red Blood Cells. *Transfusion and Apheresis Science* 50(3):479–87.
- Pegg DE, Diaper MP. On the mechanism of injury to slowly frozen erythrocytes. *Biophysical Journal*. 1988 Sep; 54(3):471-88.
- Petrášek, Zdeněk, and Petra Schwillle. 2008. Precise Measurement of Diffusion Coefficients Using Scanning Fluorescence Correlation Spectroscopy. *Biophysical Journal* 94(4):1437–48.

- Perrault R, Jackson JR, Martin-Villar J, Smiley RK. Experience with the use of frozen blood. *Canadian Medical Association Journal*. 1967 Jun 10; 96(23):1504-9.
- Piedrafita, Gabriel, Markus A. Keller, and Markus Ralser. 2015. The Impact of Non-Enzymatic Reactions and Enzyme Promiscuity on Cellular Metabolism during (Oxidative) Stress Conditions. *Biomolecules* 5(3):2101–22.
- Piomelli, Sergio, and Carol Seaman. 1993. Mechanism of Red Blood Cell Aging: Relationship of Cell Density and Cell Age. *American Journal of Hematology* 42(1):46–52.
- Piomelli, S., C. Seaman, J. Reibman, A. Tytun, J. Graziano, N. Tabachnik, and L. Corash. 1978. Separation of Younger Red Cells with Improved Survival in Vivo: An Approach to Chronic Transfusion Therapy. *Proceedings of the National Academy of Sciences of the United States of America* 75(7):3474–78.
- Polge C, Smith AU, Parkes AS. Revival of spermatozoa after vitrification and dehydration at low temperatures. *Nature*. 1949 Oct 15; 164(4172):666.
- Pribush, Alexander, Galila Agam, Tikva Yermiahu, Alexander Dvilansky, Dan Meyerstein, and Naomi Meyerstein. 1994. Radiation Damage to the Erythrocyte Membrane: The Effects of Medium and Cell Concentrations. *Free Radical Research* 21(3):135–46.
- Prickett, Richelle C., Janet A. W. Elliott, Shamina Hakda, and Locksley E. McGann. 2008. A Non-Ideal Replacement for the Boyle van't Hoff Equation. *Cryobiology* 57(2):130–36.
- Protocol for AAPH-Induced Oxidative Hemolysis. Dr. Jason Acker's Laboratory, Version 1.3. Revised 2021-08-05.
- Protocol for Biotinylation of Red Blood Cells. Dr. Jason Acker's Laboratory, Version 1.2, Revised 2023-01-10.

Protocol for Determining % Hemolysis. Dr. Jason Acker's Laboratory, Version 4.5, Revised 2008-12-16.

Protocol for Determining Microhematocrit. Dr. Jason Acker's Laboratory, Version 4.2, Revised 2015-10-28.

Protocol for Determining Osmotic Fragility. Dr. Jason Acker's Laboratory, Version 1.0, Created 2007-06-07.

Protocol for Determining P50 Using the Hemox Analyzer, Dr. Jason Acker's Laboratory, Version 5.0, Created 2017-02-14.

Protocol for Determining RBC Deformability Using the LORCA (Laser Optical Rotational Red Cell Analyzer). Dr. Jason Acker's Laboratory, Version 1.0, Created 2019-01-03.

Protocol for Osmoscan Using the LORCA (Laser Optical Rotational Red Cell Analyzer). Dr. Jason Acker's Laboratory, Version 1.0, Created 2019-01-04.

Protocol for Osmotic Hemolysis. Dr. Jason Acker's Laboratory, Version 0.2, Revised 2022-08-05.

Protocol for Preparing and Sending Supernatants for Sodium and Potassium Analysis, Acker Lab: Research and Development Operating Procedure Version 1.3 2021-02-03.

Protocol Micro Osmette 5004 Osmometer. Dr. Jason Acker's Laboratory, Version 0.3, Revised 2022-08-19.

Puchała M, Szweida-Lewandowska Z, Kiefer J. The influence of radiation quality on radiation-induced hemolysis and hemoglobin oxidation of human erythrocytes. *Journal of Radiation Research*. 2004 Jun; 45(2):275-9.

Radwanski K, Garraud O, Cognasse F, Hamzeh-Cognasse H, Payrat JM, Min K. The effects of red blood cell preparation method on in vitro markers of red blood cell aging and inflammatory response. *Transfusion*. 2013 Dec; 53(12):3128-38.

- Ramirez-Arcos, Sandra, Denese C. Marks, Jason P. Acker, and William P. Sheffield. 2016. Quality and Safety of Blood Products. *Journal of Blood Transfusion* 2016:1–2.
- Rappaz B, Cano E, Colomb T, Kühn J, Depeursinge C, Simanis V, Magistretti PJ, Marquet P. Noninvasive characterization of the fission yeast cell cycle by monitoring dry mass with digital holographic microscopy. *Journal of Biomedical Optics*. 2009 May-Jun; 14(3):034049.
- Recommendations for Reference Method for Haemoglobinometry in Human Blood (ICSH Standard 1995) and Specifications for International Haemoglobinocyanide Standard (4th Edition) International Council for Standardisation in Haematology: Expert Panel on Haemoglobinometry Introduction Scientific Symposia.
- Relevy H, Koshkaryev A, Manny N, Yedgar S, Barshtein G. Blood banking-induced alteration of red blood cell flow properties. *Transfusion*. 2008 Jan; 48(1):136-46.
- Rettig, Michael P., P. S. Low Philip S., J. Aura Gimm, Narla Mohandas, Jiazhen Wang, and John A. Christian. 1999. Evaluation of Biochemical Changes during in Vivo Erythrocyte Senescence in the Dog. *Blood* 93(1):376–84.
- Robert Valeri, C., Gina Ragno, Linda E. Pivacek, Rithy Srey, John R. Hess, Lloyd E. Lippert, Frank Mettelle, Roland Fahie, E. Mary O’Neill, and Irma O. Szymanski. 2001. A Multicenter Study of in Vitro and in Vivo Values in Human RBCs Frozen with 40-Percent (Wt/Vol) Glycerol and Stored after Deglycerolization for 15 Days at 4°C in AS-3: Assessment of RBC Processing in the ACP® 215. *Transfusion* 41(7):933–39.
- Ross-Rodriguez, Lisa U., Janet A. W. Elliott, and Locksley E. McGann. 2010a. Characterization of Cryobiological Responses in TF-1 Cells Using Interrupted Freezing Procedures. *Cryobiology* 60(2):106–16.
- Ross-Rodriguez, Lisa U., Janet A. W. Elliott, and Locksley E. McGann. 2010b. Characterization of Cryobiological Responses in TF-1 Cells Using Interrupted Freezing Procedures. *Cryobiology* 60(2):106–16.

- Ross-Rodriguez, L. U., J. A. W. Elliott, and L. E. McGann. 2010. Investigating Cryoinjury Using Simulations and Experiments. 1: TF-1 Cells during Two-Step Freezing (Rapid Cooling Interrupted with a Hold Time). *Cryobiology* 61(1):38–45.
- Roudier N, Ripoche P, Gane P, Le Pennec PY, Daniels G, Cartron JP, Bailly P. AQP3 deficiency in humans and the molecular basis of a novel blood group system, GIL. *J Biol Chem*. 2002 Nov 29; 277(48):45854-9.
- Rühl H, Bein G, Sachs UJ. Transfusion-associated graft-versus-host disease. *Transfusion Medicine Reviews*. 2009 Jan; 23(1):62-71.
- Safeukui I, Buffet PA, Deplaine G, Perrot S, Brousse V, Sauvanet A, Aussilhou B, Dokmak S, Couvelard A, Cazals-Hatem D, Mercereau-Puijalon O, Milon G, David PH, Mohandas N. Sensing of red blood cells with decreased membrane deformability by the human spleen. *Blood Advances*. 2018 Oct 23; 2(20):2581-2587.
- Saito-Benz M, Murphy WG, Tzeng YC, Atkinson G, Berry MJ. Storage after gamma irradiation affects in vivo oxygen delivery capacity of transfused red blood cells in preterm infants. *Transfusion*. 2018 Sep; 58(9):2108-2112.
- Samaja M, Rubinacci A, Motterlini R, De Ponti A, Portinaro N. Red cell aging and active calcium transport. *Experimental Gerontology*. 1990; 25(3-4):279-86.
- Scott KL, Lecak J, Acker JP. Biopreservation of red blood cells: past, present, and future. *Transfusion Medicine Reviews*. 2005 Apr; 19(2):127-42.
- Serrano, K., D. Chen, A. L. Hansen, E. Levin, T. R. Turner, J. D. R. Kurach, J. P. Acker, and D. V. Devine. 2014. “The Effect of Timing of Gamma-Irradiation on Hemolysis and Potassium Release in Leukoreduced Red Cell Concentrates Stored in SAGM.” *Vox Sanguinis* 106(4):379–81.
- Sheffield WP, Bhakta V, Jenkins C, Devine DV. Conversion to the buffy coat method and quality of frozen plasma derived from whole blood donations in Canada. *Transfusion*. 2010 May; 50(5):1043-9.

- Simak J, Gelderman MP. Cell membrane microparticles in blood and blood products: potentially pathogenic agents and diagnostic markers. *Transfusion Medicine Reviews*. 2006 Jan; 20(1):1-26.
- SMITH AU. Prevention of haemolysis during freezing and thawing of red blood-cells. *The Lancet*. 1950 Dec 30; 2(6644):910-1.
- Snyder, L. M., N. L. Fortier, J. Trainor, J. Jacobs, L. Leb, B. Lubin, D. Chiu, S. Shoheit, and N. Mohandas. 1985. Effect of Hydrogen Peroxide Exposure on Normal Human Erythrocyte Deformability, Morphology, Surface Characteristics, and Spectrin-Hemoglobin Cross-Linking. *Journal of Clinical Investigation* 76(5):1971–77.
- Snyder, L. Michael, Fred Garver, S. C. Liu, Laszlo Leb, Jane Trainor, and Normand L. Fortier. 1985. Demonstration of Haemoglobin Associated with Isolated, Purified Spectrin from Senescent Human Red Cells. *British Journal of Haematology* 61(3):415–19.
- Snyder LM, Leb L, Piotrowski J, Sauberman N, Liu SC, Fortier NL. Irreversible spectrin-haemoglobin crosslinking in vivo: a marker for red cell senescence. *British Journal of Haematology*. 1983 Mar; 53(3):379-84.
- Sparrow, Rosemary L. 2012. Time to Revisit Red Blood Cell Additive Solutions and Storage Conditions: A Role for ‘Omics’ Analyses. *Blood Transfusion* 10(SUPPL. 2):8–12.
- Sparrow, Rosemary L. 2017. Red Blood Cell Components: Time to Revisit the Sources of Variability. *Blood Transfusion* 15(2):116–25.
- Sputtek A. Cryopreservation of red blood cells and platelets. *Methods in Molecular Biology*. 2007; 368:283-301.
- Sputtek A., Kühnl P., and W. Rowe A. 2007. Cryopreservation of Erythrocytes, Thrombocytes, and Lymphocytes. *Transfusion Medicine and Hemotherapy* 34(4):262–67.

- Sputtek, Andreas, and Rebekka Sputtek. 2004. Cryopreservation in Transfusion Medicine and Hematology. Pp. 483–504 in *Life in the Frozen State*. CRC Press.
- Sputtek A, and Rau G. 1992. Cryopreservation of Human Erythrocytes with Hydroxyethyl Starch (HES)--Part 1: The Procedure. *Infusionsther Transfusionsmed* 19(6):269–75.
- Sputtek A, Bacher C, Langer R, Kron W, Henrich HA, Rau G. Cryopreservation of human erythrocytes with hydroxyethyl starch (HES)--Part 2: Analysis of survival. *Infusionsther Transfusionsmed*. 1992 Dec; 19(6):276-82. German.
- Stadnick, H., R. Onell, J. P. Acker, and J. L. Holovati. 2011. Eadie-Hofstee Analysis of Red Blood Cell Deformability. *Clinical Hemorheology and Microcirculation* 47(3):229–39.
- Stetefeld, Jörg, Sean A. McKenna, and Trushar R. Patel. 2016. Dynamic Light Scattering: A Practical Guide and Applications in Biomedical Sciences. *Biophysical Reviews* 8(4):409–27.
- Sutera, S. P., R. A. Gardner, C. W. Boylan, G. L. Carroll, K. C. Chang, J. S. Marvel, C. Kilo, B. Gonen, and J. R. Williamson. 1985. Age-Related Changes in Deformability of Human Erythrocytes. Vol. 65.
- Swindell, Christine G., Thomas A. Barker, Simon P. McGuirk, Timothy J. Jones, David J. Barron, William J. Brawn, Angela Horsburgh, and Robert G. Willetts. 2007. Washing of Irradiated Red Blood Cells Prevents Hyperkalaemia during Cardiopulmonary Bypass in Neonates and Infants Undergoing Surgery for Complex Congenital Heart Disease. *European Journal of Cardio-Thoracic Surgery* 31(4):659–64.
- Tarasev, Michael, Sumita Chakraborty, and Kenneth Alfano. 2015. RBC Mechanical Fragility as a Direct Blood Quality Metric to Supplement Storage Time. *Military Medicine* 180(3):150–57.
- Telisch M, Hoiberg R, Rao KR, Patel AR. The use of frozen, thawed erythrocytes in blood banking: a report of 28 months' experience in a large transfusion service. *American Journal of Clinical Pathology*. 1977 Aug; 68(2):250-7.

- Thiriot C, Kergonou JF, Allary M, Saint-Blancard J, Rocquet G. Effects of whole-body gamma irradiation on oxygen transport by rat erythrocytes. *Biochimie*. 1982 Jan; 64(1):79-83.
- Thomas Michael J.G., Parry Ernest S., Nash Stuart G., Bell Susan H., A method for the cryopreservation of red blood cells using hydroxyethyl starch as a cryoprotectant, *Transfusion Science*, Volume 17, Issue 3, 1996, Pages 385-396.
- Tillmann W, Levin C, Prindull G, Schröter W. Rheological properties of young and aged human erythrocytes. *Wiener klinische Wochenschrift*. 1980 Jun 2; 58(11):569-74.
- Tirri LJ, Schmidt PC, Pullarkat RK, Brockerhoff H. Studies on the hydrogen belts of membranes: II. Non-electrolyte permeability of liposomes of diester, diether, and dialkyl phosphatidylcholine and cholesterol. *Lipids*. 1977 Oct; 12(10):863-8.
- Torres-Castro K, Acuña-Umaña K, Lesser-Rojas L, Reyes DR. Microfluidic Blood Separation: Key Technologies and Critical Figures of Merit. *Micromachines (Basel)*. 2023 Nov 18; 14(11):2117.
- Treleaven, Jennie, Andrew Gennery, Judith Marsh, Derek Norfolk, Lizanne Page, Anne Parker, Frank Saran, Jim Thurston, and David Webb. 2011a. Guidelines on the Use of Irradiated Blood Components Prepared by the British Committee for Standards in Haematology Blood Transfusion Task Force. *British Journal of Haematology* 152(1):35–51.
- Treleaven, Jennie, Andrew Gennery, Judith Marsh, Derek Norfolk, Lizanne Page, Anne Parker, Frank Saran, Jim Thurston, and David Webb. 2011b. Guidelines on the Use of Irradiated Blood Components Prepared by the British Committee for Standards in Haematology Blood Transfusion Task Force. *British Journal of Haematology* 152(1):35–51.
- Triadou, P., R. Girot, D. Rebibo, D. Lemau, B. Mattlinger, P. Bolo, M. Maier, and L. Barritault. Neocytopenesis: a new approach for the transfusion of patients with thalassaemia major. *European Journal of Pediatrics* (1986) 145: 10–13.

- Tullis JL, Haynes LL, Pyle Hm, et al. Clinical Use of Frozen Red Cells. *AMA Archives of Surgery*. 1960; 81(1):151–154.
- Tuo, Wei Wei, Di Wang, Wen Jing Liang, and Yao Xiong Huang. 2014. How Cell Number and Cellular Properties of Blood-Banked Red Blood Cells of Different Cell Ages Decline during Storage. *PLoS ONE* 9(8):1–8.
- Turko, Nir A., and Natan T. Shaked. 2020. Erythrocyte Volumetric Measurements in Imaging Flow Cytometry Using Simultaneous Three-Wavelength Digital Holographic Microscopy. *Biomedical Optics Express* 11(11):6649.
- Turner, Tracey R., and Jason P. Acker. 2020. A Canadian Perspective on the Use and Preparation of Cryopreserved Red Cell Concentrates. *Transfusion and Apheresis Science* 59(4).
- Turner, Tracey R., Larissa Lautner, Angela Hill, Anita Howell, Robert Skeate, and Jason P. Acker. 2020. Evaluating the Quality of Red Blood Cell Concentrates Irradiated before or after Cryopreservation. *Transfusion* 60(1):26–29.
- Tzounakas, Vassilis L., Alkmini T. Anastasiadi, Panagiotis V. Drossos, Dimitrios G. Karadimas, Serena Valsami, Konstantinos E. Stamoulis, Issidora S. Papassideri, Marianna Politou, Marianna H. Antonelou, and Anastasios G. Kriebardis. 2021. Sex-Related Aspects of the Red Blood Cell Storage Lesion. *Blood Transfusion* 19(3):224–36.
- Tzounakas, Vassilis L., Hara T. Georgatzakou, Anastasios G. Kriebardis, Artemis I. Voulgaridou, Konstantinos E. Stamoulis, Leontini E. Foudoulaki-Paparizos, Marianna H. Antonelou, and Issidora S. Papassideri. 2016. Donor Variation Effect on Red Blood Cell Storage Lesion: A Multivariable, yet Consistent, Story. *Transfusion* 56(6):1274–86.
- Unit Sampling Protocol. Dr. Jason Acker’s Laboratory, Version 1.3, Revised 2019-03-01.
- Valeri, C. Robert, Rithy Srey, Daniel Tilahun, and Gina Ragno. 2004. The in Vitro Quality of Red Blood Cells Frozen with 40 Percent (Wt/Vol) Glycerol at -80°C for 14

- Years, Deglycerolized with the Haemonetics ACP<sup>®</sup> 215, and Stored at 4°C in Additive Solution-1 or Additive Solution-3 for up to 3 Weeks. *Transfusion* 44(7):990–95.
- Verkman AS. Water permeability measurement in living cells and complex tissues. *The Journal of Membrane Biology*. 2000 Jan 15; 173(2):73-87.
- Verkman AS, van Hoek AN, Ma T, Frigeri A, Skach WR, Mitra A, Tamarappoo BK, Farinas J. Water transport across mammalian cell membranes. *American Journal of Physiology*. 1996 Jan; 270(1 Pt 1):C12-30.
- Vraets, Adrienne, Yulia Lin, and Jeannie L. Callum. 2011a. Transfusion-Associated Hyperkalemia. *Transfusion Medicine Reviews* 25(3):184–96.
- Vraets, Adrienne, Yulia Lin, and Jeannie L. Callum. 2011b. Transfusion-Associated Hyperkalemia. *Transfusion Medicine Reviews* 25(3):184–96.
- Wachlmayr, Johann, Christof Hanneschlaeger, Armin Speletz, Thomas Barta, Anna Eckerstorfer, Christine Siligan, and Andreas Horner. 2022. Scattering versus fluorescence Self-Quenching: More than a Question of Faith for the Quantification of Water Flux in Large Unilamellar Vesicles? *Nanoscale Advances* 4(1):58–76.
- Wang, Dong, Junfeng Sun, Steven B. Solomon, Harvey G. Klein, and Charles Natanson. 2012. Transfusion of Older Stored Blood and Risk of Death: A Meta-Analysis. *Transfusion* 52(6):1184–95.
- Wang M, Liang H, Chen X, Chen D, Wang J, Zhang Y, Chen J. Developments of Conventional and Microfluidic Flow Cytometry Enabling High-Throughput Characterization of Single Cells. *Biosensors (Basel)*. 2022 Jun 23; 12(7):443.
- Watanabe, Masaru, Yuri Uehara, Namiko Yamashita, Yuu Fujimura, Kaori Nishio, Takeshi Sawada, Kazuo Takeda, Fumiaki Koizumi, and Yasuhiro Koh. 2014. Multicolor Detection of Rare Tumor Cells in Blood Using a Novel Flow Cytometry-Based System. *Cytometry Part A* 85(3):206–13.

- Weed RI, LaCelle PL, Merrill EW. Metabolic dependence of red cell deformability. *Journal of Clinical Investigation*. 1969 May; 48(5):795-809.
- Weinmann M, Hoffmann W, Rodegerdts E, Bamberg M. Biological effects of ionizing radiation on human blood compounds ex vivo. *Journal of Cancer Research and Clinical Oncology*. 2000 Oct; 126(10):584-8.
- Weisel, J. W., and R. I. Litvinov. 2019. Red Blood Cells: The Forgotten Player in Hemostasis and Thrombosis. *Journal of Thrombosis and Haemostasis* 17(2):271–82.
- Weiskopf, Richard B., Stephanie Schnapp, Kathryn Rouine-Rapp, Alan Bostrom, and Pearl Toy. 2005. Extracellular Potassium Concentrations in Red Blood Cell Suspensions after Irradiation and Washing. *Transfusion* 45(8):1295–1301.
- Willekens, Frans L. A., Bregt Roerdinkholder-Stoelwinder, Yvonne A. M. Groenen-Döpp, Harry J. Bos, Giel J. C. G. M. Bosman, Annegeet G. van den Bos, Arie J. Verkleij, and Jan M. Werre. 2003. Hemoglobin Loss from Erythrocytes in Vivo Results from Spleen-Facilitated Vesiculation. *Blood* 101(2):747–51.
- Winter, K. M., Lacey Johnson, R. G. Webb, and D. C. Marks. 2015. Gamma-Irradiation of Deglycerolized Red Cells Does Not Significantly Affect in Vitro Quality. *Vox Sanguinis* 109(3):231–38.
- Xu, Deyi, Mingxi Peng, Zhe Zhang, Guofei Dong, Yiqin Zhang, and Hongwei Yu. 2012. Study of Damage to Red Blood Cells Exposed to Different Doses of  $\gamma$ -Ray Irradiation. *Blood Transfusion* 10(3):321–30.
- Yip R, Mohandas N, Clark MR, Jain S, Shohet SB, Dallman PR. Red cell membrane stiffness in iron deficiency. *Blood*. 1983 Jul; 62(1):99-106.
- Yoshida T, Prudent M, D'alessandro A. Red blood cell storage lesion: causes and potential clinical consequences. *Blood Transfusion*. 2019 Jan; 17(1):27-52.
- Zeller, Michelle P., Bram Rochweg, Erin Jamula, Na Li, Christopher Hillis, Jason P. Acker, Ryan J. R. Runciman, Shannon J. Lane, Naveen Ahmed, Donald M. Arnold, and

- Nancy M. Heddle. 2019. Sex-Mismatched Red Blood Cell Transfusions and Mortality: A Systematic Review and Meta-Analysis. *Vox Sanguinis* 114(5):505–16.
- Zhou, Xiaoming, Zhong Liu, Zhiquan Shu, Weiping Ding, Pingan Du, Jae Hyun Chung, Carolyn Liu, Shelly Heimfeld, and Dayong Gao. 2011. A Dilution-Filtration System for Removing Cryoprotective Agents. *Journal of Biomechanical Engineering* 133(2).
- Zhurova, Mariia, Locksley E. McGann, and Jason P. Acker. 2014. Osmotic Parameters of Red Blood Cells from Umbilical Cord Blood. *Cryobiology* 68(3):379–88.
- Zhurova, Mariia, Aldo Olivieri, Andrew Holt, and Jason P. Acker. 2014. A Method to Measure Permeability of Red Blood Cell Membrane to Water and Solutes Using Intrinsic Fluorescence. *Clinica Chimica Acta* 431:103–10.
- Zhurova, Mariia. 2013. Cryobiological Characteristics of Red Blood Cells from Human Umbilical Cord Blood. University of Alberta, Edmonton, Alberta.
- Zimmermann, R., A. M. Schoetz, A. Frisch, B. Hauck, D. Weiss, J. Strobel, and R. Eckstein. 2011. Influence of Late Irradiation on the in Vitro RBC Storage Variables of Leucoreduced RBCs in SAGM Additive Solution. *Vox Sanguinis* 100(3):279–84.